Structural and thermodynamic properties of
Ca-Al-bearing amphiboles

vorgelegt von

Diplom-Mineraloge

Jens Najorka

Vom Fachbereich 9

- Bauingenieurwesen und Angewandte Geowissenschaften -

der Technischen Universität Berlin

zur Erlangung des akademischen Grades

Doktor der Naturwissenschaften

- Dr. rer. nat. -

genehmigte Dissertation

Promotionsausschuss:

Vorsitzender: Prof. Dr. Gerhard Franz

Berichter: PD Dr. Matthias Gottschalk

Berichter: Prof. Dr. Wilhelm Heinrich

Tag der wissenschaftlichen Aussprache: 16. Februar 2001

Berlin 2001

D83

EIDESSTATTLICHE ERKLÄRUNG

Hiermit erkläre ich an Eides statt, dass ich die vorliegende Arbeit selbständig und nur mit den angegebenen Mitteln angefertigt habe.

Berlin, 12.12.2000

DANKSAGUNG

Jens Najorka

ZUSAMMENFASSUNG

„Strukturelle und thermodynamische Eigenschaften von Ca-Al-haltigen Amphibolen"

In dieser Arbeit wurden die Ca-Sr-Substitution und die Mg-Tschermaks Substitution (MgSi ↔ AlAl) in dem Amphibol Tremolit sowie die Ca-Sr-Substitution in dem Pyroxen Diopsid experimentell untersucht. Die Amphibol- und Pyroxensynthesen wurden in Anwesenheit einer halogenidischen Lösung durchgeführt. Die Experimente zur Ca-Sr Substitution erfolgten bei 750°C und 200 MPa und die Experimente zur Mg-Tschermaks-Substitution bei 600-850°C und 200-2000 MPa.

Sowohl Tremolit- als auch Diopsidstruktur erwiesen sich als flexibel für den vollständigen Ersatz des Ca durch Sr. Zwischen Tremolit und Sr-Tremolit existiert eine kontinuierliche Mischkristallreihe. (SrCa)-Diopside konnten in den Bereichen von X_{Sr} = 0.00-0.31 und 0.90-1.00 synthetisiert werden. Mischkristalle entlang des Mg-Tschermaksvektors konnten zwischen Tremolit und Magnesiohornblende beobachtet werden.

Die Gitterkonstanten von Tremolit und Diopsid verändern sich mit zunehmenden Sr-Einbau linear. Zunehmender Sr-Einbau führt zur Zunahme der Zellparameter a, b und β im Tremolit sowie a, b im Diopsid, wobei sich β im Diopsid verringert. Eine lineare Änderung konnte auch mit zunehmender Mg-Tschermakskomponente im Tremolit verzeichnet werden, wobei die Zellparameter a und b abnehmen und c und β zunehmen.

IR-Untersuchungen zeigten, daß der Einbau von Sr und Al im Tremolit eine komplexe Feinstruktur der OH-Streckschwingungsbande bewirkt. Die Feinstruktur konnte hierbei im (Sr,Ca)-Tremolit der Substitution von Sr, Ca, und Mg auf der M4-Position zugeordnet werden. Im Al-Tremolit wird die Feinstruktur durch Mg-Al-Substitution auf M2- und M3-Positionen sowie Si-Al-Substitution auf T1-Positionen verursacht. Quantitative Berechnungen zu den Bandenzuordnungen deuten hierbei auf eine statistische Verteilung von Sr, Ca, und Mg auf der M4-Position sowie von Mg und Al auf M2- und M3-Positionen im Tremolit hin.

Das Verteilungsverhalten von Sr und Ca zwischen Tremolit, Diopsid und chloridischer Lösung wurde bei 750°C und 200 MPa untersucht. Sr fraktioniert hierbei stark in die Fluidphase. Die Mineral/Fluid-Verteilungskoeffizienten für Sr von $D_{Sr}^{Amphibol/Fluid}$ = 0.045 und $D_{Sr}^{Pyroxen/Fluid}$ = 0.082 wurden abgeleitet. Die Mischungsenergien in (Sr,Ca)-Tremolit- und (SrCa)-Diopsid-Serie wurde mit einem regulären Mischungsmodell berechnet, wobei die Wechselwirkungsparameter von W_{CaSr}^{Amph} = 9.8 kJ und W_{CaSr}^{Pyr} = 11.7 kJ ermittelt wurden.

Verschiedene ideale Mischungsmodelle wurden für die Mg-Tschermaks-Substitution entlang der Tremolit-Tschermakit-Mischkristallreihe getestet. Der beste Fit für die thermodynamischen Daten des Tschermakit wurde mit der Verwendung des "two-site coupled" Modells erzielt. Für Tschermakit konnte eine Enthalpie von $\Delta_f H_{ts}^{o}$ = -12528.3 ± 11.7 kJ/mol und eine Standardentropie von S_{ts}^{o} = 556.5 ± 12.0 J/K/mol extrahiert werden.

Jens Najorka

ABSTRACT

„Structural and thermodynamic properties of Ca-Al bearing amphiboles"

The Ca-Sr and Mg-tschermaks (MgSi $\leftrightarrow$ AlAl) substitutions in tremolite, and the Ca-Sr substitution in diopside were experimentally investigated. Syntheses were performed in the presence of a halogenidic fluid. Experiments about Ca-Sr substitution were carried out at 750°C and 200 MPa and experiments about Mg-tschermaks substitution were carried out at 600-850°C and 200-2000 MPa.

Both tremolite and diopside structures are flexible for a complete substitution of Sr for Ca. A continuous solid solution series exists between tremolite and Sr-tremolite. (Ca,Sr)-diopside solid solutions could be synthesized between X_{Sr} = 0.00-0.31 and 0.90-1.00. Along the Mg-tschermaks vector solid solutions between tremolite and magnesiohornblende were observed. The lattice parameters of tremolite and diopside are a linear function of the Sr-content. For (Ca,Sr)-tremolites the lattice parameters *a*, *b* and *ß* increase with increasing Sr-content. For (Ca,Sr)-diopsides *a* and *b* increase and *ß* decreases with rising Sr-content. Increasing Mg-tschermaks content in tremolite also changes the lattice parameters linearly, *a* and *b* decrease whereas *c* and *ß* increase.

Complex fine structures of the OH stretching bands can be observed in IR spectra of (Ca,Sr)-tremolites and Al-tremolites. Fine structures were assigned to substitutions of Sr, Ca and Mg on M4 sites in (Ca,Sr)-tremolite, and to Mg-Al substitution on M2 and M3 sites and to Si-Al substitution on T1 sites in Al-tremolite. The assignments were supported by quantitative calculations, which indicate a statistical distribution of Sr, Ca and Mg on M4 sites and Mg and Al on M2 and M3 sites in tremolite. The distribution of Sr and Ca between tremolite, diopside and chloridic solution were investigated at 750°C and 200 MPa. Sr fractionates strongly into the fluid.

The mineral/fluid partition coefficients for Sr are $D_{Sr}^{amphibole/fluid}$ = 0.045 and $D_{Sr}^{pyroxene/fluid}$ = 0.082. The mixing energies of (Ca,Sr)-tremolite and (Ca,Sr)-diopside series were calculated using a regular solution model. Interaction parameters of W_{CaSr}^{amph} = 9.8 kJ and W_{CaSr}^{pyr} = 11.7 kJ were derived.

The thermodynamic properties of the tschermakite endmember and the mixing properties along the tremolite-tschermakite join were extracted from six exchange reactions. Ideal mixing models were tested for Mg-tschermaks substitution along the tremolite-tschermakite join. Best fits were obtained for a two-site coupled model, resulting in an enthalpy of formation of $\Delta_f H_{ts}^o$ = -12528.3 ± 11.7 kJ/mol and a standard entropy of S_{ts}^o = 556.5 ± 12.0 J/mol/K for tschermakite endmember.

INHALTSVERZEICHNIS

Kapitel 4
Composition of synthetic tremolite-tschermakite solid solutions in amphibole-anorthite and amphibole-zoisite bearing assemblages

EINLEITUNG

Amphibol und Pyroxen sind bedeutende gesteinsbildende Mineralguppen. Sie sind ein Bestandteil vieler magmatischer und metamorpher Gesteine. Die Stabilität dieser Minerale über weite Druck- und Temperaturbereiche liegt besonders in ihrer großen chemischen Variabilität begründet. Die Strukturen dieser Kettensilikate erlauben den Einbau von Kationen verschiedenster Größen ($r_{Kationen}^{Amphibol}$ = 0.25 – 1.60 Å, Hawthorne 1981; $r_{Kationen}^{Pyroxen}$ = 0.25 – 1.16 Å, Cameron and Papike 1980) und Ladungen (+1 bis +4). In dieser Arbeit wurden die Substitutionsmechanismen von $Ca^{2+} \leftrightarrow Sr^{2+}$, $Mg^{2+} \leftrightarrow Al^{3+}$ und $Si^{4+} \leftrightarrow Al^{3+}$ in Amphibol und $Ca^{2+} \leftrightarrow Sr^{2+}$ in Pyroxen experimentell untersucht. Als experimentelles Modellsystem wurde der in der Natur weitverbreitete Ca-Amphibol Tremolit ($Ca_2Mg_5[Si_8O_{22}/(OH)_2]$) und Ca-Pyroxen Diopsid ($CaMg[Si_2O_6]$) gewählt.

Ca-Sr-Substitution in Tremolit und Diopsid

Die Elemente Ca und Sr sind in ionarer Form zweifach positiv geladen. Der Unterschied in den Ionenradien beträgt ~12% ($r_{Sr^{2+}}$ = 1.26 Å; $r_{Ca^{2+}}$ = 1.12 Å in 8-facher Koordination, Shannon 1976). Dank ihrer ähnlichen chemischen Eigenschaften können sich Sr^{2+} und Ca^{2+} gegenseitig ersetzen. Sr-Ca-Substitutionen kann man in verschiedenen gesteinsbildenden Mineralen wie in Feldspat, Glimmer, Epidot und Karbonaten beobachten. Obwohl die Kristallstrukturen für den Einbau größerer Sr-Gehalte in Amphibol und Pyroxen flexibel sind, wurde die Sr-Ca-Substitution nur in sehr geringen Konzentrationen beobachtet (< 1 Gew% SrO, Mottana and Griffin 1985; Brastad 1985). So konnte in synthetischem K-Richterit und Na-Richterit ($A(Na,Ca)Mg_5[Si_8O_{22}/(OH)_2]$ mit A = Na, K) das Ca^{2+} vollständig durch Sr^{2+} substituiert werden (Della Ventura et al. 1990; Robert et al. 1993). In synthetischem Diopsid konnten 30 Mol% des Ca^{2+} durch Sr^{2+} ersetzt werden (Benna 1982; Benna et al. 1987). Über den Sr-Einbau im Tremolit war bisher nichts bekannt.

Schwerpunkt 1 der vorliegenden Arbeit war die Frage, ob es möglich ist, Ca durch Sr im Tremolit zu ersetzen und ob 30 Mol% Sr^{2+} für Ca^{2+} im Diopsid die maximal mögliche Menge an Sr^{2+} im Diopsidgitter darstellen. Die synthetisierten Phasen wurden hierbei mit optischer Mikroskopie, Rasterelektonenmikroskopie (REM), Transmissionselektonen-mikroskopie (TEM), Elektronenstrahlmikrosonde (EMS), Pulverdiffraktometrie (XRD) und Infrarotspektroskopie (IR) charakterisiert.

Ca-Sr-Verteilungsverhalten zwischen Tremolit, Diopsid und chloridischer Lösung

Das Element Sr ist ein wichtiger petrogenetischer Indikator. Sr-Anreicherungen in Gesteinen werden häufig durch Fluid-Gesteinswechselwirkungen verursacht (Grapes and Watanabe 1984; Theye and Seidel 1988; Brastad 1985). Diese Vorgänge lassen sich rekonstruieren, wenn das Sr-Verteilungsverhalten zwischen Mineral und Fluid bekannt ist. Experimente zu Amphibol/Fluid- und Pyroxen/Fluid-Verteilungskoeffizienten des Strontiums ($D_{Sr}^{Mineral/Fluid}$) wurden von Brenan et al. (1995), Adam et al. (1997) und Ayers et al. (1997) durchgeführt. Dabei wurden Daten für pargasitische Amphibole und augitische Pyroxene ermittelt. Bisher existierten $D_{Sr}^{Mineral/Fluid}$-Werte weder für Tremolit noch Diopsid. Desweiteren lagen bisher keine thermodynamisch anwendbaren Verteilungskoeffizienten (K_D) sowie Mischungsmodelle für Sr-haltige Amphibole und Pyroxene vor.

Schwerpunkt 2 dieser Arbeit war die experimentelle Untersuchung des Verteilungsverhaltens von Sr und Ca zwischen Tremolit, Diopsid und Fluid mit dem Ziel, die Verteilungskoeffizienten $D_{Sr}^{Amphibol/Fluid}$ und $D_{Sr}^{Pyroxen/Fluid}$ sowie die Ableitung eines Mischungsmodells für (Sr,Ca)-Tremolit- und (Sr,Ca)-Diopsidmischkristalle zu ermitteln. Die Untersuchung der Festphasen erfolgte mit EMS-Technik, die fluide Phase wurde mit der Atomabsorbtionsspektrometrie charakterisiert.

Mg-Tschermaks-Substitution in Tremolit

Aufgrund seines Ionenradius kann das Aluminiumkation Al^{3+} in Sauerstoffpolyedern sowohl auf tetraedrischen als auch oktaedrischen Positionen eingebaut werden ($r_{Al^{3+}}^{[4]} = 0.39$ Å, $r_{Al^{3+}}^{[6]} = 0.53$ Å, Shannon 1976). Die gekoppelte Substitution von Al^{3+} für tetraedrisch koordiniertes Si^{4+} und oktaedrisch koordiniertes Mg^{2+} wird als Mg-Tschermaks-Substitution $Mg^{[6]}Si^{[4]} \leftrightarrow Al^{[6]}Al^{[4]}$ bezeichnet. Dieser Substitutionsmechanismus ist in Amphibolen, Pyroxenen, Glimmern und Chloriten weitverbreitet.

In der Amphibol-Mischkristallreihe Tremolit-Tschermakit ($Ca_2Mg_5[Si_8O_{22}/(OH)_2]$-$Ca_2Mg_3Al_2[Al_2Si_8O_{22}/(OH)_2]$) wurde diese Substitution von zahlreichen Autoren experimentell untersucht (Jasmund and Schäfer 1972; Oba 1978; Cao et al. 1986; Jenkins 1981, 1983, 1988, 1994, 1997; Cho and Ernst 1991; Smelik et al. 1994; Hoschek 1995; Quirion and Jenkins 1998; Hawthorne et al. 2000). Ein generelles Problem in diesen Studien war die oft unzureichende Korngröße der synthetisierten Al-Tremolite für die chemische Analyse mit der Mikrosonde. Die Zusammensetzung der Al-Tremolite wurde mittels unpolierter Mikrosondenproben bzw. röntgenographischer Methoden über die Lageänderung

des (310)-Röntgenreflexes bestimmt. Bei den Mikrosondenmessungen wurde hierbei oft energiedispersiv gemessen. Da die Genauigkeit beider Methoden nicht sehr groß ist, muß man annehmen, daß die Zusammensetzung bisher synthetisierter Al-Tremolite mit relativ großen Fehlern behaftet ist.

Für die Verwendung von Al^{3+} als petrogenetischer Indikator im Amphibol sind thermodynamische Daten der Endglieder sowie Parameter über das Mischungsverhalten der Amphibolmischkristalle erforderlich. Hierzu werden genaue Informationen über die Zusammensetzung und Al-Platzbesetzung in den Al-Tremoliten benötigt.

Schwerpunkt 3 dieser Arbeit war es, Amphibole entlang der Tremolit-Tschermakit-Mischkristallreihe zu synthetisieren, deren Zusammensetzungen sich genau mittels Mikrosonde bestimmen lassen. Auf dieser Grundlage wurden kristallchemische Untersuchungen an den Al-Tremoliten durchgeführt, mit denen die Al-Platzbesetzung auf den Oktaederplätzen erstmals quantitativ abgeleitet werden konnte. Desweiteren konnte eine Methode entwickelt werden, mit der sich die Zusammensetzung der Amphibole im ternären System Tremolit-Tschermakit-Cummingtonit anhand von Gitterparametern ableiten lässt. Die synthetisierten Phasen wurden hierbei mit optischer Mikroskopie, REM-, TEM-, EMS-, XRD- und IR-Methoden charakterisiert.

Al im Amphibol als petrogenetischer Indikator

Al-haltige Ca-Amphibole sind in der Natur weitverbreitet, man beobachtet sie z. B. in Metabasiten, Metakarbonaten und kalkalkalinen granitoiden Plutoniten. In den kalkalkalinen Plutoniten kann man eine Zunahme des Al-Gehaltes in der Hornblende mit zunehmender Tiefenlage des Plutons beobachten. Hieraus wurde ein empirisches Geobarometer 'Al in Hornblende' abgeleitet (Hammarstrom and Zen 1986; Hollister et al. 1987).

In den metamorphen Milieus war es dagegen sehr schwierig, den Al-Gehalt im Amphibol als petrogenetischen Indikator zu verwenden. Generell hängt der Al-Gehalt im Amphibol nicht nur von Druck und Temperatur ab. Bei konstantem Metamorphosegrad können die Al-Gehalte im Amphibol aufgrund verschiedener Paragenesen extrem variabel sein (Leger and Ferry 1991). Die Art der Paragenese die mit dem Al-Amphibol koexistert, spielt somit ebenfalls eine wichtige Rolle und kann geobarometrische Untersuchungen zusätzlich erschweren.

Der Al-Einbau im Amphibol kann durch verschiedene Substitutionsmechanismen erfolgen. Im System Na_2O-CaO-MgO-Al_2O_3-SiO_2-H_2O beobachtet man die Mg-Tschermaks-Substitution $(Mg_{-1}^{M1,2,3} Si_{-1}^{T1,2} Al_1^{M1,2,3} Al_1^{T1,2})$, die Edenit-Substitution

($\square^A_{-1} Si^{T1,2}_{-1} Na^A_1 Al^{T1,2}_1$) und die Glaucophan-Substitution ($Ca^{M4}_{-1} Mg^{M1,2,3}_{-1} Na^{M4}_1 Al^{M1,2,3}_1$). Bei bekannten thermodynamischen Daten für die Amphibol-Endglieder sowie bekannten Mischungsparametern wäre der Al-Gehalt leichter für petrogenetische Zwecke anwendbar. Im vereinfachten System $CaO-MgO-Al_2O_3-SiO_2-H_2O$ (CMASH) wurden mittels kalorimetrischer Untersuchungen (Smelik et al. 1994) sowie mittels Phasengleichgewichts-studien (Jenkins 1994; Hoschek 1995; Quirion and Jenkins 1998) thermodynamische Daten für Tschermakit abgeleitet und Mischungseigenschaften der Tremolit-Tschermakit-Mischkristallreihe berechnet. Wie bereits oben erwähnt, wurde die Zusammensetzung der Amphibole in diesen Studien mit relativ ungenauen Methoden ermittelt, was die Aussagekraft der abgeleiteten thermodynamischen Daten verringert.

Schwerpunkt 4 der vorliegenden Studie war die experimentelle Ableitung neuer thermodynamischer Daten für Tschermakit sowie die Ableitung der Mischungseigenschaften für die Tremolit-Tschermakit-Mischkristallreihe. Die neuen Daten wurden hierbei von Amphibolen abgeleitet, deren Zusammensetzung mit der Mikrosonde chemisch genau charakterisiert wurde, bzw. mit Hilfe der kalibrierten Gitterkonstanten ermittelbar war.

Die Kapitel 1-4 sind in englischer Sprache verfaßt und als Veröffentlichungen in Fach-zeitschriften eingereicht bzw. zur Einreichung vorbereitet. Am Ende von jedem Kapitel befindet sich eine Zusammenfassung in deutscher Sprache. Das Literaturverzeichnis wurde an das Ende eines jeden Kapitels gestellt. Die Ergebnisse von Kapitel 1 und 2 sind schon vorab in internationalen Zeitschriften erschienen:

J. Najorka, M. Gottschalk and W. Heinrich (1999) Ca-Sr distribution among amphibole, clinopyroxene, and chloride-bearing-solutions. American Mineralogist, Volume 84, 896-606.

M. Gottschalk , J. Najorka and M. Andrut (1998) Structural and compositional characteriza-tion of synthetic (Ca,Sr)-tremolite and (Ca,Sr)-diopside solid solutions. Physics and Che-mistry of Minerals, 25, 415-428.

Die Ergebnisse von Kapitel 3 und 4 sind eingereicht bzw. zur Einreichung vorbereitet:

J. Najorka and M. Gottschalk (2001) Crystal chemistry of tremolite-tschermakite solid solutions. In preparation.

J. Najorka, M. Gottschalk and W. Heinrich (2001) Compositions of tremolite-tschermakite solid solutions in amphibole-anorthite and amphibole–zoisite bearing assemblages. Submitted to American Mineralogist (Holdaway-Issue).

KAPITEL 1

Structural and compositional characterization of synthetic (Ca,Sr)-tremolite and (Ca,Sr)-diopside solid solutions by EMP, HRTEM, XRD and OH-valence vibrational spectroscopy

ABSTRACT

Solid solutions in the series tremolite–Sr-tremolite and diopside–Sr-diopside have been synthesized hydrothermally in a 1 molar $(Ca,Sr)-Cl_2$ aqueous solution at 750°C and 200 MPa. The solid run products have been investigated by optical, electron scanning and high resolution transmission electron microscopy, electron microprobe, X-ray-powder diffraction and fourier transform infrared spectroscopy. The synthesized (Ca,Sr)-tremolites are up to 2000 μm long and 30 μm wide, the (Ca,Sr)-diopsides are up to 150 μm long and 20 μm wide. In most runs the tremolites and diopsides are well ordered and chain multiplicity faults are rare. Nearly pure Sr-tremolite ($tr_{0.02}Sr-tr_{0.98}$) and Sr-Diopside ($di_{0.01}Sr-di_{0.99}$) have been synthesized. A continuous solid solution series, i.e. complete substitution of Sr^{2+} for Ca^{2+} on M4 exists for (Ca,Sr)-tremolite. Total substitution of Sr^{2+} for Ca^{2+} on M2 can be assumed for (Ca,Sr)-diopsides. For (Ca,Sr)-tremolites the lattice parameters a, b and β are linear functions of composition and increase with Sr-content whereas c is constant. For the diopside series all 4 lattice parameters are a linear function of composition; a, b, c increase and β decreases with rising Sr-content. The unit cell volume for tremolite increases 3.47% from 906.68 $Å^3$ for tremolite to 938.21 $Å^3$ for Sr-tremolite. For diopside the unit cell volume increases 4.87 % from 439.91 $Å^3$ for diopside to 461.30 $Å^3$ for Sr-diopside. The observed splitting of the OH stretching band is caused by different configurations of the next nearest neighbors, i.e the two M4 position. Resolved single bands can be attributed to the following configurations: SrSr, SrCa, CaCa and CaMg. The peak positions of these 4 absorption bands are a linear function of composition. They are shifted to lower wavenumbers with increasing Sr-content. No absorption band due to the SrMg configuration (M4) is observed. This indicates a very low or negligible cummingtonite component in Sr-rich tremolites, which is also supported by electron microprobe analysis.

INTRODUCTION

An understanding of the mineralogy, structure and energetics of cation substitutions on distinct crystallographic sites is essential for the development of mixing models for solid solutions which can then be used for the reconstruction of geological processes. Specifically a knowledge of the substitution mechanism for chemically similar elements (i.e. elements of the same group) is helpful. In 8-fold coordination the ionic radii of Mg^{2+}, Ca^{2+} and Sr^{2+} increase according to Shannon (1976) from 0.89, 1.12 to 1.26 Å, respectively. The substitution of Mg^{2+} for Ca^{2+} on the M2 site in the structure of diopside and its phase relations with ortho- and clinoenstatite are well understood (e.g. Davidson et al. 1982). Less is known about the replacement of Mg^{2+} for Ca^{2+} on the M4 site in tremolite, but experimental results indicate that this substitution seems to be rather limited (Jenkins 1987; Yang and Evans 1996; Zimmermann et al. 1996). While the substitution of Sr^{2+} for Ca^{2+} is common in various Al-bearing phases such as the feldspars, phyllosilicates and epidotes, for tremolite and diopside not much is known about this substitution. An understanding is important, however, in the case of metasomatic fluid infiltration into adjacent Al-poor rocks from intrusions or hydrothermal cells. Siliceous dolomites are rocks for example, in which tremolite and diopside are known to be stable and even coexist over a large *P-T* range. In such rocks, these processes are able to change both, the trace element and isotope characteristics of the host rock (c.f. Agrinier et al. 1993). While the Sr-contents in natural amphiboles and pyroxenes are small (< 1 wt%), systematic structural changes due to higher Sr-contents provide information about the mineralogical and crystallographic properties of the M4 sites in amphiboles and M2 sites in pyroxenes.

Della Ventura et al. (1993) and Robert et al. (1993) demonstrated that Ca^{2+} can be replaced totally by Sr^{2+} in K-richterites synthesized at 750°C and 100 MPa, i.e. at least half of the M4 sites can be occupied by Sr^{2+}. Benna (1982) and Benna et al. (1987) showed that at least 30 % of the Ca^{2+} can be substituted by Sr^{2+} in diopsides synthesized at 0.1 MPa and 1200-1300°C. The extent of the (Ca,Sr)-tremolite solid solution series and that of the (Ca,Sr)-diopside series, $(Ca,Sr)_2Mg_5[Si_8O_{22}/(OH)_2]$ and $(Ca,Sr)Mg[Si_2O_6]$ respectively, is unknown.

In order to understand the (Ca,Sr)-distribution between fluid and tremolite/diopside the following aspects have to be understood:

(1) the physical and compositional properties of endmembers and the probable (Ca,Sr)-tremolite/diopside solid solution series, and

(2) the thermodynamic properties of the (Ca,Sr)-tremolite/diopside solid solution series and the fluid with respect to Ca^{2+} and Sr^{2+}.

To study the distribution of Ca^{2+} and Sr^{2+} between (Ca,Sr)-tremolite, (Ca,Sr)-diopside and an aqueous $(Ca,Sr)Cl_2$ solution, (Ca,Sr)-tremolite and (Ca,Sr)-diopside solid solutions were synthesized at 750°C and 200 MPa. It will be the first aspect, the physical and compositional properties , which will be subject of this paper.

Because the experiments were conducted in the presence of an aqueous chloridic solution (c.f. Zimmermann et al. 1996, 1997), the synthesized tremolites and diopsides were sufficiently large enough (up to 2000×30×30 μm) for electron microprobe analysis. In addition to chemical characterization, the solid solutions were examined by electron scanning and high resolution transmission electron microscopy, X-ray powder diffraction and fourier transformed infrared spectroscopy.

The second aspect, the thermodynamic evaluation and petrologic implications of the (Ca,Sr)-tremolite/fluid and (Ca,Sr)-diopside/fluid equilibria, is presented in Najorka et al. (1999).

EXPERIMENTAL AND ANALYTICAL TECHNIQUES

Standard cold-seal hydrothermal techniques were used in this study. Temperatures were recorded with Ni-CrNi thermocouples closely adjoining the sample position. Total temperature uncertainties are estimated to be less than ±5°C. The pressure was measured with a calibrated strain gauge and is believed to be accurate to within ±10 MPa. The experiments were quenched by cooling the autoclaves with compressed air to less than 300°C in about 3 minutes. The experiments were run for 21 days at 750°C and 200 MPa.

Starting materials consisted of SiO_2, MgO, $Ca(OH)_2$, $Sr(OH)_2 \times 8H_2O$ and 1 molar $CaCl_2$-$SrCl_2$ aqueous solution. $Sr(OH)_2 \times 8H_2O$ had an impurity of 2 wt% $SrCO_3$, 0.1 wt% Ba and 0.05 wt% Ca, all other chemicals were of pro analysi quality. Except for runs 8 and 14, stoichiometric mixtures (15-25 mg) with compositions on the tremolite - Sr-tremolite join with 5 wt% of quartz in excess along with 50-200 μl chloridic aqueous solution were used. Run 8 and 14 had bulk compositions on the diopside–Sr-diopside join. The experimental setup lead to $(Ca+Sr)^{solid}/(Ca+Sr)^{total}$ ratios of 0.16 to 0.49. The experiments are divided into two series. The first series (runs 1 to 15) was performed with $(Ca+Sr)^{solid}/(Ca+Sr)^{total}$ ratios of 0.42-0.49 and the second (runs 16 to 23) was conducted with $(Ca+Sr)^{solid}/(Ca+Sr)^{total}$ ratios of 0.16-0.18. The quartz excess was chosen to compensate SiO_2 solubility at experimental conditions. All experiments were performed in

25-35 mm long gold capsules with an inner diameter of 2.6 and 4.6 mm and a wall thickness of 0.2 mm. The composition of the starting mixtures are listed in Table 1.

After each run the unopened capsules were cleaned with a weak HCl solution and hot distilled water. To extract compositional information from the aqueous solutions, the gold tubes were cut open in destilled water. The run product were then washed with aqua bidest. All fluid was recovered and diluted to yield a total of 100 ml solution for later analysis.

The solid run products were examined by optical microscopy, scanning electron microscopy (SEM), high resolution electron microscopy (HRTEM), electron microprobe (EMP), powder X-ray diffraction with Rietveld analysis (XRD) and Fourier-transform infrared spectroscopy (FTIR).

The SEM used was a HITACHI S-4000 FE-REM at the Technical University of Berlin. HRTEM investigations were carried out at the University of Kiel using a Phillips EM400T microscope and at the GeoForschungsZentrum Potsdam using a Phillips CM200T microscope, all equipped with EDX-systems.

Table 1. Composition of run charges

run	SiO_2	MgO	$Ca(OH)_2$	$Sr(OH)_2$ $\times 8\ H_2O$	$(Ca,Sr)Cl_2$ 1 m	X_{Sr} fluid start	X_{Sr} fluid final
	(mg)	(mg)	(mg)	(mg)	(µl)		
1	10.90	4.36	0.00	11.48	60	1.00	0.99
2	11.25	4.50	0.99	8.30	50	0.84	0.95
5	10.82	4.32	2.85	1.14	50	0.10	0.21
6	10.35	4.27	2.51	2.25	50	0.20	0.34
8	7.16	2.29	0.00	15.09	60	1.00	0.99
9	11.50	4.59	1.69	6.05	60	0.50	0.73
10	11.37	4.54	1.34	7.19	60	0.60	0.89
11	11.62	4.64	2.05	4.90	60	0.40	0.66
12	11.75	4.70	2.41	3.71	60	0.30	0.52
13	10.96	4.38	0.16	10.96	60	0.95	0.98
14	7.87	2.52	1.54	8.29	60	0.50	0.86
15	11.25	4.50	0.99	8.30	60	0.70	0.92
16	11.14	4.45	0.65	9.38	200	0.80	0.91
17	11.38	4.54	1.34	7.19	200	0.60	0.69
18	11.25	4.49	0.99	8.29	200	0.70	0.86
19	11.02	4.40	0.33	10.44	200	0.90	n.a.
20	9.92	3.96	0.29	9.41	200	0.90	0.96
21	10.10	4.03	0.79	7.80	200	0.73	0.83
22	10.17	4.06	1.00	7.13	200	0.67	0.76
23	9.87	3.94	0.14	9.88	200	0.95	0.98

All EMP analyses were performed with carbon coated polished samples using Cameca Camebax and SX100 microprobes at the Technical University of Berlin and the GeoForschungsZentrum Potsdam with WDS and using the PAP program of Pouchou and Pichoir (1984) for correction. Operating conditions were 15 kV and 15-20 nA. Counting time for the peaks were 20 to 40 s, the background was measured 10 to 20 s on both sides of the peak. For Sr the $Sr_{L\alpha1}$ line was chosen. Because the $Si_{K\alpha1}$, $Si_{K\beta}$, $Sr_{L\alpha1}$ and $Sr_{L\beta1}$ lines form a quadruplet, the background was measured on both sides of the line system. Well characterized natural and synthetic minerals were used as standards: wollastonite for Ca and Si, quartz for Si, forsterite and tremolite for Mg, strontianite and Sr-wollastonite for Sr. Cl concentrations in the amphiboles were always below the detection limit (< 0.05 wt%).

For the XRD measurements the run products were treated with weak HCl acid to dissolve any minor amounts of strontianite. The products were then ground in an agate mortar for several minutes, diluted with Elmer´s White glue and evenly spread on a circular foil. To minimize preferential orientation, the powder was stirred during drying. Finally, the foil was placed into the transmission sample holder and covered with a second empty foil. Powder XRD patterns were recorded in transmission using a fully automated STOE STADI P diffractometer (Cu $K_{\alpha1}$ radiation), equipped with a primary monochromator and a 7° - position sensitive detector. The normal-focus Cu X-ray tube was operated at 40 kV and 40 mA, using a take-off angle of 6°. Intensities were recorded in the 2θ range from 5 to 125°. The detector step size was 0.1° having a resolution of 0.02°. Counting times were selected to yield a maximum intensity of 2000 and 3000 counts, resulting in 5 to 20 s per detector step. Unit cell parameters, other structural parameters and phase proportions were refined using the *GSAS* software package for Rietveld refinements (Larson and Von Dreele 1987). The peakshape were defined as pseudo-Voigt with variable Lorentzian character. The peak full width at half maximum height (FWHH) was varied as a function of 2θ using the parameters U, V, W of Caglioti et al. (1958). For the Lorentzian character the parameters ´X´ and ´Y´ were used. The recorded peaks were highly symmetric due to the geometry of the STADI P diffractometer, therefore no parameters describing the asymmetry of the peaks had to be used. Background was fitted with a real space correlation function which is capable of modeling the diffuse background from the amorphous foil and glue used for the preparation. Except for the M4 site in tremolite and the M2 site in diopside, isotropic displacement factors were fixed at values approximately correct for amphiboles and pyroxenes (Della Ventura et al. 1993). The refinements were done in the following sequence: scale factor, background, zero-point correction, phase fractions, Caglioti W, lattice parameters, preferred orientation, atomic positions, individual isotropic temperature factor of the A site, Caglioti U

and V, Lorentz X and Y. Details of the Rietveld structure and quantitative phase analysis are given in Table 2.

The samples for infrared investigation were prepared by grinding 1 mg of the product and dispersing it into 450 mg KBr (dried at 170°C for 24 h). The homogenized mixture was subsequently pressed under vacuum to transparent pellets with 13 mm in diameter. The samples were dried at 170°C for 6 h before taking the spectrum. The absorption measurements were carried out in the spectral range from 3600 cm^{-1} to 3800 cm^{-1} with a resolution of 0.25 cm^{-1} using a Bruker IFS 66v FTIR spectrometer equipped with a globar as the light source, a KBr-beam splitter and DTGS-detector. Spectra were averaged over 256 scans. Phase correction mode of the interferogram was performed with a procedure after Mertz (Mertz 1965; cf. Griffiths and de Haseth 1986). Norton-Beer-weak mode was chosen as the apodization function. The sample chamber of the Bruker IFS 66v spectrometer was evacuated down to 200 Pa, therefore the influence of H_2O vapor and CO_2 is negligible. The spectra were displayed in the form of absorbance spectra as a function of wavenumber. After background correction, the band center, full width at half maximum height (FWHH) and integral intensity were determined with the program *PeakFit* by Jandel Scientific.

RESULTS

Phases and proportions

Quantitative determination of phase proportions was obtained by Rietveld analysis and is also summarized in Table 2. Because only 10 wt% of the run products (2 mg) were used for the quantitative phase analysis, the derived phase proportions have an uncertainty because of possible phase inhomogeneities in the gold tube. The first series of runs (1-15) with $(Ca+Sr)^{solid}/(Ca+Sr)^{total}$ ratios of 0.42-0.48 were quartz oversaturated whereas the second series of runs (16-23) with $(Ca+Sr)^{solid}/(Ca+Sr)^{total}$ ratios of 0.16-0.18 were quartz undersaturated. For the latter series 5 wt% quartz in excess was insufficient to saturate the fluid with SiO_2. Observed phases in the first series were (Ca,Sr)-tremolite, (Ca,Sr)-diopside and quartz. Except for the runs 8 and 14, (Ca,Sr)-tremolite was the predominant phase. Runs 8 and 14 were performed on the diopside–Sr-diopside join and both yielded 95 wt% (Ca,Sr)-diopside. Phases in the second series were (Ca,Sr)-tremolite, (Ca,Sr)-diopside, enstatite, forsterite and talc. Except for run 18, (Ca,Sr)-tremolite was the predominant phase. Amounts

of enstatite and forsterite varied from run to run and talc was only observed in run 17. In the runs 2, 15, 20, 21, 22 and 23, two distinct (Ca,Sr)-tremolites are clearly identified by separate X-ray reflections. In addition to the phases described above, minor amounts of strontianite (< 0.5 wt%) were detected by optical microscopy.

SEM

In the Figs. 1a-1d typical SEM pictures of the run products are shown. The (Ca,Sr)-tremolites were up to 2000 μm long and 30 μm wide, the (Ca,Sr)-diopsides were up 150 μm long and 20 μm wide. The tremolites in the Ca-rich runs were more fibrous than in the Sr-rich samples. The size of the (Ca,Sr)-tremolites and (Ca,Sr)-diopsides were large enough for precise electron microprobe analyses.

HRTEM

In general, the Sr-rich tremolites were more sensible to the electron beam than the Ca-rich tremolites, indicating lower lattice energies.

Phases from the runs 1, 2, 5, 6, 8, 9, 12, 13, 15, 16, 17, 23 have been investigated by HRTEM. The results can be divided into three groups. Sr-rich tremolites from runs 1, 13, 23 and diopsides from run 8 were totally free of chain multiplicity faults. (Ca,Sr)-tremolites from runs 2, 5, 6, 12, 15, 16 did show only minor concentrations of chain multiplicity faults. In run 2 for example with tremolites of intermediate composition, a total of only 4 triple chains could be detected. With increasing Ca-content in tremolite the concentration of chain multiplicity faults rises. Triple chain multiplicity faults were predominant, but single chain and 5-chain multiplicity faults were also found occasionally. Fig. 1g shows a HRTEM picture of a tremolite from run 5. The picture of this Sr-free tremolite shows 106 double chain units. Also visible are 8 triple and two 5-chain multiplicity faults. Tremolites from runs 9 and 17 did show much higher chain multiplicity fault concentrations. These were not evenly distributed, however. Large sections of undisturbed tremolite were separated by heavily disturbed sections. As one would expect from mass balance, the increased fault concentration correlates with the high diopside concentration found by quantitative phase analysis.
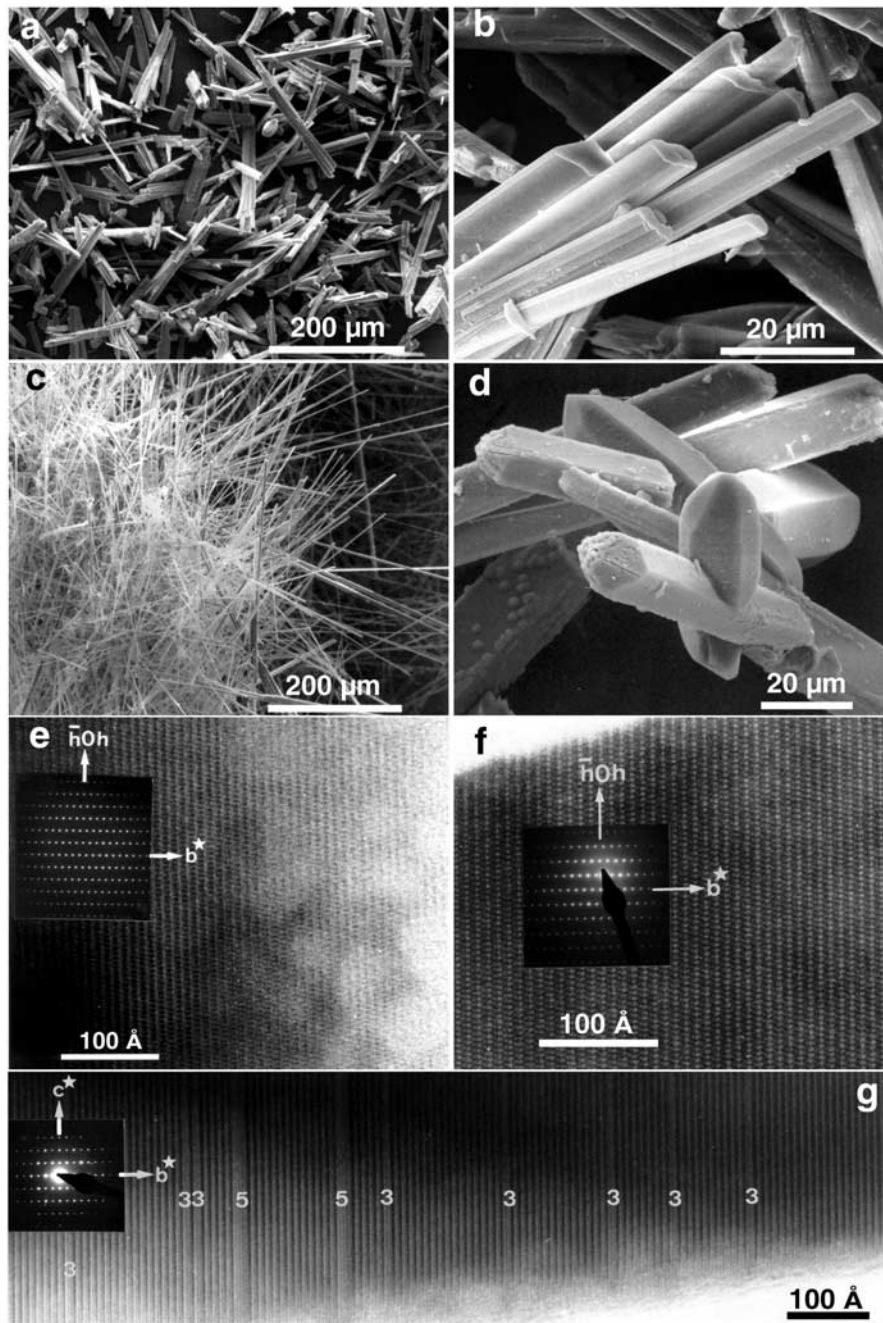
Fig. 1. SEM a)-d) and HRTEM e)-g) images of (Ca,Sr)-tremolites and (Ca,Sr)-diopsides. **a)** Reaction products (Sr-tremolite) from run 1. The average size of the Sr-tremolites is 30×200 μm. **b)** Close-up of products from run 1. **c)** The synthesized tremolites (run 5) are much more elongated in the direction parallel to *c*. **d)** Euhedral Sr-diopsides from run 8. **e)** HRTEM image of an Sr-tremolite from run 1. The spotty features on the right hand side shows the relative instability of Sr-rich tremolites with respect to the electron beam. The crystal is free of chain multiplicity faults. **f)** HRTEM image of a (Ca,Sr)-tremolite from run 2. The crystal is also free from chain multiplicity faults. **g)** HRTEM image of a tremolite from run 5. Several chain multiplicity faults are visible.

Table 2. Data collection and structure refinement details for the synthetic (Ca,Sr)-tremolite samples and results of the quantitative phase analysis

run	1	2	5	6	8	9	10	11	12	13	14	15	16	17	18	19	20	21	22	23
integration time/step interval [s]	530	340	408	848	1166	340	636	340	408	848	272	689	583	1007	1060	340	408	544	848	272
maximum counts/step	3566	2988	2690	2802	5976	2682	2900	2788	2771	3648	2587	2868	2569	2894	3060	2521	2765	2750	2652	3083
unique reflections	1512	2387	1461	1452	1510	1463	1457	1451	1453	2415	570	2381	1357	3159	1669	1247	2139	3468	3132	2166
structure parameters	54	68	53	53	21	53	35	53	36	35	21	68	35	42	55	33	33	33	55	65
experimental parameters	43	46	39	37	40	38	45	43	37	49	30	48	36	53	54	34	44	55	45	46
$N - P$	5701	5684	5706	5708	5737	5707	5718	5702	5722	5714	5747	5682	5727	5703	5689	5731	5721	5710	5698	5697
R_p	0.066	0.064	0.071	0.061	0.047	0.076	0.061	0.071	0.068	0.054	0.070	0.063	0.066	0.062	0.063	0.075	0.063	0.058	0.053	0.077
R_{wp}	0.088	0.085	0.094	0.080	0.063	0.101	0.082	0.092	0.089	0.072	0.095	0.084	0.086	0.083	0.071	0.098	0.084	0.076	0.070	0.103
χ^2	1.22	1.38	1.52	1.30	1.18	1.84	1.17	1.51	1.71	1.17	1.12	1.34	1.48	1.83	1.13	1.54	1.37	1.59	1.38	1.38
d statistics (Durbin-Watson)	1.69	1.50	1.35	1.57	1.61	1.14	1.70	1.30	1.17	1.70	1.81	1.52	1.35	1.08	1.72	1.28	1.43	1.27	1.42	1.48
results of the quantitative phase analysis [wt%]																				
(Ca,Sr)-tremolite I	89	67	85	82	1	64	92	87	87	87		65	92	49	29	100	70	80	66	59
(Ca,Sr)-tremolite II		20										26					29	13	16	41
(Ca,Sr)-diopside	7	1	12	14	95	23	6	9	5	4	95	2	8	44	60			2	8	
quartz	4	12	3	4	4	13	2	4	8	9	5	7								
enstatite														5				2	10	
forsterite														*	11		1	3		

note: $N - P$ = observations (step intervals) - least-squares parameters $R_p = \sum |y_i^{obs} - y_i^{calc}| / \sum y_i^{obs}$, $R_{wp} = \sqrt{\sum w_i (y_i^{obs} - y_i^{calc})^2 / \sum w_i (y_i^{obs})^2}$, $\chi^2 = \sum w_i (y_i^{obs} - y_i^{calc})^2 / (N-P)$,

y: intensity, $w = 1/y$: weighting factor.

*+ 2 wt% talc instead.

20

Electron microprobe

The synthesized phases were extensively examined by electron microprobe. In the case of (Ca,Sr)-tremolites the analyses were generally accepted when the sum of the oxides (not considering water) was in the range of 95 and 99 wt%. However, only few analysis were available for (Ca,Sr)-tremolites from run 22. Here analysis above 93 wt% were accepted. In the case of (Ca,Sr)-diopside a range of acceptance was set to 98-101 wt%. These criteria did lead to over 700 (Ca,Sr)-tremolite and (Ca,Sr)-diopside analyses.

Like all others, analyses for very Sr-rich tremolites and diopsides were calculated using the PAP correction program (Pouchou and Pichoir 1984). These results indicated M4 and M2 occupancies of Ca+Sr above 2 and 1, respectively. This would imply that the Sr-tremolites of run 1 would have a stoichiometry of $Sr_{2.04}Ca_{0.05} Mg_{4.91} [Si_8O_{22}/(OH)_2]$ and the Sr-diopsides of run 8 would have a stoichiometry of $Sr_{1.02}Mg_{0.98} Si_2O_6$. This effect is only observed in Sr-rich phases, however. For the range of the experimental run conditions used here (750°C and 200 MPa), it is unlikely that Ca^{2+} is incorporated on the M1,2,3 sites in tremolite or on the M1 site in diopside (e.g. Hawthorne 1983). It is more reasonable to interpret the results in a manner that the presence of a heavy element like Sr, the emitted X-ray radiation of the lowest energy, that of $Mg_{K\alpha}$, is involved in more interaction with the matrix than considered in the PAP correction program, with too low MgO contents as a result. Also secondary fluorescence of $Sr_{L\alpha1}$-radiation would lead to higher SrO contents. The MgO content was therefore corrected proportionally to the SrO content in such a way that for each wt% SrO, 0.04 wt% was added to the MgO content. This correction lead to $Sr_{1.98}Ca_{0.04} Mg_{4.98} [Si_8O_{22}/(OH)_2]$ for the Sr-tremolites in run 1 and to $Sr_{0.99}Mg_{1.01} Si_2O_6$ for the Sr-diopsides in run 8. The proposed adjustment is the minimum correction necessary to avoid structurally unreasonable site occupancies.

The electron microprobe results for (Ca,Sr)-tremolites are summarized in Table 3, those for (Ca,Sr)-diopside in Table 4. The mineral formulae were calculated on the basis of 8 Si for (Ca,Sr)-tremolites and 2 Si for (Ca,Sr)-diopsides instead of the more common 23 and 6 oxygens, respectively. In the case of the synthetic phases examined here, it is clear that all tetrahedral positions were occupied by Si^{4+}. In tremolite and diopside, SiO_2 is more than 50 wt%. Because of the charge difference with respect to the other divalent cations any analytical error in Si^{4+} will influence the other cations by a factor of 2.

Table 3. Compositions of tremolite–Sr-tremolite solid solutions

run	1	2	5	6	9	10	11	12	13	15	16	17	18	19	20	21	22	23	23
tremolite composition (wt%)																			
analyses	87	65	34	26	21	11	12	29	47	28	22	8	18	38	4	13	2	6	16
SiO_2	52.83	56.31	59.38	59.35	58.89	57.52	58.64	59.40	53.19	57.95	58.80	59.25	59.04	55.25	55.43	59.42	56.78	55.50	53.74
MgO	21.59	22.92	25.05	24.97	24.47	23.66	24.39	24.75	21.76	23.73	24.67	24.65	24.49	22.62	22.99	25.23	23.83	22.86	22.06
CaO	0.27	7.58	12.99	13.17	12.80	11.40	12.92	13.26	1.48	10.40	11.19	12.31	11.88	5.51	8.18	12.07	12.20	5.25	2.84
SrO	23.02	10.36	0.18	0.22	1.22	3.50	0.68	0.33	21.00	5.48	3.39	0.61	1.62	14.32	8.94	1.01	0.81	14.09	18.54
Σ oxides	97.71	97.24	97.60	97.71	97.38	96.08	96.64	97.74	97.43	97.57	98.05	96.82	97.04	97.69	95.53	97.74	93.62	97.70	97.17
tremolite composition on the basis of 8 Si																			
Sr	1.98	1.47	0.00	0.01	0.07	0.27	0.03	0.02	1.79	0.45	0.27	0.04	0.13	1.20	0.77	0.10	0.09	1.19	1.59
Ca	0.04	0.54	1.90	1.92	1.89	1.72	1.92	1.94	0.23	1.56	1.65	1.84	1.77	0.84	1.25	1.76	1.86	0.80	0.44
Mg	4.98	4.99	5.10	5.07	5.04	5.00	5.05	5.04	4.98	4.99	5.08	5.12	5.10	4.95	4.98	5.13	5.05	5.00	4.96
Si	8.00	8.00	8.00	8.00	8.00	8.00	8.00	8.00	8.00	8.00	8.00	8.00	8.00	8.00	8.00	8.00	8.00	8.00	8.00
occupancy on M4																			
X_{Sr}	0.98	0.43	0.00	0.01	0.04	0.13	0.02	0.01	0.88	0.22	0.14	0.02	0.07	0.59	0.38	0.05	0.04	0.60	0.79
ΔX_{Sr}	0.01	0.08	0.00	0.01	0.00	0.01	0.00	0.00	0.03	0.02	0.02	0.01	0.01	0.09	0.03	0.01	0.01	0.04	0.05
X_{Ca}	0.02	0.57	0.95	0.96	0.94	0.86	0.96	0.97	0.12	0.77	0.82	0.92	0.88	0.41	0.62	0.88	0.93	0.40	0.21
X_{Mg}	0.00	0.00	0.05	0.03	0.02	0.01	0.02	0.02	0.00	0.01	0.04	0.06	0.05	0.00	0.00	0.07	0.03	0.00	0.00

Table 4. Compositions of diopside–Sr-diopside solid solutions

run	1	2	5	6	7	8	9	10	11	12	13	14	15	16	17	18	21	22
diopside composition (wt%)																		
analyses	14	5	7	7	7	37	28	6	2	12	12	9	13	15	18	16	8	16
SiO_2	44.81	52.07	55.83	55.77	55.77	45.14	55.79	54.54	54.86	55.65	46.22	54.67	54.91	54.94	55.67	55.18	55.67	53.26
MgO	14.77	17.21	18.05	19.00	19.00	14.95	18.61	18.10	18.09	19.00	15.34	18.30	18.21	18.95	19.45	19.11	19.13	18.71
CaO	0.41	15.91	25.17	24.75	24.75	0.05	24.52	22.41	24.34	25.35	2.59	23.25	22.38	22.26	24.34	23.36	23.75	24.10
SrO	40.07	13.79	0.22	0.26	0.26	39.84	1.22	4.29	1.15	0.46	36.15	3.54	5.14	4.69	0.87	2.24	1.56	0.89
Σ oxides	100.06	98.97	99.28	99.78	99.78	99.98	100.14	99.35	98.44	100.45	100.31	99.75	100.64	100.84	100.34	99.88	100.11	96.96
diopside composition on the basis of 2 Si																		
Sr	0.99	0.31	0.00	0.00	0.00	0.99	0.02	0.09	0.02	0.01	0.90	0.07	0.11	0.10	0.02	0.05	0.04	0.03
Ca	0.02	0.67	1.00	0.97	0.97	0.00	0.96	0.90	0.97	0.98	0.12	0.92	0.89	0.87	0.94	0.91	0.92	0.95
Mg	0.99	1.02	1.00	1.03	1.03	1.01	1.02	1.01	1.01	1.02	0.98	1.01	1.00	1.03	1.04	1.04	1.04	1.03
Si	2.00	2.00	2.00	2.00	2.00	2.00	2.00	2.00	2.00	2.00	2.00	2.00	2.00	2.00	2.00	2.00	2.00	2.00
occupancy on M2																		
X_{Sr}	0.99	0.31	0.00	0.00	0.00	0.98	0.02	0.09	0.02	0.01	0.90	0.07	0.11	0.10	0.02	0.05	0.04	0.03
ΔX_{Sr}	0.02	0.07	0.00	0.00	0.00	0.01	0.01	0.01	0.00	0.00	0.02	0.03	0.03	0.01	0.00	0.01	0.00	0.00
X_{Ca}	0.01	0.67	1.00	0.97	0.97	0.00	0.96	0.90	0.97	0.98	0.12	0.92	0.89	0.87	0.94	0.91	0.92	0.94
X_{Mg}	0.00	0.02	0.01	0.03	0.03	0.02	0.02	0.01	0.02	0.02	0.00	0.01	0.01	0.03	0.04	0.04	0.04	0.03

23

In run 2 and 23 two distinct tremolite compositions were detected (c.f. Fig. 2). The distribution diagram of tremolite analyses of run 2 clearly shows two maxima. The diagram of the tremolite analyses from run 19 has only one clear maximum with a long tail towards high X_{Sr}-contents. The distribution diagram for run 13 also clearly shows one maximum. This is in agreement with the results from the quantitative phase analysis.

The solid solution series for the (Ca,Sr)-tremolites was found to be continuous however, when all available EMP analysis were taken into account (see Fig. 4). For the (Ca,Sr)-diopside solid solution series no compositions were observed in range of $0.31 > X_{Sr} > 0.90$. The content of cummingtonite ($Mg_7[Si_8O_{22}/(OH)_2]$) was highly variable (1-7%) in Ca-rich tremolites and close to 0% for Sr-rich tremolites.

X-ray diffraction

The diffraction patterns were used to define the range of compositional scatter in each sample and a Rietveld refinement was conducted. In addition to the quantitative phase analysis, the Rietveld analysis was used to derive precise lattice constants for phases in mixtures.

The positions of the (151)- and ($33\bar{1}$)-reflections of (Ca,Sr)-tremolites show different functional behaviour with respect to varying Sr-content. Starting from tremolite and going to Sr-tremolite, the (151)-reflection moves 0.18° and the ($33\bar{1}$)-reflection moves 0.77° to lower angles. Any compositional variations within a sample will affect the full with at half height (FWHH) of both reflections differently. The difference in FWHH can therefore be used as a measure of compositional variations. The diffraction patterns of all samples are plotted in the range of 31.5 and 33.5° 2θ in Fig. 3; the peak positions and their FWHH are listed in Table 5. In the runs 2, 15, 20, 21, 22 and 23 two distinct ($33\bar{1}$)-reflections could be identified.

In the course of the Rietveld refinement the space groups C 2/m for tremolite and the space group C 2/c for diopside were also found to be adequate for the Sr-rich tremolites and diopsides, respectively. The derived lattice constants are listed in Table 6 and are plotted *vs.* the Sr-content in Figs. 4 and 5. Except for run 8 and 14 the lattice parameters for (Ca,Sr)-diopsides are less precise than those for (Ca,Sr)-tremolites, because diopside was usually a minor phase in the mixtures. The lattice constants *a, b* and *ß* for (Ca,Sr)-tremolites are linear functions of X_{Sr} and increase with rising Sr-content whereas *c* is independent of composition. In contrast all constants for (Ca,Sr)-diopsides vary linearly with composition and increase, with the exception of *ß,* with rising Sr-content. In contrast to the (Ca,Sr)-tremolites where the lattice parameter *c* is
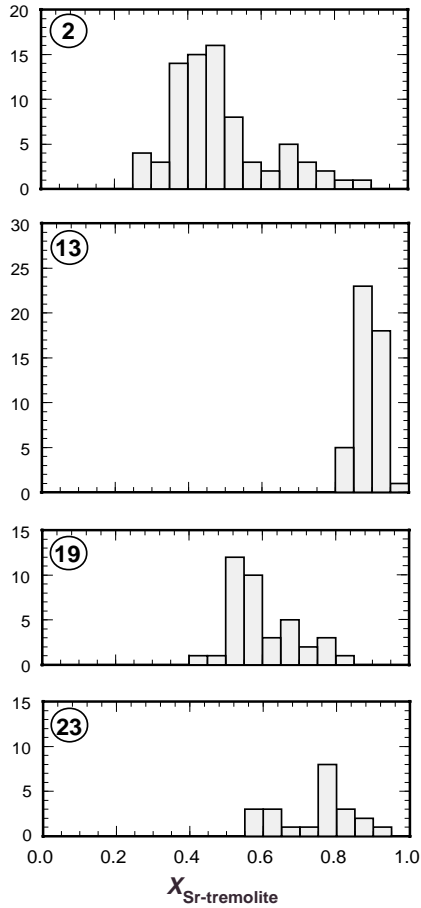
Fig. 2. Distribution of EMP analyses for (Ca,Sr)-tremolites from runs 2, 13, 19, 23. For runs 2 and 23 two distinct maxima are observed. For run 19 the distribution diagram can be interpreted as one maximum with an elongated tail towards Sr-rich tremolites. For run 13 only one maximum is observed.

Table 5. Position and FWHH of the (151) and $(33\bar{1})$ (Ca,Sr)-tremolite reflections

run	(151) of tr I and II		$(33\bar{1})$ of tr I		$(33\bar{1})$ of tr II	
	Position	FWHH	Position	FWHH	Position	FWHH
	(°2θ)		(°2θ)		(°2θ)	
1	32.91	0.12	32.00	0.13		
2	33.00	0.15	32.13	0.19	32.39	0.18
5	33.10	0.12	32.81	0.15		
6	33.09	0.12	32.79	0.14		
9	33.09	0.14	32.76	0.24		
10	33.07	0.13	32.67	0.13		
11	33.09	0.14	32.79	0.21		
12	33.07	0.14	32.79	0.23		
13	32.93	0.14	32.07	0.15		
15	33.03	0.15	32.40	0.23	32.57	0.16
16	33.07	0.16	32.69	0.21		
17	33.08	0.13	32.81	0.21		
18	33.07	0.14	32.75	0.17		
19	32.98	0.16	32.34	0.26		
20	33.00	0.16	32.41	0.14	32.52	0.18
21	33.06	0.18	32.39	0.26	32.86	0.31
22	33.01	0.20	31.99	0.36	32.79	0.27
23	32.96	0.15	32.16	0.15	32.30	0.16
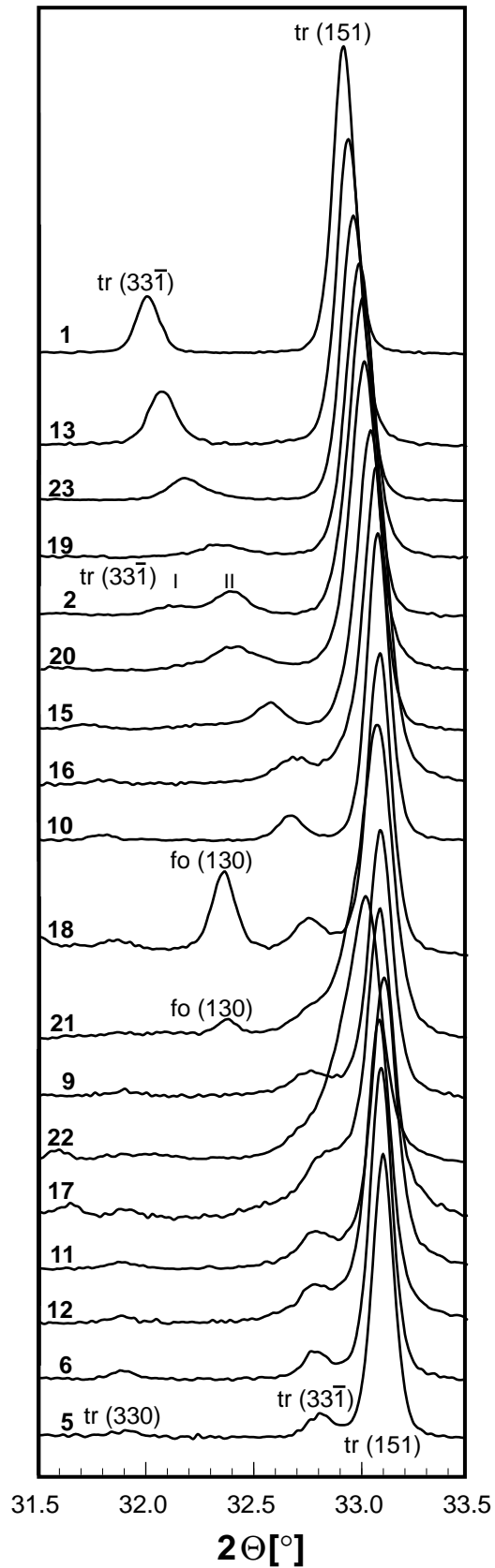
Fig. 3. X-ray patterns in the range of 31.5 to 33.5°2θ. In this range the $(33\bar{1})$- and (151)-reflection of (Ca,Sr)-tremolite are predominant. Two distinct $(33\bar{1})$-reflections for the two observed (Ca,Sr)-tremolites I and II are clearly visible in the pattern of run 2. In the patterns of the runs 18 and 21 the (130)-reflection of forsterite is observed.
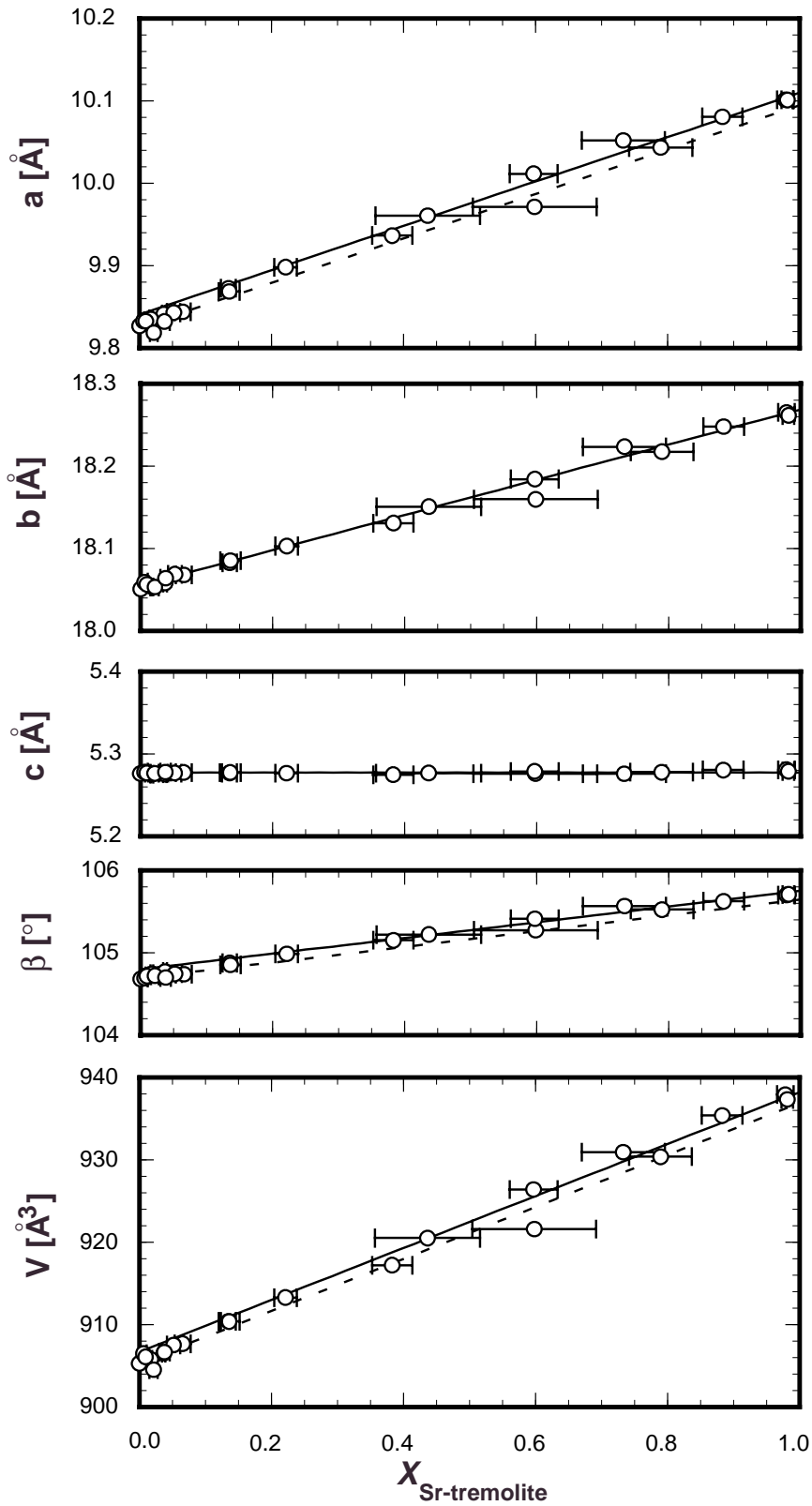
Fig. 4. The lattice constants *a*, *b*, *c*, *ß* and the unit cell volume *V* of (Ca,Sr)-tremolite as a function of X_{Sr}. All lattice constants except *c* vary linearly with composition. All compositions on the tremolite–Sr-tremolite join are represented, no limited miscibility is observed. Cummingtonite isopleths are shown as dashed lines for $X_{cum} = 0.05$ for the lattice parameters *a* and *ß* and the molar volume *V*.
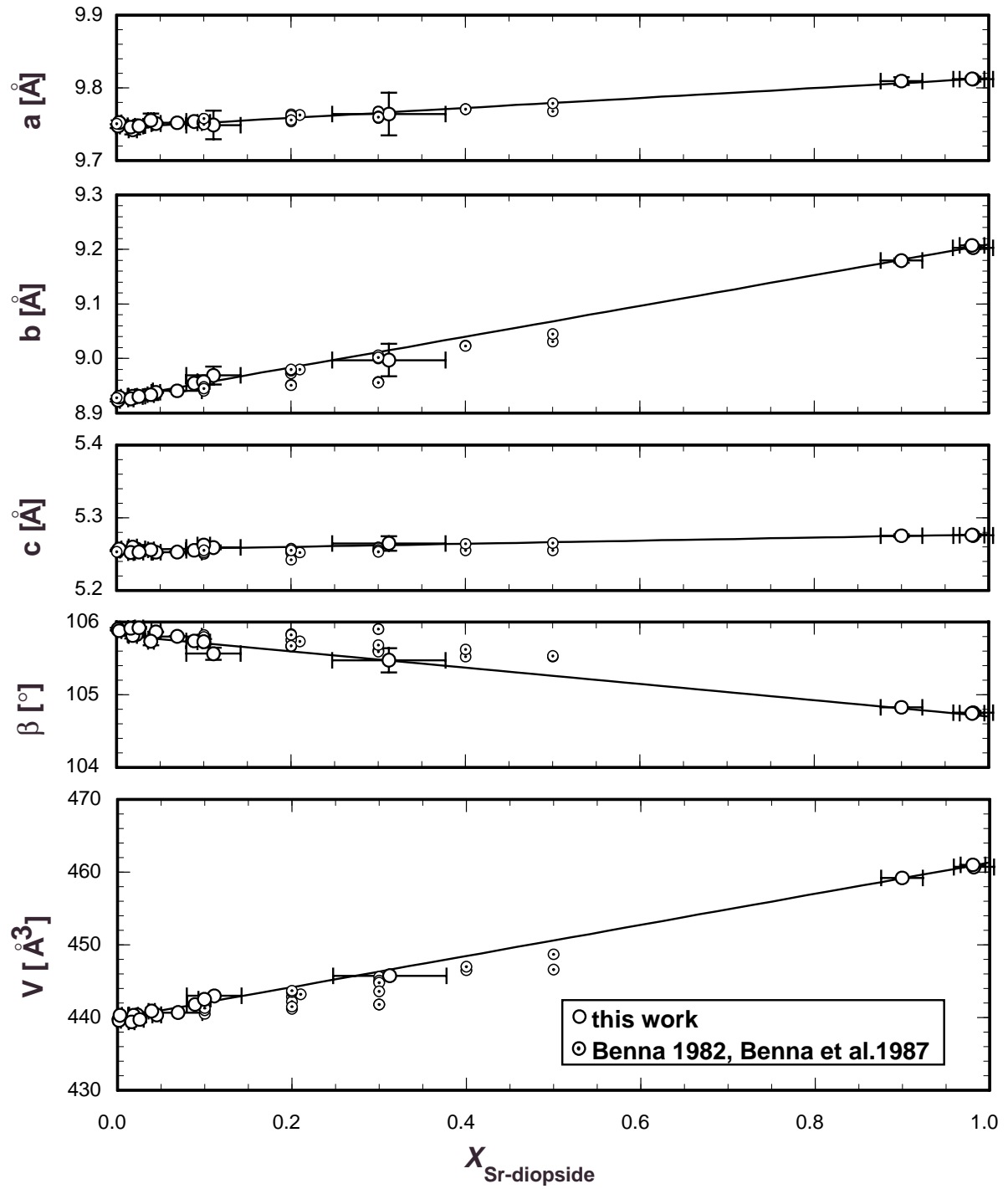
Fig. 5. The lattice constants *a, b, c, β* and the unit cell volume *V* of (Ca,Sr)-diopside as a function of X_{Sr}. All derived lattice constants vary linearly with composition. The lattice constants by Benna (1982) and Benna et al. (1987) are also shown as squares. (Ca,Sr)-diopsides in the range $0.31 > X_{Sr} > 0.90$ were not synthesized. For further discussion see text.

28

practically a constant, in (Ca,Sr)-diopside c is clearly a function of X_{Sr} in diopside. The monoclinic angle β increases with increasing Sr-content for (Ca,Sr)-tremolites and decreases with increasing Sr-content for (Ca,Sr)-diopsides. The following equations were derived using the lattice constants in Table 6:

(Ca,Sr)-tremolites

$$a = 9.8405 + 0.2691\ X_{Sr} - 0.3052\ X_{Mg} \qquad r^2 = 0.990 \qquad (1)$$
$$b = 18.0550 + 0.2136\ X_{Sr} - 0.0281\ X_{Mg} \qquad r^2 = 0.992 \qquad (2)$$
$$c = 5.2783 \qquad\qquad\qquad\qquad\qquad\qquad\qquad\qquad\qquad (3)$$
$$\beta = 104.800 + 0.9560\ X_{Sr} - 2.144\ X_{Mg} \qquad r^2 = 0.985 \qquad (4)$$

(Ca,Sr)-diopsides

$$a = 9.7454 + 0.0681\ X_{Sr} + 0.0545\ X_{Mg} \qquad r^2 = 0.984 \qquad (5)$$
$$b = 8.9272 + 0.2823\ X_{Sr} - 0.0881\ X_{Mg} \qquad r^2 = 0.997 \qquad (6)$$
$$c = 5.2555 + 0.0214\ X_{Sr} - 0.0204\ X_{Mg} \qquad r^2 = 0.900 \qquad (7)$$
$$\beta = 105.817 - 1.119\ X_{Sr} + 1.501\ X_{Mg} \qquad r^2 = 0.980 \qquad (8)$$

Except for the constants in the eqs. (1)-(4), which are the lattice parameters of pure tremolite, the parameters were determined by a least square fit. The lattice parameters for pure tremolite were derived by extrapolation from natural and synthetic samples (Yang and Evans 1996; Gottschalk unpublished).

The unit cell volume for the tremolites increases 3.47% from 906.68 Å^3 in tremolite to 938.21 Å^3 in Sr-tremolite. For diopside the unit cell volume increases 4.87 % from 439.91 Å^3 in diopside to 461.30 Å^3 in Sr-diopside.

FTIR

IR spectra were recorded for all synthesized (Ca,Sr)-tremolites in the range from 3600 cm^{-1} to 3800 cm^{-1}. The range between 3640 and 3700 cm^{-1} for all runs containing (Ca,Sr)-tremolite are plotted in Fig. 6. The main absorption band system is found in the spectral range between 3679 cm^{-1} and 3667 cm^{-1}. Number of components and their intensity vary with composition. In the case of (Ca,Sr)-tremolite endmembers at least two bands can be distinguished. For intermediate compositions up to 6 different absorption bands were necessary to describe the band system. The position of the band centers and their relative integral intensities are given in Table 7 and are plotted *vs.* composition in Fig. 7. The full width at half maximum height (FWHH) varies between 1.9 and 2.4 cm^{-1}.

Table 6. Lattice parameters of tremolite and diopside solid solutions

run	X_{Sr}	a (Å)	b (Å)	c (Å)	β (°)	V (Å^3)
tremolite–Sr-tremolite						
1	0.98	10.1012 (5)	18.2648 (6)	5.2807 (2)	105.704 (3)	937.90 (69)
2	0.73	10.0517 (41)	18.2233 (36)	5.2758 (8)	105.570 (24)	930.92 (36)
2	0.44	9.9605 (13)	18.1505 (11)	5.2767 (3)	105.224 (6)	920.49 (13)
5	0.00	9.8266 (6)	18.0506 (6)	5.2761 (2)	104.684 (3)	905.29 (10)
6	0.01	9.8326 (8)	18.0588 (8)	5.2778 (2)	104.698 (3)	906.48 (6)
8	*0.98	10.085 (18)	18.291 (34)	5.271 (12)	105.89 (15)	935.4 (9)
9	0.04	9.8410 (18)	18.0578 (13)	5.2756 (3)	104.773 (9)	906.52 (18)
10	0.13	9.8722 (7)	18.0823 (6)	5.2769 (2)	104.879 (3)	910.40 (8)
11	0.02	9.8350 (12)	18.0532 (11)	5.2753 (3)	104.749 (6)	905.78 (13)
12	0.01	9.8324 (11)	18.0562 (10)	5.2768 (2)	104.720 (6)	906.07 (12)
13	0.88	10.0804 (9)	18.2477 (10)	5.2803 (3)	105.627 (6)	935.38 (10)
15	0.22	9.8979 (11)	18.1027 (11)	5.2766 (3)	104.990 (6)	913.26 (12)
15	*0.55	9.9829 (42)	18.1823 (41)	5.2757 (9)	105.305 (24)	923.63 (39)
16	0.14	9.8684 (13)	18.0851 (10)	5.2773 (2)	104.856 (6)	910.38 (14)
17	0.02	9.8184 (20)	18.0529 (24)	5.2763 (5)	104.724 (12)	904.51 (22)
18	0.07	9.8437 (18)	18.0676 (18)	5.2773 (4)	104.742 (9)	907.67 (18)
19	0.59	9.9712 (14)	18.1594 (14)	5.2761 (3)	105.276 (6)	921.59 (17)
20	0.38	9.9363 (20)	18.1306 (18)	5.2747 (5)	105.154 (12)	917.20 (18)
20	*0.55	9.9787 (35)	18.1773 (46)	5.2743 (11)	105.346 (27)	922.57 (38)
21	0.04	9.8428 (15)	18.0685 (13)	5.2767 (3)	104.747 (6)	907.52 (17)
21	*0.70	10.0264 (76)	18.2201 (52)	5.2760 (13)	105.473 (33)	928.88 (63)
22	0.04	9.8319 (15)	18.0638 (15)	5.2778 (4)	104.702 (9)	906.65 (17)
22	*0.79	10.0548 (63)	18.2246 (50)	5.2770 (11)	105.510 (24)	931.75 (52)
23	0.60	10.0114 (35)	18.1840 (30)	5.2787 (5)	105.415 (15)	926.40 (35)
23	0.80	10.0432 (24)	18.2173 (18)	5.2777 (4)	105.526 (12)	930.36 (23)
diopside–Sr-diopside						
1	0.98	9.8122 (34)	9.2033 (31)	5.2755 (14)	104.750 (24)	460.71 (17)
2	0.31	9.764 (29)	8.997 (29)	5.264 (10)	105.47 (17)	445.8 (5)
5	0.00	9.7477 (27)	8.9235 (25)	5.2549 (8)	105.901 (15)	439.60 (11)
6	0.00	9.7525 (28)	8.9293 (24)	5.2568 (9)	105.876 (18)	440.32 (11)
8	0.98	9.8125 (04)	9.2076 (4)	5.2760 (2)	104.741 (3)	461.00 (3)
9	0.02	9.7482 (31)	8.9313 (30)	5.2570 (8)	105.823 (18)	440.35 (12)
10	0.09	9.7541 (38)	8.9547 (34)	5.2550 (13)	105.736 (24)	441.80 (15)
11	0.02	9.7425 (63)	8.9310 (57)	5.2594 (13)	105.810 (39)	440.31 (23)
13	0.90	9.8096 (55)	9.1797 (39)	5.2751 (17)	104.824 (27)	459.21 (20)
14	0.07	9.7522 (6)	8.9408 (5)	5.2526 (3)	105.800 (3)	440.69 (5)
15	0.11	9.749 (20)	8.969 (17)	5.259 (3)	105.56 (8)	443.0 (8)
16	0.10	9.7526 (53)	8.9575 (49)	5.2624 (13)	105.726 (36)	442.51 (21)
17	0.02	9.7462 (11)	8.9260 (10)	5.2521 (4)	105.909 (6)	439.40 (8)
18	0.04	9.7513 (8)	8.9381 (7)	5.2524 (3)	105.861 (3)	440.36 (6)
21	0.05	9.7556 (94)	8.9336 (95)	5.2558 (31)	105.732 (57)	440.90 (34)
22	0.03	9.7478 (20)	8.9305 (20)	5.2527 (7)	105.916 (12)	439.73 (10)

*estimated compositions from lattice parameters
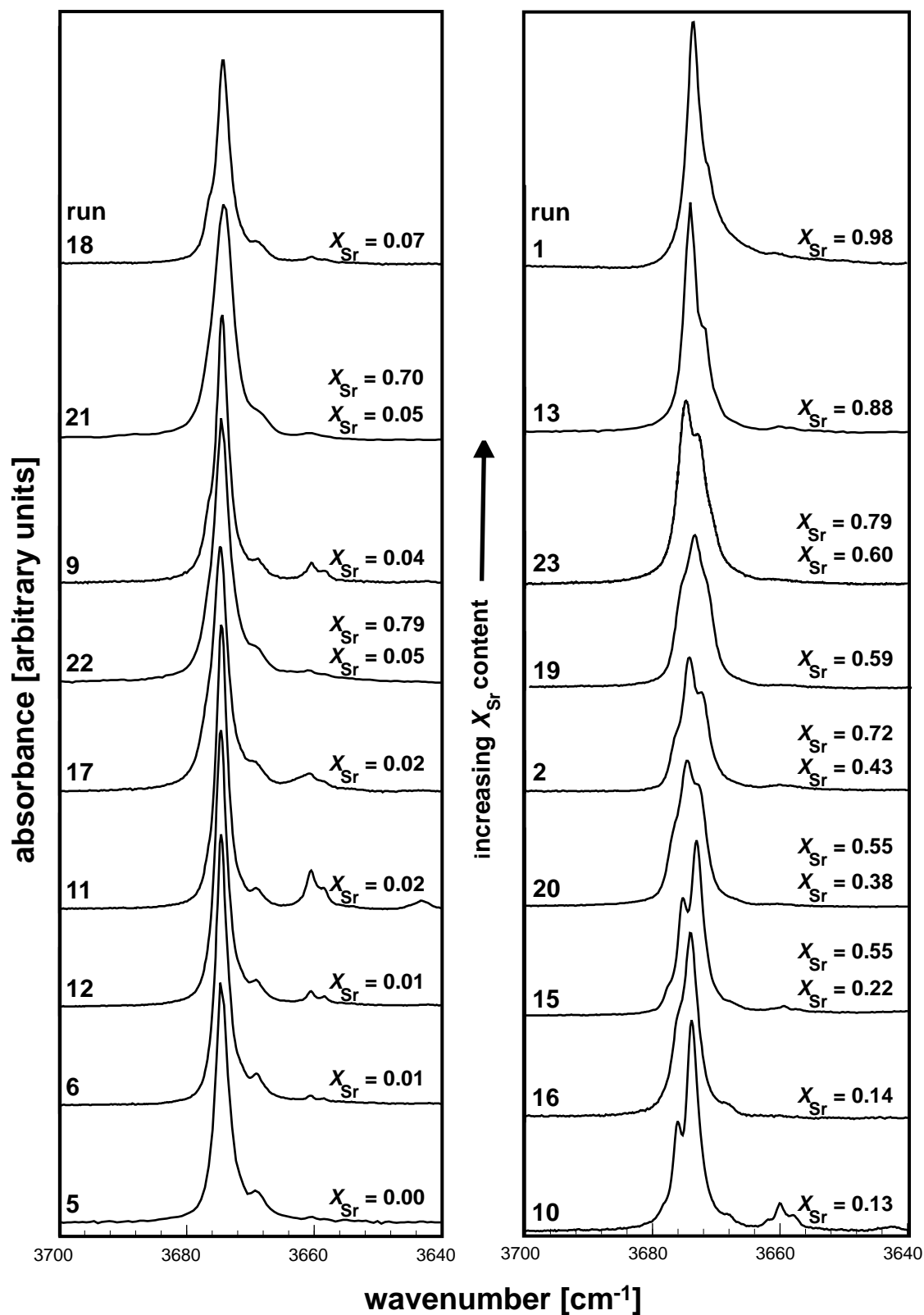
Fig. 6. The FTIR absorption spectra plotted with increasing X_{Sr}-content, starting from tremolite (run 5) to practically pure Sr-tremolite (run 1). For tremolite only absorption bands due to CaCa- and CaMg-configurations are visible. With increasing Sr-content a band due to a SrCa-configuration becomes noticeable (run 9). With further Sr increase also a band due to the SrSr-configuration appears (run 15) whereas the band due to the CaMg-configuration disappears (run 20). The band locations are listed in Table 6.
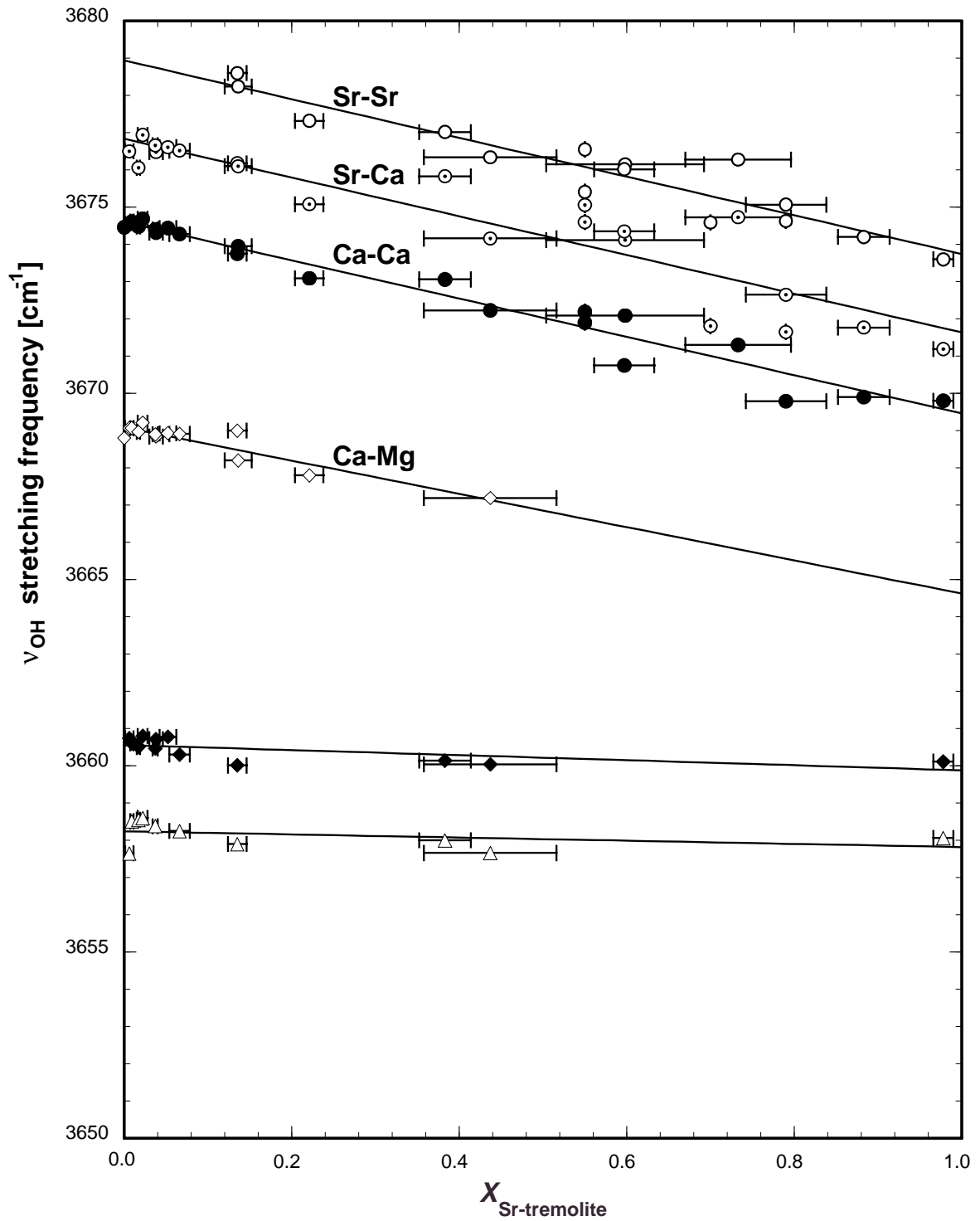
31

Besides the strong absorption, three separated but weak bands are observed in the spectra of some samples. In the products of nine runs two peaks occurred at 3660.4 and 3658.1 cm^{-1} and in three runs an additional peak was observed around 3643 cm^{-1}. The FWHH of the former two is in the order of the main absorption bands (~ 1 cm^{-1}), whereas the single band shows a FWHH of 3.2 cm^{-1}.

Table 7. Peak center of OH-vibrational bands and relative absorbance

run	SrSr (cm^{-1})	A (%)	SrCa (cm^{-1})	A (%)	CaCa (cm^{-1})	A (%)	CaMg (cm^{-1})	A (%)	additional bands (cm^{-1})	(cm^{-1})	(cm^{-1})
1	3673.6	88	3671.2	10	3669.8	2			3660.1	3658.1	
2			3674.2	36	3672.2	32			3660.0	3657.7	
2	3676.3	12	3674.7	12	3671.3	7	3667.2	1			
5					3674.5	92	3668.8	8			
6			3676.5	3	3674.5	92	3669.1	5	3660.7	3657.7	
9			3676.7	8	3674.4	88	3668.9	4	3660.5	3658.4	
10	3678.6	1	3676.2	21	3673.7	76	3669.0	2	3660.0	3657.9	3642.6
11			3676.1	4	3674.5	92	3669.0	4	3660.5	3658.5	3643.1
12					3674.6	95	3669.1	5	3660.6	3658.5	
13	3674.2	77	3671.8	19	3669.9	4					
15	3677.3	4	3675.1	16	3673.1	54	3667.8	2			
15	3675.4	14			3671.9	10					
16	3678.2	1	3676.1	20	3674.0	77	3668.2	2			
17			3676.9	9	3674.7	87	3669.2	4	3660.8	3658.6	3642.8
18			3676.5	7	3674.3	88	3668.9	5	3660.3	3658.3	
19	3676.2	20	3674.1	55	3672.1	25					
20	3677.0	6	3675.8	13	3673.1	27			3660.1	3658.0	
20	3676.6	3	3674.6	35	3672.2	16					
21			3676.6	4	3674.4	78	3668.9	5	3660.8		
21	3674.6	11	3671.8	2							
22			3676.5	7	3674.3	60	3668.8	5	3660.7		
22	3674.6	25	3671.7	3							
23	3676.0	6	3674.3	13	3670.8	7					
23	3675.1	32	3672.7	40	3669.8	2					

absorbance (A) = log(I_O/I)

Fig. 7. Plot of the peak center of the absorption bands *vs.* the (Ca,Sr)-tremolite composition. The band positions for the CaCa-, SrCa-, SrSr- and CaMg-configurations on M4 vary linearly with composition whereas the bands at 3658.5 and 3660.4 cm^{-1} show no significant variation with composition.

INTERPRETATION AND DISCUSSION

In most runs the composition of the synthesized phases are well defined by EMP analyses but for (Ca,Sr)-tremolites from some runs (see Fig. 2) rather large variations in X_{Sr} (e.g. run 2, 19 and 23) were observed. If the distribution of the compositional variations of these (Ca,Sr)-tremolites is uniform, the interpretation of the derived physical parameters for the tremolites in those runs (e.g. lattice parameters) would have been quite difficult if not impossible. The EMP-analyses, however, seem not to be evenly distributed and distinct maxima were observed. The difference in FWHH of the diffraction peaks, however, can be used as measure of compositional variations. Table 5 shows the ($33\bar{1}$)- and (151) reflections for the (Ca,Sr)-tremolites. The FWHH of the (130)-reflection of forsterite, which did not show compositional variations, was 0.13°. The (151)-reflection of the synthesized (Ca,Sr)-tremolites had, with the exception of run 21 and 22, similar FWHH-values (0.12-0.16°), indicating a crystallinity comparable to that of forsterite. The FWHH-values for the ($33\bar{1}$)-reflection did vary between 0.13° and 0.36°. In the runs 2, 15, 20, 21, 22 and 23 two distinct ($33\bar{1}$)-reflections could be identified. The (Ca,Sr)-tremolites from runs 1, 5, 6, 10, 13, 18 and one (Ca,Sr)-tremolite composition from run 15 showed no significant broadening (FWHH of 0.13- 0.17°) indicating a compositional variation with respect to X_{Sr} of less than ±0.03. The patterns from the runs 2, 20, and 23 had two distinct sharp reflections (FWHH of 0.14-0.19°) and therefore a ΔX_{Sr} of less than ±0.04. The ($33\bar{1}$)-reflections of the tremolites from the runs 9, 11, 12, 16, 17 and the second tremolite composition from run 15 had an FWHH between 0.21° and 0.24°, which corresponds to a compositional variation of less than ±0.07. The patterns from the runs 19, 21 and 22 showed at least one ($33\bar{1}$)-reflection with a FWHH in the range 0.26-0.27° (±0.09 ΔX_{Sr}). These observations indicate that the (Ca,Sr)-tremolites from almost all runs had a compositional variation which was less than ±0.07 X_{Sr}. As a consequence the compositional variation for (Ca,Sr)-tremolites from run 2, for example, was lower than one would deduce from Fig. 2 (0.25 < X_{Sr} < 0.90), but two compositional maxima at X_{Sr} = 0.43 and X_{Sr} = 0.72 with a variation of less than ±0.04 were observed. The derived lattice parameters for all (Ca,Sr)-tremolites could therefore be attributed to rather defined compositional ranges. This is additionally supported by the *Durbin-Watson* factors of the Rietveld analyses. For most runs these have a value above 1.30, which is good for complex phase mixtures. Extensive broadening of specific (Ca,Sr)-tremolite reflections would have led to much lower *Durbin-Watson* factors.

From Fig. 4 it is obvious that a continuous solid solution series exist for (Ca,Sr)-tremolites. This is in contrast to the observation that in the runs 2, 15, 20, 21, 22 and 23 two

distinct (Ca,Sr)-tremolites were detected by EMP, XRD and FTIR. However in these runs, the compositions of the (Ca,Sr)-tremolites pairs differed despite identical run conditions. This is a strong indication that these were not coexisting (Ca,Sr)-tremolites in a thermodynamical but rather in a kinetical context, i.e. they do not define coexisting amphiboles at a miscibility gap but are products of a complex reaction path. At the beginning of each experiment the composition of the fluid phase was rather badly defined. Its composition depends on the dissolution rates of the starting materials. So it is possible that in the beginning of each experiment $Sr(OH)_2 \times 8H_2O$ dissolved faster than $Ca(OH)_2$ which would have lead to more Sr-rich tremolites at that time. Later during the experiment as equilibrium conditions were approached, more Ca-rich tremolites crystallized. The primary and metastable Sr-rich tremolite was preserved in the mixture because of an energy difference too small with respect to the more Ca-rich tremolite.

A continuous solid solution series for (Ca,Sr)-diopsides can also be assumed to be stable at experimental conditions (200 MPa, 750°C) despite the fact that no (Ca,Sr)-diopsides were observed in the range of $0.31 > X_{Sr} > 0.90$. The assumption of a continuous solid solution series is based on the following arguments. First, no coexisting (Ca,Sr)-diopsides were detected by any of the methods described above for runs with intermediate bulk composition. Second, because Sr^{2+} is strongly fractionated in to the fluid (Najorka et al. 1999) only fluids with a X_{Sr}^{fluid} between 0.97 and 0.99 would lead to (Ca,Sr)-diopside compositions in the range $0.31 > X_{Sr} > 0.90$. Only one run was conducted in the required compositional range (run 23). Unfortunately no (Ca,Sr)-diopside but only (Ca,Sr)-tremolites were detected. So it is highly probable that the missing (Ca,Sr)-diopside compositions are due to chosen experimental conditions.

The variation of the lattice constants with respect to composition is linear. The curvature of the unit cell volume ($V = a\,b\,c\,\sin\,\beta$) and therefore the excess volume is negligible. The lattice constants for the most tremolitic amphiboles from runs 5 and 6 are comparable with cummingtonite poor tremolites from Yang and Evans (1996) with $a = 9.8356$ Å, $b = 18.0557$ Å, $c = 5.2785$ Å, $\beta = 104.782°$, $V = 906.4$ Å^3 and Zimmermann et al. (1996) $a = 9.824$ Å, $b = 18.061$ Å, $c = 5.279$ Å, $\beta = 104.627°$, $V = 906.36$ Å^3. The lower unit cell volume of tremolite from run 5 of 905.29 Å^3 in comparison with the one from run 6 of 906.48 Å^3 correlates with measured cummingtonite contents of 5% and 3%, respectively (Yang and Evans 1996).

From Fig. 5 it can be seen that the lattice constants for (Ca,Sr)-diopsides derived by Benna (1982) and Benna et al. (1987) show systematic deviations from the constants derived here. This can be due to the following reasons. Except for two synthesis products from

Benna et al. (1987), precise (Ca,Sr)-diopside compositions were not known. In particular, their syntheses of (Ca,Sr)-diopsides with $X_{Sr} > 0.3$ did yield additional Sr-åkermanite, so the synthesized (Ca,Sr)-diopside should be less Sr-rich. The two reported microprobe analyses show a 5-6% enstatite component, which is more than observed here. Both explanations are in agreement with the smaller lattice constants observed by Benna (1982) and Benna et al. (1987).

The assignment of the absorption bands in the IR-region (Table 7 and Fig. 7) is based on the following arguments. The vibrational frequencies of the OH-group are dependent on the interatomic forces and are sensitive to the local bonding environments which give characteristic structural information. The main OH-stretching band of the Ca-rich tremolites (e.g. 3674.5 cm^{-1} for run 5) can be attributed to 3 Mg^{2+} on 2 M1 + 1 M3 sites sharing the proton carrying oxygen O3 as a ligand and an empty A site (Rowbotham and Farmer 1973). Two Ca^{2+} are the next nearest neighbors on the adjacent M4 positions (CaCa-configuration). In the case of a partially filled A site the vibrational modes would be shifted to higher energies above 3730 cm^{-1} and the FWHH would be increased about five times (Gottschalk and Andrut 1998). In contrast, the resolved band at the lower energy wing (3668.8 cm^{-1} for run 5) was assigned to a configuration with one Ca^{2+} and one Mg^{2+} on the two neighboring M4 positions (CaMg-configuration). This assignment is supported by statistical arguments. If Ca^{2+} and Mg^{2+} are distributed statistically on M4, the probabilities p_i of CaCa-, CaMg- and MgMg-configurations can be calculated with the following equations:

$$p_{CaCa} = X_{Ca} X_{Ca} \tag{9}$$

$$p_{CaMg} = 2 X_{Ca} X_{Mg} \tag{10}$$

$$p_{MgMg} = X_{Mg} X_{Mg} \tag{11}$$

where X_{Ca} and X_{Mg} are mole fractions of Ca^{2+} and Mg^{2+} on M4. For a cummingtonite content of 5% the probabilities would be $p_{CaCa} = 0.9025$, $p_{CaMg} = 0.0950$ and $p_{MgMg} = 0.0025$.

Assuming, as a first approximation, that the CaCa-, CaMg- and MgMg-configurations have the same linear extinction coefficients which are proportional to the configuration probability, one would expect that the relative absorbancies for those configurations are 90.25%, 9.50% and 0.25%, respectively. These calculated proportions coincide with measured integral ratios of the intensity of 92 and 8% for the two observed bands of tremolite from run 5.

With increasing Sr-content in tremolite the band due to a CaCa-configuration is shifted to lower wavenumbers and an additional band becomes prominent on the high energy side (e.g. 3676.7 cm^{-1} for run 9). Following the statistical arguments given above the probability for SrCa-, SrMg- and SrSr-configurations can be calculated from:

$$p_{SrCa} = 2\, X_{Sr}\, X_{Ca} \qquad (12)$$

$$p_{SrMg} = 2\, X_{Sr}\, X_{Mg} \qquad (13)$$

$$p_{SrSr} = X_{Sr}\, X_{Sr} \qquad (14)$$

For the (Ca,Sr)-tremolite from run 9, the configuration probability would be $p_{SrSr} = 0.0016$, $p_{SrCa} = 0.0752$, $p_{CaCa} = 0.8836$, $p_{CaMg} = 0.0376$, $p_{SrMg} = 0.0016$ and $p_{MgMg} = 0.0004$. The measured intensities of the 3 strongest bands (8%, 88%, 4%) for tremolite from run 9 coincide with the three strongest calculated intensities. In runs with even higher X_{Sr} ($X_{Sr} > 0.2$), the band due to the SrSr-configuration becomes well resolved on the high energy side. So all absorption bands between 3678.2 and 3667.2 cm^{-1} can be attributed to the OH-stretching band associated to the oxygen on O3 in (Ca,Sr)-tremolite with CaCa-, CaMg-, SrCa- and SrSr-configurations on M4. The absorption bands due to MgMg- and SrMg-configurations are too weak to be detected ($< 1\%$). The observed and theoretical absorbance for the runs showing a single amphibole are plotted in Fig. 8a. This figure demonstrates the good correlation between the observed and theoretical absorbance. For runs with two amphiboles (2, 15, 20, 21, 22, 23) this correlation still exists but the deviations from the theoretical absorbance are much larger (Fig. 8b). For (Ca,Sr)-tremolites in these runs, 5 to 6 bands had to be fitted to describe the overlapping band shape. The derived positions of the individual bands were in some cases very close (< 1 cm^{-1}). Therefore errors in position and in the absorbance for these bands are larger than for bands which are separated by at least 1/2 FWHH (> 1 cm^{-1}). In Table 7 the derived band positions and intensities are listed. Fig. 7 shows the band positions plotted *vs.* the (Ca,Sr)-tremolites composition X_{Sr}. The band positions are linear function of X_{Sr} and the following equations were fitted (cm^{-1}):

$$\text{SrSr} \quad 3679.0 - 5.2\, X_{Sr} \qquad r^2 = 0.918 \qquad (15)$$

$$\text{SrCa} \quad 3676.8 - 5.2\, X_{Sr} \qquad r^2 = 0.866 \qquad (16)$$

$$\text{CaCa} \quad 3674.6 - 5.2\, X_{Sr} \qquad r^2 = 0.968 \qquad (17)$$

$$\text{CaMg} \quad 3669.1 - 4.4\, X_{Sr} \qquad r^2 = 0.860 \qquad (18)$$
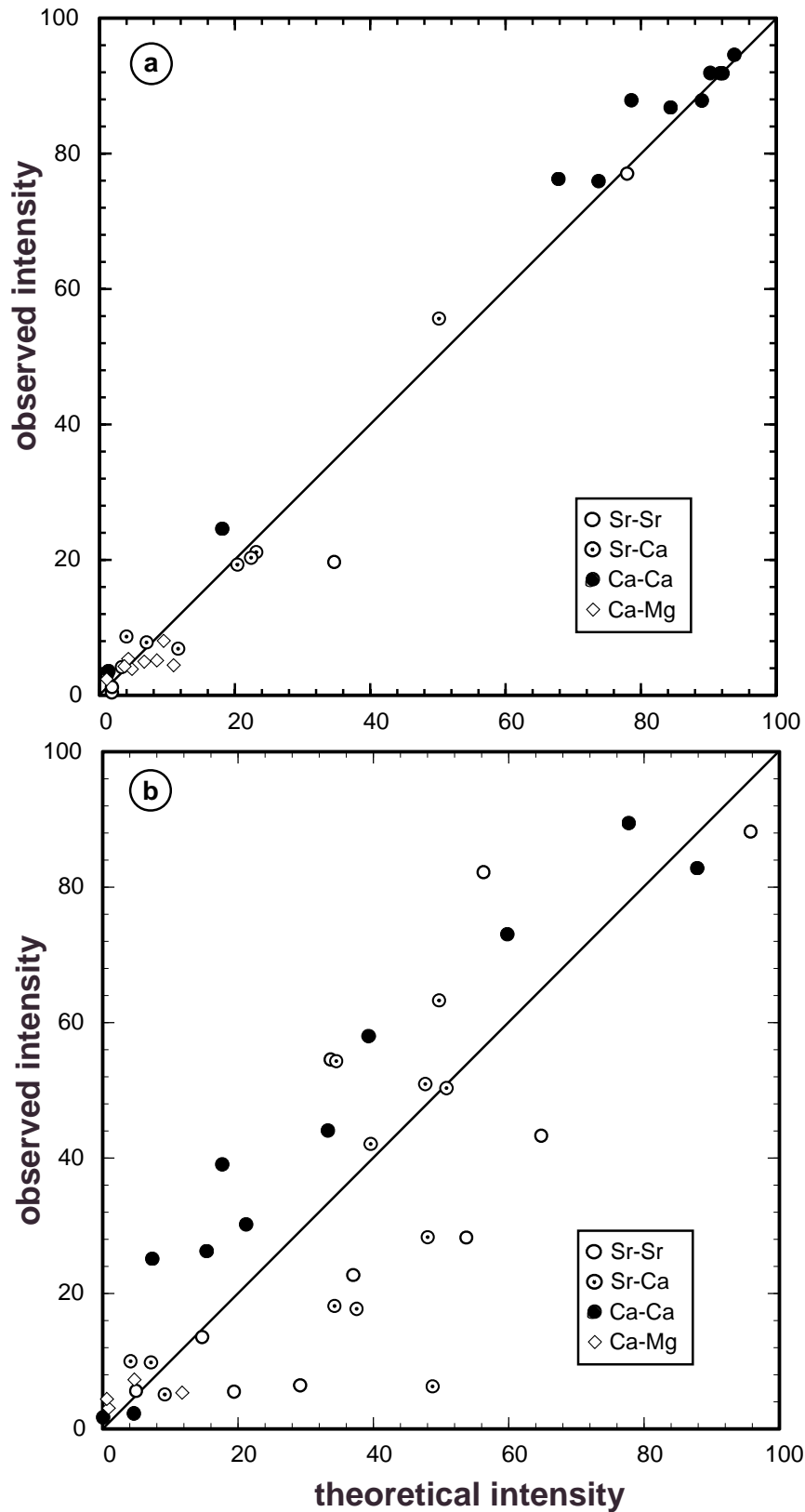
Fig. 8. Plot of the observed *vs*. theoretical FTIR integral intensity. **a)** runs with only 1 (Ca,Sr)-tremolite. **b)** runs with 2 (Ca,Sr)-tremolites. Filled circles for bands are due to CaCa-, circles with dots SrCa-, empty circles SrSr- and diamonds CaMg-configurations. For discussion see text.

The slope for the fitted CaCa-, SrCa- and SrSr-lines in all three configurations is the same. These lines are separated by 3.2 cm^{-1}. The linearity of the shift of the absorption bands suggests that the thermodynamic mixing properties of Ca^{2+} and Sr^{2+} are rather simple. This is also supported by the thermodynamic evaluation of the (Ca,Sr)-tremolite and (Ca,Sr)Cl$_2$ equilibria (Najorka et al. 1999).

Additional bands in the range of 3660.0-3660.8 cm^{-1}, 3657.7-3658.5 cm^{-1} show little compositional dependence and a band in the range 3642.6-3643.1 cm^{-1} shows none. They are also not correlated with the measured cummingtonite contents. The first two bands form a doublet, however. In the case of the (Ca,Sr)-tremolites from run 9 and 17, which did show high concentrations of chain multiplicity faults, this doublet at 3660.4 and 3658.1 cm^{-1} has a relatively high absorbance. It can be assumed that these two bands result from OH-configurations, which are associated with triple or higher chain multiplicity faults. The band around 3643 cm^{-1} is to due residual Ca(OH)$_2$.

CONCLUSIONS

Tremolite (Ca$_x$Sr$_{1-x}$)$_2$Mg$_5$[Si$_8$O$_{22}$/(OH)$_2$] and diopside (Ca$_x$Sr$_{1-x}$)Mg[Si$_2$O$_6$] solid solutions have been investigated by electron scanning and high resolution transmission electron microscopy, electron microprobe, X-ray powder diffraction and Fourier-transformed infrared spectroscopy. In most runs the tremolites and diopsides are well ordered and chain multiplicity faults are rare. Nearly pure Sr-tremolite (tr$_{0.02}$Sr-tr$_{0.98}$) and Sr-diopside (di$_{0.01}$Sr-di$_{0.99}$) have been synthesized. A continuous solid solution series, i.e. complete substitution of Sr^{2+} for Ca^{2+} on the M4 sites exists for (Ca,Sr)-tremolite. Total substituion of Sr^{2+} for Ca^{2+} on the M2 sites can be reasonable assumed for (Ca,Sr)-diopsides. The substitution of Sr^{2+} for Ca^{2+} on the M4 site in tremolite and on the M2 site in diopside extends the lattice linearly with Sr-content. IR-spectra can be interpreted with simple combinatorial assumptions and show that Sr^{2+}, Ca^{2+} and Mg^{2+} are distributed statistically on the M4 site in tremolites. Resolved single bands can be attributed to the SrSr, SrCa, CaCa and CaMg configurations on the M4 sites. The peak positions of these four absorption bands are a linear function of composition. All these observations indicate that the substitution of Sr^{2+} for Ca^{2+} in tremolites and diopsides does not involve high exchange energies.

ACKNOWLEDGMENTS

REFERENCES CITED

Agrinier P, Mével C, Bosch D, Javoy M (1993) Metasomatic hydrous fluids in amphibole peridotites from Zabargad island (Red Sea). Earth and Planetary Science Letter, 120, 187-205.

Benna P (1982) Ca-Sr substitution in clinopyroxenes along the join $CaMgSi_2O_6$-$SrMgSi_2O_6$. Tschermaks Mineralogische Petrographische Mitteilungen, 30, 37-46.

Benna P, Chiari G, Bruno E (1987) Structural modification in clinopyroxene solid solutions, the Ca-Mg and Ca-Sr substitutions in diopside structure. Mineralogy and Petrology, 36, 71-84.

Caglioti G, Paoletti A, Ricci FP (1958) Choice of collimators for crystal spectrometer for neutron diffraction. Nuclear Instruments, 3, 223-228.

Davidson PM, Grover J, Lindsley DH (1982) $(CaMg)_2Si_2O_6$ clinopyroxenes, A solution model based on nonconvergent site-disorder. Contributions to Mineralogy and Petrology, 80, 88-102.

Della Ventura G, Robert J-L, Raudsepp M, Hawthorne FC (1993) Site occupancies in monoclinic amphiboles, Rietveld structure refinement of synthetic nickel magnesium cobalt potassium richterite. American Mineralogist, 78, 633-640.

Gottschalk M, Andrut M (1998) Structural and chemical characterization of synthetic (Na,K)-richterite solid solutions by EMP, HRTEM, XRD and FTIR spectroscopy. Physics and Chemistry of Minerals, 25, 101-111.

Griffiths PR, de Haseth JA (1986) Fourier transform infrared spectroscopy. Chemical Analysis Vol. 83, John Wiley & Sons, New York.

Hawthorne FC (1983) The crystal chemistry of the amphiboles. Canadian Mineralogist, 21, 173-480.

Jenkins DM (1987) Synthesis and characterization of tremolite in the system H_2O-CaO-MgO-SiO_2. American Mineralogist, 72, 707-715.

Larson AC, Von Dreele RB (1987) Generalized structure analysis system. Los Alamos National Laboratory Report No. LA-UR-86-748.

Mertz (1965) Transformation in optics. Wiley, New York.

Najorka J., Gottschalk M., Franz G. and Heinrich W. (1999) Experimental determination of the Sr-Ca distribution between amphibole, clinopyroxene and chloridic aqueous solution. American Mineralogist, 84, 596-606.

Pouchou JL, Pichoir F (1984) Un nouveau modèle de calcul pour la microanalyse quantitative par spectroétrie de rayons X. Rech. Aérospatiale 3, 167-192.

Robert J-L, Della Ventura G, Raudsepp M, Hawthrone FC (1993) Rietveld structure refinement of synthetic strontium-rich potassium-richterites. European Journal of Mineralogy, 5, 199-206.

Rowbotham G, Farmer VC (1973) The effect of "A" site occupancy upon hydroxyl stretching frequency in clinoamphiboles. Contributions to Mineralogy and Petrology, 38, 147-149.

Shannon RD (1976) Revised effective ionic radii and systematic studies of interatomic distances in halides and chalcogenides. Acta Crystallographica Section B, 32, 751-767.

Yang H, Evans BW (1996) X-ray structure refinements of tremolite at 140 and 295 K, crystal chemistry and petrologic implications. American Mineralogist, 81, 1117-1125.

Zimmermann R, Heinrich W, Franz G (1996) Tremolite synthesis from $CaCl_2$-bearing aqueous solutions. European Journal of Mineralogy, 8, 767-776.

Zimmermann R, Knop E, Heinrich W, Pehlke I, Franz G (1997) Disequilibrium in cation exchange experiments between Na-richterite – K-richterite and aqueous solutions, effects of fractional crystallisation. European Journal of Mineralogy, 9, 97-114.

ZUSAMMENFASSUNG

Tremolit–Sr-Tremolitmischkristalle und Diopsid–Sr-Diopsidmischkristalle wurden bei 750°C und 200 MPa synthetisiert. Die synthetisierten (Sr,Ca)-Tremolite sind bis zu 2000 µm lang und 30 µm breit, (Sr,Ca)-Diopside sind bis zu 150 µm lang und 20 µm breit. In der Mehrzahl der Experimente besitzen die (Sr,Ca)-Tremolite geringe Konzentrationen an Baufehlern. Die Anzahl an Kettenmultiplizitätsfehlern ist im Sr-reichen Tremolit geringer als in Sr-armen Tremolit. Der Sr-reichste Diopsid ist baufehlerfrei.

Sowohl die Tremolitstruktur als auch die Diopsidstruktur erweisen sich flexibel für den vollständigen Ersatz des Ca^{2+} durch Sr^{2+}. Die nahezu reinen Sr-Endglieder Sr-Tremolit $((Ca_{0.02}Sr_{0.98})_2Mg_5[Si_8O_{22}/(OH)_2])$ und Sr-Diopsid $(Ca_{0.01}Sr_{0.99}Mg[Si_2O_6])$ konnten synthetisiert werden. Zwischen Tremolit und Sr-Tremolit existiert eine kontinuierliche Mischkristallreihe. (SrCa)-Diopside konnten im Bereich von $X_{Sr} < 0.31$ und $X_{Sr} > 0.90$ synthetisiert werden.

Die Gitterkonstanten von Tremolit und Diopsid verändern sich mit zunehmenden Sr-Einbau linear. Mit steigendem Sr-Gehalt vergrößern sich im (Sr,Ca)-Tremolit die Zellparameter a, b und $ß$ wobei c konstant bleibt. Im (Sr,Ca)-Diopsid vergrößern sich mit steigenden Sr-Gehalt a, b und c während $ß$ sich verkleinert. Die Tremolit- und Diopsidgitter weiten sich beträchtlich auf, das Zellvolumen zwischen Tremolit und Sr-Tremolit erhöht sich um 3.45%, zwischen Diopsid und Sr-Diopsid um 4.87%.

Die OH-Streckschwingung im (Sr,Ca)-Tremolit weist eine komplexe Feinstruktur auf. Sie wird durch verschiedene Konfigurationen von Ca^{2+}, Sr^{2+} und Mg^{2+} auf den nächsten zwei M4-Positionen um die OH-Gruppe verursacht. Einzelbanden wurden den Konfigurationen SrSr, SrCa, CaCa und CaMg zugeordnet. Die Bandenlagen verschieben sich mit steigenden Sr-Gehalten zu niedrigeren Wellenzahlen. Mit einem quantitativen Modell konnte mit einfachen kombinatorischen Annahmen die Zuordnung und Intensität der Banden bestätigt werden. Das quantitative Modell zeigt, daß Ca^{2+}, Sr^{2+} und Mg^{2+} statistisch auf der M4-Position im Tremolit verteilt sind.

Die Untersuchungen zeigen insgesamt, daß es keine strukturellen Beschränkungen für den Einbau von Sr^{2+} in Tremolit und Diopsid gibt. Die Ergebnisse deuten darauf hin, daß für die Sr-Ca-Substitution in Tremolit und Diopsid keine großen Austauschenergien benötigt werden.

KAPITEL 2

Ca-Sr distribution between amphibole, clinopyroxene and chloride-bearing solutions

ABSTRACT

The distribution of Sr between a 1 molar $(Ca,Sr)Cl_2$ solution, (Ca,Sr)-tremolite and (Ca,Sr)-diopside was determined at 750 °C and 200 MPa. The synthesized (Ca,Sr)-tremolites $(2000 \times 30$ μm$)$ and (Ca,Sr)-diopsides $(1500 \times 20$ μm$)$ were large enough for accurate microprobe analyses. The experimental results indicate that Ca^{2+} can be completely replaced by Sr^{2+} on the M4 site in tremolite and on the M2 site in diopside. The compositions of the product fluid were analyzed by AAS. In both systems, (Ca,Sr)-tremolite/fluid and (Ca,Sr)-diopside/fluid, Sr strongly fractionated into the fluid. For bulk-compositions having low Sr-concentrations, mineral/fluid partition coefficients $D_{Sr}^{mineral/fluid}$ of 0.045 for (Ca,Sr)-tremolite/fluid and 0.082 for (Ca,Sr)-diopside/fluid were derived. The experimental results were evaluated thermodynamically assuming Henry´s law and simple mixing properties for $SrCl_2$ and $CaCl_2$ in the fluid. The mixing energies of the solids were calculated using a regular solution model. In the (Ca,Sr)-tremolite–$(Ca,Sr)Cl_2$ system $\Delta\mu°$ is 59.0 kJ and W_{CaSr}^{amph} is 9.8 kJ. In the system (Ca,Sr)-diopside–$(Ca,Sr)Cl_2$ $\Delta\mu°$ is 30.8 kJ and W_{CaSr}^{px} is 11.7 kJ. The high $\Delta\mu°$ values and to a much lesser extent the W_{CaSr} values cause the strong fractionation of Sr into the fluid. The moderate values for W_{CaSr}^{amph} and W_{CaSr}^{px} strongly suggest that complete solid solution exists for (Ca,Sr)-tremolite and (Ca,Sr)-diopside at experimental run conditions. However, for the (Ca,Sr)-tremolite and (Ca,Sr)-diopside joins limited miscibilities are calculated below 316 and 430 °C, respectively.

The experimentally derived thermodynamic properties were used to determine Ca/Sr-ratios of Sr-rich metasomatic fluids, which penetrated a metaeclogite in Bjørkedalen, SW-Norway. The derived Ca/Sr-ratios from amphibole/fluid equilibria are in good agreement with those calculated from plagioclase/fluid equilibria.

INTRODUCTION

In most rock-forming minerals Sr occurs as a minor or trace element and is preferentially incorporated in Ca-bearing phases. Because both, Sr and Ca, belong to the alkaline earth group they have a similar chemical behaviour. The ionic radius in 8-fold coordination is 1.12 Å for Ca^{2+} and 1.26 Å for Sr^{2+} (Shannon 1976).

Strontium enrichment in rocks is commonly induced by fluid-rock interactions (Grapes and Watanabe 1984; Theye and Seidel 1988). An example of extreme Sr-metasomatism has been reported in a metaeclogite (Bjørkedalen SW-Norway) by Brastad (1985) with whole-rock SrO-concentrations of up to 2.4 wt%. It is clear that information about trace element distribution between fluid and minerals is required for the reconstruction of metasomatic processes.

Experimentally determined partition coefficients for Sr as a trace element between fluids and minerals have been determined for apatite (Ayers and Watson 1993), olivine (Brenan and Watson 1991), garnet (Brenan et al. 1995), clinopyroxene (Brenan et al. 1995; Adam et al. 1997; Ayers et al. 1997) and amphibole (Brenan et al. 1995; Adam et al. 1997). The distribution of Sr as a major element between fluids and minerals has been experimentally determined for (K,Sr)-feldspars by Kotelnikov and Chernysheva (1995) and Kroll et al. (1995) and for (Ca,Sr)-plagioclase by Kotelnikov and Chernysheva (1995), Kotelnikov et al. (1989) and Lagache and Dujon (1987). Thermodynamically relevant distribution coefficients and mixing models are not available for Sr-bearing amphiboles and pyroxenes. While Sr-rich amphiboles and pyroxenes are rarely observed in nature, both structures are flexible with regard to the incorporation of Sr. Della Ventura and Robert (1990) and Robert et al. (1993) synthesized (K,Sr)-richterites with Sr^{2+} completely replacing Ca^{2+} on the M4 site. Benna (1982) and Benna et al. (1987) synthesized Sr-rich pyroxenes with at least 30 mol% Sr- diopside component.

Besides the geochemical interest of quantification of the Sr incorporation in amphiboles and pyroxenes and the corresponding fluids/melts there are questions of mineralogical importance. First, how much Ca^{2+} can be replaced by Sr^{2+} in the tremolite and diopside structure? Second, how can this substitution be described structurally and thermodynamically? An appropriate mixing model along the whole composition range provides the activity coefficients at low Sr-concentrations (Henry constants) which are required for the geochemical applications.

The aim of this study is to determine the mixing behaviour of Ca and Sr in amphibole and in pyroxene by considering the Ca_1Sr_{-1} exchange vector in the simplified (Ca,Sr)-tremolite $(Ca,Sr)_2Mg_5[Si_8O_{22}/(OH)_2]$ and (Ca,Sr)-diopside $(Ca,Sr)Mg[Si_2O_6]$ systems. This is accomplished by investigating experimentally the following exchange reactions:

$$1 \text{ tremolite} \quad + 2 [SrCl_2]^{aq} \quad \leftrightarrow \quad 1 \text{ Sr-tremolite} \quad + 2 [CaCl_2]^{aq}$$

$$Ca_2Mg_5[Si_8O_{22}/(OH)_2] \qquad\qquad Sr_2Mg_5[Si_8O_{22}/(OH)_2] \qquad\qquad (1)$$

$$1 \text{ diopside} \quad + 1 [SrCl_2]^{aq} \quad \leftrightarrow \quad 1 \text{ Sr-diopside} \quad + 1 [CaCl_2]^{aq}$$

$$CaMg[Si_2O_6] \qquad\qquad SrMg[Si_2O_6] \qquad\qquad (2)$$
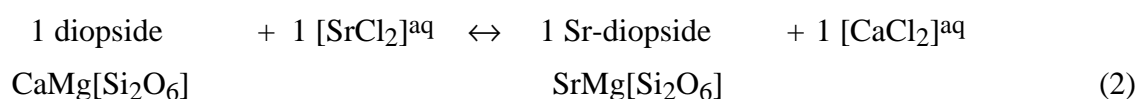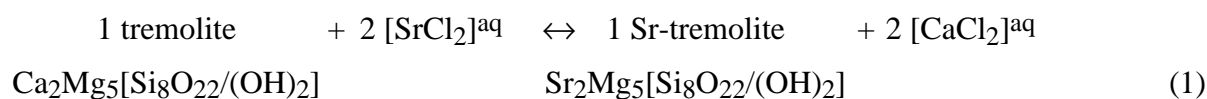
The experimentally derived Ca-Sr equilibrium distribution coefficients between tremolite, diopside and fluid allows the determination of the degree of fractionation of Sr into the fluid and to develop mixing models for the (Ca,Sr)-tremolite and the (Ca,Sr)-diopside solid solution series.

EXPERIMENTAL AND ANALYTICAL TECHNIQUES

The experimental and analytical techniques are given in detail in Gottschalk et al. (1998) and are briefly summarized as follows. Standard cold-seal hydrothermal techniques were used. Temperatures were recorded using Ni-CrNi thermocouples, which were placed inside the autoclaves adjacent to the sample capsules. Total temperature and pressure uncertainties are estimated to be less than ±5 °C and ±10 MPa, respectively. The experiments were quenched by cooling the autoclaves with compressed air to less than 300 °C in about 3 minutes. All experiments were run for 21 days at 750 °C and 200 MPa. The chosen run duration was long enough to guarantee complete reaction.

Starting materials consisted of SiO_2, MgO, $Ca(OH)_2$, $Sr(OH)_2 \bullet 8H_2O$ and a 1 molar $CaCl_2$-$SrCl_2$ solution. The compositions of the starting mixtures are listed in Table 1. The $Sr(OH)_2 \bullet 8H_2O$ powder had an impurity of 2 wt% $SrCO_3$, 0.1 wt% Ba and 0.05 wt% Ca. All other chemicals were of suprapure quality. Stoichiometric oxide and hydroxide mixtures of 15-25 mg having bulk compositions on the tremolite - Sr-tremolite join with 5 wt% of SiO_2 in excess to compensate for SiO_2 solubility at experimental conditions were used along with 50-200 μl one molar $(Ca,Sr)Cl_2$-solution. Run 8 and 14 had bulk compositions on the

Table 1. Compositions of starting mixtures and run product fluids

run	1	2	5	6	8	9	10	11	12	13	14	15	16	17	18	20	21	22	23
solid starting materials (mg)																			
SiO_2	10.90	11.25	10.82	10.35	7.16	11.50	11.37	11.62	11.75	10.96	7.87	11.25	11.14	11.38	11.25	9.92	10.10	10.17	9.87
MgO	4.36	4.50	4.32	4.27	2.29	4.59	4.54	4.64	4.70	4.38	2.52	4.50	4.45	4.54	4.49	3.96	4.03	4.06	3.94
$Ca(OH)_2$	0.00	0.99	2.85	2.51	0.00	1.69	1.34	2.05	2.41	0.16	1.54	0.99	0.65	1.34	0.99	0.29	0.79	1.00	0.14
$Sr(OH)_2 \cdot 8\,H_2O$	11.48	8.30	1.14	2.25	15.09	6.05	7.19	4.90	3.71	10.96	8.29	8.30	9.38	7.19	8.29	9.41	7.80	7.13	9.88
fluid starting materials																			
fluid (µl)	60	50	50	50	60	60	60	60	60	60	60	60	200	200	200	200	200	200	200
Sr/(Sr+Ca)	1.000	0.840	0.100	0.200	1.000	0.500	0.600	0.400	0.300	0.950	0.500	0.700	0.800	0.600	0.700	0.900	0.735	0.670	0.950
molarity	1.0	1.0	1.0	1.0	1.0	1.0	1.0	1.0	1.0	1.0	1.0	1.0	1.0	1.0	1.0	1.0	1.0	1.0	1.0
ρ fluid (g/ccm)	1.134	1.126	1.090	1.095	1.134	1.110	1.115	1.105	1.100	1.132	1.110	1.120	1.124	1.115	1.120	1.129	1.121	1.118	1.132
fluid (mg)	68.05	56.32	54.52	54.76	68.05	66.59	66.88	66.30	66.00	67.91	66.59	67.18	224.89	222.94	223.92	225.87	224.26	223.63	226.35
total run charge (mmol)																			
Si	0.181	0.187	0.180	0.172	0.119	0.191	0.189	0.193	0.196	0.182	0.131	0.187	0.185	0.189	0.187	0.165	0.168	0.169	0.164
Mg	0.108	0.112	0.107	0.106	0.057	0.114	0.113	0.115	0.117	0.109	0.063	0.112	0.110	0.113	0.112	0.098	0.100	0.101	0.098
Ca	0.000	0.021	0.084	0.074	0.000	0.053	0.042	0.064	0.075	0.005	0.051	0.031	0.049	0.098	0.073	0.024	0.064	0.079	0.012
Sr	0.103	0.073	0.009	0.018	0.117	0.053	0.063	0.042	0.032	0.098	0.061	0.073	0.195	0.147	0.171	0.215	0.176	0.161	0.227
H_2O total	3.638	3.002	2.782	2.816	3.760	3.475	3.509	3.441	3.405	3.623	3.549	3.543	11.156	11.088	11.122	11.153	11.103	11.083	11.168
H_2O in tremolite	0.022	0.022	0.021	0.021	-	0.023	0.023	0.023	0.023	0.022	-	0.022	0.022	0.023	0.022	0.020	0.020	0.020	0.020
H_2O in fluid	3.616	2.980	2.761	2.795	3.760	3.452	3.486	3.418	3.382	3.601	3.549	3.521	11.134	11.065	11.100	11.133	11.083	11.063	11.148
theoretical molarity	0.911	0.920	0.982	0.972	0.881	0.947	0.940	0.956	0.964	0.915	0.925	0.932	0.976	0.981	0.979	0.976	0.980	0.981	0.975
final fluid composition																			
Mg^{2+} (mmol)	<0.001	0.001	0.003	0.002	<0.001	0.002	<0.001	<0.001	0.002	0.001	<0.001	0.001	0.001	0.005	0.001	<0.001	<0.002	0.004	<0.001
Ca^{2+} (mmol)	<0.001	0.002	0.032	0.030	<0.001	0.005	0.003	0.012	0.026	<0.001	0.005	0.004	0.016	0.054	0.016	0.006	0.026	0.041	0.003
Sr^{2+} (mmol)	0.047	0.043	0.010	0.017	0.048	0.019	0.024	0.024	0.029	0.052	0.032	0.051	0.161	0.132	0.100	0.171	0.143	0.144	0.160
estimated molarity	0.739	0.825	0.833	0.914	0.721	0.398	0.450	0.602	0.890	0.805	0.580	0.847	0.875	0.916	0.597	0.874	0.844	0.910	0.814

note: ρ fluid derived by interpolation from the densities of 1m $CaCl_2$ solution (1.086 g/ccm) and 1m $SrCl_2$ solution (1.134 g/ccm).

H_2O in tremolite is the maximum content of water in solids in the case of only tremolite and no diopside formation.

The theoretical molarity is the value at the end of the run considering H_2O formation from hydroxides and H_2O consumption from the formation of tremolite.

48

diopside–Sr-diopside join. Two different $(Ca+Sr)^{solid}/(Ca+Sr)^{total}$ ratios of 0.42-0.49 (runs 1 to 15) and 0.16-0.18 (runs 16 to 23) were used. All experiments were performed in 25 and 35 mm long gold capsules with inner diameters of 2.6 and 4.6 mm, respectively, and wall thicknesses of 0.2 mm.

After the runs the unopened capsules were cleaned with a dilute HCl solution and hot distilled water. The gold tubes were then cut open in distilled water. The run products were washed out with double distilled water and filtered. All product fluid was collected and diluted to yield a total of 100 ml solution.

The solid products were examined by optical microscopy, scanning electron microscopy (SEM), high resolution electron microscopy (HRTEM), electron microprobe (EMP), powder X-ray diffraction with Rietveld analysis (XRD) and fourier transform infrared spectroscopy (IR). The fluids were analyzed for Ca, Sr and Mg by atomic absorption spectroscopy (AAS).

RESULTS

The reaction products of runs on the (Ca,Sr)-tremolite join consisted of 29-100 wt% tremolite, 0-60 wt% diopside, 0-10 wt% enstatite, and 0-13 wt% quartz. In the reaction products from runs 18, 20 and 21 up to 11 wt% forsterite were found instead of quartz. Talc (2 wt%) was found only in run 17. The products from runs 8 and 14 on the (Ca,Sr)-diopside join consisted of 95 wt% diopside and 5 wt% quartz.

Results from the structural characterization of the synthesized (Ca,Sr)-tremolites and (Ca,Sr)-diopsides by XRD, SEM, HRTEM and IR are discussed in detail by Gottschalk et al. (1998). Summarizing, the (Ca,Sr)-tremolites were up to 2000 μm long and 30 μm wide. The (Ca,Sr)-diopsides were up to 150 μm long and 20 μm wide. The tremolites from Ca-rich bulk compositions were more fibrous than those from Sr-rich samples. Tremolites and diopsides from most runs were well ordered with very low concentrations of chain multiplicity faults. The concentration of chain multiplicity faults increased somewhat with increasing Ca-content in (Ca,Sr)-tremolites but exceeded 5% rarely .

Both (Ca,Sr)-tremolites and (Ca,Sr)-diopsides were large enough for accurate EMP-analysis. The run products were mounted in epoxy and polished. Between 4 and 87 analyses were conducted for the amphiboles in each run. Ca-, Sr- and Mg-concentrations per formula unit (pfu) for (Ca,Sr)-tremolites from single point EMP-analysis are plotted in Fig. 1. They cover the entire compositional range between the tremolite and Sr-tremolite endmembers revealing a continuous (Ca,Sr)-tremolite solid solution series. There is, however, a small but

significant deviation from the ideal Ca_1Sr_{-1} substitution, indicating some cummingtonite $(Mg_2Mg_5[Si_8O_{22}/(OH)_2])$ component. From single point analysis this deviation was below ±0.05 pfu for most of the (Ca,Sr)-tremolites except for very Ca-rich solid solutions where the deviations were as high as ±0.15 pfu. For these Ca-rich tremolites, the Ca-content has a negative correlation with the Mg-content, which reflects the variable amount of cummingtonite-component ($X_{cum} = Mg^{M4}/(Ca+Sr+Mg)^{M4}$) in Ca-rich tremolites (Fig. 1c). All amphiboles, therefore, are solid solutions between tremolite, Sr-tremolite and cummingtonite.

The average composition of the amphiboles is given in Table 2 and Fig. 2. For amphiboles with $X_{Sr-tr} < 0.15$ ($X_{Sr-tr} = Sr^{M4}/(Ca+Sr+Mg)^{M4}$), the observed average cummingtonite-content was below 0.07. For amphiboles with higher X_{Sr-tr}-contents, X_{cum} was below 0.01. Most of the synthesized amphiboles were homogeneous within ±0.03 X_{Sr-tr} (2σ) except for (Ca-Sr)-tremolites from runs 2, 13, 20 and 23. Compositions of tremolites from runs 13 and 20 showed variations of ±0.06 and those from runs 2 and 23 of ±0.16 and ±0.11, respectively (all 2σ). In runs 2 and 23 two different compositional types of (Ca,Sr)-tremolites were distinguished by EMP, X-ray diffraction, and IR-spectroscopy with average X_{Sr-tr} compositions of 0.44 and 0.73 for run 2 and 0.59 and 0.79 for run 23 (see also Gottschalk et al. 1998). Besides the two compositional types, large (Ca,Sr)-tremolite crystals from run 2 show a clear zonation (Fig. 3). Cores from such grains had a composition of 0.25 in X_{Sr-tr} and rims of about 0.43 to 0.46. Such zonations were never observed in any (Ca,Sr)-tremolites from other runs.

The diopsides were solid solutions of diopside and Sr-diopside endmembers with only small amounts of enstatite component. Variations in the enstatite-content were somewhat larger for Ca-rich diopsides than for Sr-rich diopsides (Fig 4a and 4b). The average compositions of the diopsides from each run are listed in Table 3. In runs 20 and 23, no (Ca,Sr)-diopsides were detected. The average in enstatite component (X_{en}) did not exceed 0.05 and was below 0.02 in most runs. The compositional variations in the pyroxenes for each run was below ±0.03 X_{Sr-di} (2σ) except for (Ca,Sr)-diopsides from runs 1, 2, 13, 14 and 15. For runs 1, 13, 14 and 15 the variations in X_{Sr-di} were < 0.06. As for the tremolites run 2 shows a rather large compositional variation of ±0.13 in X_{Sr-di}. No diopsides formed in runs 20 and 23.

The Ca^{2+}, Sr^{2+} and Mg^{2+} concentrations of the final fluid are listed in Table 1. The error (2σ) was estimated to be less than 3% relative. The concentration of Cl^- was not measured. The molarity was estimated from Ca^{2+}, Sr^{2+} and Mg^{2+} concentrations assuming that these were the only cations present in the fluid. Mg^{2+}-concentrations were always very

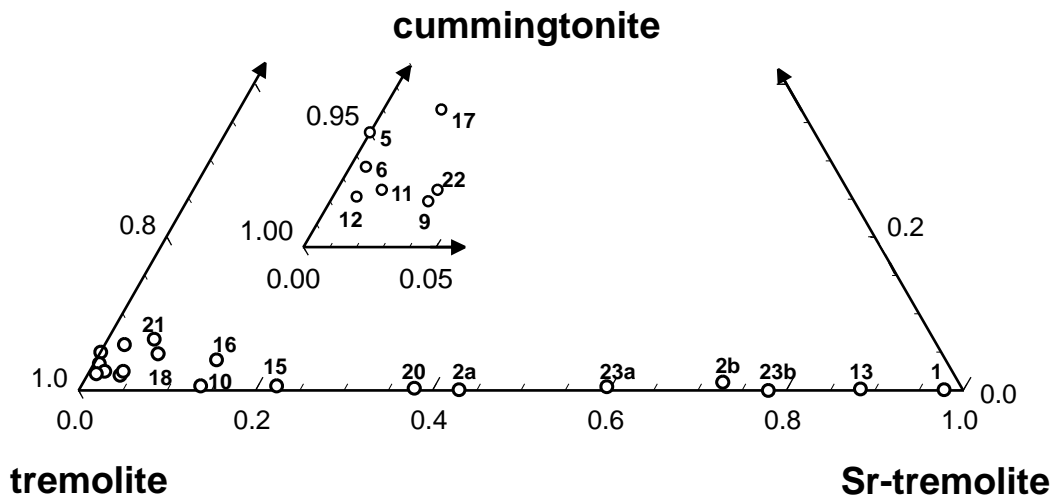**Table 2.** Average compositions of tremolite–Sr-tremolite solid solutions determined by EMP

run	1	2a	2b	5	6	9	10	11	12	13	15	16	17	18	20	21	22	23a	23b
amphibole composition (wt%)																			
number of analysis	87	65	12	34	26	21	11	12	29	47	28	22	8	18	4	13	2	6	16
SiO_2	52.83	56.31	54.63	59.38	59.35	58.89	57.52	58.64	59.40	53.19	57.95	58.80	59.25	59.04	55.43	59.42	56.78	55.50	53.74
MgO	21.59	22.92	21.97	25.05	24.97	24.47	23.66	24.39	24.75	21.76	23.73	24.67	24.65	24.49	22.99	25.23	23.83	22.86	22.06
CaO	0.27	7.58	3.42	12.99	13.17	12.80	11.40	12.92	13.26	1.48	10.40	11.19	12.31	11.88	8.18	12.07	12.20	5.25	2.84
SrO	23.02	10.36	17.22	0.18	0.22	1.22	3.50	0.68	0.33	21.00	5.48	3.39	0.61	1.62	8.94	1.01	0.81	14.09	18.54
Σ oxides	97.71	97.17	97.24	97.60	97.71	97.38	96.08	96.64	97.74	97.43	97.57	98.05	96.82	97.04	95.53	97.74	93.62	97.70	97.17
amphibole composition on the basis of 8 Si																			
Sr	1.98	0.87	1.47	0.00	0.01	0.07	0.27	0.03	0.02	1.79	0.45	0.27	0.04	0.13	0.77	0.10	0.09	1.19	1.59
Ca	0.04	1.16	0.54	1.90	1.92	1.89	1.72	1.92	1.94	0.23	1.56	1.65	1.84	1.77	1.25	1.76	1.86	0.80	0.44
Mg	4.98	4.97	4.99	5.10	5.07	5.04	5.00	5.05	5.04	4.98	4.99	5.08	5.12	5.10	4.98	5.13	5.05	5.00	4.96
Si	8.00	8.00	8.00	8.00	8.00	8.00	8.00	8.00	8.00	8.00	8.00	8.00	8.00	8.00	8.00	8.00	8.00	8.00	8.00

Table 3. Average compositions of diopside–Sr-diopside solid solutions as determined by EMP

run	1	2	5	6	7	8	9	10	11	12	13	14	15	16	17	18	22
pyroxene composition (wt%)																	
number of analysis	14	5	7	7	37	28	6	2	12	12	9	13	15	18	16	8	16
SiO_2	44.81	52.07	55.83	55.77	45.14	55.79	54.54	54.86	55.65	46.22	54.67	54.91	54.94	55.67	55.18	55.67	53.26
MgO	14.77	17.21	18.05	19.00	14.95	18.61	18.10	18.09	19.00	15.34	18.30	18.21	18.95	19.45	19.11	19.13	18.71
CaO	0.41	15.91	25.17	24.75	0.05	24.52	22.41	24.34	25.35	2.59	23.25	22.38	22.26	24.34	23.36	23.75	24.10
SrO	40.07	13.79	0.22	0.26	39.84	1.22	4.29	1.15	0.46	36.15	3.54	5.14	4.69	0.87	2.24	1.56	0.89
Σ oxides	100.06	98.97	99.28	99.78	99.98	100.14	99.35	98.44	100.45	100.31	99.75	100.64	100.84	100.34	99.88	100.11	96.96
Pyroxene composition on the basis of 2 Si																	
Sr	0.99	0.31	0.00	0.00	0.99	0.02	0.09	0.02	0.01	0.90	0.07	0.11	0.10	0.02	0.05	0.04	0.03
Ca	0.02	0.67	1.00	0.97	0.00	0.96	0.90	0.97	0.98	0.12	0.92	0.89	0.87	0.94	0.91	0.92	0.95
Mg	0.99	1.02	1.00	1.03	1.01	1.02	1.01	1.01	1.02	0.98	1.01	1.00	1.03	1.04	1.04	1.04	1.03
Si	2.00	2.00	2.00	2.00	2.00	2.00	2.00	2.00	2.00	2.00	2.00	2.00	2.00	2.00	2.00	2.00	2.00
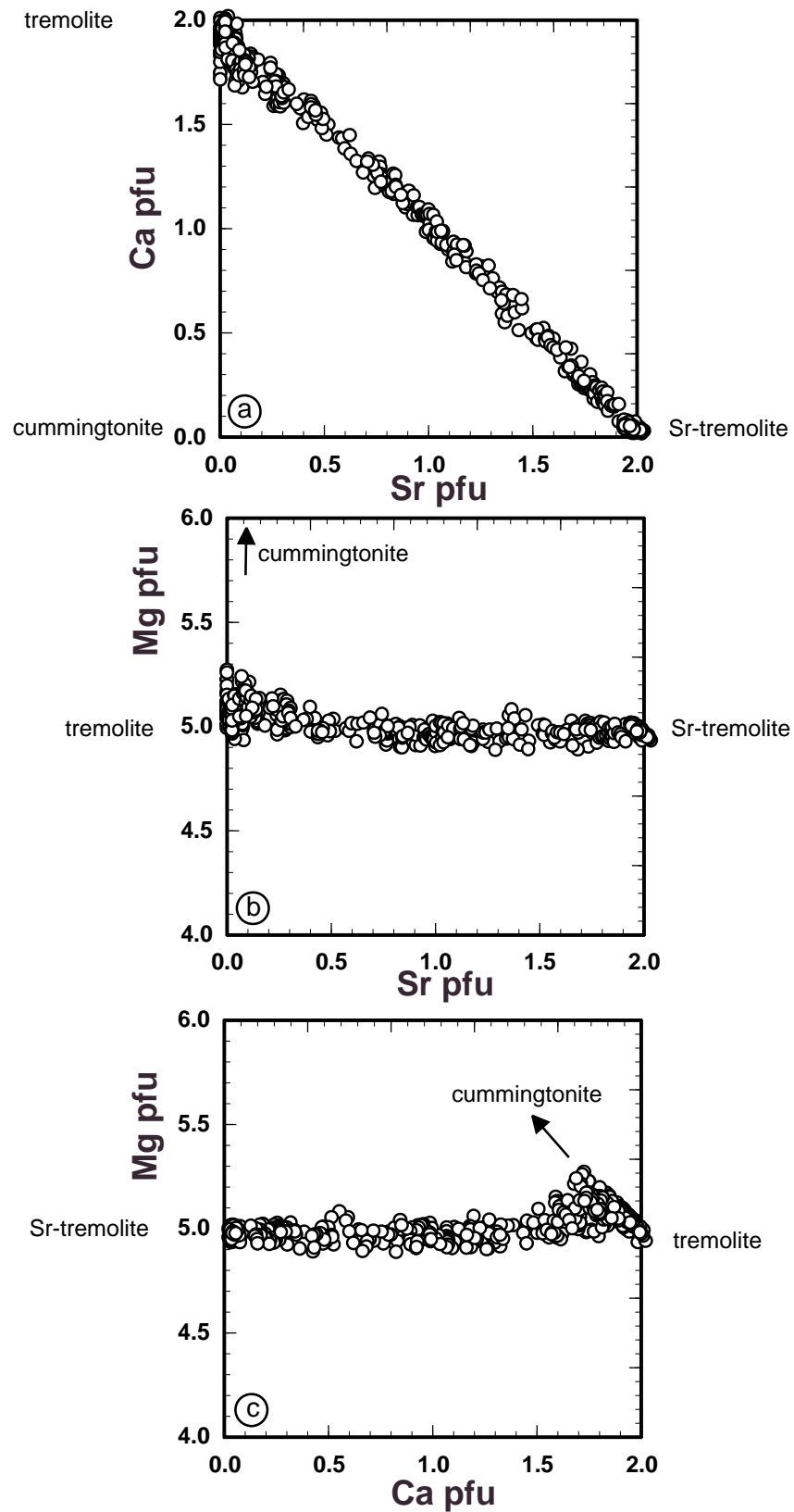
Fig. 1. Mg-, Ca- and Sr-content per formula unit (pfu) from EMP point analyses of (Ca,Sr)-tremolite. **a)** Ca-*vs*. Sr-content. **b)** Mg- *vs*. Sr-content. **c)** Ca- *vs*. Mg-content. Values > 5 for Mg corresponds to Mg^{2+} on the M4 site (cummingtonite). Mg is variable in Ca-rich tremolites with maximum cummingtonite contents of 15 mol%.

Fig. 2. Average compositions of (Ca,Sr)-tremolites from all runs plotted on the tremolite, Sr-tremolite- and cummingtonite-ternary. Ca-rich (Ca,Sr)-tremolites show variable contents of the cummingtonite component. For runs 2 and 23 the compositions of both (Ca,Sr)-tremolite populations with different X_{Sr}-contents are denoted as 2a,b and 23a,b, respectively.
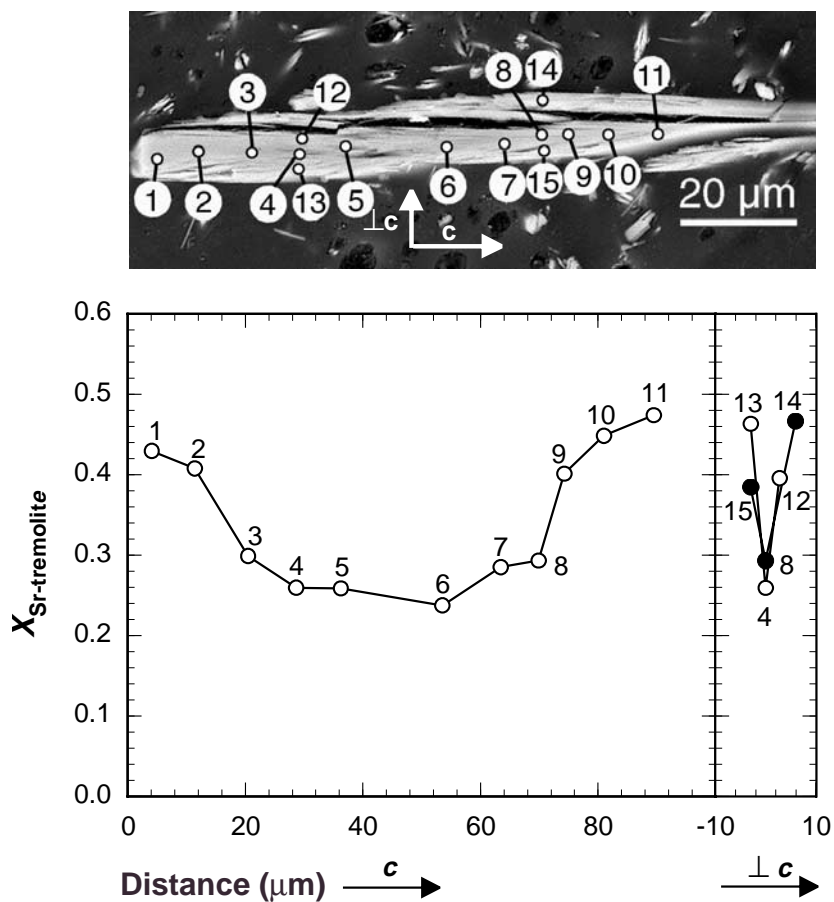
Fig. 3. Ca-Sr zonation of a tremolite crystal from run 2 along and perpendicular the crystallographic c direction. The Sr-concentration increases towards the rim. Numbers denote individual analysis spots.
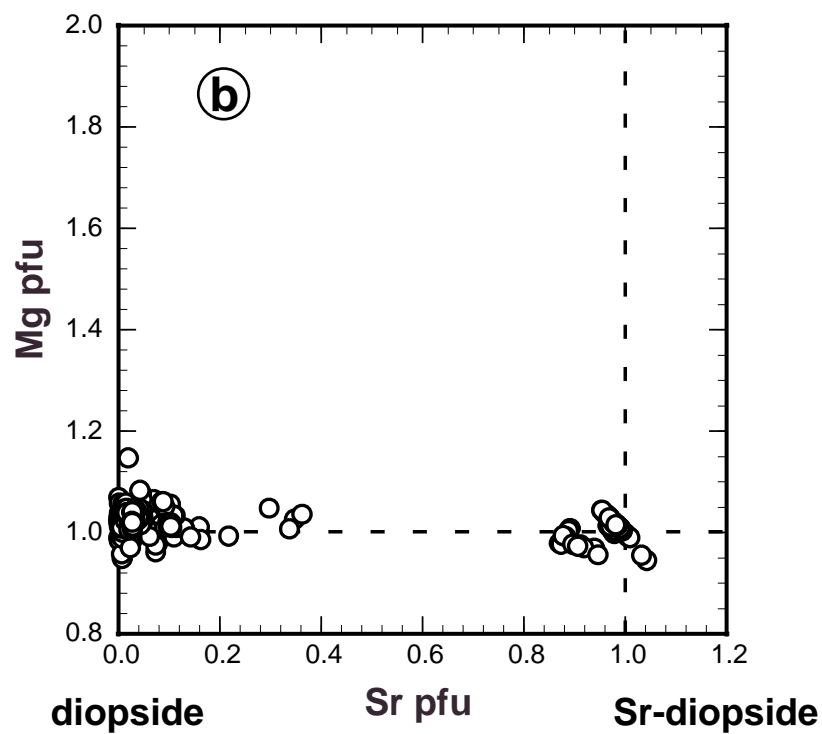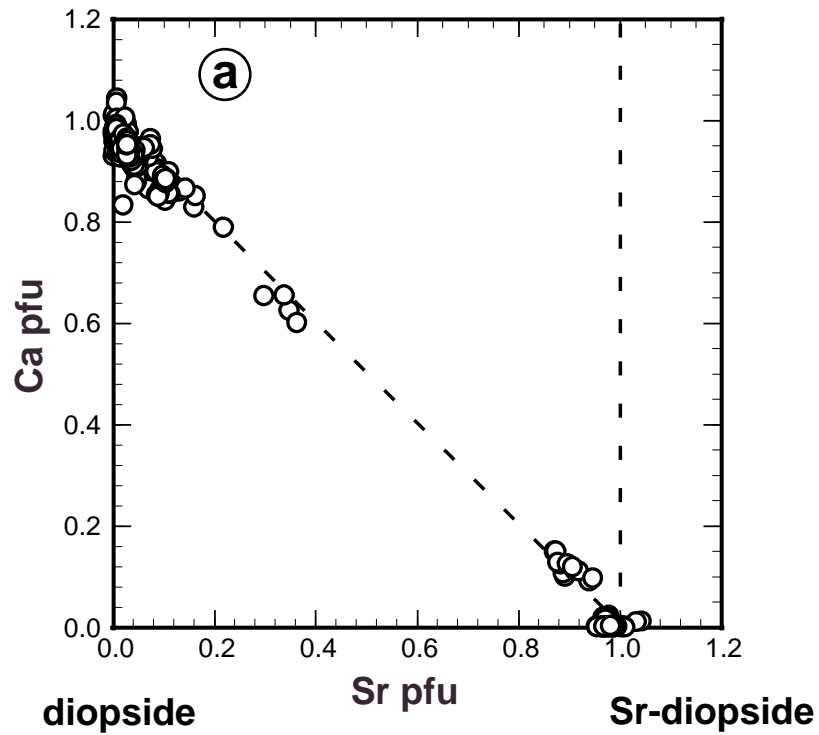
Fig. 4. Mg-, Ca- and Sr-concentrations per formula unit (pfu) from EMP point analyses of (Ca,Sr)-diopside analysis. **a)** Ca- *vs*. Sr-content. **b)** Mg- *vs*. Sr-content. Values >1 of Mg correspond to incorporation of Mg^{2+} on the M2 site (enstatite-component).

low and Mg/(Ca+Sr+Mg) values (fraction of cations, here of Mg) exceeded 0.02 only for runs with Ca-rich bulk compositions. It is interesting to note that for such Ca-rich tremolites with highly variable cummingtonite-content (Fig. 2), the variation of Mg in the fluid was also high (Fig. 5). The estimated molarity (0.40 - 0.92) was always lower than the theoretical molarity (0.88 – 0.98) which can be calculated under the assumption of complete reaction from the run charges (Table 1).

Fig.s 6 and 7 show reciprocal ternary plots for the systems (Ca,Sr)-tremolite-(Ca,Sr)Cl$_2$ and (Ca,Sr)-diopside-(Ca,Sr)Cl$_2$, respectively, along with the compositions of coexisting solids and fluids from Table 4. In Fig. 8, the distribution of Sr between (Ca,Sr)-diopside and fluid, (Ca,Sr)-tremolite and fluid, (Ca,Sr)-tremolite and(Ca,Sr)-diopside is plotted. The essential point is that in both systems, tremolite/fluid and diopside/fluid, Sr fractionates preferentially into the fluid.
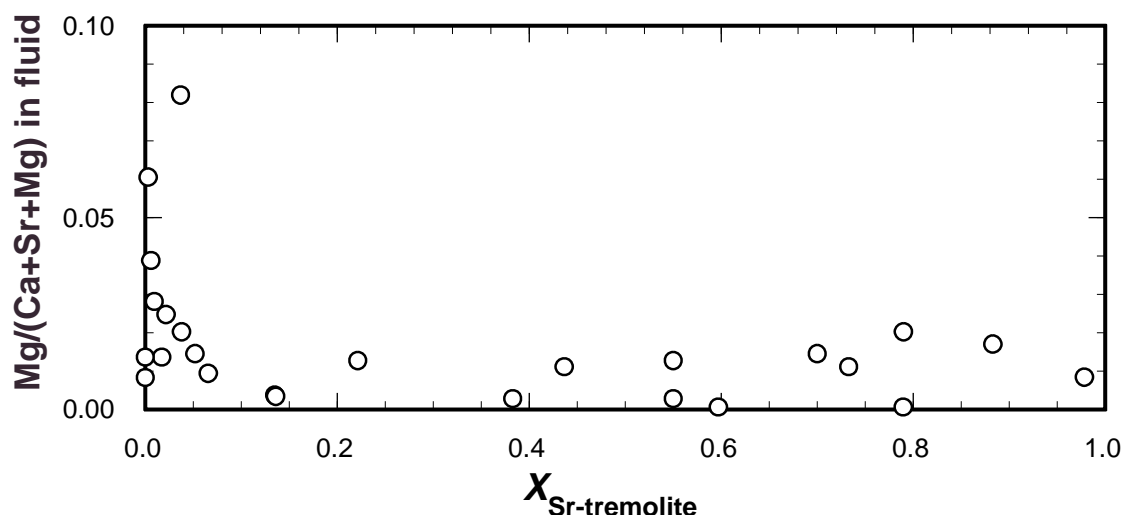
Fig. 5. Mg-concentration in the product fluid *vs.* Sr-concentrations in (Ca,Sr)-tremolite. Higher Mg-variations in the fluid correspond with increased cummingtonite contents in Ca-rich (Ca,Sr)-tremolites and -diopsides (see Fig.s 2 and 4).

INTERPRETATION AND DISCUSSION

(Ca,Sr)-tremolites from most runs were homogeneous (±0.03 X_{Sr-tr}). Only in runs 2 and 23 two populations of (Ca,Sr)-tremolites with different compositions were identified by EMP and X-ray diffraction (see also Gottschalk et al. 1998) with compositions of X_{Sr-tr} equal to 0.44 and 0.73 in run 2, 0.59 and 0.79 in run 23 (labelled as 2a, 2b, 23a and 23b in Table 2).

Table 4. Ca, Sr and Mg concentrations in terms of molar ratios in coexisting amphibole, pyroxene and fluid

run	1	2	5	6	8	9	10	11	12	13	14	15	16	17	18	20	21	22	23
fluid																			
X_{SrCl2} ×100	1.288	1.417	0.340	0.589	1.255	0.541	0.687	0.699	0.855	1.411	0.880	1.423	1.427	1.176	0.895	1.508	1.273	1.275	1.415
X_{CaCl2} ×100	0.003	0.052	1.154	1.065	0.003	0.136	0.082	0.352	0.755	0.011	0.132	0.098	0.141	0.475	0.139	0.055	0.235	0.363	0.027
X_{MgCl2} ×100	0.011	0.017	0.096	0.067	0.011	0.060	0.003	0.014	0.047	0.025	0.014	0.020	0.005	0.042	0.010	0.004	0.022	0.034	0.001
X_{H2O}	0.987	0.985	0.984	0.983	0.987	0.993	0.992	0.989	0.983	0.986	0.990	0.985	0.984	0.983	0.990	0.984	0.985	0.983	0.986
Sr/(Ca+Sr+Mg)	0.990	0.954	0.214	0.342	0.990	0.734	0.890	0.655	0.516	0.975	0.857	0.923	0.908	0.694	0.858	0.962	0.832	0.763	0.981
ΔSr/(Ca+Sr+Mg)(2σ)	0.001	0.003	0.015	0.020	0.001	0.014	0.008	0.019	0.021	0.001	0.010	0.005	0.007	0.017	0.010	0.003	0.011	0.015	0.016
Ca/(Ca+Sr+Mg)	0.002	0.035	0.725	0.619	0.002	0.184	0.106	0.331	0.456	0.008	0.129	0.064	0.089	0.281	0.133	0.035	0.153	0.217	0.019
Mg/(Ca+Sr+Mg)	0.008	0.011	0.061	0.039	0.008	0.082	0.004	0.014	0.028	0.017	0.014	0.013	0.003	0.025	0.009	0.003	0.015	0.020	0.001
amphibole																			
$X_{Sr\text{-}tr}$	0.978	0.437	0.003	0.006	-	0.037	0.135	0.017	0.010	0.883	-	0.221	0.136	0.022	0.066	0.383	0.052	0.038	0.797
$\Delta X_{Sr\text{-}tr}$ (2σ)	0.025	0.158	0.002	0.002	-	0.006	0.022	0.004	0.005	0.061	-	0.034	0.031	0.012	0.024	0.061	0.020	0.016	0.107
X_{tr}	0.021	0.579	0.950	0.959	-	0.943	0.859	0.958	0.969	0.115	-	0.773	0.824	0.918	0.886	0.627	0.881	0.937	0.221
X_{cum}	0.001	0.001	0.047	0.035	-	0.020	0.006	0.025	0.021	0.002	-	0.006	0.040	0.060	0.048	0.003	0.067	0.025	0.000
pyroxene																			
$X_{Sr\text{-}di}$	0.982	0.312	0.001	0.003	0.980	0.020	0.089	0.015	0.008	0.900	0.069	0.111	0.100	0.016	0.045	-	0.039	0.026	-
$\Delta X_{Sr\text{-}di}$ (2σ)	0.046	0.130	0.005	0.005	0.029	0.020	0.018	0.010	0.003	0.048	0.056	0.063	0.014	0.006	0.010	-	0.007	0.009	-
X_{di}	0.019	0.665	0.998	0.965	0.018	0.960	0.899	0.965	0.975	0.119	0.921	0.887	0.870	0.939	0.914	-	0.925	0.949	-
X_{en}	0.007	0.023	0.001	0.032	0.018	0.020	0.012	0.020	0.017	0.001	0.010	0.012	0.030	0.045	0.041	-	0.036	0.025	-
$X_{Sr\text{-}bulk}$	1.000	0.774	0.100	0.200	1.000	0.500	0.600	0.400	0.300	0.950	0.546	0.700	0.800	0.600	0.700	0.900	0.745	0.669	0.950
$\Delta X_{Sr\text{-}bulk}$ (2σ)	0.000	0.015	0.008	0.014	0.000	0.021	0.020	0.020	0.018	0.004	0.021	0.018	0.014	0.020	0.018	0.008	0.017	0.019	0.004
(Sr+Ca) solid/bulk	0.419	0.472	0.461	0.459	0.486	0.431	0.429	0.435	0.437	0.420	0.464	0.427	0.181	0.184	0.182	0.164	0.167	0.168	0.163
reaction 1: tremolite + 2 CaCl₂ ↔ Sr-tremolite + 2 SrCl₂																			
lnK_D	-4.62	-7.18	-9.07	-8.96	-	-9.25	-7.95	-9.41	-9.50	-5.65	-	-7.84	-8.24	-9.30	-8.93	-7.61	-9.05	-8.92	-5.36
Δ lnK_D	2.36	1.30	1.35	0.69	-	0.36	0.42	0.50	1.02	1.20	-	0.43	0.56	1.16	0.81	0.54	0.84	0.89	1.33
$D_{Sr}^{amph/fluid}$	3.28	1.41	0.04	0.05	-	0.31	0.90	0.11	0.05	2.75	-	0.74	0.45	0.09	0.34	0.12	0.20	0.14	2.45
reaction 2: diopside + SrCl₂ ↔ Sr-diopside + CaCl₂																			
lnK_D	-2.20	-4.07	-5.21	-5.25	-0.19	-5.14	-4.44	-4.65	-4.50	-2.84	-4.49	-4.75	-4.48	-4.97	-4.87	-	-4.85	-4.87	-
Δ lnK_D	2.57	0.61	2.92	1.66	1.52	0.92	0.24	0.55	0.43	0.54	0.87	0.64	0.18	0.40	0.25	-	0.20	0.38	-
$D_{Sr}^{pyr/fluid}$	7.41	2.57	0.08	0.06	7.59	0.51	1.55	0.33	0.11	6.31	0.97	0.97	0.87	0.18	0.62	-	0.39	0.25	-

note: X_{SrCl2} = SrCl₂/(SrCl₂+CaCl₂+MgCl₂+H₂O) in the fluid, $X_{Sr\text{-}tr}$ = Sr/(Sr+Ca+Mg) on M4 in tremolite, $X_{Sr\text{-}di}$ = Sr/(Sr+Ca+Mg) on M2 in diopside, $X_{Sr\text{-}bulk}$ = Sr/(Sr+Ca) in the bulk, $X_{Ca\text{-}fluid}$, $X_{Mg\text{-}fluid}$, X_{tr}, X_{cum}, X_{di} and X_{en} for Ca, Mg in the fluid, tremolite, cummingtonite, diopside and enstatite, respectively. For the calulation of the K_D-values more digits were used than given in Table 4.
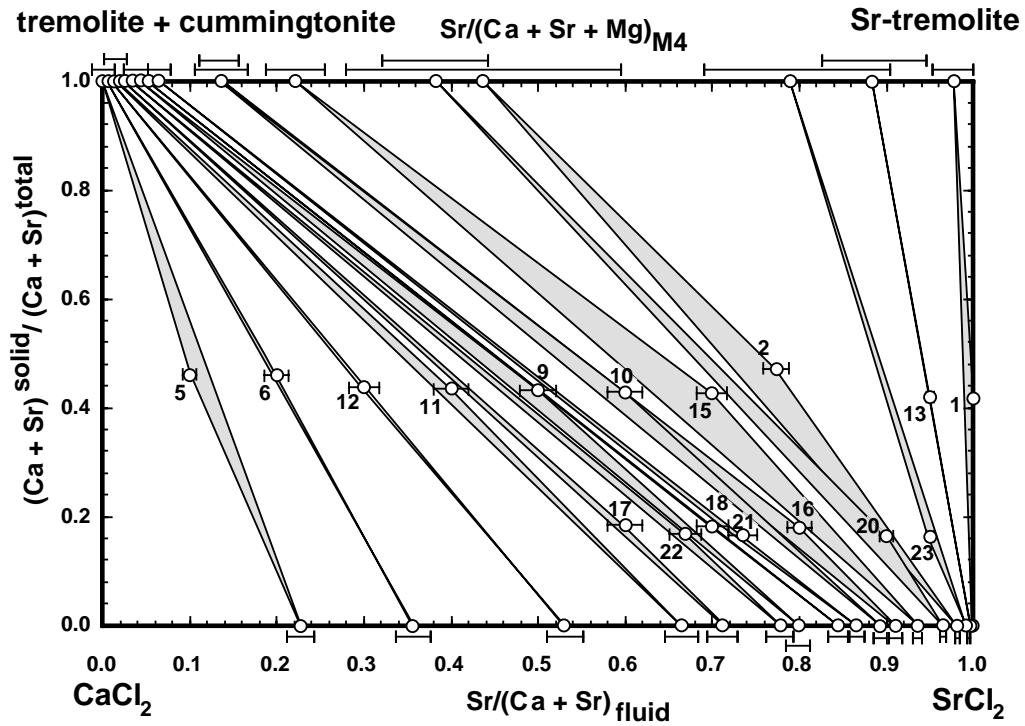
Fig. 6. Amphibole-, fluid- and bulk-composition plotted in the reciprocal ternary system (Ca,Sr)-tremolite-(Ca,Sr)Cl$_2$ as a function of X_{Sr}. Error bars denote the 2σ variations in composition. Consistent phase relations are evident by subparallel tie lines, which are close to their respective bulk compositions. Sr fractionates strongly into the fluid.
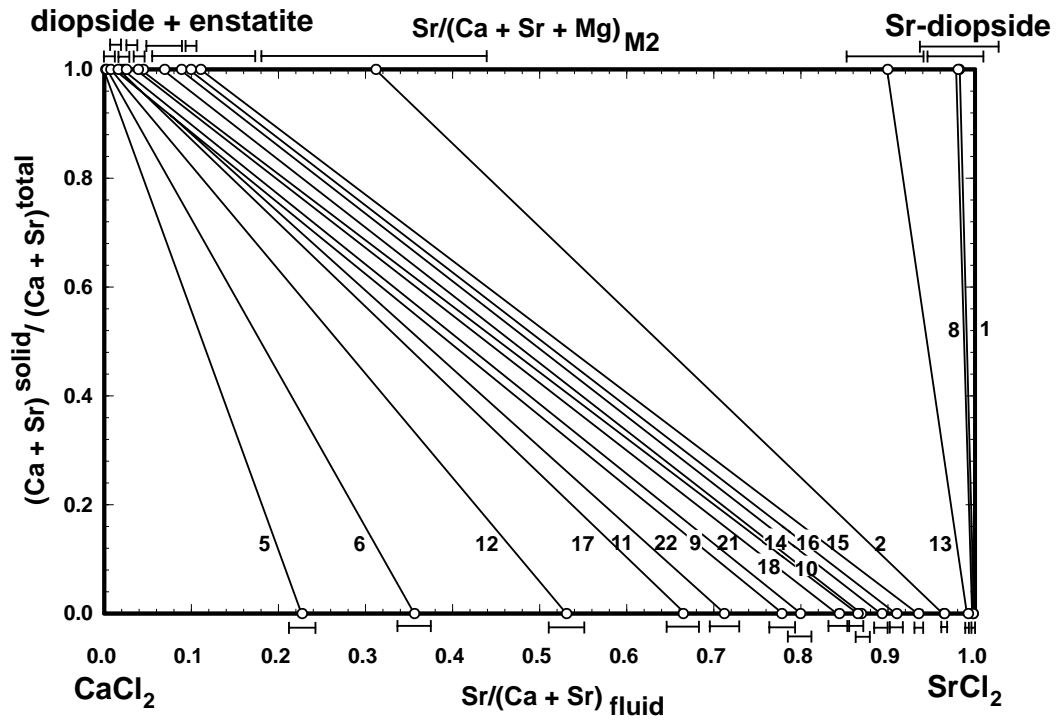
Fig. 7. Pyroxene- and fluid-composition plotted in the reciprocal ternary system (Ca,Sr)-diopside-(Ca,Sr)Cl$_2$ as a function of X_{Sr}. Error bars denote the 2σ variations in composition. As in the tremolite/fluid system, Sr fractionates strongly into the fluid.
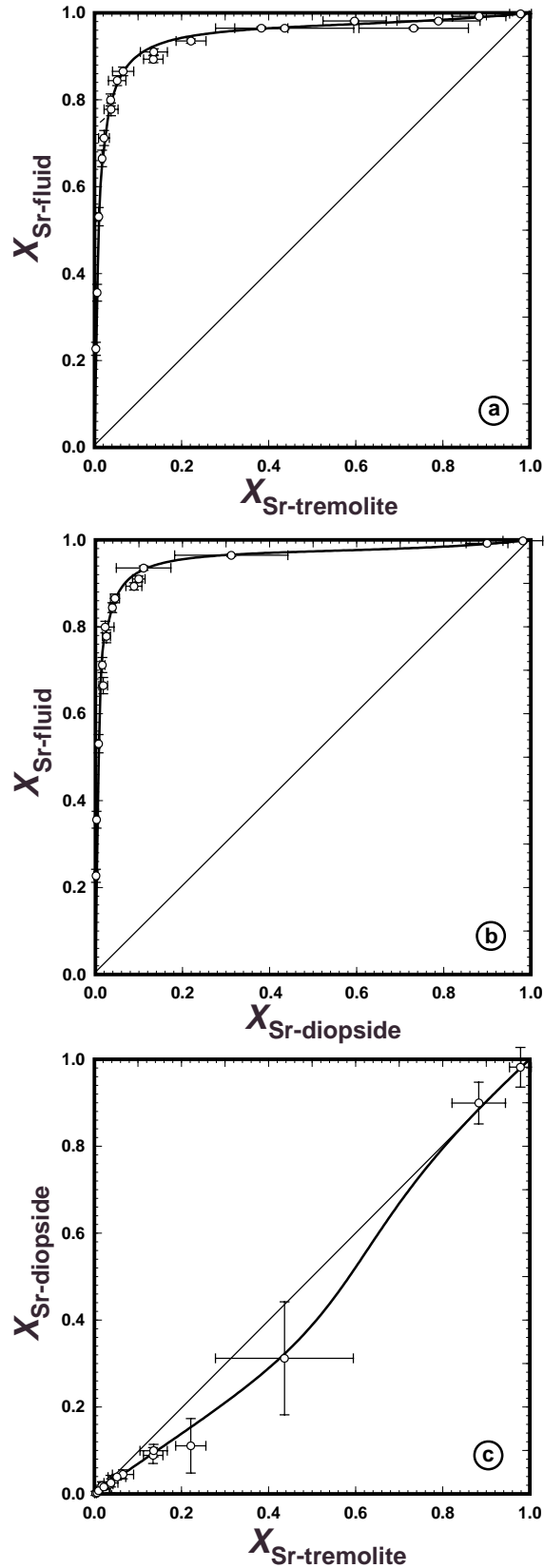
Fig. 8. Distribution diagrams in terms of X_{Sr} between **a)** (Sr,Ca)-tremolite and fluid, **b)** (Sr,Ca)-diopside and fluid, and **c)** (Sr,Ca)-tremolite and (Sr,Ca)-diopside. Data are from Table 4. The curves are calculated equilibrium distributions using the derived values of $\Delta\mu° = 59.0$ kJ and for $W_{CaSr}^{amph} = 9.8$ kJ for (Ca,Sr)-tremolite, and $\Delta\mu° = 30.8$ kJ and $W_{CaSr}^{px} = 11.7$ kJ for (Ca,Sr)-diopside.

58

The two populations from either run can not be interpreted as coexisting (Ca,Sr)-tremolites at a miscibility gap but rather as a result of a complex reaction path during those runs. It is possible that at the very beginning of those two experiments fluctuations in the composition of the fluid occurred due to inhomogeneities of the starting materials within each capsule. Its composition may also have depended on the different dissolution rates of the starting materials. Such local compositional variations in the fluid may have initially produced (Ca,Sr)-tremolites which were not in equilibrium with the bulk fluid but were metastable. The sensibility of the tremolite composition in respect to compositional variations of the fluid is enhanced for fluid compositions of Sr/(Ca+Sr) > 0.95 in comparison to fluids with lower Sr-contents (Fig. 8). It is obvious from Fig. 8a that in this range, the distribution of Sr between (Ca,Sr)-tremolite and fluid is very flat. Small compositional variations in the fluid lead to amplified variations in the coexisting solids. The final fluids of run 2 and 23 had compositions of Sr/(Ca+Sr) = 0.954 and 0.981. For the runs 2 and 23, the amphibole population for which the tie-lines in Fig. 6 are closest to their respective bulk compositions are the most probable candidates which were in equilibrium with the fluid (amphibole 2a and 23b from Table 2). This is also supported by the observation that these populations lead to thermodynamically consistent subparallel tie-lines.

Fig. 3 shows that in run 2 besides the two distinct tremolite populations, large (Ca,Sr)-tremolite crystals were zoned with cores enriched in Ca relative to the rims. It is reasonable to assume that the (Ca,Sr)-tremolite compositions of the rims were in equilibrium with the final fluid. The average composition (65 EMP analyses; $X_{\text{Sr-tr}} = 0.44$) for most small crystals from run 2 were practically identical to the rim composition (0.43 to 0.46) of the grain shown in Fig. 3. Such a zonation is interpreted as the result of a fractional crystallization process (for detailed discussion see Zimmermann et al. 1997a). At the beginning of the run the X_{Sr}-composition of the fluid should be close to that of the bulk composition, which is always lower in Sr than the final fluid. Because Sr fractionates strongly into the fluid, (Ca,Sr)-tremolites crystallizing initially were more Ca-rich than those in equilibrium at the end of the experiment. This process is especially enhanced for Sr-rich bulk compositions and resulting final fluids with a X_{Sr} of more than 0.95 (see discussion above). This is supported by observations made from run 20, which was performed at almost identical conditions than run 2, except for the fluid/solid ratio. In run 20 there was 4 times more fluid in respect to amphibole present than in run 2 and therefore the fluid had a much higher buffer capacity. Significantly smaller variations in composition were observed in amphiboles from run 20 compared to run 2. Chemical variations in (Ca,Sr)-tremolites from run 2 ($\Delta X_{\text{Sr-tr}} = \pm0.16\ 2\sigma$) were, by far, the highest ones observed. We emphasize, however, that in the vast majority of

the runs, the (Ca,Sr)-tremolites and (Ca,Sr)-diopsides were homogeneous with a compositional variation (2σ) in X_{Sr-tr} of less than ±0.03 and in X_{Sr-di} of less than ±0.05 (Fig.s 6, 7, 8).

No (Ca,Sr)-diopside compositions were observed in the range between $0.31 > X_{Sr-di} > 0.90$. In principle, this might be due either to a limited miscibility or to an extreme fractionation behaviour. As shown above, pyroxene/fluid Sr fractionation is even more enhanced than in the system amphibole/fluid. Pyroxenes with a X_{Sr-di} of 0.31 coexist with a fluid with a X_{Sr} of 0.954 whereas pyroxenes with a X_{Sr-di} of 0.90 coexist with a fluid with a X_{Sr} of 0.975. Thus, a difference in X_{Sr} in the fluid of only 0.021 leads to a change in X_{Sr-di} of 0.31 to 0.90 in the pyroxenes. If this effect is disregarded one might argue, then, that a fluid composition anywhere between these values would coexist with two diopside compositions. However, the thermodynamic treatment of the system (see below) reveals that a miscibility gap along the (Ca,Sr)-diopside join at the experimental conditions is highly improbable. The absence of compositions in the range of $0.31 < X_{Sr-di} < 0.90$ is simply the result of the chosen bulk compositions.

The molarity in the fluid calculated from the experimentally determined cation concentrations was always somewhat lower than the theoretical values calculated from the starting materials (Table 1). This is most likely due to fluid loss when opening the capsules and probably also to insufficient washing of the solid run products. However the important cation ratios are not affected by fluid loss.

The reciprocal ternary plots of the systems (Ca,Sr)-tremolite-(Ca,Sr)Cl$_2$ and (Ca,Sr)-diopside-(Ca,Sr)Cl$_2$ (Fig.s 6 and 7) show subparallel tie-lines. This is a good argument for thermodynamic equilibrium in the runs because for thermodynamic consistency such subparallel tie-lines are required. If only (Ca,Sr)-tremolite had formed the tie-lines would coincide with the bulk compositions plotted in Fig. 6. That in some cases the bulk compositions are slightly off the tie-lines is mainly due to the formation of (Ca,Sr)-diopside and cummingtonite component in the (Ca,Sr)-tremolites. The offset is most pronounced for the (Ca,Sr)-tremolites from runs 2 and 15. For all other runs, the tie-lines are very close to their bulk composition.

Zimmermann et al. (1997b) tried to demonstrate equilibrium of the Na-K-Ca exchange between amphibole and an aqueous chloride solution with reversed experiments. They showed that such experiments did not approach overall equilibrium corresponding to the respective bulk chemistry. Due to a dissolution fractional-crystallization process only small amounts of the starting amphiboles were dissolved and product amphibole only precipitated as very thin rims epitactically on the amphiboles used as starting phases. While it can be

assumed that these rims were in equilibrium with the fluid present at the time of precipitation, the fluid did evolve with time together with the coexisting amphibole rims. As a result a large array of amphibole compositions was observed which made the runs useless for the demonstration of equilibrium. Synthesizing amphiboles with an excess fluid, however, allows the exchange of cations between fluid and solid to a much larger extent (Zimmermann et al. 1997a) therefore minimizing the effect of fractional crystallization.

Summarizing, we believe that equilibrium distributions were achieved based on three main arguments: First, in the vast majority of the runs the (Ca,Sr)-tremolites are within a very narrow compositional range. Second, the (Ca,Sr)-tremolites are well crystallized with almost no stacking or multiplicity faults (Gottschalk et al. 1997). Third, the phase relations in the reciprocal ternary show overall consistency. All these are good arguments for thermodynamic equilibrium.

THERMODYNAMIC EVALUATION

Assuming thermodynamic equilibrium, the mixing parameters for the (Ca,Sr)-tremolite solid solutions are extracted. At constant pressure and temperature an equilibrium such as (1) can be formulated thermodynamically with the expression

$$\Delta\mu^o + RT \ln \frac{a_{Sr-tr}^{amph} \left(a_{CaCl_2}^{aq}\right)^2}{a_{tr}^{amph} \left(a_{SrCl_2}^{aq}\right)^2} = 0 \tag{3}$$

and

$$\Delta\mu^o = \mu_{Sr-tr}^o + 2\mu_{CaCl_2}^o - \mu_{tr}^o - 2\mu_{SrCl_2}^o \tag{4}$$

where a are the activities of the components and μ^o are the chemical potentials at their standard state. Mixing in (Ca,Sr)-tremolites takes place on the two M4 sites. Because the M4 site has a multiplicity of two, the activities of tremolite and Sr-tremolite are written as the squared product of the M4 site occupancy and its activity coefficient:

$$a_{tr}^{amph} = \left(X_{Ca}^{amph} \gamma_{Ca}^{amph}\right)^2 \tag{5}$$

$$a_{Sr-tr}^{amph} = \left(X_{Sr}^{amph} \gamma_{Sr}^{amph}\right)^2 \tag{6}$$

61

Using the definitions for the activities of $CaCl_2$ and $SrCl_2$ ($a_i = X_i\,\gamma_i$) and the definition of the distribution coefficient K_D,

$$K_D = \frac{X_{Sr}^{amph}\,X_{CaCl_2}^{aq}}{X_{Ca}^{amph}\,X_{SrCl_2}^{aq}} \tag{7}$$

eq. (3) becomes:

$$\Delta\mu^o + 2RT\ln K_D + 2RT\ln\frac{\gamma_{Sr}^{amph}\,\gamma_{CaCl_2}^{aq}}{\gamma_{Ca}^{amph}\,\gamma_{SrCl_2}^{aq}} = 0 \tag{8}$$

Because the runs were conducted with a 1 molar solution it is reasonable to assume that in the fluid Henry´s law is obeyed. Furthermore it is assumed that the Henry´s constants of both, $CaCl_2$ and $SrCl_2$ (or Ca^{2+} and Sr^{2+}) are equal because of their chemical similarities. This simplifies eq. (8) to:

$$\Delta\mu^o + 2RT\ln K_D + 2RT\ln\frac{\gamma_{Sr}^{amph}}{\gamma_{Ca}^{amph}} = 0 \tag{9}$$

If the Henry´s constants of $CaCl_2$ and $SrCl_2$ (or Ca^{2+} and Sr^{2+}) are not equal, a constant value is simply added to $\Delta\mu°$, but eq. (9) still holds.

Ideal mixing, i.e. $\gamma_i = 1$, on the M4 site in the amphiboles is improbable. The simplest activity model is that of a regular solution. Using the formulation after Wohl (1946) a regular solution in the ternary system tremolite, Sr-tremolite and cummingtonite including a ternary interaction parameter can be formulated as

$$G_{M4}^{EM} = X_{Ca}X_{Sr}W_{CaSr} + X_{Ca}X_{Mg}W_{CaMg} + X_{Sr}X_{Mg}W_{SrMg} + X_{Ca}X_{Sr}X_{Mg}C \tag{10}$$

where W_{CaSr}, W_{CaMg} and W_{SrMg} are the binary parameters and C is the ternary interaction parameter. The activity coefficient of a component can be derived by multiplying eq. (10) with ($n_{Ca}+n_{Sr}+n_{Mg}$) and differentiating the result with respect to the mole number of the specific component:

$$R\,T\ln\gamma_{Ca}^{amph} = X_{Sr}^2 W_{CaSr} + X_{Mg}^2 W_{CaMg} + X_{Sr}X_{Mg}\left(W_{CaSr} + W_{CaMg} - W_{SrMg}\right) + X_{Sr}X_{Mg}\left(1 - 2X_{Ca}\right)C$$

$$R\,T\ln\gamma_{Sr}^{amph} = X_{Ca}^2 W_{CaSr} + X_{Mg}^2 W_{SrMg} + X_{Ca}X_{Mg}\left(W_{CaSr} + W_{SrMg} - W_{CaMg}\right) + X_{Ca}X_{Mg}\left(1 - 2X_{Sr}\right)C \quad (11)$$

$$R\,T\ln\gamma_{Mg}^{amph} = X_{Sr}^2 W_{SrMg} + X_{Ca}^2 W_{CaMg} + X_{Ca}X_{Sr}\left(W_{SrMg} + W_{CaMg} - W_{CaSr}\right) + X_{Ca}X_{Sr}\left(1 - 2X_{Mg}\right)C$$

With the assumption that the ternary interaction parameter C is zero, in conjunction with eq. (11), eq. (9) becomes:

$$\Delta\mu^o + 2RT\ln K_D + 2\left(W_{CaSr}^{amph}(X_{Ca} - X_{Sr}) + X_{Mg}\left(W_{SrMg}^{amph} - W_{CaMg}^{amph}\right)\right) = 0 \quad (12)$$

The last term in eq. (12) will have a large effect for (Ca,Sr)-tremolites of intermediate compositions when $X_{Ca} \sim X_{Sr}$. However, their cummingtonite content X_{Mg} is very low and the last term in eq. (12) can be neglected:

$$\Delta\mu^o + 2RT\ln K_D + 2W_{CaSr}^{amph}(X_{Ca} - X_{Sr}) = 0 \quad (13)$$

In Fig. 9, -lnK_D is plotted *vs.* $(X_{Ca} - X_{Sr})$. If the regular solution model and the simplifications are appropriate, this plot should yield a linear relationship. The intercept is $\Delta\mu^o/(2RT)$ and the slope is the binary interaction parameter W_{CaSr}^{amph}/RT. From Fig. 9 it follows that the derived lnK_D´s do indeed obey a linear relationship with respect to the M4 occupancy within the error range. Linear regression results in 59.0 ± 0.8 kJ for $\Delta\mu^o$ and 9.8 ± 0.5 kJ for W_{CaSr}^{amph} ($R^2 = 0.962$).

For reaction (2) the equilibrium between (Ca,Sr)-diopside and fluid can be formulated in the same fashion:

$$\Delta\mu = \Delta\mu^o + RT\ln\frac{a_{Sr-di}^{px}\,a_{CaCl_2}^{aq}}{a_{di}^{px}\,a_{SrCl_2}^{aq}} \quad (14)$$

and

$$\Delta\mu^o + RT\ln K_D + W_{CaSr}^{px}(X_{Ca} - X_{Sr}) = 0 \quad (15)$$

Fig. 10 shows the -lnK_D *vs.* $(X_{Ca} - X_{Sr})$ plot for the system (Ca,Sr)-diopside/fluid. Again a linear relationship holds and values for $\Delta\mu^o$ and W_{CaSr}^{px} of 30.8 ± 0.5 kJ and for 11.7 ± 0.6 kJ ($R^2 = 0.961$) were obtained, respectively. Fig. 8b shows that also the regular solution model fits the measured values well.
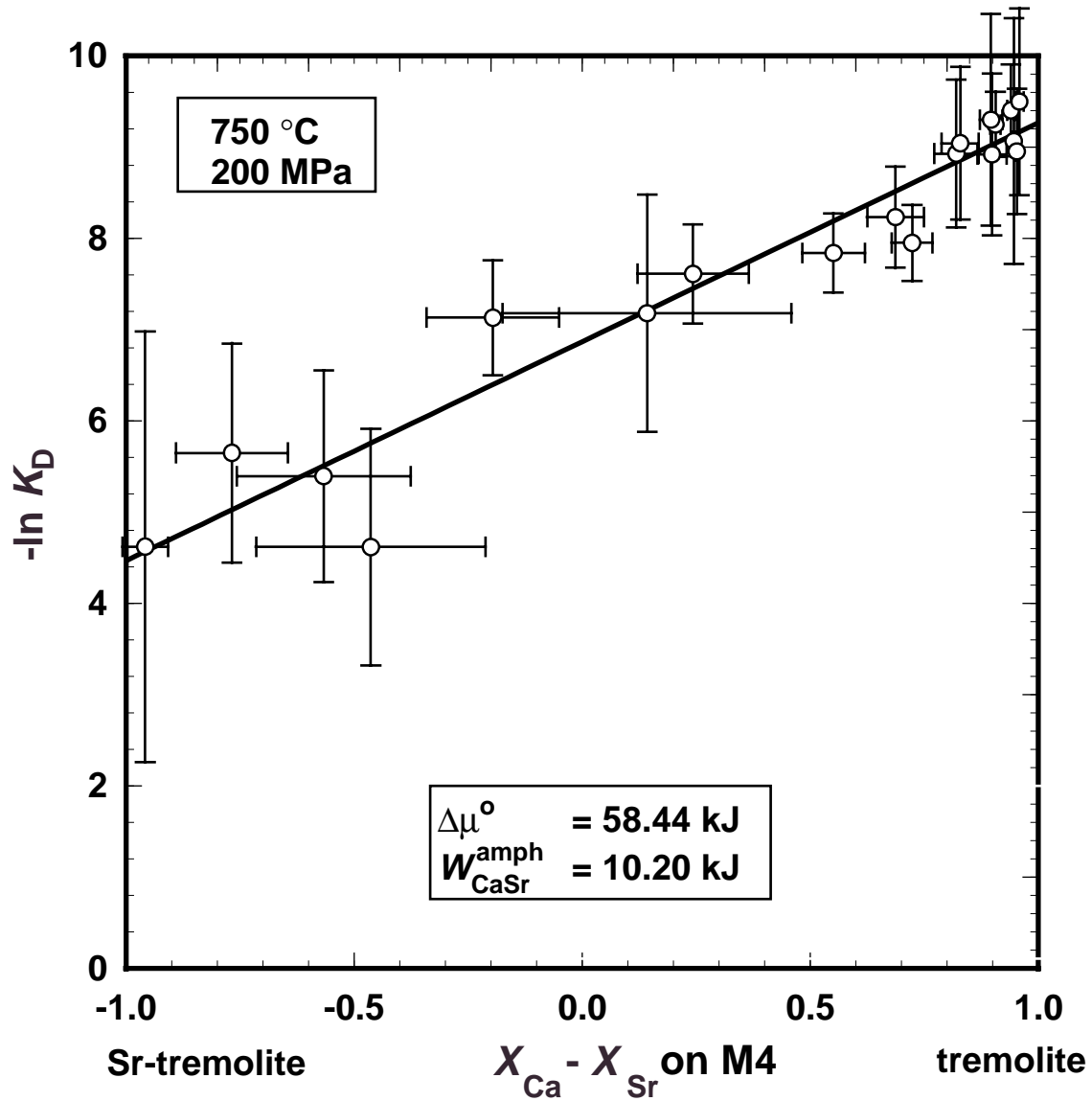
Fig. 9. Plot of $-\ln K_D$ *vs.* $(X_{Ca} - X_{Sr})$ for (Ca,Sr)-tremolite. A linear relationship (regular solution model) is consistent with the experimentally derived values for K_D. within errors. $\Delta\mu°$ (intercept) and W (slope) were calculated by linear regression.

The interaction parameters for (Ca,Sr)-tremolite and (Ca,Sr)-diopside solid solutions, $W_{CaSr}^{amph} = 9.8$ and $W_{CaSr}^{px} = 11.7$ kJ are similar. The same is true for $\Delta\mu°$ for the exchange reactions (1) and (2) if normalized to one cation exchange (i.e. 29.5 *vs.* 30.8 kJ).

Comparing the values of $\Delta\mu°$ and W_{CaSr} it becomes evident that $\Delta\mu°$ dominates the Ca-Sr distribution between (Ca,Sr)-tremolite/(Ca,Sr)-diopside and fluid. The excess term G_{M4}^{EM} (eq. 10) attains its maximum for both (Ca,Sr)-tremolites and (Ca,Sr)-diopsides at $X_{Sr} \sim 0.5$ and becomes then 2.5 kJ and 2.8 kJ, respectively, for the two binaries. This is less than 10% of the value of $\Delta\mu°$. The difference in *Gibbs* free energy of Ca^{2+} and Sr^{2+} in aqueous solution is small, i.e. 5.9 kJ at 298.15 K and 0.1 MPa (Robie et al. 1979). Assuming that the two fluid

species have similar heat capacities, it is mainly the difference in the *Gibbs* free energy of the endmembers tremolite/Sr-tremolite and diopside/Sr-diopside, i.e. their enthalpies and entropies, which governs the Ca/Sr distribution between solids and fluid and only to a minor extend the mixing behaviour of Ca^{2+} and Sr^{2+} on their specific crystallographic sites.
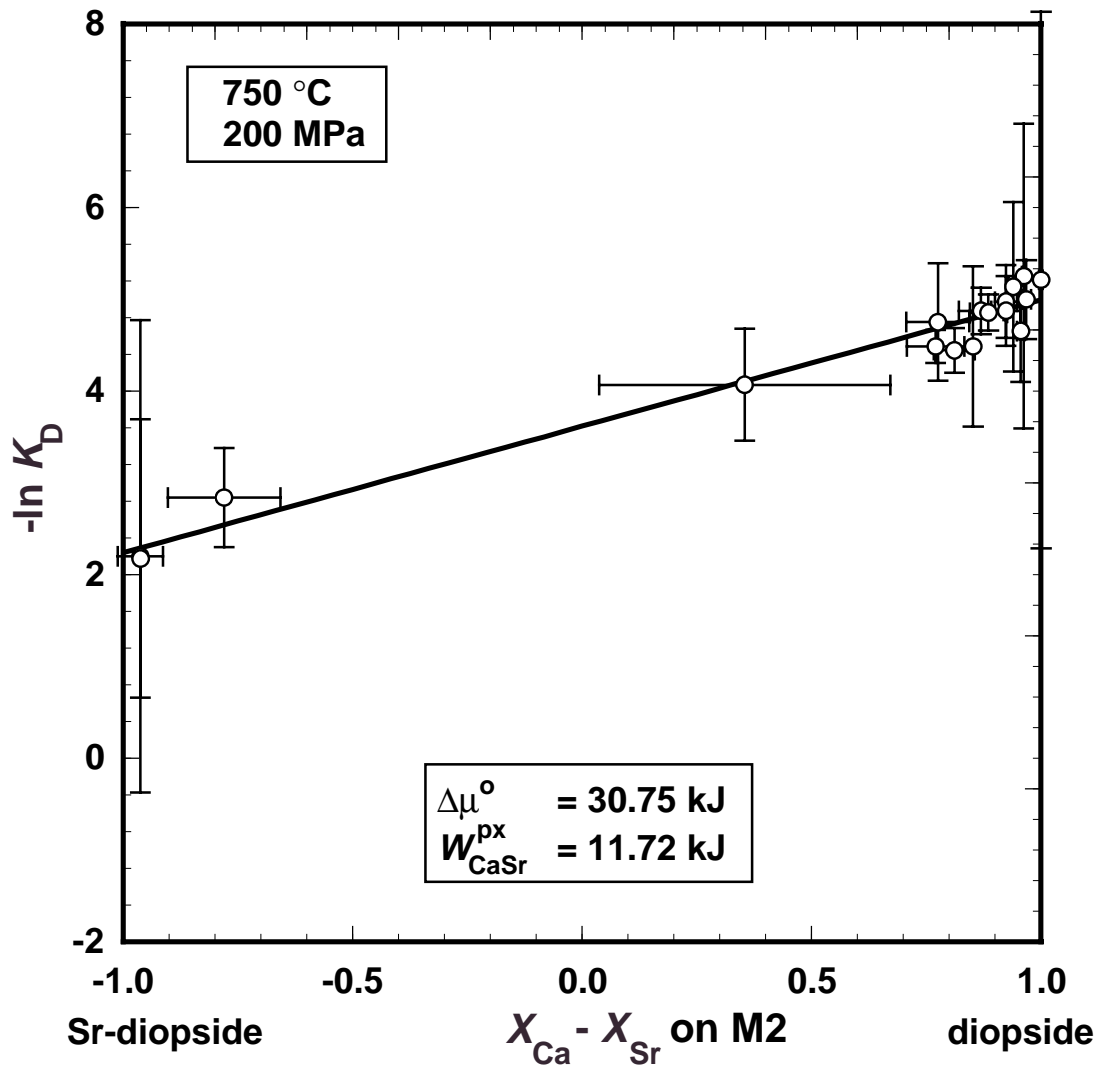

Fig. 10. Plot of $-\ln K_D$ *vs.* $(X_{Ca} - X_{Sr})$ for (Sr,Ca)-diopside. A linear relationship (regular solution model) is consistent with the experimentally derived values for K_D within errors. $\Delta\mu^\circ$ (intercept) and W (slope) were calculated by linear regression.

The thermodynamic evaluation of the observed fractionation of Sr between diopside and fluid using a regular solution model for (Ca,Sr)-diopsides (see below) yields a value for the exchange parameter W_{CaSr}^{px} of 11.7 kJ. For regular solutions the critical mixing temperature T_c can be calculated using the relation $2\,RT_c = W_{CaSr}^{px}$ (e.g. Guggenheim 1967). Above T_c a continuous solid solution series exists. Under the assumption that the derived

value for W_{CaSr}^{px} is independent from temperature a critical temperature of 430 °C is calculated for the diopside-Sr-diopside solid solution series. With this value for W_{CaSr}^{px} there is no immiscibility in the (Ca,Sr)-diopside solid solution series at 200 MPa and 750 °C; W_{CaSr}^{px} must be at least 50% higher than the observed value to indicate a miscibility gap. A value of 316 °C for T_c is calculated for the tremolite-Sr-tremolite solid solution series.

PETROGENETIC IMPLICATIONS

The experimental results show that on the M4 site of amphibole and the M2 site of clinopyroxene, Ca^{2+} can be completely replaced by Sr^{2+}. It is clear that for these two mineral groups, the incorporation of Sr is not governed by structural restrictions (e.g. limited miscibility) but by the absolute element abundances and the fractionation behaviour within a given system.

The average abundance of Sr in crustal rocks is in the range of 100 to 500 ppm with Ca/Sr ratios of about 100 to 300 (Turekian and Wedepohl 1961). For the geochemical modeling of fractionation processes, partition coefficients must be available. Application of the equations (13) and (15) to such low Sr-concentrations in the bulk rock (Sr/(Sr+Ca) < 0.01) result in mineral/fluid partition coefficients ($D_{Sr}^{mineral/fluid} = c_{Sr}^{mineral}(wt\%)/c_{Sr}^{fluid}(wt\%)$) of 0.045 and 0.082 for coexisting (Ca,Sr)-tremolite/fluid and (Ca,Sr)-diopside/fluid pairs, respectively. The derived Sr partition coefficient for (Ca,Sr)-tremolites is almost identical with the partition coefficient of Rb in (Na,K,Rb)-richterite/fluid equilibria (Melzer et al. 1997) which ranges from 0.055 and 0.064 depending on the K-concentration in richterite. In contrast, the Sr partition coefficients $D_{Sr}^{mineral/fluid}$ derived by Brenan et al. (1995), Ayers et al. (1997) and Adam et al. (1997) are considerably larger. For pargasites, augites and chloride solution at 900 °C and 2 GPa Brenan et al. (1995) reported a value of 1.7 for $D_{Sr}^{amph/fluid}$ and values in the range between 0.48 and 4.6 for $D_{Sr}^{cpx/fluid}$. For the equilibrium of clinopyroxene and a H_2O-rich fluid at 900-1100 °C and 2-3 GPa Ayers et al. (1997) reported $D_{Sr}^{cpx/fluid}$ values in the range of 1-2. Adam et al. (1997) examined the distribution of Sr between aqueous fluid, basanitic melt and amphibole/clinopyroxene at 1100 °C and 2 GPa. They reported $D_{Sr}^{amph/fluid}$ and $D_{Sr}^{cpx/fluid}$ values of 6.6 and 3, respectively. For amphibole/melt systems, Adam et al. (1993) give a value of 0.33-0.35 for $D_{Sr}^{amph/melt}$ at 875-1100 °C and 1-2 GPa for pargasites and both, basanitic and andesitic melt.

The partition coefficients from Brenan et al. (1995), Ayers et al. (1997) and Adam et al. (1997) were determined at higher temperatures and higher pressures and for complex bulk

compositions close to natural rocks. This is, however, not sufficient to explain the rather large difference in the experimental results and the reasons remain unclear. The presence of Cl⁻ in our fluids may play a certain role, however. Brenan et al. (1995) observed lower $D_{Sr}^{cpx/fluid}$ values for Cl-bearing fluids than for pure H_2O. On the other hand, partition coefficients for Sr between clinopyroxene and basaltic melt of 0.075 to 0.136 at 1250-1345 °C, 0.1 MPa (Ray et al. 1983) and of 0.079 at 1300 °C, 1GPa (Skulski et al. 1994) are also much lower than the values obtained by Brenan et al. (1995), Ayers et al. (1997) and Adam et al. (1997).

It is clear that experimentally derived *partition* coefficients *D* are strictly applicable only for systems, which are close to the experimental system. The essential point is that in simplified model systems the exchange reactions are precisely defined whereas in complex natural systems they are not. The *distribution* coefficients K_D and the equilibrium constants as derived here are thermodynamically more meaningful values and more universal; an understanding or at least reasonable assumptions of the mixing behaviour of the phases involved is required, however. Comparing partition coefficients derived in different systems is a rather dangerous task.

Natural examples, such as the metaeclogite of Bjørkedalen in SW-Norway with whole rock concentrations of up to 2.4wt% SrO (Brastad 1985) are, however, well suited to compare the derived distribution coefficients with those predicted from studies of exchange reactions. This rock was metasomatized by an anomalously Sr-rich fluid. The maximum contents of Sr-bearing components are up to 27 mol% $Sr_2Al_2Si_2O_8$ in plagioclase, 20 mol% $Sr_2Al_3[SiO_4/Si_2O_7/O/(OH)]$ in epidote, 51 mol% $Na_4Sr_8[Al_{20}Si_{20}O_{80}] \cdot 24H_2O$ in thomsonite, 2 mol% $Sr_5(PO_4)_3(OH)$ in apatite and 1 mol% $Sr_2Mg_5[Si_8O_{22}/(OH)_2]$ in amphibole. The experimentally determined distribution coefficient K_D is used to derive the Ca/Sr-ratio of the fluid which caused the metasomatism. With a value for K_D of 1.2×10^{-4} for Sr-poor tremolites (Fig. 9) a Ca/Sr ratio (wt%) of 0.55 is calculated for the coexisting fluid using eq. (16):

$$\left(c_{Ca}^{fluid} / c_{Sr}^{fluid} \right)^2 = K_{D(Sr-Ca)}^{amph-fluid} \cdot \left(c_{Ca}^{amph} / c_{Sr}^{amph} \right)^2 \tag{16}$$

Experimentally determined equilibria between (Ca,Sr)-anorthite and fluid are available from Lagache and Dujon (1987) at 750 °C and 200 MPa and from Kotelnikov et al. (1989) at 700-800 °C and 100-200 MPa. Application of these results to the plagioclase in the Bjørkedalen metaeclogite leads to a Ca/Sr ratio (wt%) in the fluid of 0.81 for the distributions derived by Lagache and Dujon (1987) and of 0.79 using the results from

Kotelnikov et al. (1989). Considering that neither the amphibole nor the plagioclase in the Bjørkedalen metaeclogite are pure (Ca,Sr)-solid solutions, the derived Ca/Sr ratios (wt%) are in good agreement with the value of 0.55 derived here.

ACKNOWLEDGMENTS

REFERENCES CITED

Adam, J., Green, T.H., Sie, S.H., and Ryan, C.G. (1997) Trace element partitioning between aqueous fluids, silcate melts and minerals. European Journal of Mineralogy, 9, 569-584.

Ayers, J.C., Dittmer, S.K., and Layne, G.D. (1997) Partitioning of elements between peridotite and H_2O at 2.0-3.0 GPa and 900-1100 °C. and application to models of subduction zone processes. Earth and Planetary Science Letters, 150, 381-398.

Ayers, J.C., and Watson, E.B. (1993) Apatite/ fluid partitioning of rare-earth elements and strontium; experimental results at 1.0 GPa and 1000 degrees C and application to models of fluid-rock interaction. Chemical Geology, 110, 299-314.

Benna, P. (1982) Ca-Sr substitution in clinopyroxenes along the join $CaMgSi_2O_6$-$SrMgSi_2O_6$. Tschermaks Mineralogische und Petrographische Mitteilungen, 30, 37-46.

Benna, P., Chiari, G., and Bruno, E. (1987) Structural modification in clinopyroxene solid solutions: the Ca-Mg and Ca-Sr substitutions in diopsid structure. Mineralogy and Petrology, 36, 71-84.

Brastad, K. (1985) Sr metasomatism, and partition of Sr between the mineral phases of a meta-eclogite from Bjorkedalen, West Norway. Tschermaks Mineralogische und Petrographische Mitteilungen, 34, 87-103.

Brenan, J.M., Shaw, H.F., Ryerson, F.J., and Phinney, D.L. (1995) Mineral-aqueous fluid partitioning of trace elements at 900 degrees C and 2.0 GPa; constraints on the trace element chemistry of mantle and deep crustal fluids. Geochimica et Cosmochimica Acta, 59, 3331-3350.

Brenan, J.M., and Watson, E.B. (1991) Partitioning of trace elements between olivine and aqueous fluids at high P-T conditions; implications for the effect of fluid composition on trace-element transport. Earth and Planetary Science Letters, 107, 672-688.

Della Ventura, G., and Robert, J.-L. (1990) Synthesis, XRD and FTIR studies of strontium richterites. European Journal of Mineralogy, 2, 171-175.

Gottschalk, M., Najorka, J., and Andrut, M. (1998) Structural and compositional characterization of synthetic (Ca,Sr)-tremolites and (Ca,Sr)-diopsides. Physics and Chemistry of Minerals, in press.

Grapes, R., and Watanabe, T. (1984) Al-Fe^{3+} and Ca-Sr^{2+} epidotes in metagreywacke-quartzofeldspathic schist, Southern Alps, New Zealand. American Mineralogist, 69, 490-498.

Guggenheim, E.A. (1967) Thermodynamics: an advanced treatment for chemists and Ohysicists. Elsevier Science Publishers.

Kotelnikov, A.R., and Chernysheva, I.V. (1995) Excess free energies of mixing of Sr, Ba-bearing binary feldspar solid solutions (experimental data). Mineralogical Magazine, 59, 79-91.

Kotelnikov, A.R., Chernysheva, I.V., Romanenko, I.M., and Tikhomirova, E.I. (1989) Experimental determination of energy of mixing of Ca-Sr- anorthites from data on cation-exchange equilibria. Geochimia, 11, 1575-1586.

Kroll, H., Kotelnikov, A.R., Göttlicher, J., and Valyashko, E.V. (1995) (K,Sr)-feldspar solid solutions: the volume behaviour of heterovalent feldspars. European Journal of Mineralogy, 7, 489-499.

Lagache, M., and Dujon, S.C. (1987) Distribution of strontium between plagioclases and 1 molar aqueous chloride solutions at 600 degrees C, 1.5 kbar and 750 degrees C, 2 kbar. Bulletin de Mineralogie, 110, 551-561.

Melzer, S., Gottschalk, M., Heinrich, W., and Franz, G. (1997) Experimentally determined partioning of RB between richterites and aqueous (Na,K)-chloride solutions. Contributions to Mineralogy and Petrology, submitted.

Ray, G.L., Shimizu, N., and Hart, S.R. (1983) An ion microprobe study of partitioning of trace elements between clinopyroxene and liquid in the system diopside-albite-anorthite. Geochimica et Cosmochimica Acta, 47, 2131-2140.

Robert, J.L., Della Ventura, G., Raudsepp, M., and Hawthrone, F.C. (1993) Rietveld structure refinement of synthetic strontium-rich potassium-richterites. European Journal of Mineralogy, 5, 199-213.

Robie, R.A., Hemingway, B.S., and Fisher, J.R. (1979) Thermodynamic properties of minerals and related substances at 298.15 K and 1 bar (10^5 pascals) pressure and at higher temperatures. US.Geol.Surv.Bull., 1452, 456.

Shannon, R.D. (1976) Revised effective ionic radii and systematic studies of interatomic distances in halides and chalcogenides. Acta Crystallographica Section A, 32, 751-767.

Skulski, T., Minarik, W., and Watson, E.B. (1994) High-pressure experimental trace-element partitioning between clinopyroxene and basaltic melts. Chemical Geology, 117, 127-147.

Theye, T., and Seidel, E. (1988) Fluorine, lithium and strontium metasomatism in high pressure metamorphic rocks, Crete. Fortschritte der Mineralogie, Beiheft 66, 157.

Turekian, K.K., and Wedepohl, K.H. (1961) Distribution of the elements in some major units of the Earth's crust. Geological Society of America Bulletin, 72, 175-96.

Wohl, K. (1946) Thermodynamic evaluationof binary and ternary liquid systems. Trans. Am. Inst. Chem. Eng., 42, 215-249.

Zimmermann, R., Gottschalk, M., Heinrich, W., and Franz, G. (1997a) Experimental Na-K distribution between amphiboles and aqueous chloride solutions, and a mixing model along the richterite – K-richterite join. Contributions to Mineralogy and Petrology, 126, 252-264.

Zimmermann, R., Knop, E., Heinrich, W., Pehlke, I., and Franz, G. (1997b) Disequilibrium in cation exchange experiments between Na-richterite – K-richterite and aqueous solutions: effects of fractional crystallisation. European Journal of Mineralogy, 9, 97-114.

ZUSAMMENFASSUNG

Die Verteilung von Sr und Ca zwischen Tremolit, Diopsid und chloridischer Lösung wurde bei 750°C und 200 MPa untersucht. Die synthetisierten (Sr,Ca)-Tremolite sind bis zu 2000 μm lang und 30 μm breit, (Sr,Ca)-Diopside sind bis zu 150 μm lang und 20 μm breit. Idiomorphe Kornformen, nahezu baufehlerfreie Strukturen sowie chemische Homogenität weisen auf Gleichgewichtsbedingungen in den Versuchen.

Die Sr-Ca-Verteilungskurven der Systeme (Ca,Sr)-Tremolit-Fluid und (Ca,Sr)-Diopsid-Fluid zeigen extreme Abweichungen von der 1:1-Verteilung. Sr fraktioniert hierbei stark in die Fluidphase. Erst bei sehr hohen Sr/Ca-Verhältnissen im Fluid (> 0.8) können signifikante Sr-Gehalte im Tremolit und Diopsid erzeugt werden. Für geringe Sr-Gesamtzusammensetzungen wurden Mineral/Fluid-Verteilungskoeffizienten ($D_{Sr}^{Mineral/Fluid}$) ermittelt, wobei für das (Sr,Ca)-Tremolit/Fluid-System ein $D_{Sr}^{Tremolit/Fluid}$ von 0.045 und für das (Sr,Ca)-Diopsid/Fluid-System ein $D_{Sr}^{Diopsid/Fluid}$ von 0.082 abgeleitet wurde.

Anhand der Austauschreaktionen (1) Tremolit + 2 SrCl$_2$ ↔ Sr-Tremolit + 2 CaCl$_2$ sowie (2) Diopsid + SrCl$_2$ ↔ Sr-Diopsid + CaCl$_2$ wurden die Mischungsparameter für die Mischkristallreihen (Sr,Ca)-Tremolit und (Sr,Ca)-Diopsid berechnet. Die Berechnungen erfolgten unter der Annahme von Henryschen Verhalten für SrCl$_2$ und CaCl$_2$ im Fluid. Die Mischungsenergien der Festkörper wurden mit regulären Mischungsmodellen berechnet. Für die Reaktion (1) wurde ein chemisches Standardpotential $\Delta\mu° = 59.0$ kJ und ein Wechselwirkungsparameter $W_{CaSr}^{Amph} = 9.8$ kJ berechnet, für die Reaktion (2) wurde $\Delta\mu° = 30.8$ kJ und $W_{CaSr}^{Px} = 11.7$ kJ berechnet. Für beide Systeme (Ca,Sr)-Tremolit-Fluid und (Ca,Sr)-Diopsid-Fluid ist das große $\Delta\mu°$ für die starke Fraktionierung von Sr ins Fluid hauptverantwortlich, während der W–Parameter einen geringen Beitrag hierfür liefert. Die kritischen Mischungstemperaturen liegen für die (Ca,Sr)-Tremolit-Mischkristallreihe bei 316°C und für die (Ca,Sr)-Diopsid-Mischkristallreihe bei 430°C. Somit sind unter den experimentellen Bedingungen bei 750°C und 200 MPa keine Mischungslücken zu erwarten.

KAPITEL 3

Crystal chemistry of tremolite-tschermakite solid solutions

ABSTRACT

Tremolite-tschermakite solid solutions have been synthesized between 700-850°C and 200-2000 MPa. The starting materials were oxide-hyroxide mixtures and an additional 0.1-1.8 molal $CaBr_2$-solution. The run products were characterized using SEM, HRTEM, EMP, XRD and FTIR. The synthesized Al-tremolites formed needles and lath shaped crystals of up to 300×20 μm. HRTEM-investigations showed that the majority of the amphiboles were well ordered. The EMP-analysis revealed that the Al-tremolites were solid solutions in the ternary tremolite-tschermakite-cummingtonite. The highest observed Al-content was close to the composition of magnesiohornblende (X_{ts} = 0.54). Different cummingtonite concentrations (X_{cum} = 0.00-0.18) were observed, which generally increased with Al-content.

Rietveld refinements of the lattice constants showed a linear decrease of the cell parameters *a* and *b* with increasing Al-content, whereas *c* and *ß* increased. Small deviations from the linear behavior were caused by variable amounts of the cummingtonite component. For pure tschermakite lattice parameters of *a* = 9.7438(11) Å, *b* = 17.936(14) Å, *c* = 5.2995(3) Å, *ß* = 105.68(9) °, and *V* = 891.7 ± 1.4 Å^3 were extrapolated by least square regression. Using the *a* and *ß* lattice parameters for tremolite, tschermakite and cummingtonite, it was possible to derive amphibole compositions using powder XRD.

IR-spectra of the Al-tremolites showed a total of 12 individual bands. The FWHMs of all bands increased with increasing Al-content. According to their FWHMs, these bands were grouped into three band systems at 3664-3676 cm^{-1} (I), 3633-3664 cm^{-1} (II) and 3526-3633 cm^{-1} (III).

Assuming [6]Al substitution at M2 and/or M3 and [4]Al at T1, three principal different configurational groups could be assigned as local environments for the proton. I: only Si^{4+} at T1 and one or two Al^{3+} at M2 and/or $M3_{far}$, II: one Al^{3+} at T1 and one to three Al^{3+} at M2 and/or at $M3_{far}$, III: either Al^{3+} on $M3_{near}$ and/or two Al^{3+}on T1 and additional one to four Al^{3+} at M2. It is assumed that these three configurational groups correspond to the three groups of observed bands. This was quantitativly supported by Monte-Carlo simulations. A model with random distribution at M2 and M3 including Al-avoidance at tetrahedral and octahedral sites yielded the best agreement with the spectroscopical results.

INTRODUCTION

In rock-forming silicates such as amphiboles, pyroxenes, micas and chlorites the Mg-tschermaks substitution of the type $Mg^{2+} + Si^{4+} \leftrightarrow Al^{3+} + Al^{3+}$ is quite common. Generally the amount of the tschermaks component is controlled by pressure, temperature and bulk composition or is even buffered by a phase assemblage. In the latter case if the thermodynamic properties of this substitution were understood the Al-content could be used for geothermobarometric purposes.

The content of tschermaks component in amphiboles has been studied experimentally by Jasmund and Schäfer (1972), Oba (1978), Cao et al. (1986), Jenkins (1981, 1983, 1988, 1994, 1997), Cho and Ernst (1991), Smelik et al. (1994), Hoschek (1995), Quirion and Jenkins (1998) and Hawthorne et al. (2000) using the simplified system tremolite-tschermakite $(Ca_2Mg_5[Si_8O_{22}/(OH)_2]$ - $Ca_2Mg_3Al_2[Al_2Si_6O_{22}/(OH)_2)])$. The synthetic tremolite-tschermakite crystals were usually very small and the fibrous needles rarely exceeded a thickness of 5 μm. The small grain size made the chemical characterization using the electron microprobe difficult if not impossible. To avoid preparation difficulties, unpolished grain mounts were often used for EMP-analyses (Cao et al. 1986; Jenkins 1988, 1994; Hoschek 1995; Quirion and Jenkins 1998). The precision of this method is rather low and standard deviations are on the order of 5% (Jenkins 1994). Several investigations (Jenkins 1981, 1983, 1988, 1994; Cho and Ernst 1991; Hoschek, 1995) used the d-value variation of the (310) reflection as a function of composition for the determination of the Al-content in tremolite-tschermakite solid solutions. The uncertainty using this approach is also high, however (6 %, Cho and Ernst 1991) and the influence of additional components (e.g. cummingtonite) is generally neglected. Therefore the analytical error in the chemical composition of most of the previously synthesized tremolite-tschermakite solid solutions seems to be large.

In addition to uncertainties in composition, the crystal chemistry of Al^{3+} in tremolite-tschermakite solid solutions has not been resolved univocally. A fragment of the structure of the monoclinic C 2/m amphiboles is shown in Fig. 1. The main feature of the amphibole structure are two double chains of SiO_4 tetrahedra connected by a strip of octahedra which form an *I*-beam in the *z* direction. In tremolite the octahedra sites M1, M2 and M3 are occupied by Mg^{2+}, M4 by Ca^{2+} and the tetrahedra sites T1 and T2 by Si^{4+}. At least theoretically the cation Al^{3+} could occupy the octahedral M1, M2 and M3 and the tetrahedral T1 and T2 sites; it is regarded to be too small for the M4 site.
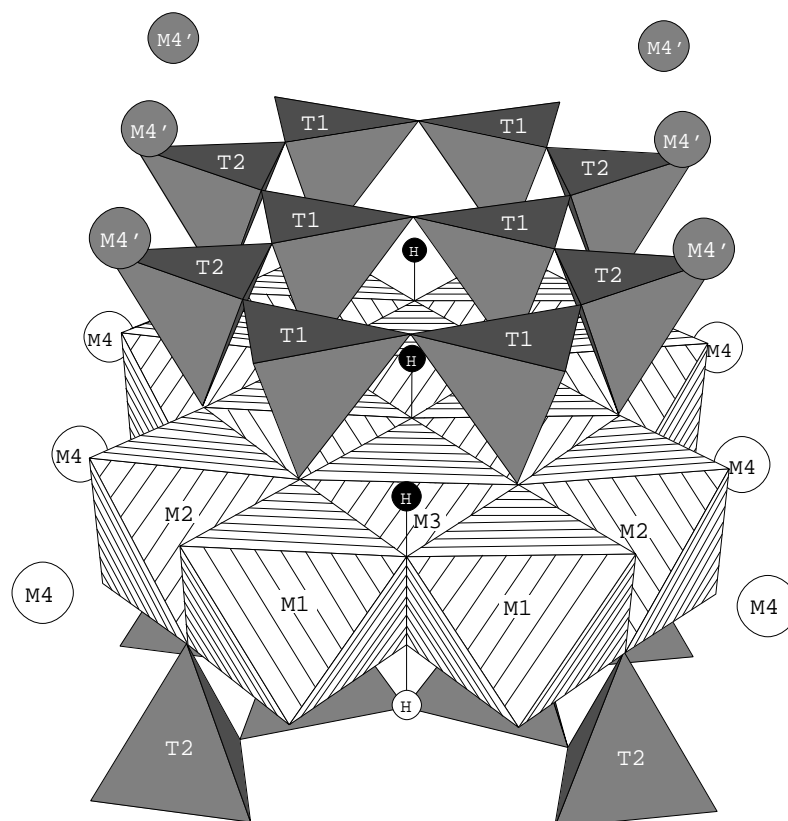
Figure 1. *I*-beam of the C 2/m amphibole structure with surrounding M4 sites. A strip of edge-sharing octahedra is intercalated between two corner-sharing double tetrahedral chains in apex-to-apex arrangement. The M2 and M4 sites provide the linkages to adjacent *I*-beams (after Hawthorne 1983).

Using natural monoclinic amphibole, Hawthorne (1981) deduced from mean bond length *vs*. ionic radius relationships, that octahedral Al^{3+} ([6]Al) is strongly ordered on the M2 site. Recent IR and NMR studies of synthetic pargasites indicated [6]Al disorder over M2, M1 and/or M3 sites (Raudsepp et al. 1987; Welch 1994). A direct [6]Al assignment to M1 or M3 was not possible with these methods, however. Single crystal X-ray structure refinements of natural pargasites and pargasitic hornblendes (Oberti et al. 1995a) showed that octahedral Al^{3+} is distributed over the M2 and M3 sites. This is in accordance with a neutron powder diffraction study of synthetic pargasite (Welch and Knight 1999) and an IR investigation of synthetic richterite-pargasite solid solutions (Della Ventura et al. 1999). In a recent study synthetic tremolite-magnesiohornblende solid solutions were investigated by Hawthorne et al. (2000) using IR and NMR. The IR and NMR spectra showed that [6]Al occupies two different octahedral sites, the M2 site and the M1 or M3 site.

In monoclinic amphiboles tetrahedral Al ([4]Al) is preferentially incorporated on the T1 site (Hawthorne 1981) which was derived from mean bond-length considerations. Oberti et al. (1995b) showed in a single crystal study of calcic amphiboles that for amphiboles with contents of [4]Al < 2 atoms per formula unit (apfu), Al^{3+} strongly prefers the T1 site. However, Al^{3+} on T1 and T2 sites is observed in amphiboles with [4]Al > 2 apfu. Al^{3+} disorder over T1 and T2 sites is also a function of temperature (Oberti et al. 1995b). This is in agreement with ^{29}Si MAS NMR investigations (Welch et al. 1998) of pargasite synthesized at 930°C and 100 MPa. Al^{3+} ordering on the T1 site was observed, however, in fluoro-edenite synthesized at 1000°C and 200 MPa (Welch et al. 1998). A reason for the strong preference of [4]Al to the T1 site could be the underbonded oxygen O4 which is connected to the T2 site. An incorporation of Al^{3+} on T2 would increase the charge deficiency of the O4 bond valence (Oberti et al. 1995b; Welch et al. 1998).

Jenkins et al. (1997) investigated synthetic tremolite-tschermakite solid solutions up to the composition of magnesiohornblende ($Ca_2Mg_4Al[AlSi_7O_{22}/(OH)_2)]$) using EMP, XRD, IR and NMR. This study indicated that Al^{3+} is distributed over all T and M sites in the Al-tremolites. However, a detailed quantitative analysis of the site occupancies for Al^{3+} was not possible.

Difficulties in the determination of site occupancies of Al^{3+} in synthetic Al-tremolites are due mainly to the following reasons. Similar X-ray scattering factors for Al, Si and Mg make site-scattering refinements using XRD-data very difficult if not impossible. The error of the mean-bond lengths (e.g. variations in <T1-O>, <T2-O> distances for [4]Al and variations in <M2-O>, <M3-O> distances for [6]Al) deduced from structure refinements using X-ray powder diffraction (Jenkins et al. 1997) are large. In addition, due to the small grain size of the synthetic tremolite-tschermakite solid solutions, single crystal X-ray diffraction studies of the site occupancies are not possible. And finally, the band broadening of the IR and NMR spectra of Al-rich tremolite makes the quantitative interpretation of Al^{3+} occupancies difficult (Jenkins et al. 1997, Hawthorne et al. 2000).

The derivation of thermodynamic mixing properties, however, requires the knowledge of the crystal chemistry. Especially if these are to be applied over a larger *P-T*-range than obtained experimentally. Entropies of ideal mixing are crucial for the derivation of such models. Therefore, if the amount of tschermaks substitution is to be used as a petrogenetic indicator, a good knowledge of the site occupancies for [4]Al and [6]Al along the tremolite-tschermakite join is needed.

In this study amphiboles along the tremolite-tschermakite join were synthesized in the presence of halogenidic fluids. With this method it was possible to get amphibole crystals that were large enough for electron microprobe measurements (cf. Zimmermann et al. 1996; Gottschalk et al. 1998; Melzer et al. 1998). The synthesized tremolite-tschermakite solid solutions were characterized using scanning electron microscopy (SEM), high-resolution transmission electron microscopy (HRTEM), electron microprobe (EMP), powder X-ray diffraction (XRD) and Fourier transform infrared spectroscopy (FTIR). The combination of results from EMP and XRD were used for the derivation of a more precise method to deduce the compositions of the amphiboles from lattice parameters in the ternary system tremolite-tschermakite-cummingtonite. Quantitative [6]Al site occupancies were derived using IR-spectroscopy of the OH-stretching vibration in conjunction with derived compositions of the tremolite-tschermakite solid solutions.

EXPERIMENTAL AND ANALYTICAL TECHNIQUES

Experimental Methods

The experiments were performed using standard cold-seal hydrothermal and piston cylinder techniques. The hydrothermal experiments were carried out between 700-800°C and 200-500 MPa using H_2O and CO_2 as a pressure medium. Temperatures were measured closely to the sample with a Ni-CrNi thermocouple and were accurate within ±5°C, pressures were measured with a calibrated strain gauge with an precision of ±5 MPa. At the end of each run the samples were quenched isobarically with compressed air. The samples were quenched to 300°C within 3 minutes.

The piston cylinder experiments were performed between 700-850°C and 1150-2000 MPa. The accuracy of the temperature measurement with the Ni-CrNi thermocouple was ±15°C. The pressure uncertainties were ±50 MPa. NaCl ($T < 800$°C) and CaF_2 ($T > 800$°C) assemblies were used. Because of its higher friction for the CaF_2 assemblies the pressure had to be corrected by 10%.

Mixtures of SiO_2, MgO, Al_2O_3 and $Ca(OH)_2$ (analytical grade) and a 0.1-1.8 molal aqueous $CaBr_2$-solution were used as starting materials. The solid/fluid ratio varied between 0.5-3.0. The bulk compositions of the runs were chosen to be close but not on the tremolite-tschermakite join. An excess of SiO_2 (3-8 wt%) was used in order to compensate the

solubility of SiO_2 at *P* and *T* (Manning 1994). The samples for the hydrothermal experiments were sealed in gold capsules of 25-35 × 3 mm with a wall thickness of 0.2 mm. For the piston cylinder runs platinum and gold capsules of 10-12 × 3 mm and a wall thickness of 0.2 mm were used. The charges contained between 30-60 mg solids and 30-60 mg fluid in the hydrothermal runs and between 6-12 mg solids and 2-6 mg fluid in the piston cylinder runs. The run charges and the synthesis conditions of the experiments are listed in Table 1.

Table 1. Run charges and synthesis conditions

run	$Ca(OH)_2$ [mg]	$CaBr_2$ [mg]	MgO [mg]	Al_2O_3 [mg]	SiO_2 [mg]	H_2O [mg]	$CaBr_2$- molality	*T* [°C]	*P* [MPa]	time [days]
TS-6	4.04	1.31	5.22	1.05	14.98	50.91	0.13	750	500	26
TS-15	3.56	5.71	4.61	0.61	11.98	28.56	0.97	750	500	7
TS-16	3.55	5.71	2.91	4.89	9.40	28.55	0.97	750	500	7
TS-18	1.48	1.70	1.47	1.09	4.62	8.49	0.96	800	1500	5
TS-19	1.43	1.70	1.59	0.88	4.74	8.52	0.96	800	1500	5
TS-20	3.70	2.85	4.35	0.75	11.65	14.28	0.94	800	200	7
TS-30	5.15	5.73	5.86	4.11	15.39	28.66	0.96	750	500	14
TS-33	5.59	5.71	6.59	0.89	17.34	28.55	0.95	750	500	30
TS-40	4.68	3.52	5.20	1.34	14.51	17.58	0.94	750	350	17
TS-41	4.69	6.84	5.38	0.97	14.56	34.21	0.97	700	350	27
TS-48	1.54	2.12	1.35	1.09	4.78	10.58	0.97	750	1500	7
TS-50	1.54	2.30	1.36	1.08	5.00	11.53	0.97	750	2000	7
TS-52	1.07	0.97	1.26	0.98	5.25	10.14	0.47	850	1500	5
TS-53	1.05	0.97	1.27	0.97	5.64	10.17	0.47	850	2000	10
TS-54	1.13	1.01	1.28	0.76	4.76	9.92	0.50	800	1500	13
TS-56	2.62	2.35	3.77	1.19	10.73	30.07	0.38	750	350	14
TS-64	4.17	3.75	5.41	1.61	15.74	45.70	0.40	750	200	14
TS-70	1.57	1.49	1.24	1.21	4.95	4.96	1.40	750	1500	7
TS-82	6.82	6.16	9.45	4.22	23.69	25.06	1.15	800	200	14
TS-83	5.85	5.31	11.14	0.56	27.64	25.06	1.00	800	200	14
TS-86	8.19	7.37	12.72	3.91	27.84	19.88	1.69	800	200	14
TS-90	1.48	1.37	2.14	1.35	6.55	5.98	1.08	850	1150	6
TS-91	1.73	1.54	1.56	1.59	6.48	5.97	1.21	850	1150	6
TS-92	1.92	0.92	1.65	2.35	5.55	2.45	1.58	850	1300	8
TS-93	1.69	0.94	2.21	1.40	6.13	2.58	1.57	850	1300	8
STR080	15.12[*]	10.07	14.21	10.27	40.34	28.65	1.76	700	500	14
Tr-II-5[#]	43.43[*]	-	114.15	-	272.38	80.00	0.00	660	700	50

[*]$CaCO_3$ instead of $Ca(OH)_2$, [#]run Tr-II-5 from Gottschalk et al. (2000)

Analytical Methods

The synthesized products were characterized by optical, scanning electron (SEM) and high-resolution transmission electron microscopy (HRTEM), electron microprobe (EMP), powder X-ray diffraction (XRD) and Fourier transform infrared spectroscopy (FTIR).

The SEM and HRTEM investigations were performed using a Zeiss DSM962 scanning electron microscope and a Philips CM200T transmission electron microscope. The EMP-analyses were performed on polished and carbon coated samples with Cameca SX50 and SX100 microprobes. The data were collected in wavelength dispersive spectrometry mode and corrected using the PAP program (Pouchou and Pichoir 1984). The following standards were used: wollastonite for Si and Ca, synthetic plagioclase for Al and natural tremolite for Mg. Peak counting times were 40 sec for Ca and Mg and 20 sec for Si and Al. For the background counting times were 20 and 10 sec, respectively.

For XRD measurements the solid run products were ground in an agate mortar to a grain size of less than 2 μm. The powder was diluted with Elmer´s White glue and mounted on a circular foil. To minimize preferred orientation, the powder was stirred during drying. The foil was then placed into the sample holder and covered with a second empty foil. Powder XRD patterns were recorded in transmission using a fully automated STOE STADI P diffractometer ($Cu_{K\alpha 1}$ radiation), equipped with a primary monochromator and a 7° - wide position sensitive detector (PSD). Operating conditions were 40 kV and 40 mA, with a take off angle of 6°. The spectra were recorded in the range of 5 to 125° (2 θ) using a step interval of 0.1°. The resolution of the PSD was set to 0.02°. Counting times were selected to yield a maximum intensity of 2000 to 3000 counts for each sample, resulting in 5 to 20 sec per detector step. The unit cell and other structural parameters were refined using the *GSAS* software package for Rietveld refinement (Larson and Von Dreele 1987). The isotropic displacement factors of tremolite were fixed at values approximately correct for amphiboles (Della Ventura et al. 1993). The following algorithm was used during the refinement procedure: scale factor, background (real space correlation function), zero-point correction, phase fractions, lattice constants, Caglioti W, preferred orientation, atomic positions, Caglioti U+V, Lorentz LX+LY. Further details of the refinement procedure are described by Gottschalk and Andrut (1998).

IR absorption spectra were recorded in the spectral range of 3500 cm^{-1} to 3800 cm^{-1} with a resolution of 0.25 cm^{-1} using a Bruker IFS 66V FTIR spectrometer equipped with a globar light source, a KBr-beam splitter and a DTGS-detector. The sample chamber was

evacuated to 300 Pa. Transparent pellets (mixtures of 1 mg amphibole and 450 mg KBr) were pressed under vacuum and dried at 170°C for at least 48 hours but typically for several weeks. The spectra were averaged over 1024 scans and evaluated using the program PeakFit™ (SPSS Science). The background was subtracted using in most cases a linear function and only in some cases a cubic function. A combination of a Gaussian and a Lorentzian function with equal full-width at half-maximum (FWHM) was used to fit the bands.

RESULTS

REM

Typical SEM images of the synthesized products are shown in Fig. 2. Amphibole was the principal phase in the experiments and formed idiomorphic needle or lath-shaped crystals with widths of 1-20 μm and lengths of 10-300 μm. In general, the grain size of the amphiboles increased with rising *P-T* conditions as well as with increasing concentration of the bromidic solution. The thinnest amphibole needles were synthesized at 200-500 MPa and 750°C, where the grain width rarely exceeded 3 μm (Fig. 2c). At 800°C and 200 MPa many crystals with a thickness of 5-10 μm were observed (Fig. 2d). High pressures runs between 1.3–2.0 GPa generally yielded large amounts of amphiboles with lath shaped habitus and a thickness of up to 10-20 μm (Fig. 2a-2b). Amorphous SiO_2 was observed in several runs (e.g. Fig. 2b).

HRTEM

Al-tremolites from runs TS-6, TS-15, TS-16, TS-18, TS-19, TS-20, TS-33, TS-41, TS-52, TS-64, TS-93 were investigated by HRTEM. Fig. 3a-3b show representative HRTEM-images of the synthesized amphiboles. The majority of the Al-tremolites were well ordered with only a minor concentration of chain multiplicity faults (≤ 5%). Higher concentrations of chain multiplicity faults (~10%) were observed only in runs TS-15 and TS-33 (Fig. 3b). Fig. 3b shows an Al-tremolite crystal of run TS-33 with 40 double chain units, 3 triple and 2 quadruple chain multiplicity faults. Typically single, triple, quadruple and quintuple chain multiplicities faults were observed. Faults with multiplicities ≥3 occured mostly as isolated
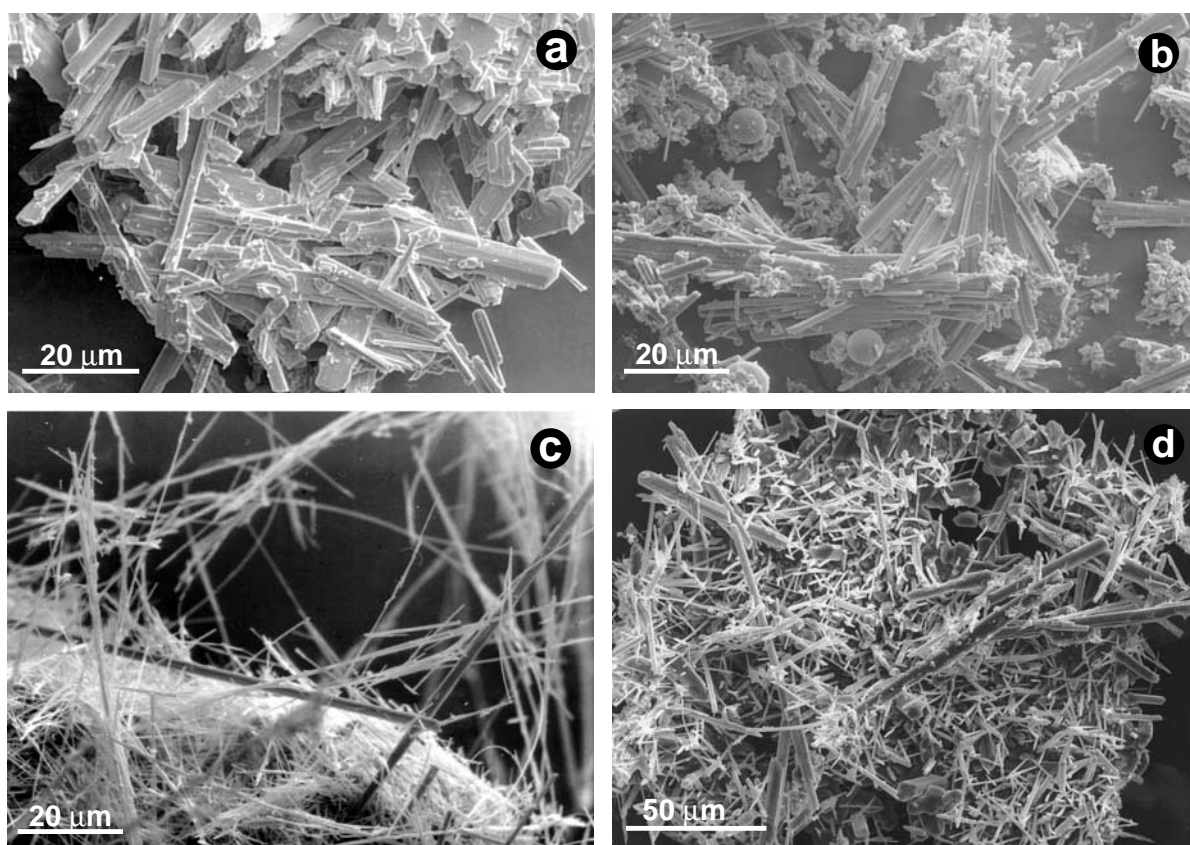
Fig. 2. Typical SEM images of the synthesized amphiboles from high pressure runs (≥ 1150 MPa) a)-b) and low pressure runs (≤ 500 MPa) in c)-d). Lath-shaped amphiboles with **a)** X_{ts} = 0.54 (run TS-93) and **b)** X_{ts} = 0.31 (run TS-70). **c)** amphibole needles from run TS-6 (X_{ts} = 0.22). **d)** needle to lath-shaped amphiboles from run TS-20 (X_{ts} = 0.12).

chains and passed through the whole crystal. High overall chain fault concentrations were often observed to be concentrated in small areas of the crystal.

EMP

Except for the runs TS-6, TS-15, TS-30, TS-40 and TS-83, the compositions of the synthesized amphiboles were determined by EMP. These results are presented in Table 2. The analyses were normalized to 23 oxygens and the cations were distributed according to the formula $AB_2C_5[T_8 O_{22}/(OH)_2]$ (A = vacant; B = Ca, Mg; C = Mg, Al; T = Al, Si). The total Al content was distributed equally (Al^{tot} /2) over the C and T sites, assuming that tschermaks substitution is obeyed. A single analysis was accepted if the total oxide sum was

Table 2. Composition of the synthesized Al-tremolites

| run	TS-16	TS-18	TS-19	TS-20	TS-33	TS-41	TS-48	Ts-50	TS-52	TS-53	TS-54	TS-56	TS-64	TS-70	Ts-82	TS-86	TS-90	TS-91	TS-92	TS-93	STR080
no.of analyses	15	10	3	20	2	3	8	14	23	20	32	7	8	18	12	8	13	9	26	35	23
CaO	12.40	12.21	11.84	13.05	13.27	13.50	13.02	12.97	11.25	13.01	12.85	12.23	11.98	12.76	12.33	12.15	11.85	12.96	12.15	12.20	13.16
MgO	20.63	21.35	21.04	23.22	23.89	22.76	22.24	22.77	22.83	22.69	21.78	23.18	21.79	22.52	24.05	23.69	22.42	21.54	21.07	20.05	21.17
Al_2O_3	10.20	8.33	8.00	2.83	2.76	3.07	6.82	4.91	8.85	6.91	7.81	6.78	3.49	7.79	3.30	4.27	7.96	8.84	11.21	13.36	9.19
SiO_2	51.23	52.52	50.56	56.46	57.60	56.58	54.33	55.68	53.50	54.94	54.35	55.78	51.31	54.93	56.83	56.10	54.37	54.70	52.84	50.81	53.65
Σ oxides	94.45	94.42	91.44	95.56	97.52	95.90	96.41	96.33	96.42	97.54	96.78	97.97	88.56	98.01	96.50	96.21	96.59	98.03	97.27	96.43	97.18
2σ standard deviation of the mean																					
ΔCaO	1.27	0.40	0.79	0.49	0.70	0.97	0.51	0.55	1.58	0.95	0.43	0.53	0.55	0.40	1.06	1.19	0.31	0.22	0.43	1.26	0.41
ΔMgO	2.41	2.11	0.48	1.42	0.54	0.86	1.54	1.33	2.26	1.06	1.29	0.88	1.39	1.06	1.82	1.17	0.85	1.10	1.31	1.20	1.20
$ΔAl_2O_3$	3.77	2.03	1.22	0.87	0.24	0.22	2.14	1.34	2.52	3.85	2.89	2.22	0.49	2.15	1.14	0.60	1.97	2.28	2.93	3.88	2.86
$ΔSiO_2$	3.38	2.70	1.25	2.70	0.80	1.47	3.51	2.66	2.93	1.65	1.63	1.46	3.63	1.88	3.12	3.18	1.81	1.60	1.72	3.17	2.34
amphibole composition based on 23 oxygens																					
Ca	1.86	1.83	1.83	1.93	1.92	1.99	1.91	1.90	1.64	1.89	1.88	1.76	1.92	1.84	1.80	1.78	1.73	1.87	1.76	1.79	1.92
Mg	4.30	4.44	4.53	4.78	4.82	4.67	4.54	4.65	4.64	4.58	4.43	4.64	4.85	4.52	4.89	4.83	4.55	4.32	4.25	4.09	4.29
Al	1.68	1.37	1.36	0.46	0.44	0.50	1.10	0.79	1.42	1.10	1.25	1.07	0.62	1.23	0.53	0.69	1.28	1.40	1.79	2.15	1.47
Si	7.16	7.33	7.30	7.80	7.80	7.79	7.45	7.63	7.29	7.44	7.41	7.49	7.66	7.39	7.76	7.68	7.40	7.36	7.15	6.95	7.29
X_{ts}	0.42	0.34	0.34	0.12	0.11	0.12	0.28	0.20	0.36	0.28	0.31	0.27	0.15	0.31	0.13	0.17	0.32	0.35	0.45	0.54	0.37
$ΔX_{ts}$	0.07	0.04	0.02	0.02	0.00	0.01	0.05	0.03	0.05	0.08	0.06	0.04	0.01	0.04	0.02	0.02	0.04	0.05	0.06	0.07	0.05
X_{cum}	0.07	0.09	0.08	0.03	0.04	0.00	0.04	0.05	0.18	0.06	0.06	0.12	0.04	0.08	0.10	0.11	0.14	0.07	0.12	0.11	0.03
X_{tr}	0.51	0.57	0.58	0.85	0.85	0.87	0.68	0.75	0.47	0.67	0.62	0.61	0.80	0.61	0.77	0.72	0.55	0.58	0.43	0.36	0.60
Σ M4	2.00	2.00	2.00	2.00	2.00	2.00	2.00	2.00	2.00	2.00	2.00	2.00	2.00	2.00	2.00	2.00	2.00	2.00	2.00	2.00	2.00
Σ M1-3	5.00	4.96	5.04	4.94	4.96	4.91	5.01	4.95	4.99	5.02	4.93	4.94	5.07	4.98	4.96	4.96	4.92	4.89	4.91	4.95	4.94
Σ T	8.00	8.02	7.98	8.03	8.02	8.04	8.00	8.02	8.00	7.99	8.04	8.03	7.96	8.01	8.02	8.02	8.04	8.06	8.05	8.02	8.03
Σ cations	15.00	14.98	15.02	14.97	14.98	14.96	15.00	14.98	15.00	15.01	14.96	14.97	15.04	14.99	14.98	14.98	14.96	14.94	14.95	14.98	14.97

$Σ$ M1-3 = Mg − (2 - Ca) + Al / 2; $Σ$ T = Al / 2 + Si; X_{ts} = Al / 4; X_{cum} = (2 − Ca) / 2
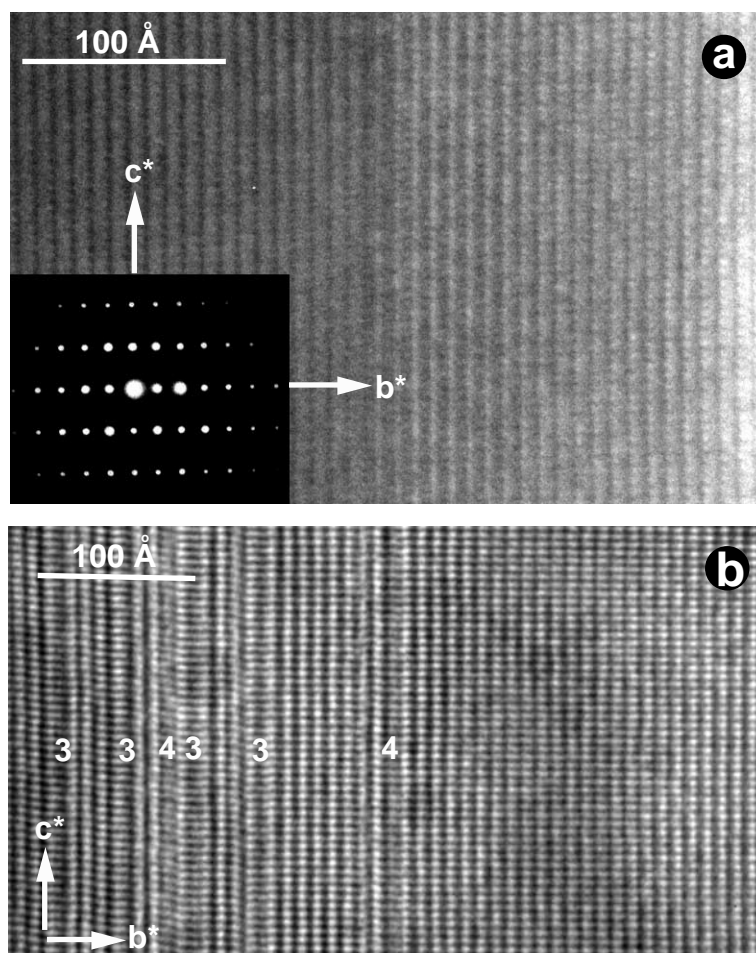
Fig. 3. HRTEM images of (020) lattice fringes of the synthesized amphiboles. **a)** a defect-free amphibole crystal from run TS-19 (X_{ts} = 0.32). **b)** randomly distributed triple and quadruple chains in an amphibole crystal from run TS-33 (X_{ts} = 0.13)

in the range of 91-99 wt%. Because of the small crystal size of the amphiboles in run TS-64, the total oxide sum were mostly below 90 wt%. Therefore, a total oxide sum between 85-99 wt% was accepted for amphiboles from run TS-64. Some analyses showed unusually high T site occupancies larger than 8. From a crystal chemical view, such occupancies are not allowed and are believed to be an analytical artefact. Therefore site occupancies were used as an additional criteria if these deviations were larger than the analytical error (2σ). If the site occupancies exceeded the nominal value by ±1 % on the T sites, ±2 % on the B and C sites and ±0.5 % for the total sum of all cation sites (= 15) the analysis was also rejected.

The average amphibole compositions of the runs are summarized in Table 2 and Fig. 4. The synthesized Al-tremolites are solid solutions of the ternary tremolite-tschermakite-cummingtonite. Along the tschermaks vector $Si_{-1}Mg_{-1}Al_2$, amphibole compositions were between 11 mol% and 54 mol% tschermakite. The Al-richest composition was observed in run TS-93 (X_{ts} = 0.54) which is close to the composition of magnesiohornblende. Ca^{2+} was
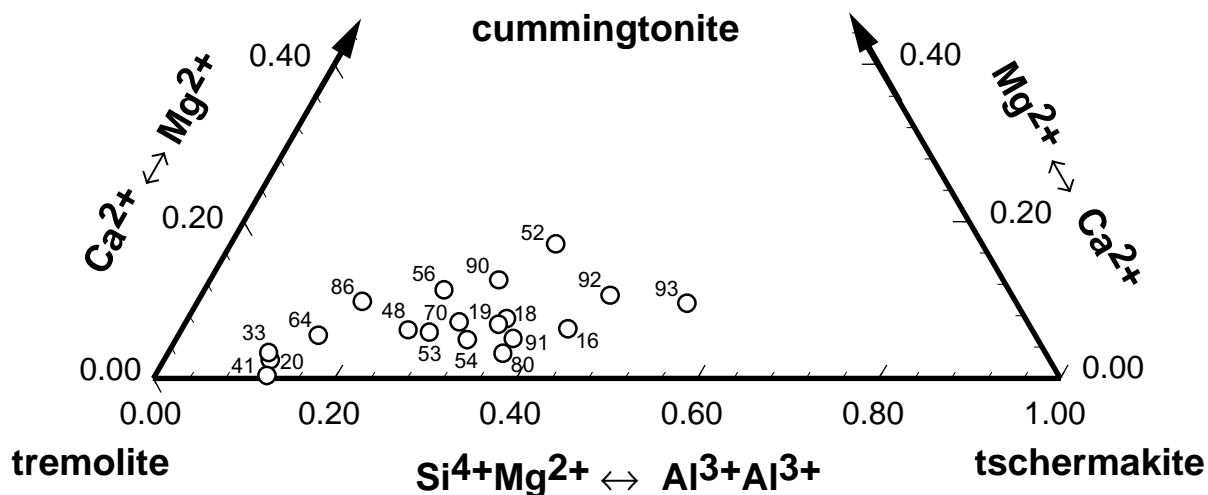
Fig. 4. Average compositions of the Al-tremolites determined by EMP plotted in the ternary tremolite-tschermakite-cummingtonite. The Al-richest amphibole sample with $X_{ts} = 0.54$ (run TS-93) is close to the composition of magnesiohornblende. Variable cummingtonite contents are observed.

replaced, to a small extent, by Mg^{2+} on the M4 site and cummingtonite concentrations of up to $X_{cum} = 0.18$ were observed. The cummingtonite content for most runs was in the range of $X_{cum} = 0.00$-0.10, however. Br-contents were always below the detection limit (< 0.1 wt%).

XRD

A Rietveld structure refinement was performed for each run product. The derived phase proportions and amphibole lattice parameters are presented in Table 3. The amphibole yield was between 40-100 wt %. Up to three additional minor solid phases were detected. These were quartz, anorthite, diopside, talc, chlorite, zoisite and enstatite.

Fig. 5 shows that the lattice parameters of the synthesized amphiboles are a linear function of the Al-content. With increasing amount of Al-substitution in tremolite, the cell parameters *a* and *b* decrease whereas the parameters *c* and *ß* increase. Some variations are observed for the lattice parameters *a* and *ß*. These variations correlate with the amount of cummingtonite component in Al-tremolite (see below). As a result of increasing cummingtonite content the values of the *a* and *ß* parameters decrease.

Table 3. Results of the Rietveld refinement: statistics, phase proportions and lattice constants of the Al-tremolites. X_{ts} XRD is Tschermaks component derived from lattice constant

| run	R_p	R_{wp}	χ^2	DW	phase proportions [wt%]	a [Å]	b [Å]	c [Å]	β [°]	V [Å³]	X_{ts} XRD	X_{ts} EMP
TS-6	0.073	0.054	1.63	1.27	90 amph + 9 di + 1 qtz	9.7860(10)	18.0282(13)	5.2801(3)	104.74(3)	900.9(1)	0.22	-
TS-15	0.057	0.042	1.48	1.32	90 amph + 7 di + 2 qtz + 1 tc	9.8033(2)	18.0356(12)	5.2781(3)	104.78(3)	902.3(1)	0.17	-
TS-16	0.075	0.057	1.63	1.19	40 amph + 24 an + 4 cln	9.7636(2)	17.9990(2)	5.2898(4)	104.90(1)	898.4(2)	0.42	0.42
TS-18	0.067	0.049	1.28	1.59	78 amph + 22 zo	9.7767(7)	18.0099(7)	5.2875(2)	104.84(2)	899.9(1)	0.33	0.34
TS-19	0.061	0.045	1.26	1.58	95 amph + 5 zo	9.7749(9)	18.0055(9)	5.2833(2)	104.82(2)	898.9(1)	0.32	0.34
TS-20	0.073	0.055	1.24	1.66	68 amph + 20 di + 6 qtz + 6 an	9.8138(4)	18.0516(5)	5.2798(1)	104.76(1)	904.5(1)	0.11	0.12
TS-30	0.061	0.045	1.60	1.25	76 amph + 24 an	9.7632(12)	18.0090(18)	5.2835(1)	104.74(1)	898.4(2)	0.32	-
TS-33	0.062	0.046	1.35	1.43	74 amph + 4 qtz	9.8083(8)	18.0434(14)	5.2766(3)	104.76(3)	903.0(1)	0.13	0.11
TS-40	0.063	0.046	1.86	1.20	66 amph + 18 di + 10 an + 6 qtz	9.8009(15)	18.0449(31)	5.2790(7)	104.80(7)	902.6(2)	0.19	-
TS-41	0.062	0.065	1.36	1.38	64 amph + 30 di + 6 qtz	9.8082(12)	18.0423(22)	5.2772(4)	104.80(4)	902.9(2)	0.16	0.12
TS-48	0.059	0.043	1.41	1.44	73 amph + 21 zo + 6 tc	9.7913(6)	18.0178(6)	5.2808(1)	104.86(1)	900.5(1)	0.27	0.28
TS-50	0.065	0.048	1.27	1.57	43 amph + 33 zo + 22 tc + 1 qtz	9.8034(8)	18.0323(10)	5.2817(2)	104.83(4)	902.6(1)	0.20	0.20
TS-52	0.064	0.047	1.34	1.48	99 amph + 1 zo	9.7516(7)	17.9890(8)	5.2836(2)	104.76(2)	896.3(1)	0.39	0.36
TS-53	0.062	0.046	1.27	1.53	59 amph + 34 di + 7 fluorite	9.7913(11)	18.0048(9)	5.2813(2)	104.82(2)	900.1(1)	0.24	0.28
TS-54	0.080	0.058	1.31	1.49	91 amph + 9 zo	9.7850(7)	18.0126(6)	5.2835(1)	104.90(1)	899.9(1)	0.33	0.31
TS-56	0.072	0.054	1.42	1.41	74 amph + 11 qtz + 11 an + 4 tc	9.7790(8)	18.0276(17)	5.2805(4)	104.72(4)	900.4(1)	0.24	0.27
TS-64	0.078	0.059	1.43	1.37	67 amph + 24 an + 9 qtz	9.7976(7)	18.0371(13)	5.2787(3)	104.75(3)	902.1(1)	0.18	0.15
TS-70	0.047	0.035	1.37	1.41	63 amph + 29 zo + 6 qtz + 2 tc	9.7822(5)	18.0119(7)	5.2816(1)	104.84(1)	899.6(1)	0.30	0.31
TS-82	0.059	0.043	1.29	1.47	69 amph + 21 an + 8 en + 2 qtz	9.7874(5)	18.0373(7)	5.2777(2)	104.65(2)	901.4(1)	0.16	0.13
TS-83	0.069	0.051	1.26	1.57	80 amph + 13 qtz + 7 en	9.8024(5)	18.0450(6)	5.2767(2)	104.64(2)	903.0(1)	0.08	-
TS-86	0.068	0.050	1.36	1.52	70 amph + 18 en + 12 an	9.7949(4)	18.0391(5)	5.2800(1)	104.75(1)	902.2(1)	0.19	0.17
TS-90	0.058	0.042	1.27	1.55	97 amph + 2 en + 1 tc	9.7601(5)	18.0071(8)	5.2830(2)	104.75(2)	897.9(1)	0.34	0.32
TS-91	0.057	0.042	1.23	1.54	100 amph	9.7694(5)	18.0011(9)	5.2827(2)	104.87(2)	897.9(1)	0.37	0.35
TS-92	0.070	0.051	1.49	1.38	100 amph	9.7480(5)	17.9821(8)	5.2898(2)	104.83(2)	896.4(1)	0.44	0.45
TS-93	0.065	0.046	1.44	1.34	78 amph + 18 an + 4 cor	9.7457(8)	17.9610(11)	5.2903(3)	104.93(3)	894.8(1)	0.52	0.54
STRO80	0.063	0.047	1.47	1.36	69 amph + 24 an + 7 tc	9.7740(7)	17.9961(10)	5.2848(2)	104.87(2)	898.4(1)	0.36	0.37
TR-II-5	0.083	0.064	1.31	1.56	95 amph + 4 di + 1 qtz	9.8364(5)	18.0540(8)	5.2768(2)	104.73(2)	906.3(1)	0.00	0.00

note: $R_p = \sum |y_i^{obs} - y_i^{calc}| / \sum y_i^{obs}$, $R_{wp} = \sqrt{\sum w_i (y_i^{obs} - y_i^{calc})^2 / \sum w_i (y_i^{obs})^2}$, $\chi^2 = \sum w_i (y_i^{obs} - y_i^{calc})(N - P)$, y: intensity, w: 1/y weighting factor

N-P: observations (step intervals) – least square parameters, DW: Durbin-Watson statistics

abbrevations: amph amphibole, di diopside, qtz quartz, tc talc, zo zoisite, en enstatite, cor corundum.

*Fluorite content in run TS-53 was caused by impurity induced from the pressure medium after experiment.
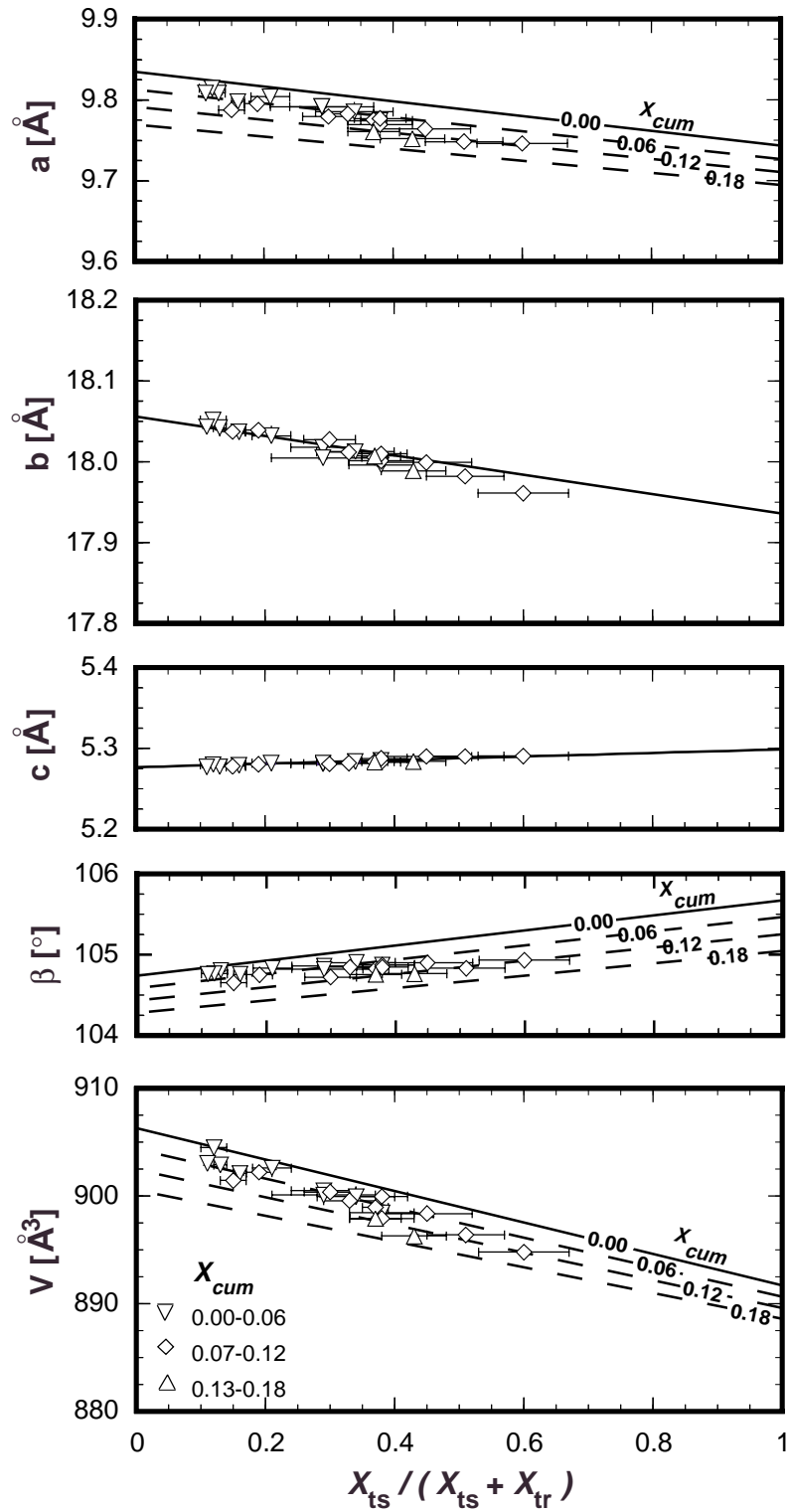
Fig. 5. Lattice constants *a*, *b*, *c*, *β* and cell volume *V* of the synthesised Al-tremolites as a function of X_{ts} / (X_{ts} + X_{tr}) determined by EMP. Cummingtonite isopleths are shown as solid lines for X_{cum} = 0.00 and as dashed lines for X_{cum} = 0.06, 0.12 and 0.18.

IR

Powder spectra were recorded in the range of OH-stretching vibrations between 3500-3800 cm^{-1} and are shown in Fig. 6. Only samples with > 70 wt% amphibole and < 5 wt% of additional OH-bearing phases (chlorite, talc, zoisite) are shown. Starting from tremolite systematic variations are observed with increasing Al-content. A sharp band at 3675 cm^{-1} is visible in Al-poor tremolites. This band is known as the typical band of tremolite (e.g. Burns and Strens 1966). With increasing Al-content in tremolite, the intensity of this band decreases, the band center shifts to 3672 cm^{-1}, the full width at half maximum (FWHM) increases and additional bands centered at 3652, 3624 and 3608 cm^{-1} appeared. With increasing Al-content, the intensity and FWHM of these bands increase. Due to this broadening for Al-rich amphiboles ($X_{ts} > 0.30$) many bands overlaped.

DISCUSSION

Phase composition and XRD

The EMP data show that the synthesized amphiboles are solid solutions in the ternary system tremolite-tschermakite-cummingtonite. A continuous solid solution series along the tremolite-tschermakite join up to roughly magnesiohornblende composition ($X_{ts} = 0.50$) with a maximum tschermakite content of $X_{ts} = 0.54$ was observed. Amphiboles with higher tschermakite contents could not be synthesized. This is in aggreement with previous experimental studies (Cao et al. 1986; Jenkins 1988; Cho and Ernst 1991; Smelik et al. 1994; Hoschek 1995; Jenkins et al. 1997). Cho and Ernst (1991) synthesized amphiboles at 1250 MPa and 900 °C containing up to 60 mol% tschermakite. Oba (1978) has claimed to have synthesised pure tschermakite at 800-850°C and 700-1700 MPa. However, this has never been reproduced (Jenkins 1988). Other syntheses with higher Al-contents have not been reported yet. The crystal-chemical constraints for this limitation on the Al-content is unknown. Only 1/8 of all tetrahedral sites or only one quarter of the T1 sites are filled with Al^{3+} in magnesiohornblende and therefore Al-avoidance seems not to be ultimatively involved. One may also speculate that the observed maximum Al-content is not a rigid crystal chemical constraint but is due to systematic changes of the thermodynamic properties. Tremolite-tschermakite solid solutions could be just less stable with respect to
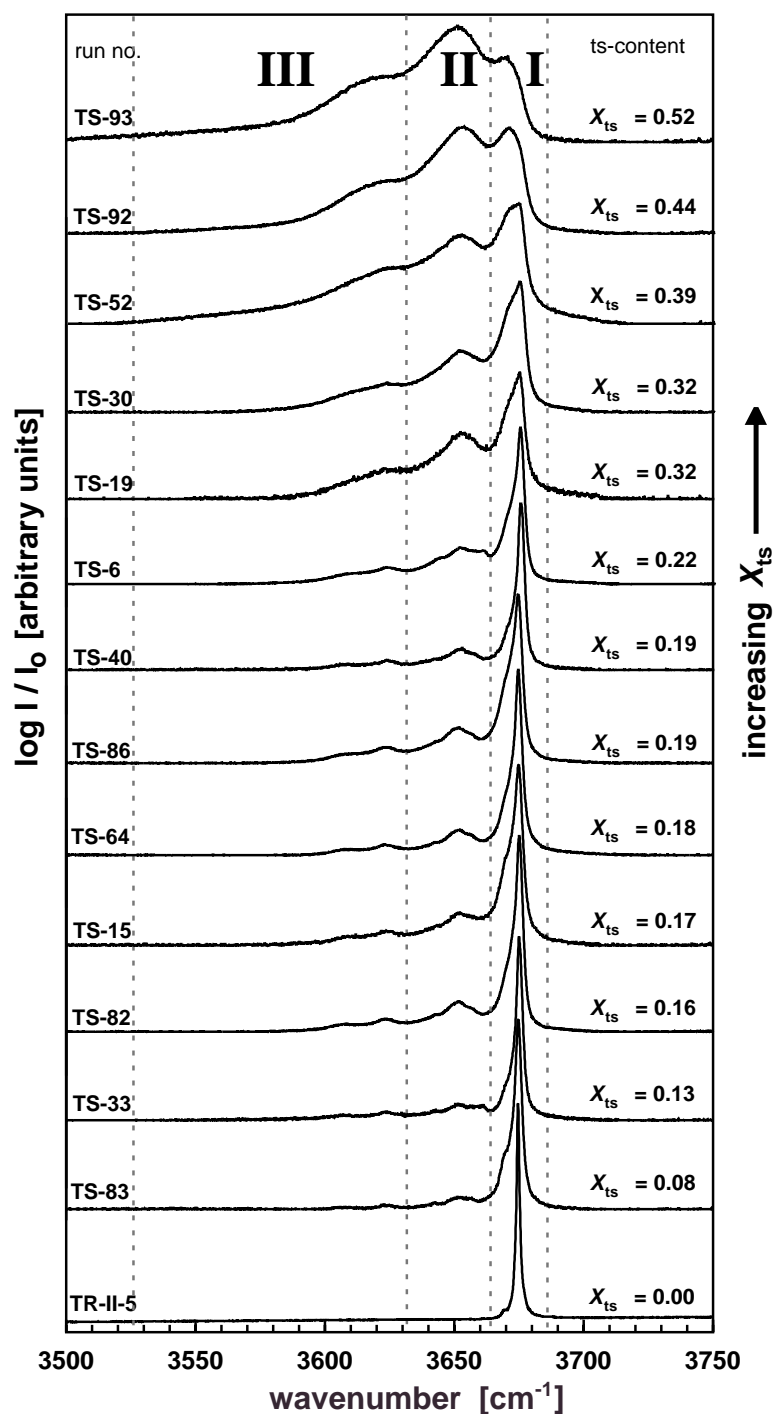
Fig. 6. FTIR-spectra of the OH-stretching vibration of Al-tremolites (background subtracted). The spectra are sorted with increasing values of X_{ts}, derived from XRD-data. The sharp band in Al-poor tremolites at 3675 cm^{-1} decreases with increasing X_{ts} and new bands appear at 3652, 3624 and 3608 cm^{-1}. The FWHM´s of all bands increase with increasing X_{ts}. 3 band regions were distinguished at 3664-3676 cm^{-1} (I), 3633-3664 cm^{-1} (II) and 3526-3633 cm^{-1} (III) (see text).

other assemblages containing phases like anorthite, corundum and melt. For otherwise fixed phase assemblages, the cummingtonite-content of the amphibole (Gottschalk et al. 1999) increases with temperature. This seems also to be the case for the tschermakite-content. In this case before higher Al-contents are reached the amphibole decomposes to form a partial melt.

The measured cummingtonite concentrations were in the range of 0-18 mol%. At a constant tschermakite content large variations in cummingtonite component were observed (Table 2, Fig. 4). In general cummingtonite concentrations increased with increasing tschermakite content. As a consequence of the observed increasing cummingtonite content phases like diopside, anorthite and zoisite become more abundant.

Cummingtonite as an additional component in synthetic tremolitic and richteritic amphiboles is widely observed (e.g. Jenkins 1987; Graham et al. 1989; Pawley et al. 1993; Smelik et al. 1994; Melzer et al. 2000) and concentrations of up to 10 mol% have been reported (Jenkins 1987). Because EMP analyses are often lacking a cummingtonite content of 10 mol% had been assumed in synthetic Al-tremolites (Jenkins 1994; Quirion and Jenkins 1998; Hawthorne et al. 2000).

The lattice parameters of the synthesized amphiboles are a systematic function of the Al-content (Fig. 5) and cummingtonite concentration (Gottschalk et al. 1999). The a, b and β parameters of cummingtonite are significantly lower than those of tremolite. Therefore variations in lattice parameters (Fig. 5) are due to variations in cummingtonite content. It has been shown by Gottschalk et al. (1999) that for the system tremolite-cummingtonite the lattice parameters are a linear function of composition. Assuming that the lattice parameters are also a linear function of the Al-content and using the respective values for pure tremolite (Gottschalk et al. 1999) and cummingtonite (Hirschmann et al. 1994) the values $a = 9.7438(11)$ Å, $b = 17.936(14)$ Å, $c = 5.2995(3)$ Å, $\beta = 105.68(9)$ °, and $V = 891.7 \pm 1.4$ Å^3 for tschermakite were obtained by least square regression and eqs. (1)-(4) can be used to calculate the lattice parameters of tremolite-tschermakite-cummingtonite solid solutions.

$$a\,[\text{Å}] = 9.8354\,X_{tr} + 9.7438\,X_{ts} + 9.4700\,X_{cum} \qquad r^2 = 0.999994 \qquad (1)$$

$$b\,[\text{Å}] = 18.0562\,X_{tr} + 17.936\,X_{ts} + 17.925\,X_{cum} \qquad r^2 = 0.999997 \qquad (2)$$

$$c\,[\text{Å}] = 5.2768\,X_{tr} + 5.2995\,X_{ts} + 5.2700\,X_{cum} \qquad r^2 = 0.999999 \qquad (3)$$

$$\beta\,[°] = 104.74\,X_{tr} + 105.68\,X_{ts} + 102.18\,X_{cum} \qquad r^2 = 0.999996 \qquad (4)$$

The high correlations of the linear regressions ($r^2 > 0.999$) supports the assumption that the lattice parameters are in fact a linear function of the composition. Jenkins (1994) extrapolated a similar cell volume of $892.9 \pm 1.2 \, \text{Å}^3$ for tschermakite endmember. The results of the regression are also plotted in Fig. 5 which demonstrates that the lattice parameters a and β are also sensitive to the cummingtonite content of the solid solution.

Because of their small grain size, compositions of synthetic tremolite-tschermakite solid solutions often have been determined by XRD using the location of the (310) reflection (Jenkins 1981, 1983, 1988; Cho and Ernst 1991; Hoschek 1995). The location of the (310) reflection calculated using eqs. (1)-(4) for cummingtonite contents of 0 and 10 mol% and the calibration curves used by Jenkins (1988), Cho and Ernst (1991) and Hoschek (1995) are shown in Fig. 7. These calibration curves coincide with the calculated line for a cumming-
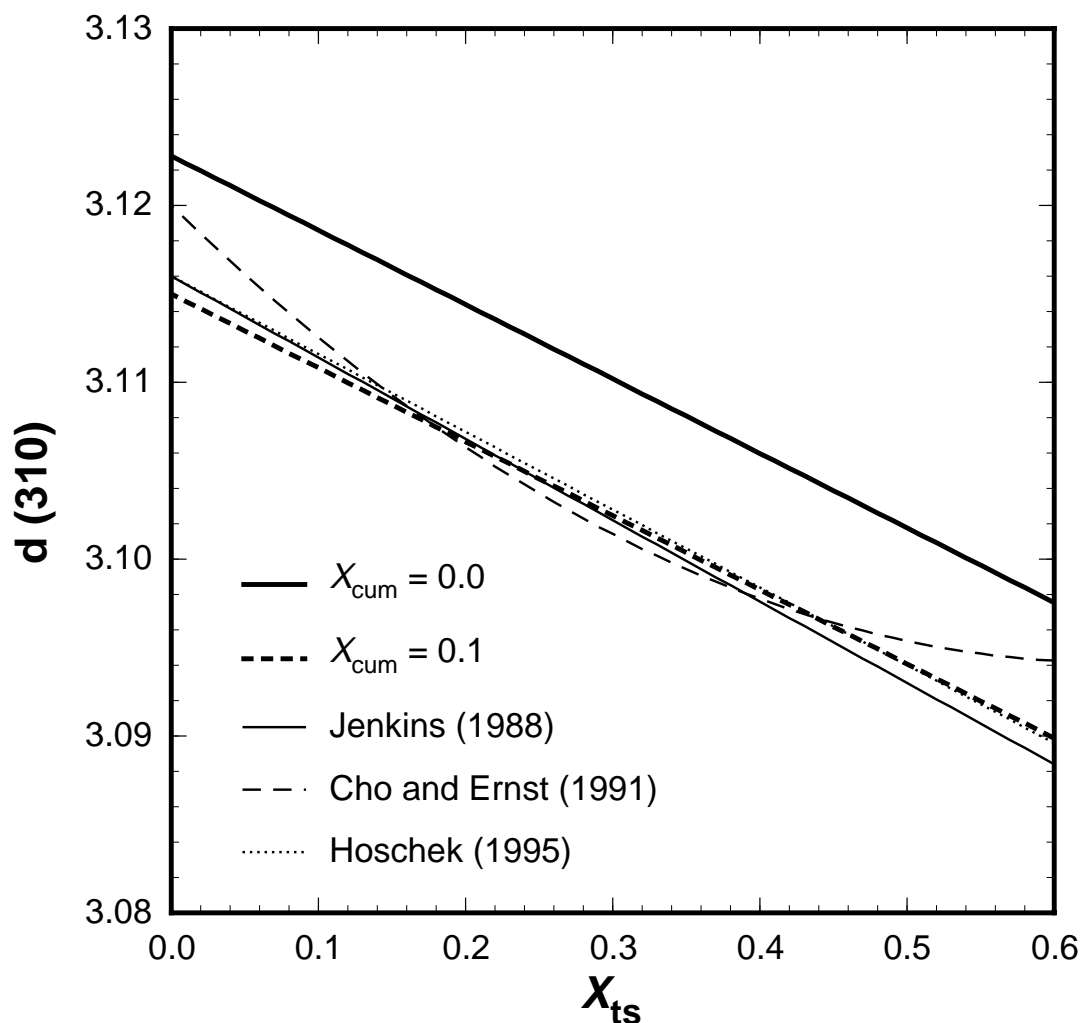
Fig. 7. Variation of the d(310) reflection with composition of Al-tremolites.

tonite content of 10 mol%. If these later curves were used for amphiboles with lower cummingtonite contents, the tschermakite content would be severely underestimated. If the cummingtonite content is 0 instead of 10 mol%, the so derived tschermakite content will be 18 mol% too low using the calibration curves previously available.

A better way to determining compositions by XRD is the use of the compositional dependence of the lattice parameters. The lattice parameters a and β are sensitive to both the tschermakite and cummingtonite content. While a decreases with increasing tschermakite and increasing cummingtonite content, β shows a contrary behaviour for both components. The combination of eqs. (1) and (4) yields expressions for the composition of an amphibole sample, if its lattice parameters are known, on the tremolite-tschermakite-cummingtonite ternary:

$$X_{ts} = \frac{\left(a_{sample} - a_{cum}\right)\left(\beta_{tr} - \beta_{cum}\right) - \left(a_{tr} - a_{cum}\right)\left(\beta_{sample} - \beta_{cum}\right)}{\left(a_{tr} - a_{cum}\right)\left(\beta_{cum} - \beta_{ts}\right) - \left(a_{cum} - a_{ts}\right)\left(\beta_{tr} - \beta_{cum}\right)} \tag{5}$$

$$X_{tr} = \frac{\left(a_{sample} - a_{cum}\right)\left(\beta_{ts} - \beta_{cum}\right) - \left(a_{ts} - a_{cum}\right)\left(\beta_{sample} - \beta_{cum}\right)}{\left(a_{ts} - a_{cum}\right)\left(\beta_{cum} - \beta_{tr}\right) - \left(a_{cum} - a_{tr}\right)\left(\beta_{ts} - \beta_{cum}\right)} \tag{6}$$

$$X_{cum} = \frac{\left(a_{sample} - a_{tr}\right)\left(\beta_{tr} - \beta_{ts}\right) - \left(a_{tr} - a_{ts}\right)\left(\beta_{sample} - \beta_{tr}\right)}{\left(a_{tr} - a_{ts}\right)\left(\beta_{ts} - \beta_{cum}\right) - \left(a_{ts} - a_{cum}\right)\left(\beta_{tr} - \beta_{ts}\right)} \tag{7}$$

Oba (1978) presented lattice constants of several tschermakites which were synthesised between 800-850°C and 700-1700 MPa. The composition of these tschermakites were evaluated using the a-β relationship of equations (5) - (7). The derived tschermaks contents were between $X_{ts} = 0.36 - 0.55$. This is a strong indication that pure tschermakite was not synthesised in this study. In Fig. 8 the mean <M-O> and <T-O> bond distances for the synthesized amphiboles are shown. Run TS-16 yielded only 40 wt% amphibole and runs TS-30 and TS-40 had values for the Durbin-Watson statistics below 1.25. Because of uncertain errors in the bond distances they are omitted in Fig. 8. Due to the preferred orientation of the samples and the fact that they did not consist of a single phase, errors of the mean bond distances are relatively high. Nevertheless the following can be deduced. The <M1-O> and <T2-O> distances for the synthesized amphiboles are constant within error (2σ). The <M2-O>, <M3-O> and <M4-O> distances decrease whereas the <T1-O> distance increases with
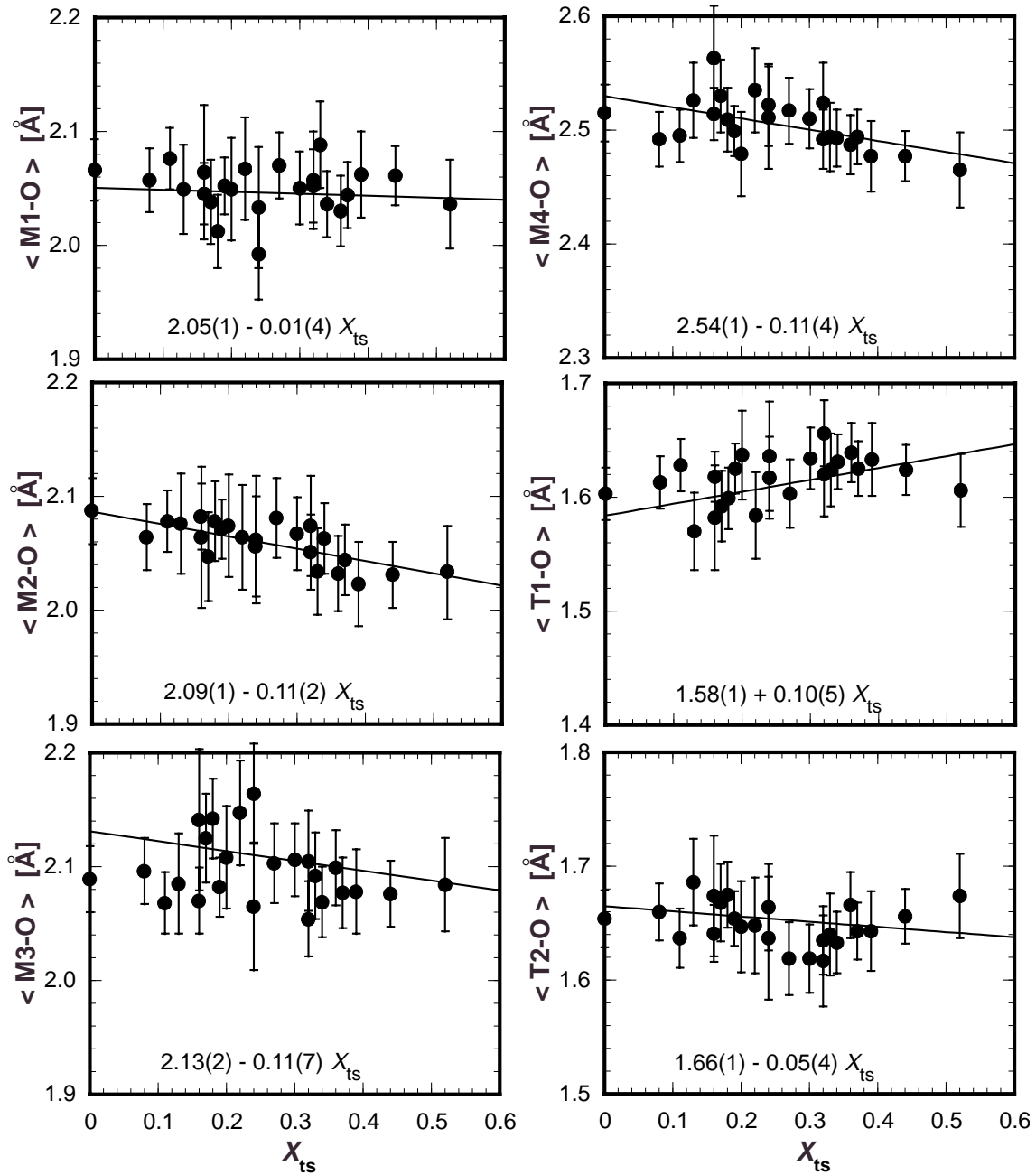
Fig. 8. Variation in individual <M-O> and <T-O> bond distances as a function of the composition of the Al-tremolites.

increasing Al-content. This can be interpreted by the M1 and the T2 sites always being occupied by Mg^{2+} and Si^{4+}, respectively. Whereas substitution of Al^{3+} for Mg^{2+} occurs on the M2 and M3 sites. This leads to a decrease of the M2 and M3 mean bond distances because of the smaller cation radius of Al^{3+}. Al^{3+} is substituted for Si^{4+} on the T1 site which leads to an increase in the mean bond distance because Al^{3+} is larger than Si^{4+}. Increasing Mg^{2+} for Ca^{2+} on M4 (cummingtonite content) which is correlated with the Al-content (Fig. 4) leads to a decrease in the mean bond distance for the M4 site.

IR

OH-stretching vibration and occupancy of sites

The frequency of the fundamental OH-stretching vibration is a function of the local charge distribution in the neighbourhood of the proton (Burns and Strens 1966; Hawthorne 1981). The cation sites in the vicinity of the proton are illustrated in Fig. 9. This figure shows the central layer of octahedral sites within the amphibole *I*-beam, the tetrahedra belonging to the upper $(Si,Al)_4O_{11}$ chain, the M4-sites belonging to this *I*-beam and the upper left and right neighbour *I*-beams (M4'). The tetrahedra of the lower double chain are
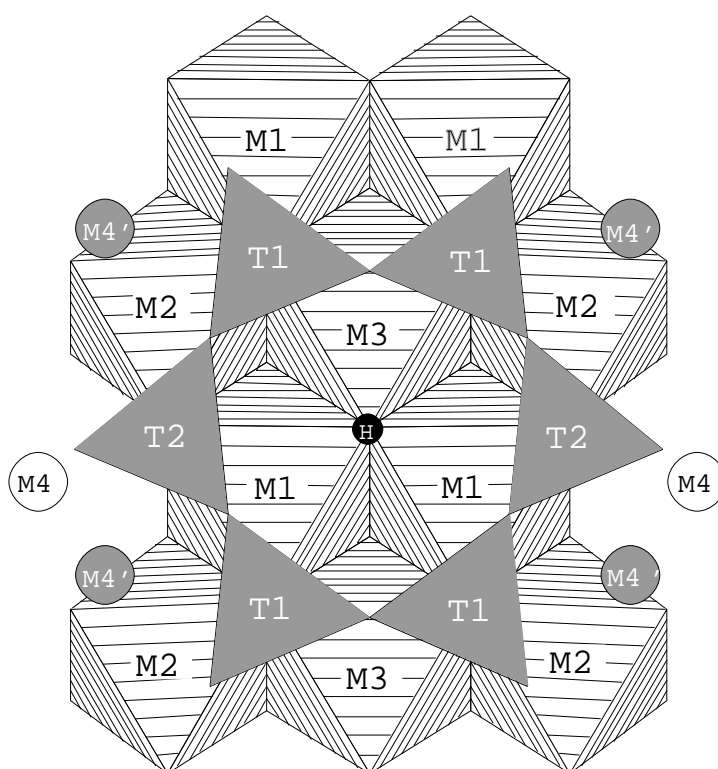
Fig. 9. Local environment of the proton in the tremolite structure. The M4 sites (white) are on a level with the octahedral strip. The M4' sites (grey) belong to adjacent upper left and right neighbour *I*-beams.

not shown because the effect of any variation in charge distribution in this chain which could influence the vibration of the upper proton is, as a first approximation, shielded by the octahedral chain. In the following, proton-cation distances up to 6 Å were considered which

are calculated using the structure of tremolite as determined by Hawthorne and Grundy (1976) (cf. Table 4). These distances range between 2.67 and 5.81 Å. It must be noted that several sites (e.g. M2, M3, M4) occur with different distances in the immediate vicinity of the proton. In tremolite, cations in the immediate vicinity of the proton are Mg^{2+} on M1, M2 and M3, Ca^{2+} on M4 and Si^{4+} on T1 and T2 sites. The corresponding band is located at 3675 cm-1 (Burns and Strens 1966). If cations with other radii and charges are substituted on these sites, the band position for this local configuration will be different. In solid solutions various

Table 4. Cation-proton distances up to 6 Å in tremolite (Hawthorne and Grundy, 1976)

proton distance to	near [Å]	far [Å]
M1	2.692	5.105
M2	4.164	5.144
M3	2.670	4.032
M4	5.465	-
M4´	5.318	5.812
T1	3.120	3.126
T2	3.183	-

configurations occur simultaneously and various bands are observed (e.g. Burns and Strens 1966; Della Ventura et al. 1999; Gottschalk et al. 1998, 1999; Hawthorne et al. 2000). The absorbance of such bands will be proportional to the probability of its corresponding configuration. If the absorbance of each band is evaluated, then the probability of each configuration and therefore the site occupancies can be determined. The problem is the effective size of the configuration shell, the assignment of a band to a certain configuration, and the wavenumber dependency of the absorbency, however.

Band positions

A detailed inspection of the IR-spectra in range of the OH-stretching vibrations revealed that the observed bands, centred at 3675, 3652, 3624 and 3608 cm^{-1}, had shoulders and/or were asymmetric. By fitting the spectra to symmetric bands of a gaussian-lorentzian character up to 12 individual bands could be identified which are listed in Table 5. The identified bands had within each sample a variety of different FWHMs which increased with decreasing wavenumber and generally increased with increasing Al-content. In addition the absorbance of some bands increased with Al-content while others decreased. According to their FWHMs the bands were grouped into three band systems which were located between 3664-3676 cm^{-1} (I), 3633-3664 cm^{-1} (II) and 3533-3625 cm^{-1} (III). To simplify the process of the quantification and interpretation of the bands, the FWHMs within each band system were constrained to one single value. With this constrain it was possible to get consistent band positions also for the band systems with high FWHMs (II + III) along the whole solid solution series. Band positions, relative integral absorbances and FWHMs of the detected bands are shown Table 5. The fitted bands for the runs TS-30, TS-64, TS-92 and TS-93 with different Al-contents are shown in Fig. 10.

Local configurations

Previous studies concluded that Al^{3+} in octahedral coordination ([6]Al) either predominantly occupies only the M2 (Hawthorne 1981, 1983), the M2 and M1/M3 (Raudsepp et al. 1987; Welch 1994) or the M2 and M3 sites (Oberti et al. 1995a; Welch and Knight 1999; Della Ventura et al. 1999; Hawthorne et al. 2000). Jenkins et al. (1997) concluded from their ^{29}Si NMR spectra that Al^{3+} is equally distributed between the T1 and T2 sites. According to Hawthorne (1981, 1983) and Welch et al. (1998), tetrahedral Al ([4]Al) is preferentially incorporated at the T1 site. Oberti et al. (1995b) observed that high Al contents ([4]Al > 2 apfu) and equilibration at high temperatures lead to increasing [4]Al occupancies at T2.

For the following considerations it is assumed that in the tremolite-tschermakite solid solution [6]Al occupies either only the M2 or the M2 and M3 sites. The M1 site will always be filled by Mg^{2+}. Synthesis temperatures were below 850°C and the maximum [4]Al contents was 1.04 apfu. Therefore it has been assumed that [4]Al is preferentially located at the T1 site. For simplicity the substitution of Mg^{2+} for Ca^{2+} on the M4 site (cummingtonite component) is neglected. The resulting relevant cluster is shown in Fig. 11 and contains four

Table 5. Data of the OH-stretching vibration of the synthesised Al-Tremolites. Position, relative absorbance, full with at half maximum (FWHM) of fitted bands. Runs are listed with increasing X_{ts}, derived from XRD-data.

| run		TS-83	TS-33	TS-82	TS-15	TS-64	TS-86	TS-40	TS-6	TS-19	TS-30	TS-52	TS-92	TS-93
X_{ts}		0.08	0.13	0.16	0.17	0.18	0.19	0.19	0.22	0.32	0.32	0.39	0.44	0.52
Band system I														
Band A	[cm⁻¹]	3674.7	3675.1	3674.9	3675.1	3675.0	3674.9	3675.3	3675.0	3675.0	3675.1	3674.9	3674.9	3675.4
rel. absorb.	[%]	58.2	50.9	35.6	38.5	46.8	31.9	45.0	26.9	17.0	17.0	9.8	6.3	2.7
Band B	[cm⁻¹]	3671.7	3672.1	3671.9	3672.1	3671.9	3671.7	3672.2	3671.9	3672.0	3671.9	3671.7	3672.4	3672.4
rel. absorb.	[%]	10.1	6.4	9.5	10.8	9.1	11.7	9.2	9.5	7.9	9.1	5.0	4.5	3.7
Band C	[cm⁻¹]	3669.1	3669.6	3669.4	3669.5	3669.5	3669.1	3669.5	3669.2	3669.2	3669.1	3669.3	3669.4	3669.5
rel. absorb.	[%]	10.6	4.9	9.4	7.2	7.4	9.0	6.4	6.7	6.7	7.6	4.3	6.5	3.1
Band D	[cm⁻¹]	3666.3	3667.4	3666.5	3666.5	3666.6	3665.9	3666.2	3666.1	3666.0	3665.8	3666.2	3665.5	3665.5
rel. absorb.	[%]	2.2	0.7	3.3	2.8	2.2	3.4	2.0	2.3	2.6	3.3	2.6	3.3	2.5
FWHM A-D	[cm⁻¹]	3.2	2.9	3.9	3.3	3.5	3.8	3.2	3.5	4.6	4.6	5.4	6.5	7.6
Band system II														
Band E	[cm⁻¹]	3660.7	3658.6	3661.4	3660.2	3659.7	3660.6	3660.7	3660.3	3660.2	3661.3	3660.9	3660.5	3660.3
rel. absorb.	[%]	3.4	7.0	8.1	6.3	4.2	6.9	4.6	9.5	11.3	11.4	12.6	12.8	9.0
Band F	[cm⁻¹]	3651.9	3651.3	3651.6	3650.9	3651.6	3651.1	3651.6	3651.7	3651.9	3651.0	3651.4	3651.9	3652.5
rel. absorb.	[%]	8.7	12.1	13.8	13.3	15.2	14.1	12.1	15.2	24.2	16.8	18.0	19.8	17.5
Band G	[cm⁻¹]	3641.1	3640.8	3640.5	3640.0	3640.7	3640.5	3640.6	3641.6	3641.6	3640.1	3641.3	3641.2	3641.9
rel. absorb.	[%]	2.8	4.9	5.5	5.6	4.9	6.4	5.0	8.3	8.6	7.3	7.4	9.0	9.5
FWHM E-G	[cm⁻¹]	10.2	11.4	11.9	10.9	11.0	11.3	10.2	12.3	15.0	13.0	15.7	16.0	16.9
Band system III														
Band H	[cm⁻¹]	3623.7	3623.7	3624.1	3624.2	3623.9	3624.5	3624.2	3624.5	3624.2	3624.8	3625.4	3625.1	3624.8
rel. absorb.	[%]	2.6	7.3	9.9	10.3	6.6	11.0	10.6	13.4	16.7	19.1	22.0	24.5	31.0
Band I	[cm⁻¹]	3607.2	3607.0	3608.4	3607.1	3608.3	3607.9	3607.0	3607.4	3608.0	3606.8	3607.9	3608.2	3607.0
rel. absorb.	[%]	1.3	5.0	4.8	5.3	3.7	5.6	5.2	6.8	5.1	8.5	9.0	8.7	10.5
Band J	[cm⁻¹]											3583.4	3578.3	3567.9
rel. absorb.	[%]											5.7	3.2	7.1
Band K	[cm⁻¹]											3555.4	3552.9	3526.3
rel. absorb.	[%]											3.4	1.4	3.4
FWHM H-K	[cm⁻¹]	7.2	10.9	15.2	15.4	12.8	15.8	14.5	19.4	26.9	25.7	34.5	35.8	42.5
Triple chain band														
	[cm⁻¹]		3660.8						3660.8					
rel. absorb	[%]		0.8						1.4					
FWHM	[cm⁻¹]		2.8						3.8					

96
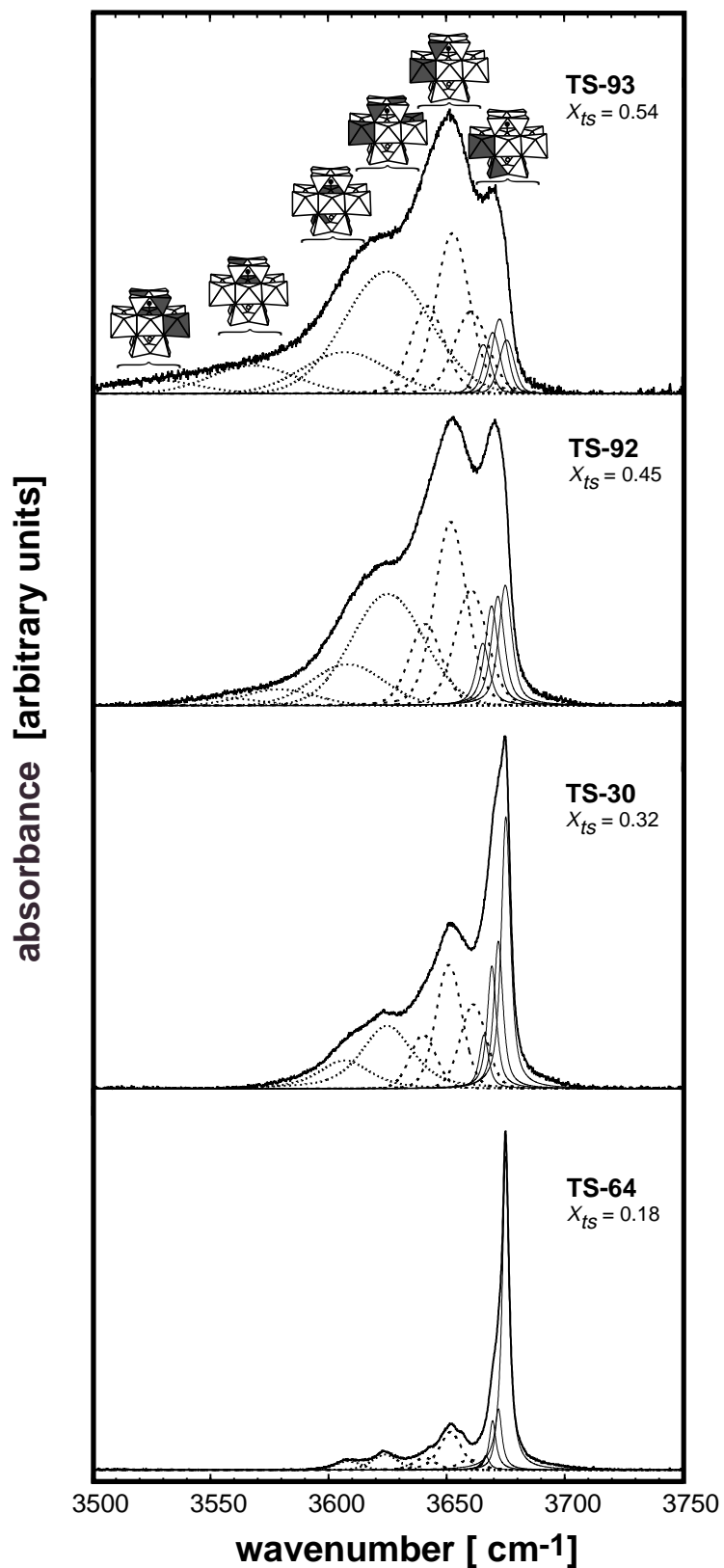
Fig. 10. Selected FTIR spectra of the runs TS-93, TS-92, TS-30 and TS-64. Up to 11 individual bands were necessary for a consistent fitting procedure along the whole solid solution series. An exemplary band assignment to the configurations is shown.

M2, two M3 and eight T1 sites, two protons, one above (H) and one below (H') the octahedral strip. The tetrahedra above and below the octahedral chain will be further also labelled T1 and T1', respectively. Because of the assumption that the octahedral chain acts as a shield, the vibrational mode of a proton is only influenced by the four T1 cations on the same level. The distances between the proton and the M2 and M3 sites in the front and in the back (according to Fig. 11) are different (Table 4) and therefore the $M2_{near}$, $M3_{near}$ and $M2_{far}$, $M3_{far}$ sites are treated separately. In the following as a short hand notation, each configuration will be designated by M2M3M2:T1T1-T1T1:M2M3M2 which lists, according to Fig. 11, the front (far) sites first (all sites from left to right). In this notation the configuration typical for tremolite will MgMgMg:SiSi-SiSi:MgMgMg (configuration A1, see Fig. 12).
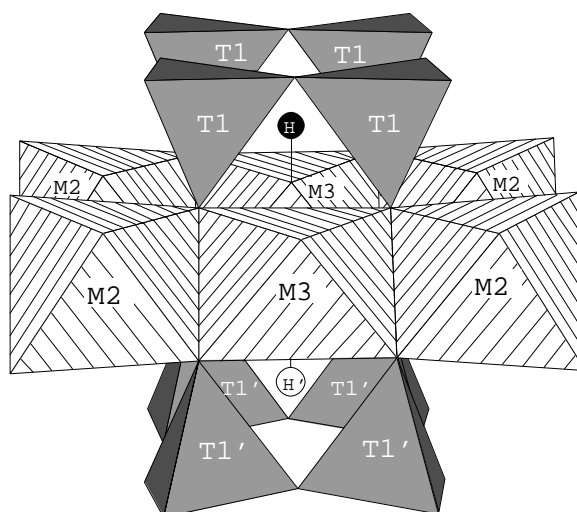
Fig. 11. Cluster around the H atom only consisting of polyhedra where Al substitution is assumed.

Due to local charge balance, the tschermaks exchange is supposed to be a coupled substitution. It is now reasonable to assume that the substitution of Al^{3+} for Mg^{2+} on either M2 or M3 is charge balanced by Al^{3+} for Si^{4+} on the closest T1 site. If one Al^{3+} is substituted on the left front M2 site, the upper proton H will have either the configuration AlMgMg:AlSi-SiSi:MgMgMg (A4) or AlMgMg:SiSi-SiSi:MgMgMg (A2). For the second configuration the charge balance occurs on a T1' site. The lower proton H' will have one of the corresponding and matching configuration either A2 or A4, respectively. The adjacent cluster to the front is formed in the *c* direction by the next two T1, two T1', two M2 and one M3 sites. As a consequence this cluster will then either have the configuration MgMgMg:SiSi-SiAl:AlMgMg (C1) or MgMgMg:SiSi-SiSi:AlMgMg (B1) if no additional

Al^{3+} substitution occurs. If Al^{3+} is substituted on the front M3 site, the occurring configurations for H are either MgAlMg:AlSi-SiSi:MgMgMg (A6) or MgAlMg:SiSi-SiSi:MgMgMg (A3). In the more Al-rich amphiboles, it is possible that configurations with multiple substitutions will occur. Bond valence considerations (Oberti et al. 1995b; Hawthorne 1997) implied that ^{T1}Al-O-^{T1}Al dimers are very unlikely in amphiboles and that therefore Al-avoidance operates. Bond valence considerations also showed that cation arrangements with Al^{3+} on adjacent octahedral sites are improbable (Hawthorne 1997; Della Ventura et al. 1999; Hawthorne et al. 2000). These considerations lead to a total of 121 configurations. This number is reduced to 48 because some configurations are not distinguishable, e.g. the configuration MgAlMg:SiAl-SiSi:MgMgMg is equivalent to configuration MgAlMg:AlSi-SiSi:MgMgMg (A6) which therefore has a multiplicity of two. For each configuration there will be an OH-vibrational band with an absorbance proportional to its probability. If it will be further assumed that the effect of substitution of two Al^{3+} at equivalent M2 or T1 sites either in *cis* and *trans* configuration is indistinguishable (e.g. AlMgMg:SiSi-SiSi:AlMgMg (B2) and AlMgMg:SiSi-SiSi:MgMgAl) the total number of different configurations is reduced to 36. These configurations with their multiplicities are summarized in Fig. 12.

It must be noted, that the definition of the configuration shell as in Fig. 11 for IR interpretation comprises a larger size (and more cations) than in previous studies of synthetic Al-tremolites. Jenkins et al. (1997) considered Al-Mg substitution at two M1 and one M3$_{near}$ sites in the nearest vicinity of the proton for an interpretation model of the IR-bands. Hawthorne et al. (2000) observed a fine structure in the IR-bands of Al-tremolites that could not be interpreted with this model. It was concluded that the OH-stretching vibration of Al-tremolites is not only influenced by the nearest neighbor of the proton (M1M1M3$_{near}$), but also by the next nearest neighbors (T1T1: M2$_{near}$M3$_{far}$M2$_{near}$) . Hawthorne et al. (2000) discussed an expanded model including Mg-Al substitution on M2$_{near}$, M3$_{near}$ and M3$_{far}$ sites and including Si-Al substitution at T1 sites of the back of the cluster (Fig.11). In contrast to this study, the T1 sites and M2$_{far}$ sites in the front cluster were not included in the model by Hawthorne et al. (2000). However, T1 sites at both, the front and back of the cluster are nearly in the same distance to the proton (Table 4, 3.13 Å and 3.12 Å). Si-Al substitutions on the T1 sites of the front cluster should have almost the same influence on the OH-stretching vibration as T1 sites of the back cluster. Assuming Al-avoidance on T1 sites,
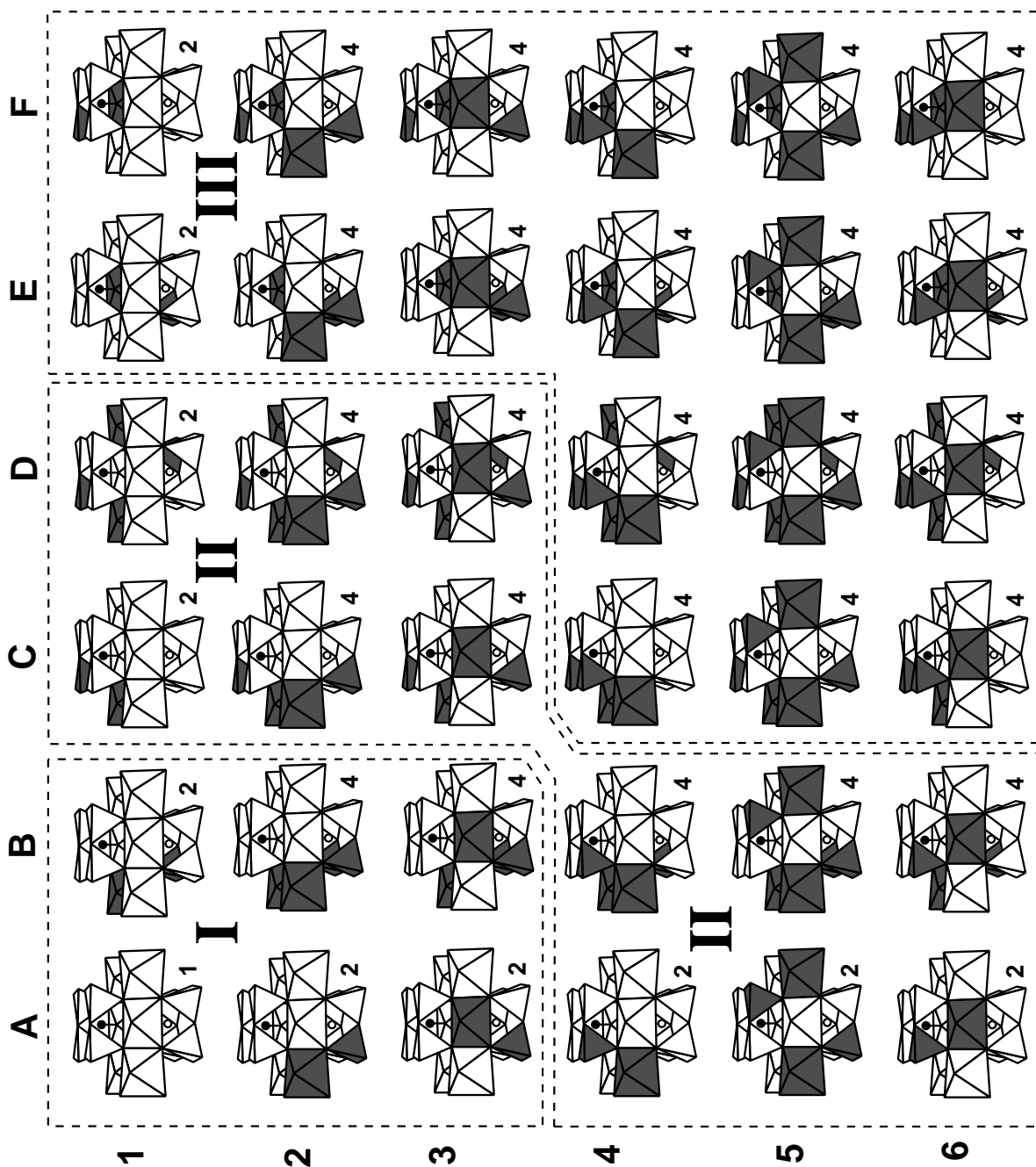
Fig. 12. The 36 possible configurations for Al-incorporation assuming Al-Mg substitution on M2 and M3 and Al-Si substitution on T1 including charge coupled substitution and Al-avoidance. The numbers are the multiplicities of the configurations. White tetrahedra are occupied by Si and white octahedra are occupied by Mg. Grey tetrahedra and octahedra are occupied by Al.

two Si-Al substitutions are possible on the 4 T1 sites around a proton. Configurations with two Al^{3+} at T1 (Fig. 12, configurations C4-C6, D4-D6 and F4-F6) were not considered in the study by Hawthorne et al. (2000). The effect of Si-Al substitution at two T1 sites should be significantly different from Si-Al substitution on one T1 site. Therefore all four T1 sites around the proton were included in the model of this study.

In comparison to the study of Hawthorne et al. (2000) also the $M2_{far}$ sites were included in the model because a higher number of bands were observed. These additional bands could not be explained with the model from Hawthorne et al. 2000. For the quantification of these bands an expanded model including the $M2_{far}$ sites were necessary.

Band assignment

Up to 12 bands have been detected in the amphiboles synthesized here. This number is significantly lower than the expected 36. Many bands will overlap and are not resolved others will be of low absorbance because of the low probability of their corresponding configuration. From these 12 detected bands only the one with the highest wavenumber at 3675 cm^{-1} is definitely known to correspond to the tremolite configuration (A1).

For synthetic tremolite-tschermakite solid solutions Jenkins et al. (1997) observed with increasing Al-content a decrease in the absorbance of the tremolite-type band at 3675 cm^{-1} and an increase in the band at 3652 cm^{-1}. Without considering the fine structure, the band at 3652 cm^{-1} was attributed to the Al^{3+} substitution on either the M1 or M3 site. Hawthorne et al. (2000) reported bands at 3675, 3671, 3655, 3642, 3624 and 3608 cm^{-1}. The model for band assignments based on 4 distinct substitutions: (1) Al $\leftrightarrow$ Mg at $M3_{near}$, (2) Al $\leftrightarrow$ Si at T1, (3) Al $\leftrightarrow$ Mg at $M2_{near}$ and Al $\leftrightarrow$ Mg at $M3_{far}$. The band at 3671 cm^{-1} was assigned to the substitution (3) and the band at 3655 cm^{-1} to the substitution (2). The band at 3642 cm^{-1} was attributed to either a combination of substitution (2) and (3) or only a substitution (1). Substitutions of either (1) and (3) or (1) and (2) caused the band at 3624 cm^{-1}. The band at 3608 cm^{-1} was assigned to combinations of substitution (1), (2) and (3). As discussed above, T1 sites and $M2_{far}$ sites of the front cluster were not included in the model for the band assignments. Therefore, effects from Si-Al substitutions at two T1 sites as well as from Al-Mg substitutions at M_{far}-sites of the proton H' were not included in the model.

In this study a larger fine structure of the bands were observed which could not be explained with the model from Hawthorne et al. (2000). The quantitative interpretation of the IR-spectra of the Al-tremolites required a more expanded model.

The physical environmental differences between the 36 configurations are due to differences in cation charge and cation radii of Al^{3+} (0.39 Å) *vs*. Si^{4+} (0.26 Å) in tetrahedral coordination and of Al^{3+} (0.54 Å) *vs*. Mg^{2+} (0.72 Å) in octahedral coordination, respectively (Shannon 1976). The influence of both differences in charge and size on the electrostatic field is complex and not easily predicted. Furthermore the substitution of a larger cation with

a lower charge (tetrahedral) and of a smaller cation with a higher charge (octahedral), but at the opposite site of the proton, both yield bands at lower wavenumbers. For purpose of simplification it is assumed that the shift of the band position with respect to the tremolite band is correlated with the distance at which Al^{3+} substitution occurs. The distances of the M2, M3 and T1 sites to the proton (Table 4) can be also divided into three groups. One of the two M3 sites is closest to the proton (2.67 Å). This is followed by the four T1 sites (3.12 and 3.13 Å). The two M2 sites (far and near) and the other $M3_{far}$ site show the largest distances (4.16, 5.14 and 4.03 Å, respectively). Therefore an Al^{3+} substitution on the most remote sites should have the least influence on band position. The influence of Al^{3+} on T1 sites would be larger followed by Al^{3+} substitution on the $M3_{near}$ site with the largest influence on band position. Similarly the effect of the two Al^{3+} substitutions should be a linear combination. According to these assumptions, the configurations can be assigned to three groups. I: only Si^{4+} at T1 and one to two Al^{3+} at M2 and/or $M3_{far}$, II: one Al^{3+} at T1 and one to three Al^{3+} at M2 and/or at the $M3_{far}$, III: either Al^{3+} on $M3_{near}$ and/or two Al^{3+}on T1 and an additional one to four Al^{3+} on M2.

It is now assumed that the three configurational groups (I-III) correspond to the three groups of bands with fundamental differing FWHMs (Table 5). The six configurations of the group I (A1 to A3 and B1 to B3) are assigned to the Band A, B, C and D. The bands B, C and D closest to the tremolite band A were all characterized by a low FWHM (Table 5). If only octahedral substitutions are relevant for a configuration, such low FWHMs are commonly observed (e.g. Gottschalk et al. 1998, 1999). Therefore it seems reasonable to assign these bands to the group I. The shift of positions for bands B, C and D with respect to band A was in the range of -3 to -10 cm^{-1}. With increasing Al-content, the absorbance of A decreased and those of B, C and D increased. The D-band always showed the lowest absorbance of these. Because the total X_{ts} of the synthesized amphiboles does not exceed 0.54, the probability of corresponding configurations with two Al^{3+} substitutions in one cluster is lower than those of the other four. Therefore one might speculate that the B- and D- bands correspond to the configurations B2 and B3. As a consequence of the distance argument the B-band would correspond to the A2, the C-band to A3+B1 and the D-band to B2+B3 configurations.

There are 12 configurations with one Al^{3+} on T1 and one Al^{3+} on M2 and $M3_{far}$. These resulting bands are assumed to be those of the group II. The shift in the position of bands E, F and G with respect to band A was in the range of -15, -24 and -34 cm^{-1}, respectively.

The remaining configurations have either Al^{3+} on $M3_{near}$ and/or two Al^{3+} on T1. The corresponding bands are considered to be those of group III. The position of bands H, I, J and K showed a shift of -51, -68, ~-90 and ~-120 cm^{-1}, respectively.

An exact assignment of the bands in the groups II and III to distinct configurations is ambiguous. One could, however, speculate that the shift of the H-band (-51 cm^{-1}) is due to two Al^{3+} substitutions on T1 because the average shift of the group II bands (one Al^{3+} on T1) is -24 cm^{-1}. The I-band (-68 cm^{-1}) could then be assigned to a single substitution on $M3_{near}$. Consequently the J-band could be due to a $M3_{near}$ and one T1 (~-90 cm^{-1}) and the K band to a $M3_{near}$ and two T1 (~-120 cm^{-1}) substitutions. This band assignment is shown in Fig. 10.

An additional small sharp band of low absorbance was observed in the samples TS-6 and TS-33 at 3660.8 cm^{-1} which is not consistent with the bands systems described above. Gottschalk et al. (1998, 1999) reported minor bands in synthetic tremolites at 3660 cm^{-1} which correlated with the concentrations of chain multiplicity faults. This is in agreement with the results of HRTEM investigations for TS-33 which showed a high concentration of chain multiplicity faults.

Quantification of site occupancies

Hawthorne et al. (2000) discussed that it is not possible to quantify the OH-bands of synthetic Al-tremolites because no satifactory background could be fitted. Powder IR samples of amphiboles were usually prepared from a mixture of the amphibole sample and KBr. KBr contains small amounts of water under normal conditions. IR spectra of water-bearing KBr show very broad absorbance bands which overlape with the region of the OH-stretching vibration of amphiboles. The overlapping broad water band makes a quantitativ evaluation of the OH-band rather difficult. Good results can be obtained however, if the KBr powder and the prepared KBr pellets are dried at 170°C for at least 48 hours, but typically for several weeks to minimize water contamination in the samples. After such procedure the IR spectra showed a flat baseline. In most cases the background could be subtracted using a linear function and only in some rare cases using a cubic function. Using these samples a quantitative interpretation of the IR-spectra was possible.

As described above, the observed 3 band systems in Al-tremolites are assigned to 3 configurational groups. The absorbance of each band should be proportional to the probability of its underlying configuration. The observed absorbances should therefore

provide some information about the actual site occupancies. To do this, the functional dependence of absortivity with respect to wavenumber is required.
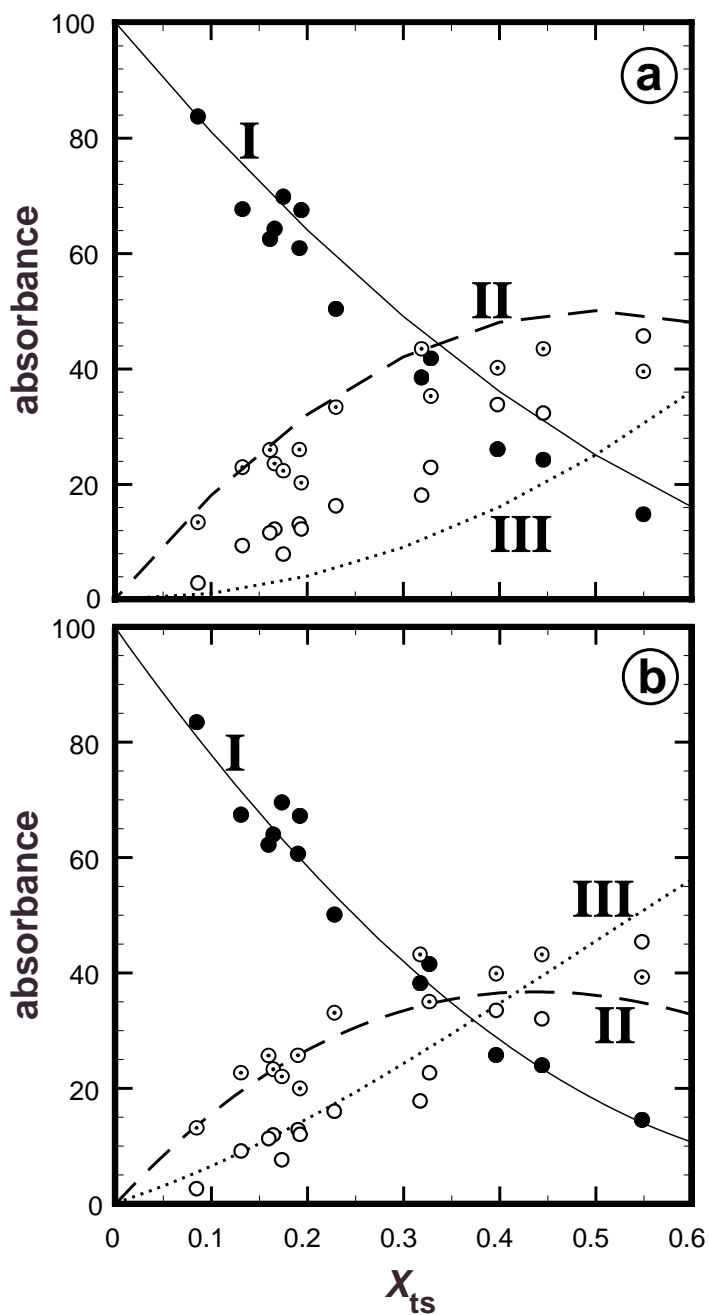
Fig. 13. Comparison of observed (points) and calculated (lines) absorbances for each group (I-III). **a)** Random distribution of Al-Mg on the M2 sites. **b)** Random distribution of Al-Mg on the M2 and M3 sites. filled circles: band group I, open circles with dots: band group II, open circles: band group III.

The absorbtivity of the OH-stretching vibration is a linear function of wavenumber (Skogby and Rossmann 1991). Hawthorne et al. (1997) determined and Melzer et al. (2000) further quantified the required proportionality factor using synthetic K-richterite-tremolite and K-richterite-richterite-tremolite solid solutions, respectively. Melzer et al. (2000) derived the following expression for the absorbtivity of an OH-stretching band at the wavenumber w relative to the tremolite band at 3674.6 cm^{-1}:

$$\varepsilon_w/\varepsilon_{3674.6\ \text{cm}^{-1}} = 1 - 0.00703\ (w - 3674.6) \tag{8}$$

This expression was derived in the range of 3674-3730 cm^{-1} and for the synthetic Al-amphiboles it had to be extrapolated to lower wavenumbers. All absorbances were corrected using equation (8). The corrected absorbances should be directly proportional to the probabilities of a single configuration or group of configurations.

The probability of possible configurations were simulated with a Monte-Carlo approach. Using a model crystal containing 3000 tremolite configurations of the type A1, a chosen number of Al^{3+} cations corresponding to a desired X_{ts} content were randomly distributed. The constraints of local charge balance and Al-avoidance were applied. At the end of each simulation the probabilities of all configurations were determined.

Two models were set up: (1) Al^{3+} substitution only on M2 and (2) Al^{3+} substitution on M2 and M3 with no next neighbour [6]Al. The simulation was carried out for 7 different tschermakite contents between X_{ts} = 0.0-0.6 using step intervals of 0.1. The results are presented in Fig. 13 which shows the sum of probabilities $vs.$ the corrected absorbances within each group (I-III) of configurations. Fig. 13a shows that the assignment of bands to certain groups of configurations is correct. Furthermore the second model ([6]Al^{3+} on M2 and M3) (Fig. 13b) seems to be more appropriate. This indicates that octahedral substitution of Al^{3+} is not only restricted to the M2 site in Al-tremolites. This is in agreement with NMR and IR investigations of synthetic Al-tremolites (Jenkins et al. 1997; Hawthorne et al. 2000). Incorporation of Al^{3+} on M2 and M3 sites seems to be a very good model for interpretation of the IR-spectra. It supports the results of a single crystal X-ray studies of pargasites and pargasitic hornblendes (Oberti et al. 1995a) and a neutron powder diffraction study of synthetic pargasite (Welch and Knight 1999) where Al is distributed over M2 and M3 sites.

ACKNOWLEDGMENTS

REFERENCES CITED

Burns, R.G., and Strens, R.G.J. (1966) Infrared study of the hydroxyl bands in clinoamphiboles. Science, 153, 890-892.

Cao, R.-L., Ross, C., and Ernst, W.G. (1986) Experimental studies to 10 kb of the bulk composition tremolite$_{50}$-tschermakite$_{50}$ + excess H_2O. Contributions to Mineralogy and Petrology, 93, 160-167.

Cho, M., and Ernst, W.G. (1991) An experimental determination of calcic amphibole solid solution along the join tremolite-tschermakite. American Mineralogist, 76, 985-1001.

Della Ventura, G., Hawthorne, F., Robert, J.-L., Delbove, F., Welch, M., and Raudsepp, M. (1999) Short-range order of cations in synthetic amphiboles along the richterite-pargasite join. European Journal of Mineralogy, 11, 79-94.

Della Ventura, G., Robert, J.-L., Raudsepp, M., and Hawthrone, F.C. (1993) Site occupancies in monoclinic amphiboles: Rietveld structure refinement of synthetic nickel magnesium cobalt potassium richterite. American Mineralogist, 78, 633-640.

Gottschalk, M., Andrut, M., and Melzer, S. (1999) The determination of cummingtonite content of synthetic tremolite. European Journal of Mineralogy, 11, 967-982.

Gottschalk, M., Najorka, J., and Andrut, M. (1998) Structural and compositional characterisation of synthetic (Ca,Sr)-tremolite and (Ca,Sr)-diopside solid solutions. Physics and Chemistry of Minerals, 25, 415-428.

Graham, C.M., Maresch, W.V., Welch, M.D., and Pawley, A.R. (1989) Experimental studies on amphiboles: A review with thermodynamic perspectives. European Journal of Mineralogy, 1, 535-555.

Hawthorne, F.C. (1981) Crystal chemistry of the amphiboles. In D.R. Veblen, Ed. Amphiboles and other hydrous pyriboles - mineralogy, 9a, p. 1-102. Mineralogical Society of America.

Hawthorne, F.C. (1983) The crystal chemistry of the amphiboles. Canadian Mineralogist, 21, 173-480.

Hawthorne, F.C. (1997) Short-range order in amphiboles: a bond-valence approach. The Canadian Mineralogist, 35, 201-216.

Hawthorne, F.C., Della Ventura, G., Robert, J.-L., Welch, M., Raudsepp, M., and Jenkins, D. M. (1997) A Rietveld and infrared study of synthetic amphiboles along the potassium-richterite.tremolite join. American Mineralogist, 82, 708-716.

Hawthorne, F.C., and Grundy, H.D. (1976) The crystal chemistry of amphiboles. IV. X-ray and neutron refinements of the crystal structure of tremolite. Canadian Mineralogist, 14, 334-345.

Hirschmann, M., Evans, B.W., and Yang, H. (1994) Composition and temperature dependence of Fe-Mg ordering in cummingtonite-grunerite as determined by X-ray diffraction. American Mineralogist, 79, 862-877.

Hoschek, G. (1995) Stability relations and Al content of tremolite and talc in CMASH assemblages with kyanite + zoisite + quartz + H_2O. European Journal of Mineralogy, 7, 353-362.

Jasmund, K., and Schäfer, R. (1972) Experimentelle Bestimmung der P-T-Stabilitätsbereiche in der Mischkristallreihe Tremolit-Tschermakite. Contributions to Mineralogy and Petrology, 34, 101-115.

Jenkins, D.M. (1981) Experimental phase relations of hydrous peridotites modelled in the system H_2O-CaO-MgO-Al_2O_3-SiO_2. Contributions to Mineralogy and Petrology, 77, 166-176.

Jenkins, D.M. (1983) Stability and composition relations of calcic amphiboles in ultramafic rocks, Contributions to Mineralogy and Petrology, 83, 375-384.

Jenkins D.M. (1987) Synthesis and characterization of tremolite in the system H_2O-CaO-MgO-SiO_2. American Mineralogist, 72, 707-715.

Jenkins, D.M. (1988) Experimental study of the join tremolite-tschermakite: A reinvestigation. Contributions to Mineralogy and Petrology, 99, 392-400.

Jenkins, D.M. (1994) Experimental reversal of the aluminium content in tremolitic amphiboles in the system H_2O-CaO-MgO-Al_2O_3-SiO_2. American Journal of Science, 294, 593-620.

Jenkins, D.M., Sherriff, B.L., Cramer, J., and Xu, Z. (1997) Al, Si, and Mg occupancies in tetrahedrally and octahedrally coordinated sites in synthetic aluminous tremolite. American Mineralogist, 82, 280-290.

Larson, A.C., and Von Dreele, R.B. (1987) Generalized structure analysis system. Los Alamos National Laboratory Report.

Manning, G.E. (1994) The solubility of quartz in H_2O in the lower crust and upper mantle. Geochimica et Cosmochimica Acta, 58, 4831-4839.

Melzer, S., Gottschalk, M., and Heinrich, W. (1998) Experimentally determined partitioning of Rb between richterites and aqueuos (Na,K)-chloride solutions. Contributions to Mineralogy and Petrology, 133, 315-328.

Melzer, S., Gottschalk, M., Andrut, M., Heinrich, W. (2000) Crystal chemistry of K-richterite-richterite-tremolite solid solutions: a SEM, EMP, XRD, HRTEM and IR study. European Journal of Mineralogy, 12, 273-291.

Oba (1978) Phase relations of $Ca_2Mg_3Al_2[Al_2Si_6O_{22}/(OH)_2)$ - $Ca_2Mg_5[Si_8O_{22}/(OH)_2]$ join at high temperature and pressure - the stability of tschermakite. J. Fac. Sci. Hokkaido Univ., ser. IV, 18, 339-50.

Oberti, R., Hawthorne, F.C., Ungaretti, L., and Cannillo, E. (1995a) [6]Al disorder in amphiboles from mantle peridotites. Canadian Mineralogist, 33, 867-878.

Oberti, R., Ungaretti, L., Cannillo, E., Hawthorne, F.C., and Memmi, I. (1995b) Temperature-dependent Al order-disorder in the tetrahedral double chain of C2/m amphiboles. European Journal of Mineralogy, 7, 1049-1063.

Pawley, A.R., Graham, C.M., and Navrotsky, A. (1993) Tremolite-richterite amphiboles: Synthesis, compositional and structural characterization, and thermochemistry. American Mineralogist, 78, 23-35.

Pouchou, J.L., and Pichoir, F. (1984) Un nouveau modèle de calcul pour la microanalyse quantitative par spectroétrie de rayons X. Rech. Aérospatiale, 3, 167-192.

Quirion, D.M., and Jenkins, D.M. (1998) Dehydration and partial melting of tremolitic amphibole coexisting with zoisite, quartz, anorthite, diopside, and water in the system $H_2O\text{-}CaO\text{-}MgO\text{-}Al_2O_3\text{-}SiO_2$. Contributions to Mineralogy and Petrology, 130, 379-389.

Raudsepp, M., Turnock A.C., Hawthorne, F.C., Sherriff, B.L., and Hartman, J.S. (1987) Characterization of synthetic pargasitic amphiboles ($NaCa_2Mg_4M^{3+}Si_6Al_2O_{22}(OH,F)_2$; M^{3+} = Al, Cr, Ga, Sc, In) by infrared spectroscopy, Rietveld structure refinement, and ^{27}Al, ^{29}Si, and ^{19}F MAS NMR spectroscopy. American Mineralogist, 72, 580-593.

Shannon, R.D. (1976) Revised effective ionic radii and systematic studies of interatomic distances in halides and chalcogenides. Acta Crystallographica, A32, 751-767.

Skogby, H., and Rossmann, G.R. (1991) The intensity of amphibole OH bands in the infrared absorption spectrum. Physics and Chemistry of Minerals, 18, 64-68.

Smelik, E.A., Jenkins, D.M., and Navrotsky, A. (1994) A calorimetric study of synthetic amphiboles along the tremolite-tschermakite join and the heats of formation of magnesiohornblende and tschermakite. American Mineralogist, 79, 1110-1122.

Welch, M.D. (1994) A multinuclear study of synthetic pargasite. American Mineralogist, 79, 261-268.

Welch, M.D., and Knight, K.S. (1999) A neutron powder diffraction study of cation ordering in high-temperatur synthetic amphiboles. European Journal of Mineralogy, 11, 321-331.

Welch, M.D., Shuangxi, L., and Klinowski, J. (1998) ^{29}Si MAS NMR systematics of calcic and sodic-calcic amphiboles. American Mineralogist, 83, 85-96.

Zimmermann, R., Heinrich, W., and Franz, G. (1996) Tremolite synthesis from $CaCl_2$-bearing aqueous solutions. European Journal of Mineralogy, 8, 767-776.

ZUSAMMENFASSUNG

Tremolit–Tschermakitmischkristalle wurden zwischen 700-850°C und 200-2000 MPa synthetisiert. Die synthetisierten Al-Tremolite bildeten nadel- bis leistenförmige Kornformen, mit bis zu 300 μm Länge und 20 μm Breite. Die Realstruktur des Al-Tremolit weist nur eine geringe Konzentration an Baufehlern auf. Zunehmender Al-Einbau im Tremolit führt nicht zu einer Zunahme an Kettenmultiplizitätsfehlern.

Die Mehrzahl der synthetisierten Al-Tremolite war für die chemische Analyse mit der Mikrosonde groß genug. Die Al-Tremolite sind Mischkristalle im ternären System Tremolit-Tschermakit-Cummingtonit. Die Al-reichste Tremolitprobe besitzt eine Zusammensetzung nahe dem Magnesiohornblende-Endglied (X_{ts} = 0.54). Al-reichere Tremolite konnten nicht synthetisiert werden. Variable Cummingtonitgehalte zwischen X_{cum} = 0.00-0.18 wurden beobachtet, die generell mit steigendem Al-Gehalt im Amphibol zunehmen.

Die Gitterkonstantverfeinerungen der Al-Tremolite zeigen, daß zunehmender Al-Gehalt eine lineare Änderung der Zellparameter bewirkt. Die Zellparameter a und b verringern sich wobei c und β ansteigen. Für reinen Tschermakit wurden die Gitterparameter a = 9.7438(11) Å, b = 17.936(14) Å, c = 5.2995(3) Å, β = 105.68(9) °, and V = 891.7 ± 1.4 Å^3 extrapoliert. Mit den Zellparametern a und β war es möglich, die Zusammensetzung der Amphibole im ternären System Tremolit-Tschermakit-Cummingtonit über die Gitter-konstanten zu bestimmen.

Die IR-Spekren im Bereich der OH-Streckschwingung zeigten insgesamt 12 Einzelbanden. Die Halbwertsbreiten aller Banden steigen mit zunehmendem Al-Gehalt an. Gemäß ihrer Halbwertsbreite wurden die Banden in folgende drei Bandensysteme eingeteilt: 3664-3676 cm^{-1} (I), 3633-3664 cm^{-1} (II) und 3526-3633 cm^{-1} (III).

Unter der Annahme, daß [6]Al-Substitution auf den M2- und/oder M3-Positionen sowie [4]Al auf den T1-Positionen stattfindet, können drei Konfigurationsgruppen als lokale Umgebung für das Proton zugeordnet werden: (I) nur Si^{4+} auf T1 und ein oder zwei Al^{3+} auf M2 und/oder M3$_{far}$, (II) ein Al^{3+} auf T1 und ein bis drei Al^{3+} auf M2 und/oder auf M3$_{far}$, (III) entweder Al^{3+} auf M3$_{near}$ und/oder zwei Al^{3+} auf T1 sowie zusätzlich ein bis vier Al^{3+} auf M2. Es besteht die Annahme, daß diese drei Konfigurationsgruppen mit den drei beobachteten Banden korrespondieren. Das konnte quantitativ durch Monte-Carlo-Simulationen untermauert werden. Das Modell der statistischen Verteilung von Al auf M2 und M3 - einschließlich Al-avoidance auf tetraedischen und oktaedrischen Positionen - ergab die beste Übereinstimmung mit den spektroskopischen Ergebnissen.

KAPITEL 4

Composition of synthetic tremolite-tschermakite solid solutions in amphibole-anorthite and amphibole-zoisite bearing assemblages

ABSTRACT

The composition of synthetic amphiboles was investigated experimentally along the tremolite-tschermakite join in the system $CaO-MgO-Al_2O_3-SiO_2-H_2O-Br_2$. Compositions of these amphiboles were studied within the phase assemblages amphibole-anorthite-quartz-diopside (I), amphibole-anorthite-quartz-talc (II), amphibole-anorthite-quartz-enstatite (III), amphibole-anorthite-talc-clinochlore (IV), amphibole-zoisite-talc-quartz (V), and amphibole-zoisite-talc-clinochlore (VI). Assemblages were synthesized from oxide-hydroxide mixtures in the presence of a $CaBr_2$-bearing solution between 600-800°C and 200-2000 MPa. Solid phases were investigated using SEM, HRTEM, EMP and XRD techniques. EMP-data show that the produced amphiboles are solid solutions of the ternary tremolite-tschermakite-cummingtonite. Enstatite, diopside, talc and clinochlore showed small deviations from the respective endmember composition due to some Al-incorporation.

The thermodynamic properties of the tschermakite endmember and the mixing properties along the tremolite-tschermakite join were extracted from corresponding exchange reactions of the experimentally produced phase assemblages (I)-(VI). Various ideal mixing models were tested for Al-Mg and Al-Si substitution at octahedral M2 and M3 sites and at tetrahedral T1 sites. Best fits were obtained for a two-site coupled model, resulting in $\Delta_f H^o_{ts} = $ -12528.3 ± 11.7 kJ/mol and $S^o_{ts} = $ 556.5 ± 12.0 J/mol/K for tschermakite endmember. Similar calculations were carried out for magnesiohornblende, and values of $\Delta_f H^o_{Mghb} = $ -12418.7 ± 5.9 kJ/mol and $S^o_{Mghb} = $ 562.8 ± 6.1 J/mol/K were extracted. Calculated phase relations and amphibole compositions agree well with experimental data if the derived thermodynamical data of tschermakite and a two-site mixing model for Al-incorporation in amphibole solid solutions are applied.

In natural rocks, the Al concentration in amphibole is widely used as a geobarometer because Al contents increase mainly with pressure. Our results suggest that, at a given pressure, more Al is incorporated than indicated by previous experimental studies. Thus, pressures indicated by the "Al in hornblende" geobarometer are probably overestimated.

INTRODUCTION

In greenschist to granulite facies rocks, Al-bearing calcic amphiboles are common. They occur either in metabasites (e.g. Robinson et al. 1982), metamorphosed marls (e.g. Baker and Matthews 1994) or in calcalkaline granitoids (e.g. Hammarstrom and Zen 1986; Hollister et al. 1987). In calcalkaline granitoids the Al-content of amphibole commonly increases with depth. This has been used to derive an empirical "Al in hornblende" geobarometer (Hammarstrom and Zen 1986; Hollister et al. 1987; Johnson and Rutherford 1989; Thomas and Ernst 1990; Schmidt 1992). The Al-content in amphibole, however, is not only a function of pressure and temperature but also depends on bulk composition given by a particular mineral assemblage. This complicates the Al-content in amphibole to be used as a simple petrogenetic indicator. Leger and Ferry (1991) demonstrated that calcic amphiboles in metabasites from the Wait River formation (N. Vermont) at the same metamorphic grade have highly variable Al-contents of 0.4 to 3.3 Al^{3+} pfu due to the presence of different Al-bearing minerals.

Al^{3+} enters various tetrahedral and octahedral sites in the amphibole lattice because of its suitable ionic size ($^{[4]}Al^{3+}$ = 0.39 Å, $^{[6]}Al^{3+}$ = 0.54 Å; Shannon 1976). The octahedral M2 site and the tetrahedral T1 site are the most probable locations (Hawthorne 1983; Makino and Tomita 1989), but the M3 site (Oberti et al. 1995a; Welch and Knight 1999) and the T2 sites (Oberti et al. 1995b; Welch et al. 1998) have also been suggested for Al incorporation in pargasites. Jenkins et al. (1997) considered the incorporation of Al^{3+} at all octahedral sites (M1-M3) and tetrahedral sites (T1-T2). In synthetic amphiboles along the tremolite-tschermakite join, incorporation of octahedral Al^{3+} at M2 and M3 sites and of tetrahedral Al^{3+} at T1 sites has been discussed in recent studies (Hawthorne et al. 2000; Najorka and Gottschalk, submitted).

Taking Al-free tremolite ($Ca_2Mg_5[Si_8O_{22}/(OH)_2]$) as a reference, Al is incorporated by the $^{[4]}Al_1^{3+[6]}Al_1^{3+[4]}Si_{-1}^{4+[6]}Mg_{-1}^{2+}$ exchange vector. The thermodynamic properties of Al-bearing amphibole, i.e. its Gibbs free energy, depend on the intracrystalline Al-distribution at the different tetrahedral and octahedral sites. It is clear that the Al concentrations in calcic amphiboles could be used more effectively in geothermobarometry if the thermodynamic properties of the amphibole endmembers, their mixing properties and particularly the distribution of Al^{3+} between different crystallographic sites were known better.

There is a large number of experimental studies on the tschermaks substitution $^{[4]}Al_1^{3+[6]}Al_1^{3+[4]}Si_{-1}^{4+[6]}Mg_{-1}^{2+}$ in amphibole, its respective phase equilibria and thermodynamic

properties (e.g. Jasmund and Schäfer 1972; Jenkins 1981, 1994; Cao et al. 1986; Cho and Ernst 1991; Smelik et al. 1994; Hoschek 1995; Quirion and Jenkins 1998). However, except for the study of Cho and Ernst (1991) all work encountered the crucial difficulty that the synthesized amphiboles were mostly too small for appropriate EMP analysis. To obtain compositional information often unpolished grain mounts for energy dispersive analysis (Cao et al. 1986; Jenkins 1983, 1988, 1994; Hoschek 1995; Quirion and Jenkins 1998) or systematic variations of X-ray reflections were used instead (Jenkins 1981, 1983, 1988, 1994; Cho and Ernst 1991; Hoschek 1995). However, either method is hampered by inherent difficulties. Uneven surfaces of unpolished grain mounts make absorbtion corrections for characteristic X-rays difficult if not impossible. Consequently, such analyses are not precise enough. Moreover, the system tremolite-tschermakite ($Ca_2Mg_5[Si_8O_{22}/(OH)_2]$ - $Ca_2Mg_3Al_2[Al_2Si_6O_{22}/(OH)_2)]$ is not a binary but a ternary system because varying amounts of cummingtonite component ($Mg_2Mg_5[Si_8O_{22}/(OH)_2]$) of up to 18mol% have been observed (Najorka and Gottschalk, submitted). The shifts of X-ray reflections do not provide sufficiently precise chemical information if the exact amounts of X_{cum} are not considered. Fig. 1 shows the location of the (310) reflection for X_{cum} of 0 and 0.10 (Najorka and Gottschalk, submitted). The XRD-calibration curves for X_{cum} used by Jenkins (1988), Cho and Ernst (1991) and Hoschek (1995) all coincide with the calculated line for a X_{cum} of 0.10 (Fig. 1). However, if X_{cum} is 0.05 instead of 0.10, the derived tschermakite content in amphibole (X_{ts}) were too low by 9 mol% if the calibration curve mentioned above is applied. It is clear that accurate compositions are indispensable for any correct thermodynamic evaluation.

With the use of chloridic or bromidic solutions it is possible to synthesize amphiboles large enough for electron microprobe analysis (Zimmermann et al. 1996; Gottschalk et al. 1998; Melzer et al. 1998). Using this experimental approach, Najorka and Gottschalk (submitted) presented a precise characterization of tremolite-tschermakite-(cummingtonite) solid solutions in the compositional range between $Tr_{100}Ts_0$ and $Tr_{45}Ts_{55}$ by EMP, IR, X-Ray and TEM methods.

In this study, large amphiboles along the tremolite-tschermakite join have been synthesized in presence of various Al-bearing phase assemblages at varying P and T. The following equilibria were investigated in detail:

$$1 \text{ tschermakite} + 2 \text{ diopside} + 2 \text{ quartz} \leftrightarrow 1 \text{ tremolite} + 2 \text{ anorthite} \tag{1}$$
$$1 \text{ tschermakite} + 2 \text{ quartz} \leftrightarrow 1 \text{ talc} + 2 \text{ anorthite} \tag{2}$$

$$2 \text{ tschermakite } + 2 \text{ quartz} \leftrightarrow 4 \text{ anorthite} + 3 \text{ enstatite} + 2 \text{ H}_2\text{O} \tag{3}$$

$$5 \text{ tschermakite } + 4 \text{ H}_2\text{O} \leftrightarrow 1 \text{ tremolite} + 8 \text{ anorthite} + 2 \text{ clinochlore} \tag{4}$$

$$3 \text{ tremolite} + 9 \text{ tschermakite} + 14 \text{ quartz} + 8 \text{ H}_2\text{O} \leftrightarrow 12 \text{ zoisite} + 14 \text{ talc} \tag{5}$$

$$5 \text{ tremolite} + 43 \text{ tschermakite} + 60 \text{ H}_2\text{O} \leftrightarrow 14 \text{ clinochlore} + 28 \text{ talc} + 48 \text{ zoisite} \tag{6}$$
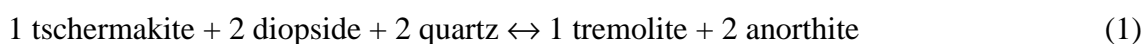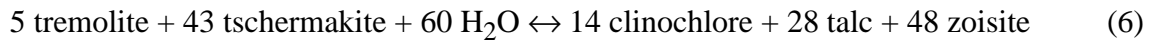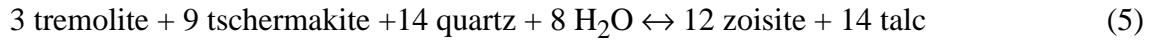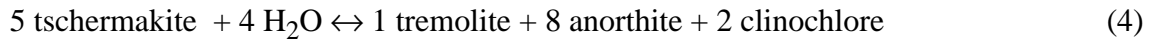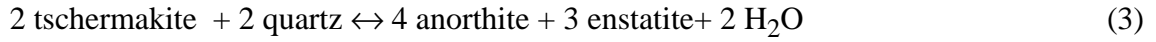
Al-concentrations in amphibole solid solutions have been measured, and thermodynamic properties of the tschermakite endmember and mixing properties along the tremolite-tschermakite join are presented.
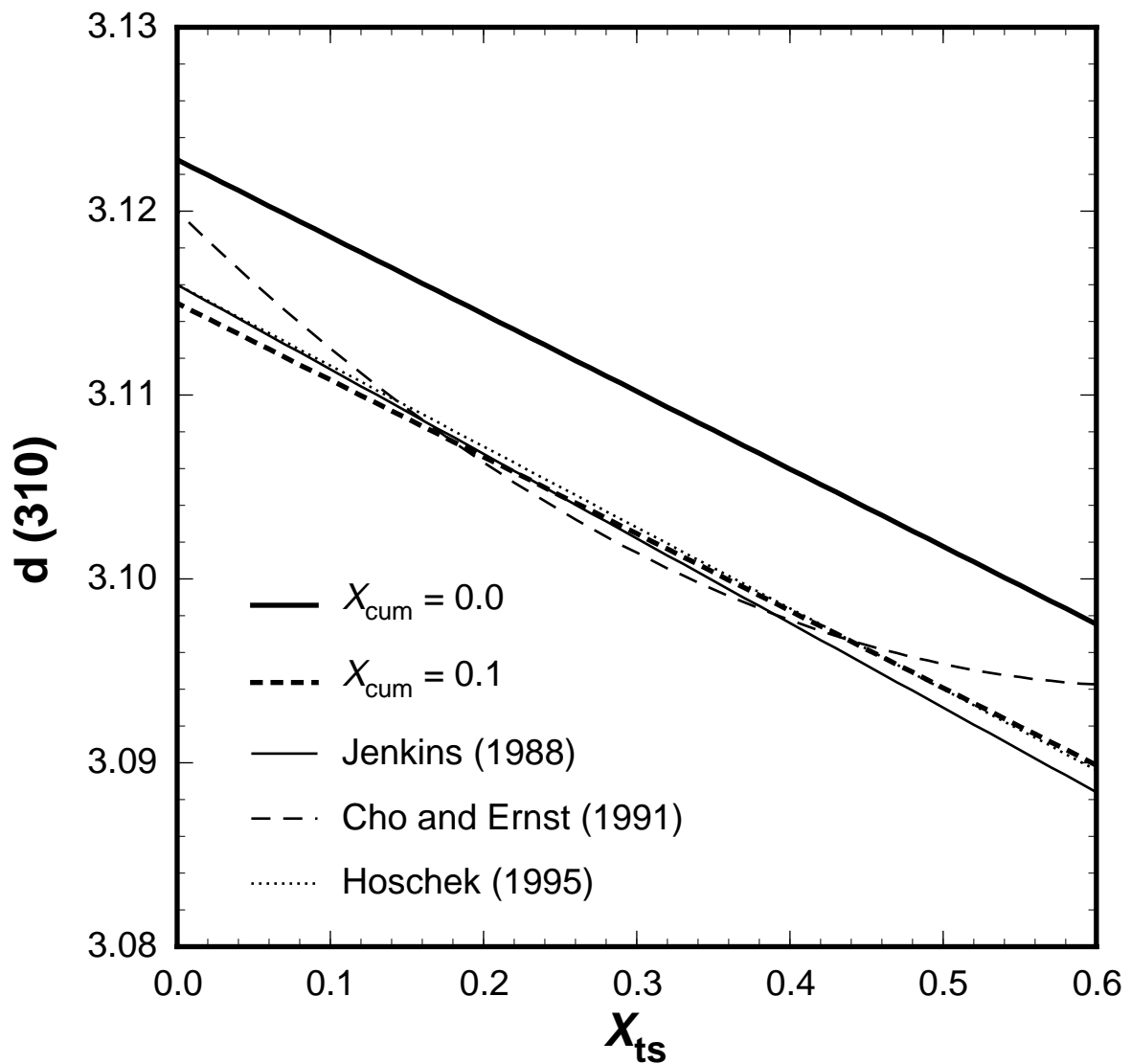
Fig. 1. Variation of the $d_{(310)}$ – reflection with composition in ternary tremolite-tschermakite-cummingtonite amphiboles. Calibration lines of previous studies coincide with the calculated line for $X_{\text{cum}} = 0.1$ (Najorka and Gottschalk submitted).

EXPERIMENTAL AND ANALYTICAL TECHNIQUES

The experimental strategy follows the "synthesis exchange technique" (Zimmermann et al. 1997; Melzer et al. 1998; Najorka et al. 1999) where synthesis and exchange reaction are combined in one experiment. Experiments were performed from 200 to 500 MPa and 600 to 850°C in standard cold-seal hydrothermal vessels. H_2O and CO_2 were used as pressure media. Temperatures were measured inside the vessels with Ni-CrNi thermocouples closely placed to the sample. The pressure was controlled with a calibrated strain gauge. The uncertainties in temperature and pressure are estimated to be less than ±5°C and ±5 MPa. At the end of each run the samples were quenched isobarically to 300°C within 3 minutes using compressed air.

For runs at 1500 and 2000 MPa and 650°C to 750°C a piston cylinder apparatus with NaCl assemblies was used. The estimated uncertainties of temperature and pressure were ±15°C and ±50 MPa, respectively.

The starting materials were mixtures of analytical grade SiO_2, MgO, Al_2O_3, $Ca(OH)_2$, and aqueous $CaBr_2$-solution (≤ 2 molal). The solid/fluid ratio varied between 1.0 and 3.0. With respect to CaO, MgO, Al_2O_3 and SiO_2, the bulk compositions were chosen to lie within the amphibole-anorthite-quartz-diopside (I), the amphibole-anorthite-quartz-talc (II), the amphibole-anorthite-quartz-enstatite (III), the amphibole-anorthite-clinochlore-talc (IV), the amphibole-zoisite-quartz-talc (V), the amphibole-zoisite-clinochlore-talc (VI), and the amphibole-zoisite-kyanite-clinochlore (VII) subsystems. The respective bulk compositions and the run conditions are listed in Table 1. In Fig. 2 the bulk compositions of the runs are presented as subtetrahedra in the $CaO-MgO-SiO_2-Al_2O_3$ space.

The synthesized products were characterized by optical microscopy, scanning electron microscopy (SEM), high-resolution transmission electron microscopy (HRTEM), electron microprobe (EMP) and powder X-ray diffraction (XRD). Details of the analytical procedures are given by Najorka and Gottschalk (submitted).

Table 1. Starting conditions of the runs

run	$Ca(OH)_2$ (mg)	$CaBr_2$ (mg)	MgO (mg)	Al_2O_3 (mg)	SiO_2 (mg)	H_2O (mg)	$CaBr_2$-molality	$X_{H_2O}^{before}$	$X_{H_2O}^{after}$	T (°C)	P (MPa)	time (days)
bulk (I) amph-an-di-qtz												
TS-3	3.94	1.19	5.18	0.77	13.93	51.26	0.11	0.99	0.99	750	200	60
TS-14	4.64	2.85	5.39	1.08	14.72	14.24	0.93	0.98	0.98	750	500	7
TS-20	3.70	2.85	4.35	0.75	11.65	14.28	0.94	0.98	0.98	800	200	7
TS-34	4.63	3.41	5.33	1.23	14.22	17.06	0.94	0.98	0.98	600	500	14
TS-35	4.67	3.45	5.21	1.35	14.23	17.27	0.94	0.98	0.98	700	200	17
TS-36	4.68	3.42	5.21	1.34	14.09	17.13	0.94	0.98	0.98	600	200	16
TS-38	9.37	3.50	10.41	2.68	27.55	17.51	0.88	0.98	0.98	600	350	14
TS-40	4.68	3.52	5.20	1.34	14.51	17.58	0.94	0.98	0.98	750	350	17
TS-47	1.43	1.29	1.71	0.45	5.53	3.64	1.62	0.97	0.97	850	350	19
TS-57	5.76	5.19	6.87	1.83	20.74	17.02	1.41	0.98	0.97	700	350	17
TS-58	5.75	5.18	6.86	1.83	20.76	17.04	1.41	0.98	0.97	650	500	18
TS-59	5.75	5.18	6.86	1.82	20.61	17.05	1.40	0.98	0.97	650	200	18
TS-60	5.76	5.19	6.87	1.83	20.89	16.76	1.43	0.97	0.97	800	350	16
TS-69	8.08	10.92	4.43	6.46	20.72	25.09	2.02	0.96	0.96	700	500	12
bulk (II) amph-an-ta-qtz												
TS-9	1.10	0.99	1.85	0.81	5.36	3.59	1.29	0.98	0.98	600	500	19
TS-13	1.10	1.00	1.85	0.81	5.38	3.54	1.31	0.98	0.98	650	350	19
TS-61	4.38	3.95	7.36	3.22	21.38	12.99	1.41	0.98	0.97	650	200	18
TS-62	4.38	3.95	7.36	3.21	21.36	13.00	1.40	0.98	0.97	650	500	18
TS-67	6.46	4.97	6.09	5.34	21.47	22.48	1.03	0.98	0.98	600	200	32
TS-68	8.48	9.65	6.36	8.76	25.65	30.20	1.50	0.97	0.97	700	500	12
TS-94	4.38	3.95	7.35	3.21	21.35	13.04	1.40	0.98	0.97	800	350	16
TS-95	4.38	3.95	7.35	3.21	21.34	12.95	1.41	0.98	0.97	700	350	17
bulk (III) amph-an-en-qtz												
Ts-87	6.41	5.84	13.30	5.49	31.58	19.88	1.36	0.98	0.98	800	200	14
bulk (IV) amph-an-ta-cln												
TS-21	4.75	0.00	6.71	3.55	15.14	9.74	0.00	1.00	1.00	650	350	19
TS-22	1.58	0.00	2.23	1.18	5.03	4.33	0.00	1.00	1.00	750	350	19
TS-37	4.75	0.00	6.72	3.55	15.15	9.79	0.00	1.00	1.00	600	500	19
TS-55	5.06	4.57	9.30	6.74	20.71	22.54	0.96	0.98	0.98	700	500	15
TS-66	5.07	4.54	9.40	6.50	20.85	22.38	0.96	0.98	0.98	600	200	32
bulk (V) amph-zo-ta-qtz												
TS-71	1.44	1.30	1.93	1.37	6.41	6.00	1.02	0.98	0.98	750	1500	7
TS-72	1.42	1.29	1.98	1.25	6.32	6.00	1.02	0.98	0.98	650	2000	7
TS-76	1.43	1.31	1.95	1.32	6.23	7.01	0.89	0.98	0.98	650	1500	8
TS-88	1.34	1.25	2.22	1.03	6.61	5.99	0.99	0.98	0.98	700	2000	7
bulk (VI) amph-zo-ta-cln												
TS-85	1.51	1.40	2.25	1.84	5.32	6.06	1.09	0.98	0.98	700	1500	8
bulk (VII) amph-zo-ky-cln												
TS-84	1.27	1.19	2.08	2.64	5.03	6.04	0.94	0.98	0.98	700	1500	8

note: $X_{H_2O} = \dfrac{n_{H_2O}}{n_{CaBr_2} + n_{H_2O}}$
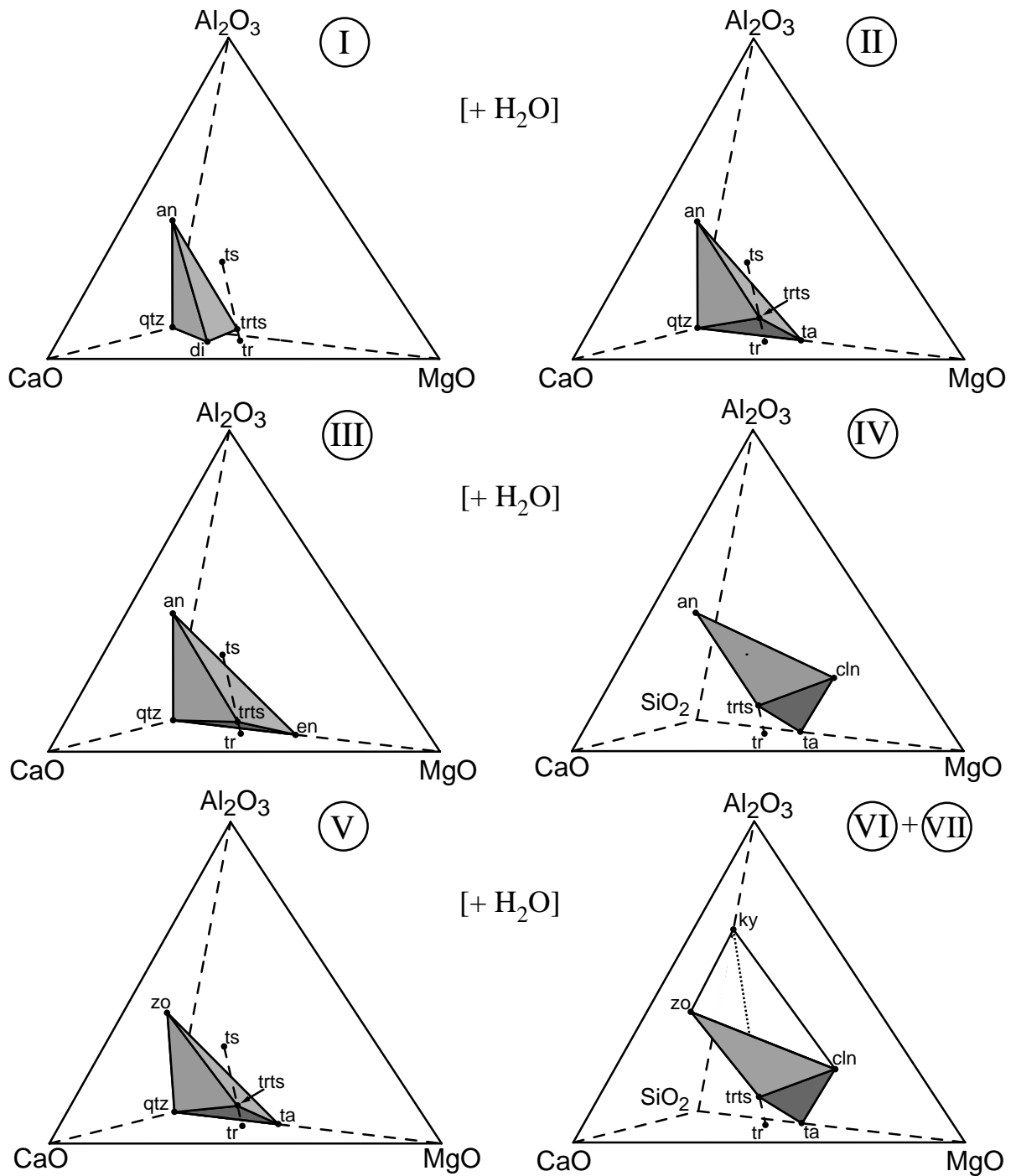
Fig. 2. The phase assemblages (I)-(VII) plotted into the CMAS-tetrahedron with excess water. The bulk compositions were chosen to lie within the subtetrahedra of the phase assemblages (I)-(VII). Abbreviations: an anorthite, cln clinochlore, di diopside, en enstatite, ky kyanite, qtz quartz, ta talc, tr tremolite, trts tremolite-tschermakite solid solutions, ts tschermakite, zo zoisite. Dashed line: tremolite-tschermakite join. Note that a small amount of cummingtonite component in amphibole shifts the trts join slightly towards the MgO-apex.

RESULTS

Phase characterization

SEM-images of run products are shown in Fig. 3. The shapes of the synthesized crystals were subhedral or euhedral. Amphibole was the major phase produced in most runs. The size of the needles or lath-shaped crystals were in the range of $1\text{-}20 \times 10\text{-}300$ μm. Talc usually occurred as distinct leaf-like crystals (5 to 300 μm) and smaller grains often had a pseudohexagonal shape. Anorthite formed euhedral platy crystals of up to 50×150 μm in size. Quartz crystallized as euhedral prisms (< 20 μm). Diopside, zoisite, enstatite and forsterite crystallized as thin prisms with sizes in the range of $2\text{-}5 \times 10\text{-}50$ μm. Occasionally, amorphous SiO_2 was observed. However, because of the similar habitus of amphibole, diopside, zoisite, enstatite and forsterite it was difficult to distinguish between these phases by SEM-imaging. Traces of remaining starting materials were never observed.
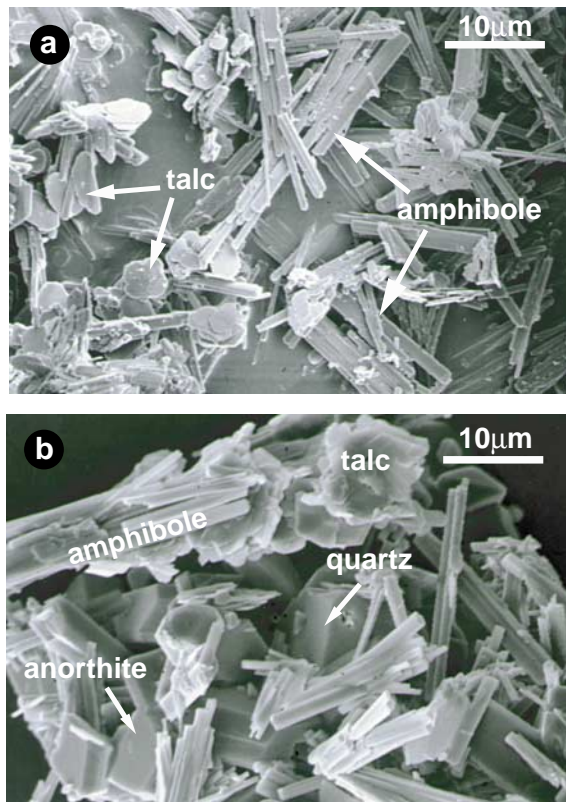
Fig. 3. SEM images of run products. **a)** lath-shaped amphibole crystals ($20 \times 2\text{-}5$ μm) and leaf like talc crystals (4×4 μm) from run TS-88 **b)** amphibole, talc, anorthite and quartz crystals (run TS-68).

All experimental products were investigated by powder XRD. For each run product, a Rietveld refinement was performed which provided quantiative phase proportions of solids as well as their lattice parameters. The derived phase proportions are listed in Table 2. In the products of most runs amphibole was the predominant phase. As predicted by the chosen bulk compositions, the intended divariant phase assemblages consisting of 4 solids and 1 fluid were observed in most cases. For runs at 200, 350 and 500 MPa, amphibole and anorthite were observed together with either quartz and diopside, quartz and talc, quartz and enstatite or clinochlore and talc. At 1500 and 2000 MPa, amphibole and zoisite formed along with either quartz and talc, or clinochlore and talc. In runs TS-34, TS-36, TS-38, TS-58, and TS-59, which produced the phase assemblage amphibole-anorthite-diopside-quartz, talc was observed as an additional phase. In run TS-22, the assemblage amphibole-anorthite-clinochlore-talc was expected, however, amphibole-anorthite-enstatite-forsterite formed instead. In the runs TS-47 and TS-84 no amphibole was produced.

Compositions of amphibole in the tremolite-tschermakite-cummingtonite ternary were determined using the compositional dependence of the lattice parameters a and β (Najorka and Gottschalk, submitted). The compositional dependence of the lattice parameters was cross-checked with measurements by EMP and FTIR. Results agree within error limits of either method (Najorka and Gottschalk, submitted; see also below). Lattice parameters for amphibole solid solutions and the derived compositions are listed in Table 2 and 3. Refinement of the lattice parameters for anorthite, quartz, forsterite and zoisite indicated that these were of nearly pure endmember composition. Deviations from endmember lattice parameters were observed for talc, clinochlore, diopside and enstatite due to the incorporation of Al-bearing components (Table 4) and these were used to determine the compositions of the respective phases. The extent of tschermaks-substitution in ortho- and clinopyroxenes ($Ca_{-1}Si_{-1}Al_2$ and $Mg_{-1}Si_{-1}Al_2$, respectively) was estimated by applying the compositional dependence of the lattice parameters suggested by Gasparik (1986) and Danckwerth and Newton (1978). The Al-concentrations in talc and chlorite were determined using the calibrations by Hoschek (1995) and Baker and Holland (1996), respectively. The derived compositions of orthopyroxene, clinopyroxene, talc, and chlorite are also listed in Table 2. The determined Al concentrations correspond to 2 to 5 mol% Mg-tschermaks component in orthopyroxene, 0 to 8 mol% Ca-tschermaks component in clinopyroxene, 0 to 19 mol% tats component in talc, and 5 to 34 mol% amesite component in chlorite.

The synthesized amphiboles were often sufficiently large enough for reliable EMP analyses. The composition of amphiboles from 18 runs are presented in Table 5. The

Table 2. Phase proportions of the runs and compositions of amphiboles along with Al-bearing minor phases determined by EMP and XRD. (I) to (VII) denote the respective bulk compositions explained in text.

run	T (°C)	P (MPa)	time (days)	phase proportions (wt%)	group	amph X_{ts}^{EMP}	X_{cum}^{EMP}	X_{tr}^{EMP}	X_{ts}^{XRD}	X_{cum}^{XRD}	X_{tr}^{XRD}	cpx X_{di}^{EMP}	X_{Cats}^{EMP}	X_{Cats}^{XRD}	X_{di}^{XRD}	opx X_{Mgts}^{EMP}	X_{en}^{EMP}	X_{Mgts}^{XRD}	X_{en}^{XRD}	talc X_{tats}^{XRD}	X_{ta}^{XRD}	chl X_{ames}^{XRD}	X_{cln}^{XRD}
				(I) amph-di-qtz-an																			
TS-36	600	200	16	12 amph, 40 di, 6 qtz, 13 an, 29 ta	(iii)				0.22	0.03	0.74	0.94	0.06	0.03	0.97					0.00	1.00		
TS-38	600	350	14	36 amph, 30 di, 7 qtz, 7 an, 19 ta	(iii)				0.30	0.04	0.65			0.06	0.94					0.04	0.96		
TS-34	600	500	14	1 amph, 49 di, 6 qtz, 11 an, 33 ta	(iii)									0.05	0.95					0.09	0.91		
TS-59	650	200	18	46 amph, 19 di, 16 qtz, 10 an, 9 ta	(iii)				0.19	0.07	0.74			0.07	0.93					0.00	1.00		
TS-58	650	500	18	49 amph, 20 di, 19 qtz, 5 an, 7 ta	(iii)				0.22	0.05	0.73			0.08	0.92					0.04	0.96		
TS-35	700	200	17	75 amph, 10 di, 4 qtz, 11 an	(i)	0.14	0.00	0.86	0.15	0.04	0.80			0.03	0.97								
TS-57	700	350	17	73 amph, 2 di, 15 qtz, 10 an	(i)	0.18	0.00	0.82	0.16	0.05	0.80												
TS-69	700	500	12	41 amph, 10 di, 10 qtz, 40 an	(i)				0.26	0.03	0.71	0.95	0.05	0.03	0.97								
TS-3	750	200	60	93 amph, 1 di, 4 qtz, 2 an	(i)				0.14	0.04	0.82												
TS-40	750	350	17	66 amph, 18 di, 6 qtz, 10 an	(i)				0.19	0.05	0.76			0.01	0.99								
TS-14	750	500	7	78 amph, 15 di, 4 qtz, 3 an	(i)				0.23	0.08	0.69			0.04	0.96								
TS-20	800	200	7	68 amph, 20 di, 6 qtz, 6 an	(i)	0.12	0.03	0.85	0.11	0.03	0.86	0.97	0.03	0.00	1.00								
TS-60	800	350	16	84 amph, 1 di, 9 qtz, 5 an	(i)				0.19	0.06	0.75												
TS-47	850	350	19	60 dio, 40 fo, melt	(ii)							0.94	0.06										
				(II) amph-qtz-an-ta																			
TS-67	600	200	32	44 amph, 10 qtz, 34 an, 11 ta	(i)	0.23	0.00	0.77	0.18	0.03	0.79									0.00	1.00		
TS-9	600	500	19	50 amph, 13 qtz, 17 an, 20 ta	(i)	0.26	0.04	0.70	0.24	0.05	0.71									0.02	0.98		
TS-61	650	200	18	49 amph, 12 qtz, 19 an, 20 ta	(i)	0.23	0.01	0.76	0.19	0.05	0.76									0.00	1.00		
TS-13	650	350	19	48 amph, 15 qtz, 17 an, 20 ta	(i)	0.24	0.00	0.75	0.22	0.05	0.73									0.00	1.00		
TS-62	650	500	18	50 amph, 13 qtz, 16 an, 21 ta	(i)	0.26	0.01	0.73	0.25	0.06	0.69									0.02	0.98		
TS-95	700	350	17	48 amph, 13 qtz, 19 an, 20 ta	(i)	0.24	0.01	0.75	0.23	0.06	0.71									0.02	0.98		
TS-68	700	500	12	45 amph, 8 qtz, 43 an, 3 ta	(i)	0.29	0.05	0.66	0.33	0.07	0.60												
TS-94	800	350	16	63 amph, 10 qtz, 22 an, 5 ta	(i)				0.23	0.11	0.66												
				(III) amph-qtz-an-en																			
TS-87	800	200	14	35 amph, 3 qtz, 25 an, 37 en	(i)	0.14	0.13	0.73	0.16	0.10	0.75					0.02	0.98	0.02	0.98				
				(IV) amph-an-ta-cln																			
TS-66	600	200	32	25 amph, 33 an, 22 ta, 20 cln	(i)	0.30	0.03	0.68	0.31	0.04	0.65									0.00	1.00	0.05	0.95
TS-21	650	350	19	74 amph, 13 an, 8 ta, 6 cln	(i)				0.29	0.05	0.65									0.07	0.93	0.07	0.93
TS-37	600	500	19	76 amph, 13 an, 5 ta, 6 cln	(i)	0.36	0.02	0.62	0.33	0.05	0.62									0.19	0.81	0.06	0.94
TS-55	700	500	15	41 amph, 26 an, 20 ta, 12 cln	(i)	0.37	0.03	0.60	0.36	0.06	0.58									0.01	0.99	0.09	0.91
TS-22	750	350	19	70 amph, 19 an, 8 en, 4 fo	(i)	0.28	0.08	0.08	0.33	0.09	0.58							0.05	0.95				
				(V) amph-zo-ta-qtz																			
TS-76	650	1500	8	16 amph, 36 zo, 42 ta, 6 qtz	(i)	0.24	0.10	0.65	0.24	0.06	0.69									0.06	0.94		
TS-72	650	2000	7	12 amph, 33 zo, 42 ta, 10 qtz	(i)	0.21	0.04	0.75	0.19	0.04	0.77									0.03	0.97		
TS-71	750	1500	7	25 amph, 28 zo, 40 ta, 7 qtz	(i)				0.32	0.08	0.61									0.09	0.91		
TS-88	700	2000	7	37 amph, 22 zo, 32 ta, 8 qtz	(i)				0.23	0.05	0.72									0.00	1.00		
				(VI) amph-zo-ta-cln																			
TS-85	700	1500	8	8 amph, 40 zo, 42 ta, 10 cln	(i)	0.34	0.07	0.59	0.33	0.05	0.63									0.05	0.95	0.16	0.84
				(VII) amph-zo-ky-cln																			
TS-84	700	1500	8	43 ta, 30 zo, 14 cln, 13 cor	(i)															0.12	0.88	0.34	0.66

note: Phase proportions of the runs were refined using the Rietveld method. X_{ts} =Al^{tot}/4 = Al^{M2}/2 in amphibole; X_{cum} = Mg^{M4}/2 in amphibole; X_{cats} =Al^{tot}/2 = Al^{M1} in diopside; X_{Mgts} = Al^{tot}/2 = Al^{M1} in enstatite; X_{tats} = Al^{tot}/2 = Al^{M3} in talc; X_{ames} = Al^{tot}/4 = Al^{M1} in chlorite. Al contents (XRD) were derived from cell parameter b for enstatite (Danckwerth and Newton 1978) and diopside (Gasparik 1986) and from cell parameter c for clinochlore (Baker and Holland 1996) and talc (Hoschek 1995). For explanation of groups (i, ii, iii) see text.

Table 3. Refined lattice constants of solid solutions of the tremolite-tschermakite-cummingtonite ternary

run	a (Å)	b (Å)	c (Å)	β (°)
TS-3	9.8066(7)	18.0400(13)	5.2763(3)	104.76(1)
TS-9	9.7942(12)	18.0160(18)	5.2818(4)	104.83(1)
TS-13	9.7958(14)	18.0191(23)	5.2825(5)	104.81(2)
TS-14	9.7858(12)	18.0281(20)	5.2790(5)	104.76(1)
TS-20	9.8138(4)	18.0516(5)	5.2798(1)	104.76(1)
TS-21	9.7889(8)	18.0125(13)	5.2841(28)	104.88(1)
TS-22	9.7729(7)	18.0093(13)	5.2823(3)	104.82(1)
TS-35	9.8054(15)	18.0450(26)	5.2774(6)	104.77(2)
TS-36	9.802(11)	17.9732(26)	5.2984(8)	104.86(18)
TS-37	9.7863(6)	17.9930(9)	5.2846(2)	104.92(1)
TS-38	9.7869(45)	17.9746(90)	5.2754(28)	104.89(7)
TS-40	9.8009(15)	18.0449(31)	5.2790(7)	104.80(2)
TS-55	9.7803(10)	18.0063(0)	5.2851(0)	104.92(0)
TS-57	9.8041(13)	18.0437(20)	5.2797(4)	104.77(1)
TS-58	9.7950(20)	18.0312(30)	5.2804(7)	104.81(2)
TS-59	9.7936(40)	18.0403(83)	5.2823(19)	104.74(6)
TS-60	9.7964(9)	18.0300(10)	5.2777(2)	104.77(1)
TS-61	9.7993(12)	18.0270(24)	5.2797(5)	104.79(1)
TS-62	9.7903(14)	18.0136(21)	5.2832(4)	104.82(2)
TS-66	9.7932(19)	18.0205(32)	5.2847(6)	104.94(2)
TS-67	9.8094(15)	18.0322(26)	5.2822(6)	104.84(2)
TS-68	9.7811(11)	18.0005(17)	5.2819(4)	104.88(1)
TS-69	9.8015(13)	18.0264(20)	5.2807(5)	104.91(2)
TS-71	9.7822(5)	18.0119(7)	5.2816(1)	104.84(1)
TS-72	9.8017(32)	18.0190(40)	5.2818(7)	104.81(3)
TS-76	9.7889(23)	18.0152(31)	5.2839(6)	104.81(2)
TS-85	9.7876(30)	18.0036(30)	5.2843(2)	104.88(1)
TS-87	9.7861(8)	18.0376(11)	5.2783(3)	104.75(1)
TS-88	9.7925(16)	18.0160(17)	5.2856(3)	104.83(1)
TS-94	9.7732(16)	18.0175(23)	5.2812(5)	104.66(2)
TS-95	9.7908(14)	18.0222(27)	5.2807(6)	104.79(2)

amphiboles are solid solutions of the ternary tremolite-tschermakite-cummingtonite. Br concentrations were found to be below the EMP detection limit (0.1wt%). The analyses were normalized to 23 oxygens and the cations were distributed according to the formula $AB_2C_5[T_8 O_{22}/(OH)_2]$, where A = vacant; B = Ca, Mg; C = Mg, Al; T = Al, Si. The total Al concentration was distributed equally ($Al^{tot}/2$) over the C and T sites assuming that the tschermaks substitution is obeyed. A single analysis was accepted if the total oxide sum was in the range of 91 to 99 wt%. Because of the small crystal size of the amphiboles in three runs (TS-9, TS-35, TS-57) the total oxide sum was often below 90 wt%, and a sum between 84-99 wt% was accepted here. T-site occupancies of larger than 8 were calculated from a number of analyses. Such occupancies are unlikely and interpreted as an analytical artifact. Therefore, site occupancies were used as additional criteria and analyses were rejected if these deviations were larger than the analytical error (2σ). If these occupancies exceeded the nominal value by $\pm1\%$ at the T-sites, $\pm3\%$ at the B- and C-sites and $\pm0.5\%$ for the total sum of 15 on all cation sites the analysis was also rejected.

Table 4. Refined lattice constants of Al-bearing phases

run	a (Å)	b (Å)	c (Å)	β (°)
enstatite				
TS-22	18.2241(57)	8.7765(58)	5.1763(23)	
TS-87	18.2262(9)	8.8036(6)	5.1791(2)	
diopside				
TS-14	9.7565(32)	8.9122(25)	5.2656(13)	106.09(2)
TS-20	9.7463(7)	8.9217(7)	5.2544(3)	105.95(1)
TS-34	9.7431(12)	8.9084(10)	5.2596(5)	106.00(1)
TS-35	9.7663(67)	8.9127(47)	5.2669(10)	105.99(3)
TS-36	9.7569(15)	8.9147(16)	5.2601(7)	106.00(1)
TS-38	9.7483(26)	8.9061(24)	5.265528	106.03(2)
TS-40	9.7617(29)	8.9190(26)	5.26758(8)	106.01(2)
TS-58	9.7395(36)	8.9033(25)	5.2659(10)	105.99(3)
TS-59	9.7393(26)	8.9036(21)	5.2646(8)	106.00(2)
TS-69	9.7424(34)	8.9133(26)	5.2576(18)	105.92(3)
clinochlore				
TS-21	5.3207(15)	9.2139(32)	14.3756(86)	96.85(4)
TS-37	5.3207(16)	9.2088(28)	14.3781(77)	96.79(3)
TS-55	5.3181(5)	9.2112(16)	14.3705(42)	96.95(2)
TS-66	5.3188(3)	9.2139(16)	14.3793(48)	96.90(2)
TS-84	5.3133(3)	9.1998(10)	14.3068(33)	96.93(1)
TS-85	5.3141(4)	9.1981(11)	14.3513(99)	96.89(3)

run	a (Å)	b (Å)	c (Å)	α (°)	β (°)	γ (°)
talc						
TS-9	5.2936(10)	9.1647(8)	9.4882(31)	90.54(2)	99.96(2)	90.00(1)
TS-13	5.2955(20)	9.1649(14)	9.4943(40)	90.57(3)	99.89(5)	89.98(2)
TS-21	5.2948(33)	9.1670(31)	9.4645(61)	90.76(5)	99.69(7)	90.00(3)
TS-34	5.2979(10)	9.1633(15)	9.4763(32)	90.22(2)	100.29(2)	89.96(1)
TS-36	5.2921(22)	9.1642(15)	9.5076(31)	90.41(3)	100.07(3)	90.03(3)
TS-37	5.3095(44)	9.1619(36)	9.4106(86)	90.47(8)	99.39(8)	90.03(6)
TS-38	5.2736(22)	9.1627(34)	9.4899 (39)	90.40(4)	100.27(4)	89.68(3)
TS-55	5.2923(9)	9.1619(10)	9.4984(42)	89.98(2)	100.24(3)	89.85(2)
TS-58	5.2834(70)	9.1652(79)	9.485(11)	90.79(10)	100.04(10)	90.11(7)
TS-59	5.2891(35)	9.1631(38)	9.4843(68)	90.64(7)	99.42(8)	90.09(4)
TS-61	5.2930(22)	9.1622(15)	9.4862(33)	90.67(3)	99.61(5)	90.01(2)
TS-62	5.2946(23)	9.1650(15)	9.4889(42)	90.54(3)	100.06(5)	90.00(2)
TS-66	5.2965(9)	9.1688(11)	9.4926(33)	90.56(2)	99.85(3)	89.96(1)
TS-67	5.3052(33)	9.1643(33)	9.5039(46)	90.65(5)	100.06(7)	89.88(4)
TS-71	5.2955(7)	9.1663(6)	9.4689(19)	90.56(1)	100.06(2)	90.01(1)
TS-72	5.3004(8)	9.1639(7)	9.4828(15)	90.30(1)	99.87(2)	90.11(1)
TS-76	5.2933(7)	9.1651(6)	9.4772(16)	90.43(1)	99.99(2)	90.01(1)
TS-84	5.2919(6)	9.1668(5)	9.4639(15)	90.32(1)	100.24(2)	90.03(1)
TS-85	5.2929(4)	9.1656(5)	9.4816(24)	90.41(1)	100.04(1)	90.01(1)
TS-88	5.2955(7)	9.1672(5)	9.4933(23)	90.51(1)	99.92(2)	90.01(1)
TS-95	5.2942(23)	9.1628(16)	9.4862(34)	90.56(3)	99.88(5)	90.00(2)

Table 5. Compositions of synthesized amphibole solid solutions from EMP measurements

run	TS-9	TS-13	TS-20	TS-21	TS-22	TS-35	TS-37	TS-55	TS-57	TS-61	TS-62	TS-67	TS-68	TS-72	TS-76	TS-85	TS-87	TS-95
no. of analyses	9	18	20	11	9	3	10	15	1	11	6	9	9	7	2	15	10	13
CaO	12.38	13.16	13.05	13.07	12.35	12.85	13.23	13.21	12.04	13.36	13.36	13.75	12.84	13.10	11.70	12.52	12.04	13.16
MgO	20.69	20.99	23.22	20.84	21.79	21.44	20.73	21.09	19.38	21.81	21.58	22.16	21.65	22.43	21.41	21.22	24.30	21.46
Al_2O_3	5.94	5.77	2.83	7.20	6.91	3.15	8.83	9.04	3.80	5.75	6.45	5.64	7.21	5.25	5.81	8.34	3.44	5.68
SiO_2	51.62	53.33	56.46	53.76	53.48	52.06	53.21	53.08	49.37	54.56	53.88	55.66	53.80	55.37	53.12	52.87	57.53	53.48
Σ oxides	90.63	93.25	95.56	94.87	94.53	89.49	96.00	96.42	84.59	95.48	95.25	97.21	95.51	96.15	92.04	94.95	97.31	93.78
2σ standard deviation of the mean																		
ΔCaO	1.22	0.49	0.49	1.03	1.63	0.64	1.08	0.85	-	0.53	0.32	0.54	0.62	0.97	1.40	1.08	0.66	0.60
ΔMgO	1.85	1.94	1.42	0.82	1.28	1.08	0.82	1.12	-	1.31	0.32	1.32	1.52	1.66	0.22	1.42	1.17	0.85
ΔAl_2O_3	0.93	2.92	0.87	1.28	0.95	0.17	0.96	1.16	-	0.41	0.19	0.39	1.30	1.89	0.73	1.49	0.41	0.67
ΔSiO_2	4.02	3.73	2.70	2.29	3.25	2.76	2.44	2.34	-	2.16	1.41	1.92	3.16	2.79	2.04	2.38	1.63	1.50
amphibole composition based on 23 oxygens																		
Ca^{M4}	1.93	2.00	1.93	1.95	1.84	2.04	1.95	1.94	2.01	1.98	1.99	2.00	1.90	1.93	1.79	1.86	1.74	1.99
Mg^{M4}	0.07	0.00	0.07	0.05	0.16	0.00	0.05	0.06	0.00	0.02	0.01	0.00	0.10	0.07	0.21	0.14	0.26	0.01
$Mg^{M1,2,3}$	4.43	4.43	4.71	4.27	4.38	4.73	4.21	4.25	4.51	4.48	4.45	4.50	4.36	4.52	4.35	4.26	4.64	4.50
$Al^{[6]}$	0.51	0.48	0.23	0.59	0.57	0.27	0.72	0.73	0.35	0.47	0.53	0.45	0.59	0.42	0.49	0.68	0.27	0.47
$Al^{[4]}$	0.51	0.48	0.23	0.59	0.57	0.27	0.72	0.73	0.35	0.47	0.53	0.45	0.59	0.42	0.49	0.68	0.27	0.47
Si	7.52	7.56	7.80	7.48	7.46	7.70	7.32	7.28	7.71	7.55	7.48	7.57	7.44	7.60	7.59	7.35	7.77	7.54
X_{ts}	0.26	0.24	0.12	0.30	0.28	0.14	0.36	0.37	0.18	0.23	0.26	0.23	0.29	0.21	0.24	0.34	0.14	0.24
ΔX_{ts}	0.02	0.06	0.02	0.02	0.02	0.01	0.02	0.02	0.00	0.01	0.00	0.01	0.02	0.03	0.01	0.03	0.01	0.01
X_{cum}	0.04	0.00	0.03	0.03	0.08	0.00	0.02	0.03	0.00	0.01	0.01	0.00	0.05	0.04	0.10	0.07	0.13	0.01
X_{tr}	0.71	0.75	0.85	0.68	0.64	0.86	0.62	0.60	0.82	0.76	0.73	0.77	0.66	0.75	0.65	0.59	0.73	0.75
Σ M1-3	4.94	4.92	4.94	4.86	4.95	5.00	4.92	4.98	4.86	4.95	4.98	4.95	4.95	4.94	4.84	4.94	4.91	4.97
Σ T	8.03	8.04	8.03	8.07	8.03	7.98	8.04	8.01	8.06	8.02	8.01	8.03	8.02	8.03	8.08	8.03	8.05	8.01
Σ cations	14.97	14.96	14.97	14.93	14.97	15.02	14.96	14.99	14.94	14.98	14.99	14.98	14.98	14.97	14.92	14.97	14.95	14.99

note: Σ M1-3 = Mg^{M1,2,3} + Al$^{[6]}$; Σ T = Al$^{[4]}$ + Si; X_{ts} = (Al$^{[4]}$ + Al$^{[6]}$)/ 4; X_{cum} = Mg^{M4} / 2

Compositions of diopside from runs TS-20, TS-36, TS-47 and TS-69 as well as of enstatite from run TS-87 were also obtained by EMP. Amounts of Al of up to 0.12 apfu in diopside and 0.04 apfu in enstatite were observed (Table 6). Because of the small size of the pyroxene crystals, the total oxide sum was often below 100 wt%. Therefore, single analyses with a total oxide sum as low as 90 wt% were accepted. The analyses were calculated on the basis of six oxygens according to the pyroxene formula XY $[T_2 O_6]$ with X = Ca, Mg; Y = Mg, Al; T = Al, Si. Again, the total Al content (Al^{tot}) was distributed equally ($Al^{tot}/2$) over the X and T sites assuming that tschermaks substitution is obeyed.

Table 6. Composition of Al-bearing ortho- and clinopyroxenes

run	TS-20	TS-36	TS-47	TS-69	TS-87
phase	di	di	di	di	en
no. of analyses	5	2	2	4	3
CaO	24.9	23.02	24.79	23.67	0.54
MgO	18.2	15.81	15.48	17.43	38.24
Al_2O_3	1.27	2.59	2.56	2.49	1.19
SiO_2	54.3	50.28	51.69	52.64	59.51
Σ oxides	98.7	91.69	94.51	96.24	99.48
2σ standard deviation of the mean					
ΔCaO	1.37	1.11	0.66	2.28	0.14
ΔMgO	1.19	2.99	1.25	2.09	0.05
$ΔAl_2O_3$	0.33	4.30	0.62	0.77	0.31
$ΔSiO_2$	2.15	1.15	3.03	5.14	0.90
pyroxene composition based on 6 oxygens					
Ca^{M2}	0.97	0.96	1.01	0.95	0.02
Mg^{M2}	0.03	0.04	0.00	0.05	0.96
Mg^{M1}	0.96	0.89	0.88	0.91	0.96
$Al^{[6]}$	0.03	0.06	0.06	0.05	0.02
$Al^{[4]}$	0.03	0.06	0.06	0.05	0.02
Si	1.98	1.97	1.97	1.96	2.00
X_{ts}	0.03	0.06	0.06	0.05	0.02
$ΔX_{ts}$	0.00	0.05	0.01	0.01	0.01
X_{en}	0.03	0.04	0.00	0.05	0.96
X_{di}	0.94	0.91	0.94	0.89	0.02
Σ M1-2	1.99	1.95	1.95	1.97	1.96
Σ T	2.01	2.03	2.03	2.02	2.02
Σ cations	3.99	3.97	3.97	3.98	3.98

note: $Σ M1\text{-}2 = Ca^{M2} + Mg^{M1,2} + Al^{[6]}$; $Σ T = Al^{[4]} + Si$; $X_{ts} = (Al^{[4]} + Al^{[6]})/2$; $X_{en} = Mg^{M2}$

Anorthite, quartz, forsterite and zoisite had endmember compositions. The talc and chlorite crystals were too small (< 1 μm) to obtain reasonable EMP-analyses. The results from EMP and XRD measurements show that the observed phases amphibole, orthopyroxene, clinopyroxene, talc and chlorite were always solid solutions of two or more

endmembers. The compositions of the amphiboles from many runs were obtained by EMP and XRD and the results generally agree (Table 2). In a few runs, amphiboles were too small for accurate EMP analyses and total sums were low. In addition, their cummingtonite contents as obtained by EMP are of low accuracy (Najorka and Gottschalk, submitted). On the other hand, reasonable lattice parameters were obtained for all phases in mineral mixtures even if the total amount of a particular phase within the assemblage was as low as 5 wt%. Furthermore, precise relationships between lattice parameters and composition in the tremolite-tschermakite-cummingtonite ternary do exist (Najorka and Gottschalk, submitted). This holds also for pyroxene compositions, where similar results with EMP and XRD were obtained (Table 2). For talc and chlorite solid solutions only compositions from XRD were available. In the following, all compositional details rely on data obtained by XRD.

Compositions of amphiboles in the *P-T-X*-space

Stability fields of the water-saturated assemblages amphibole-anorthite-quartz-diopside, amphibole-anorthite-quartz-talc, amphibole-anorthite-quartz-enstatite, amphibole-anorthite-clinochlore-talc, amphibole-zoisite-quartz-talc, amphibole-zoisite-clinochlore-talc, and amphibole-zoisite-kyanite-clinochlore have been calculated for the respective bulk compositions (I) to (VII) using VERTEX (Connolly 1990) and assuming $a_{H_2O} = X_{H_2O}$ (values from Table 1). Results are shown in Fig.s 4a-4d. Thermodynamic properties for mineral endmembers are from the internally consistent data set of Gottschalk (1997). The activities of diopside in clinopyroxene, enstatite in orthopyroxene, clinochlore in chlorite, and talc in talc-tats solid solutions were calculated with compositions from Table 2 and mixing models explained in a section below. In Fig.s 4a-d the measured X_{ts}–values are plotted into the calculated stabilitiy fields along with X_{ts}–isopleths that were calculated using a two-site coupled model for Al incorporation into amphibole (see also discussion below).

Bulk composition amphibole-anorthite-quartz-diopside

Fourteen runs were performed at 200 to 500 MPa and 600 to 850°C using bulk composition (I) that should have produced the assemblage amphibole-anorthite-quartz-diopside. Amphibole coexisting with anorthite-quartz-diopside was observed in eight runs at 700°C, 750°C, and 800°C (filled circles in Fig. 4a). X_{ts} in amphibole is strongly pressure dependent and increases from 0.11-0.15 at 200 MPa to 0.23-0.26 at 500 MPa. In experiments
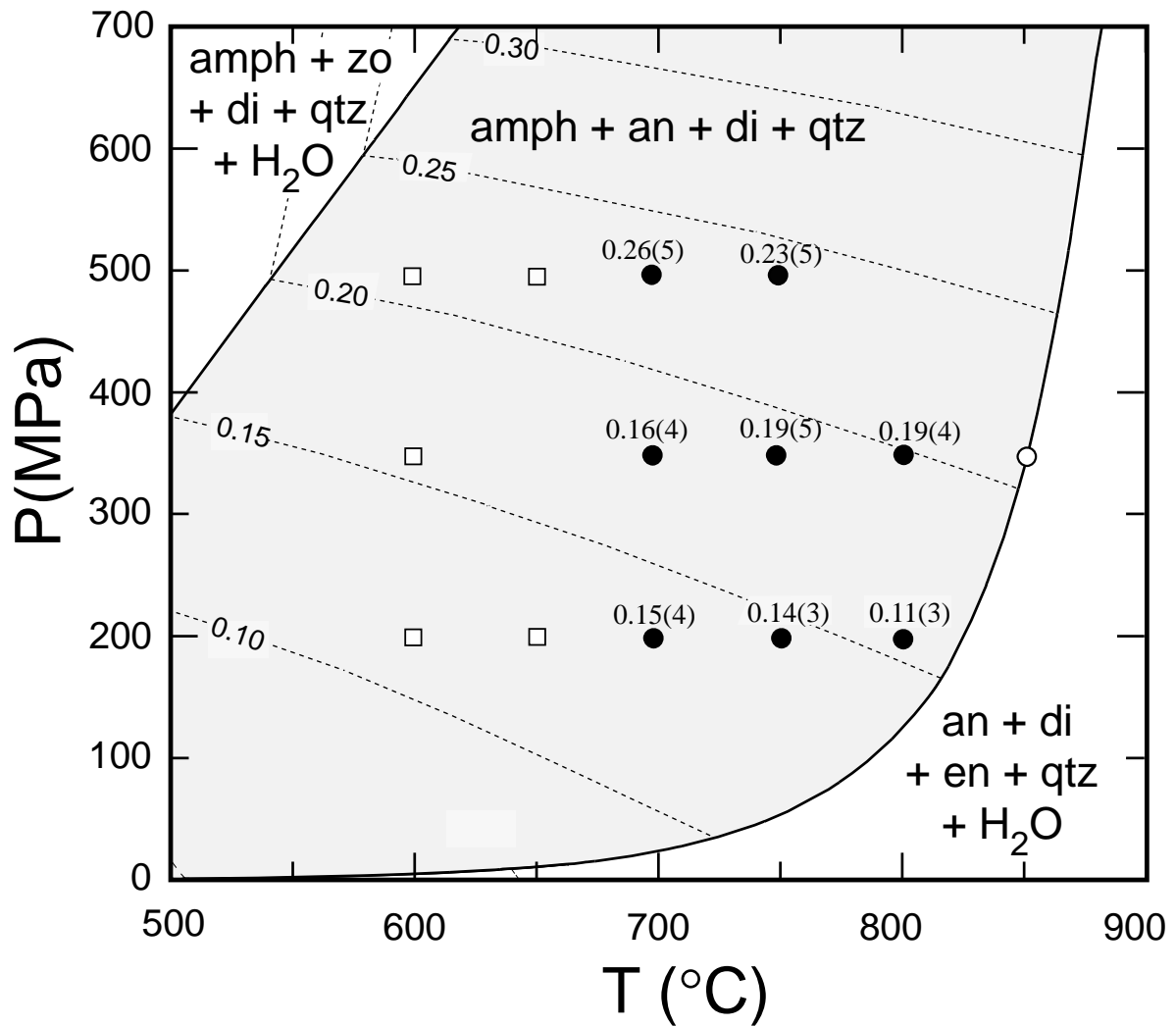
Fig. 4a. *P-T* plot of the stability field of the assemblage amphibole-anorthite-diopside-quartz for bulk composition (I) calculated with VERTEX (Connolly 1990) and assuming $a_{H_2O} = 0.98$ (Table 1). Runs between 700 and 800°C yielded the assemblage amphibole-anorthite-diopside-quartz (filled circles). In runs between 600-650°C talc occurred as additional phase (open squares). At 850°C and 350 MPa diopside, forsterite plus melt formed (open circle). Dashed lines denote X_{ts}-isopleths calculated using a two-site coupled model for Al-incorporation in amphibole (see below). Note that exchange reaction (1) does not depend on a_{H_2O}.

between 600-650°C, talc occurred as an additional phase (open squares in Fig. 4a). In talcbearing runs, X_{ts} in amphiboles is significantly higher and ranges from 0.19 to 0.30. Obviously, there is a metastable phase in this assemblage (see discussion below) and values for X_{ts} were therefore omitted in Fig. 4a. No amphibole formed in run TS-47 (850°C, 350 MPa) where only diopside, forsterite and melt were detected.

Bulk composition amphibole-anorthite-quartz-talc

Eight runs were performed at 200-500 MPa and 600-800°C using bulk composition (II) in the amphibole-anorthite-quartz-talc subsystem (filled circles in Fig. 4b). This phase assemblage was produced in all runs. The tschermakite component in amphibole is, again, strongly pressure dependent and increases from 0.18 at 200 MPa to 0.24-0.33 at 500 MPa.

Bulk composition amphibole-anorthite-quartz-enstatite

One experiment was conducted at 200 MPa and 800°C using bulk composition (III) in the amphibole-anorthite-quartz-enstatite subsystem. This phase assemblage was produced and X_{ts} of the amphibole was 0.16 (filled square in Fig. 4b).

Bulk composition amphibole-anorthite-clinochlore-talc

Five runs were carried out at 200-500 MPa and 600-750°C using bulk composition (IV) in the subsystem amphibole-anorthite-clinochlore-talc. At 600 to700°C this assemblage was actually produced (filled circles in Fig. 4c). X_{ts} in amphibole increased with pressure and temperature from 0.29 (650°C, 350 MPa) to 0.36 (700°C, 500 MPa). At 750°C and 350 MPa clinochlore was not stable and, as predicted by VERTEX, the assemblage amphibole-anorthite-enstatite-forsterite was observed instead (square in Fig. 4c).

Bulk composition amphibole-zoisite-talc-quartz

Four runs were performed at 1500-2000 MPa and 650-750°C with bulk composition (V) in the subsystem amphibole-zoisite-talc-quartz. The phase assemblage amphibole-zoisite-talc-quartz always formed (Fig. 4d), despite the fact that at 1500 MPa and 750°C calculations by VERTEX predict presence of kyanite instead of talc. X_{ts} in amphibole varies with temperature and pressure. The lowest (0.19) and the highest (0.32) X_{ts} were observed at 650°C, 2000 MPa and 750°C, 1500 MPa, respectively.

Bulk composition amphibole-zoisite-talc-clinochlore

One run, using bulk composition (VI) in the amphibole-zoisite-talc-clinochlore subsystem, was performed at 1500 MPa and 700°C (TS-85). Indeed, the assemblage amphibole-zoisite-talc-clinochlore formed and X_{ts} in amphibole is 0.33.

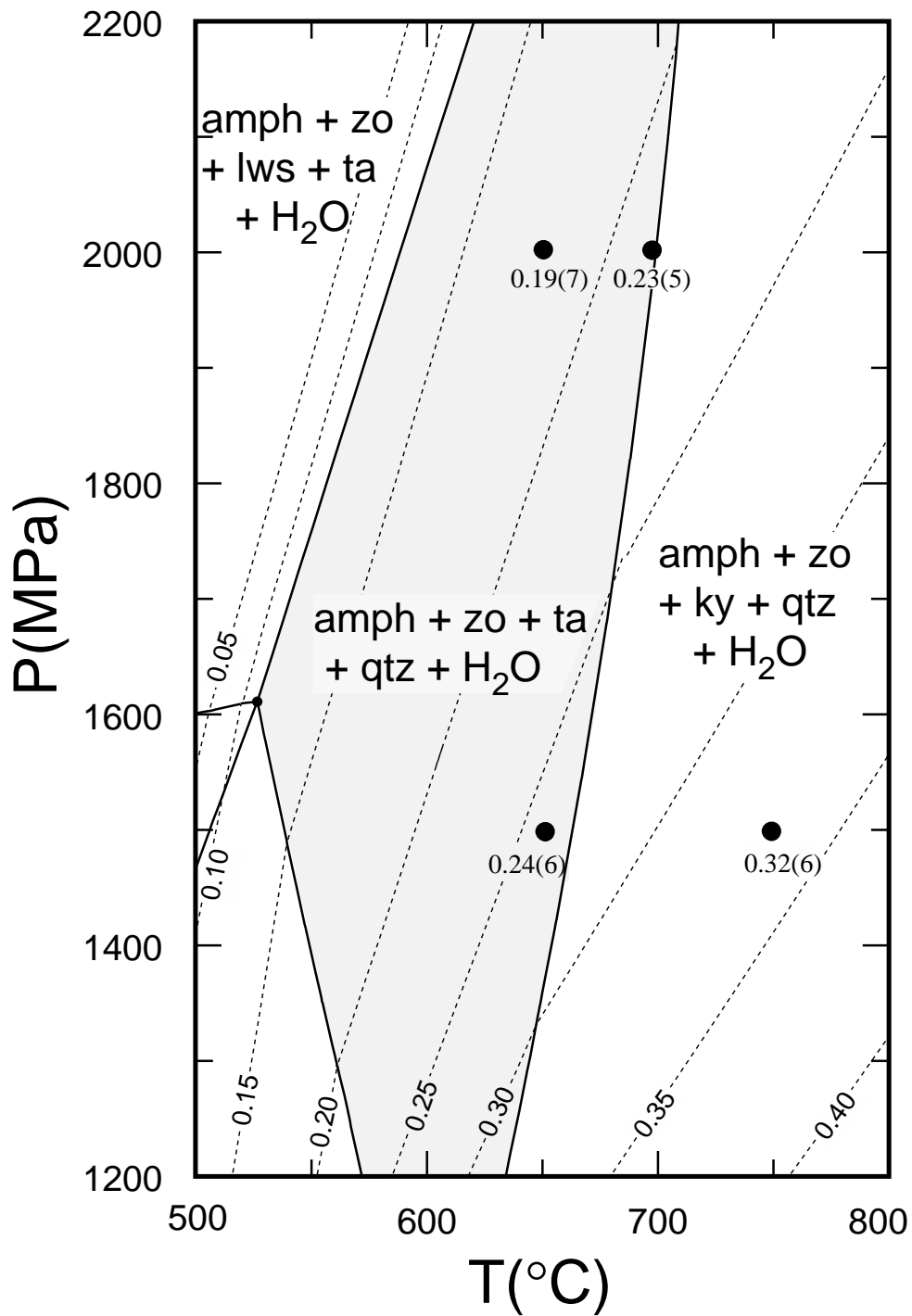*Bulk composition amphibole-zoisite-kyanite-clinochlore*

One run was performed at 700°C and 1500 MPa with bulk composition (VII) in the amphibole-zoisite-kyanite-clinochlore subsystem. No amphibole formed and only the phases talc, zoisite, clinochlore and corundum crystallized (TS-84).
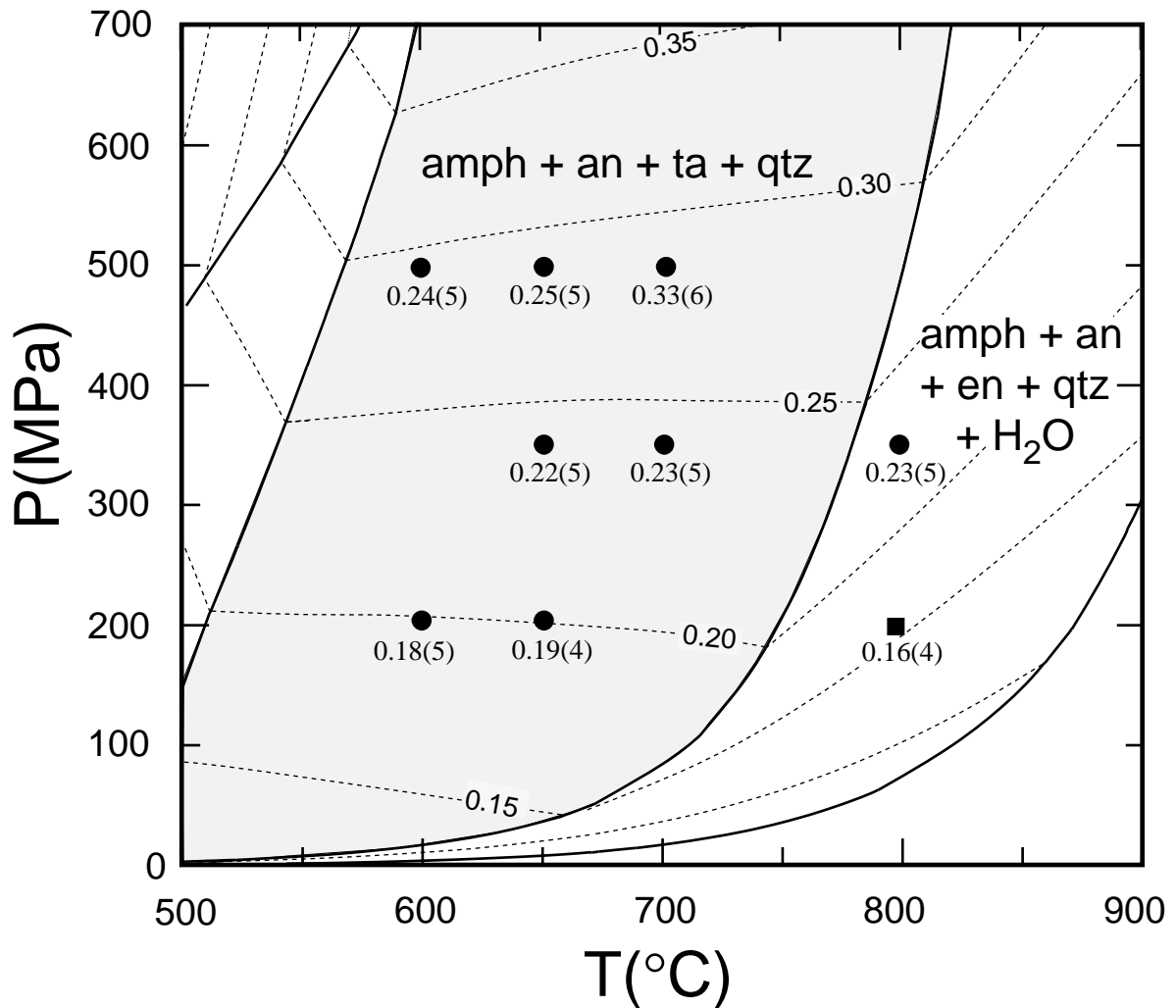
Fig. 4b. *P-T* plot of the stability fields of the assemblages amphibole-anorthite-talc-quartz and amphibole-anorthite-enstatite-quartz for bulk compositions (II) and (III) calculated with VERTEX (Connolly 1990) and assuming a_{H_2O} = 0.97 (Table 1). Filled circles represent runs which yielded the assemblage amphibole-anorthite-talc-quartz. Square represents run TS-87 which yielded the assemblage amphibole- anorthite-enstatite-quartz. Dashed lines show X_{ts}-isopleths calculated using a two-site coupled model for Al-incorporation in amphibole (see below).
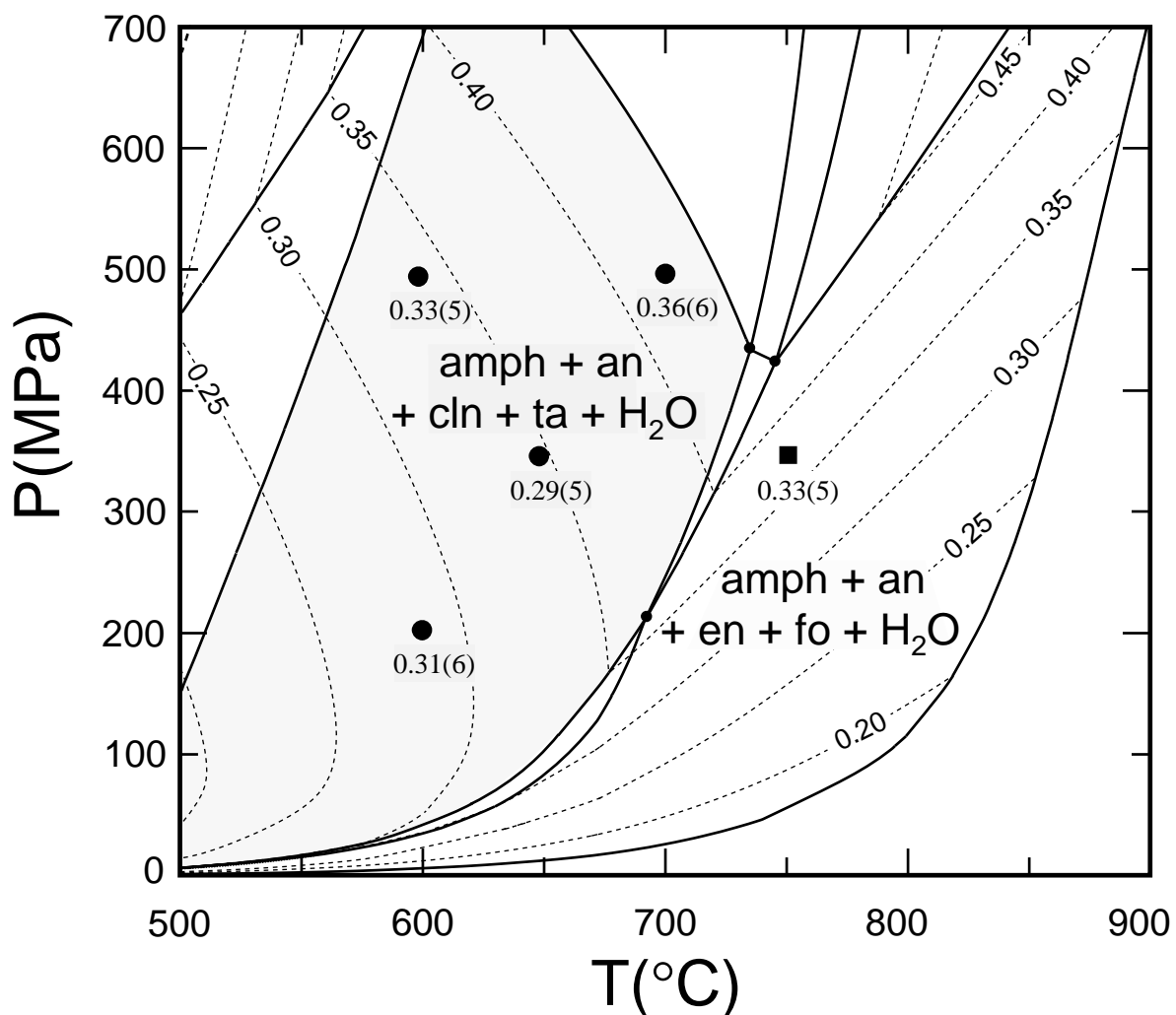
Fig. 4c. *P-T* plot of the stability fields of the assemblages amphibole-anorthite-clinochlore-quartz and amphibole-anorthite-enstatite-forsterite for bulk composition (IV) calculated with VERTEX (Connolly 1990) and assuming $a_{H_2O} = 0.99$. Filled circles represent runs yielding the assemblage amphibole-anorthite-clinochlore-quartz. Square represents run TS-22 which yielded the assemblage amphibole-anorthite-enstatite-forsterite, in agreement with the stability fields calculated by VERTEX. Dashed lines show X_{ts}-isopleths calculated using a two-site coupled model for Al-incorporation in amphibole (see below).

Fig. 4d. *P-T* plot of the stability field of the assemblage amphibole-zoisite-talc-quartz for bulk composition (V) calculated with VERTEX (Connolly 1990) and assuming $a_{H_2O} = 0.98$. Filled circles represent runs which yielded the assemblage amphibole-zoisite-talc-quartz. Dashed lines show X_{ts}-isopleths calculated using a two-site coupled model for Al-incorporation in amphibole (see below).

DISCUSSION

Phase assemblages

In the five component system CaO-MgO-Al_2O_3-SiO_2-H_2O equilibrium assemblages of five phases are divariant. If fluid is present, stable assemblages then consist of four solids, shown as group (i) in Table 2. For any given pressure and temperature, the compositions of all phases are fixed even if the bulk chemistry varies within certain compositional limits. Such assemblages form subtetrahedra within the CaO-MgO-Al_2O_3-SiO_2 tetrahedron (Fig. 2) and have stability fields in the P-T-space (Fig. 4). An additional degree of freedom is introduced if only three solids are observed. In this case, variations in the bulk composition are accompanied by changes in the composition of one or more phases. Such three solid assemblages are represented by triangles within a tetrahedron. We found no amphibole-bearing three solid assemblages in our experiments. Obviously, the chosen bulk compositions did not allow for formation of reduced assemblages except from run TS-47 where at 850°C and 350 MPa diopside, forsterite and melt were produced (group (ii) in Table 2). Equilibrium assemblages of five solids are univariant. In Fig. 2, such assemblages are represented by a distorted ditrigonal pyramid, where a triangle is common to two adjacent tetrahedra on which the respective starting bulk composition resides. In P-T-space they are stable along the univariant reaction curves denoted in Fig.s 4a-d. However, the presence of five solids (group (iii) in Table 2) in our experimental products does not necessarily mean that this actually constitutes a stable univariant assemblage because one of the phases may have formed metastably. If a stable amphibole-bearing univariant assemblage formed, compositions of amphibole solid solutions at the univariant boundaries must agree with the intersecting X_{ts}-isopleths from the divariant field. If not, metastable formation of at least one phase is indicated.

The majority of the runs yielded four solids plus fluid (group (i)) with phase assemblages according to the chosen bulk compositions and amphibole solid solutions of the tremolite-tschermakite-cummingtonite ternary. Within each phase assemblage, X_{ts} of the amphiboles systematically varied with pressure and temperature and the compositional scatter was low. At given pressure and temperature, different bulk compositions produced different four solid assemblages with varying amphibole compositions. This is in line with chemographical considerations because, in this case, adjacent subtetrahedra are not allowed to intersect (Fig. 2). At 500 MPa and 700°C, for example, three different assemblages were

produced: amphibole-anorthite-quartz-diopside from bulk composition (I), amphibole-anorthite-quartz-talc from bulk composition (II) and amphibole-anorthite-clinochlore-talc from bulk composition (IV), with amphibole solid solutions having X_{ts}–values of 0.26, 0.33 and 0.36, respectively. Increasing X_{ts} in amphiboles from assemblages (I), (II) and (IV) is consistent because the corresponding subtetrahedra for these assemblages indeed do not intersect. For any other compositional sequence, the subtetrahedra would overlap at that corner that is represented by the amphibole composition along the trts-join (Fig. 2) and, if present, would indicate inconsistency. Similarly, at 500 MPa and 700°C, X_{cum} of 0.07 in amphiboles from assemblage (II) and of 0.06 from (IV) were higher than that of 0.03 from assemblage (I), again indicating internal consistency. Also, the cummingtonite component within each assemblage increases with temperature as predicted by Gottschalk et al. (1999).

These observations indicate that the assemblages and phase compositions of group (i) experiments represent equilibrium or are at least close to equilibrium. Although oxides and hydoxides were used as starting materials and no reversed runs were conducted, three observations argue for equilibrium: First, the compositional scatter of the solid solutions is low. Second, the synthesized amphiboles are well ordered with low chain multiplicity fault concentrations (Najorka and Gottschalk, submitted). Third, phase relations and compositions of solid solutions are consistent. This holds with the exception of the three runs, TS-94, TS-71, and TS-84. Run TS-94, conducted with bulk composition (II) at 800°C and 350 MPa should have produced amphibole-quartz-anorthite-talc, and it did. However, calculations by VERTEX predict the stability of enstatite instead of talc at these conditions (Fig. 4b). The calculated reaction boundary is only lower by 18°C at 350 MPa, which is probably within the error limits of the calculation scheme, and amphibole-quartz-anorthite-talc is considered to be the stable assemblage. Run TS-71, conducted with bulk composition (V) at 750°C and 1500 MPa, should have produced amphibole-zoisite-talc-quartz, and it also did. VERTEX predicts the stability of kyanite instead of talc, which is unstable above 650°C (Fig. 4d). It is well known that in experiments kyanite notoriously fails to nucleate, and because of that, the stability field of amphibole-zoisite-talc-quartz is believed to have extended metastably to higher temperatures. Nucleation problems of kyanite probably also caused formation of corundum in run TS-84 and prevented formation of amphibole. We have therefore no information from the experiment using bulk composition (VII).

Five experiments at 600 to 650°C and 200 to 500 MPa (TS-34, TS-36, TS-38, TS-58, TS-59) performed with bulk composition (I) produced talc in addition to the expected four solid assemblage amphibole-anorthite-quartz-diopside (group (iii) in Table 2). In these runs,

X_{ts} in amphiboles is significantly higher than indicated for the four solid assemblage amphibole-anorthite-quartz-diopside (Table 2, Fig. 4a). Measured X_{ts} in amphiboles from 0.19 to 0.30 from the five solid assemblage would fit somewhat better into the compositional pattern of the assemblage amphibole-anorthite-quartz-talc. According to the arguments given above, one of the observed phases is metastable. This is probably talc, which might have nucleated rapidly during heating up at lower temperatures and failed to decompose between 600 and 650°C, but did at temperatures above. In any case, the five solid assemblage does not represent a univariant assemblage and results are excluded from further considerations.

Comparison with earlier results

Amphiboles along the tremolite-tschermakite join have been synthesized and studied experimentally by Jasmund and Schäfer (1972), Oba (1978), Cao et al. (1986), Cho and Ernst (1991), Jenkins (1981, 1983, 1988, 1994), Smelik et al. (1994), Hoschek (1995), Jenkins et al. (1997) and Najorka and Gottschalk (submitted). The synthesis of pure endmember tschermakite was claimed by Oba (1978), however, our recalculation of his lattice constants using the compositional dependence of the a and β lattice parameters (Najorka and Gottschalk, submitted) results in a maximum X_{ts} of 0.55, far from the assumed composition of tschermakite endmember. This is in accordance with an experimental study by Jenkins (1988), where a maximum X_{ts} of about 0.50 was determined. Limited tremolite-tschermakite solid solutions of up to roughly magnesiohornblende (X_{ts} = 0.50) were also observed in experimental studies by Jasmund and Schäfer (1972), Cho and Ernst (1991), Smelik et al. (1994), Jenkins et al. (1997), Hoschek (1995), and Najorka and Gottschalk (submitted). The highest X_{ts} of up to 0.60 in tremolite-tschermakite solid solutions were reported by Cho and Ernst (1991) at 1250 MPa and 900 °C.

It is not clearly understood yet if structural or thermodynamical restrictions were responsible for the limited incorporation of the tschermakite component into tremolite. Measured Al-concentrations for different assemblages at varying bulk compositions show that X_{ts} does not exceed 0.36 at our experimental P-T conditions, and calculated X_{ts}-isopleths reveal that X_{ts} is always lower than 0.5 over the whole P-T range (Fig.s 4a-d). This suggests that possible Al-rich tremolite-tschermakite solid solutions are thermodynamically unstable with respect to other phase assemblages. This is also seen in the CMAS(H)-tetrahedron (Fig. 2). We found, for example, that at 700°C and 500 MPa bulk composition (IV) produced amphibole-anorthite-clinochlore-talc with X_{ts} of 0.36 (TS-55; Fig. 4c). If, at identical P-T

134

conditions, the bulk composition is shifted towards the Al_2O_3 apex, the Al-concentration in amphibole is buffered to some extent by anorthite-clinochlore-talc at relatively low X_{ts} (Fig. 2, IV). If, on the other hand, the *P-T* conditions are changed to 750° and 350 MPa at identical bulk composition, the new assemblage amphibole-anorthite-enstatite-forsterite becomes stable (TS-22; Fig.s 4c and 5). Again, X_{ts} in amphibole is buffered by anorthite-enstatite-forsterite at somewhat lower values within narrow compositional limits. It can be shown, that for common bulk compositions large stability ranges of four solid assemblages in the *P-T*-space exist, which preclude tremolite-tschermakite solid solutions with high tschermakite contents.
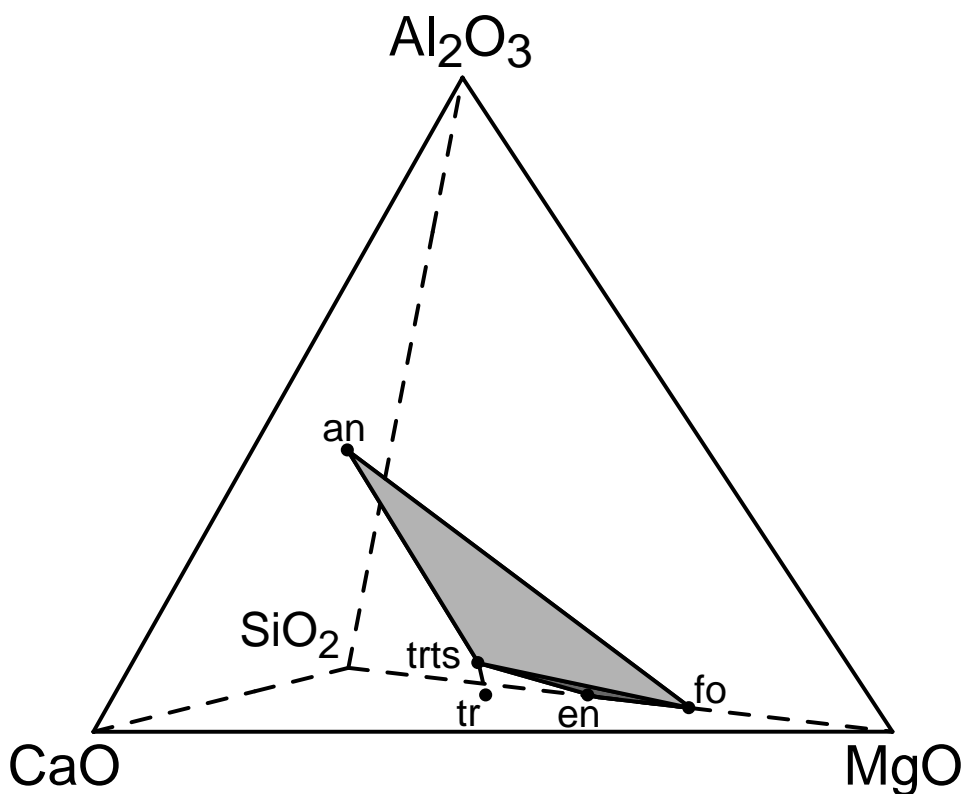
Fig. 5. The phase assemblage amphibole-anorthite-enstatite-forsterite produced by bulk composition (IV) plotted into the CMAS-tetrahedron with excess water (see also Fig. 4c)

Our measured Al-concentrations in amphiboles from the assemblage amphibole-anorthite-quartz-diopside (I) show distinct differences compared to the results of Jenkins (1994) who investigated the same assemblage between 600-800°C and 200-700 MPa. Both studies agree insofar as a significant pressure dependence of the Al-isopleths in amphibole was detected. However, Jenkins (1994) suggested that at 700°C, X_{ts} would increase from 0.07 to 0.12 as pressure increases from 200 to 500 MPa, whereas our study shows that at 700°C X_{ts} increases from 0.15 to 0.26 over the same pressure range. The pressure effect in our study is much more pronounced. These discrepancies possibly reflect errors in the analytical methods. The compositions of the amphiboles in Jenkins' (1994) study rely in part on the location of the (310) reflection in the XRD-pattern where presence of cummingtonite component of 10 mol% was assumed (see Fig. 1). Our results show that most X_{cum}–values are between 0.03 to 0.06 (Table 2). Overestimation of X_{cum}, however, results in a large underestimation of the tschermakite component (see also Najorka and Gottschalk, submitted) and this is probably the main reason for the observed discrepancy. On the other hand, EDS-analyses of amphiboles in unpolished grain mounts as used by Jenkins (1994) are probably not precise enough for accurate amphibole compositions.

Our measured Al-concentrations in amphiboles that were produced with bulk composition (IV) show overall agreement with the results of Cao et al. (1986) on the three solid assemblage amphibole-anorthite-clinochlore (without talc) and on the four solid assemblage amphibole-anorthite-enstatite-forsterite. For the former, Cao et al. (1986) detected X_{ts} to about 0.40 at 720°C/1000 MPa using a few EMP measurements of unpolished grain mounts, and in our experiments X_{ts} was 0.29 at 650°C/350 MPa, and 0.37 at 700°C/500 MPa. For the latter, they found $X_{ts} = 0.20$ at 795°C/200 MPa. Our value is 0.33 at 750°C/350 MPa. Given the relatively large compositional scatter in our experiments (see Fig. 4c), a similar *P-T-X* dependence of the Al concentrations in amphibole for bulk composition (IV) is indicated.

THERMODYNAMIC EVALUATION

Thermodynamic properties of tschermakite and magnesiohornblende

At fixed pressure and temperature, a five phase assemblage (four solids plus fluid) in the CMASH system is invariant. For such an assemblage, a reaction can be formulated and used to evaluate the thermodynamic properties of one or more phases or phase components. For the experimentally observed assemblages (I-VI), the corresponding exchange reactions are given by eqs. (1)-(6). Using these exchange reactions, the experimental results are used to extract the thermodynamic properties of tschermakite endmember and the mixing properties of the tremolite-tschermakite-cummingtonite solid solutions. The equilibrium of each reaction is given by

$$\Delta G_r = 0 = \sum_i \nu_i \left(G_i^o + RT \ln a_i \right) + \nu_{H_2O} RT \ln f_{H_2O}^o \tag{7}$$

in which G_i^o is the molar standard Gibbs free energy of the pure phase i, ν_i its stoichiometric coefficient, a its activity and $f_{H_2O}^o$ the fugacity of pure H_2O. Introducing the standard Gibbs free energy of tschermakite G_{ts}^o explicitly

$$\sum_i \nu_i G_i^o = \sum_{j \neq ts}^{k-1} \nu_j G_j^o + \nu_{ts} G_{ts}^o, \tag{8}$$

eq. (7) is rearranged:

$$-\nu_{ts} G_{ts}^o = \sum_{j \neq ts}^{k-1} \nu_j G_j^o + \sum_i^k \nu_i RT \ln a_i + \nu_{H_2O} RT \ln f_{H_2O}^o \tag{9}$$

Considering the reference conditions $T°$ and $P°$ at 298 K and 0.1 MPa, and introducing the temperature and pressure dependence for G_i^o, the apparent Gibbs free energy $(\Delta_f H_i^o - TS_i^o)$ instead of G_i^o, and the definition of the equilibrium constant K, eq. (9) becomes:

$$\Delta_f H_{ts}^o - TS_{ts}^o = -\frac{1}{\nu_{ts}} \left(\sum_{j \neq ts}^{k-1} \nu_j \left(\Delta_f H_j^o - TS_j^o \right) + RT \ln K_{(P,T)} - \int_{T^o}^{T_f} \int_{T^o}^{T_f} \frac{\Delta c_P^o}{T} dTdT + \int_{P^o}^{P} \Delta V_{solids}^o dP \right) \tag{10}$$

If the right hand side of eq. (10) is evaluated for equilibria (1) to (6) at various *P-T* conditions, a plot of the results *versus* temperature results in a straight line, where the enthalpy of formation from the elements $\Delta_f H_{ts}^o$ and the third law entropy S_{ts}^o of tschermakite endmember is determined from the intersect and slope, respectively.

In the following, the right hand side of eq. (10) is assessed for each experimentally observed five phase (four solids plus fluid) assemblage. The required thermodynamic properties ($\Delta_f H_j^o, S_j^o, c_{P,j}^o, V_{j,\text{solid}}^o$) of all components are from Gottschalk (1997) except for tschermakite. For tschermakite, $c_{P,\text{ts}}^o$ and V_{ts}^o (268.5 cm^3/mol) was taken from Holland and Powell (1998) and from Najorka and Gottschalk (submitted), respectively, and the coefficients of thermal expansion and compression of tremolite (Gottschalk 1997) were used as a first approximation. The fugacities of pure water $f_{H_2O}^o$ were calculated using the equation of state of Kerrick and Jacobs (1981).

The activities of all phases are required for the calculation of the equilibrium constant (eq. 10). Since anorthite, forsterite, quartz and zoisite have endmember compositions, their activities were treated as unity. Deviations from endmember composition were observed in diopside, enstatite, clinochlore and talc due to small amounts of Al-incorporation (Table 2). Their activities were calculated assuming ideal mixing using compositions from Table 2 and compositional variables from Table 7. Since in most experimental runs a bromidic solution was present, the activity of water was slightly reduced. Because of low molalities (Table 1) the activity of H$_2$O was approximated using Raoult´s law ($a_{H_2O} = X_{H_2O}$).

The activities of tschermakite and tremolite in amphbibole solid solutions depend both on the site occupancies as well as the degree of short range ordering. Consequently, the evaluation of the mixing properties is not straightforward. Various sites have been discussed at which the Al substitution in amphiboles is assumed to occur (Hawthorne 1983; Oberti et al. 1995a, 1995b; Welch and Knight 1999; Welch et al. 1998). Recent studies using NMR- and IR-spectroscopy indicate that in tremolite-tschermakite solid solutions Al occupies the octahedral M2, M3 and the tetrahedral T1 sites (Hawthorne et al. 2000; Najorka and Gottschalk, submitted). Random distribution on these sites is restricted, however, if the rule of Al-avoidance on adjacent T1 tetrahedra (Oberti et al. 1995b; Hawthorne 1997) and M2-, M3-octahedra (Hawthorne et al. 2000; Najorka and Gottschalk, submitted) is considered. Further restrictions are imposed by local charge balance, which requires that the tetrahedral substitution of Al for Si is accompanied by octahedral substitution of Al for Mg at the next M2 or M3 sites.

The activities of the endmembers tremolite and tschermakite are commonly expressed using ideal mixing models, which consider substitution on the M2, M3 and T1 sites (e.g. Jenkins 1994; Smelik et al. 1994; Hoschek 1995; Quirion and Jenkins 1998). Local charge balance is assumed to a certain extent in all but one of these ideal mixing models. Difficulties arise, however, because the amounts of octahedral and tetrahedral sites per formula unit are not equal and the means by which charge is locally balanced are not unique. This adds a contribution to the configurational entropy. For example, if Al is substituted at a M3 site, local charge can be balanced at four equivalent T1 sites above or below the octahedral band within the amphibole *I*-beam. Substitution of Al on M2 can be locally charge balanced at two equivalent T1 sites. On the other hand, incorporation of Al on a distinct T1 site can be charge-balanced by either a coupled substitution on a M2 or M3 site. The configurational entropies for various mixing models are shown in Fig. 6 and the corresponding expressions for the respective activities are listed in Table 7. The highest entropies are calculated for models which neglect charge balance by assuming total random distribution at the M2 and T1 sites as shown for model (f). In contrast to model (f), model (g) (Holland and Powell 1998) considers random mixing at only two of the four T1 sites which lowers the configurational entropy. Despite this decrease in configurational entropy, model (g) does not include local charge balance because the substitution of Al at the octahedral and tetrahedral sites is still independent in this case. From the mixing models shown in Table 7 only model (c) considers true charge balance by using clusters of $Si_{T1}Mg_{M2}Si_{T1}$, $Si_{T1}Al_{M2}Al_{T1}$ and $Al_{T1}Al_{M2}Si_{T1}$. However, because this model adds only a linear compositional term to model (b), the resulting expressions for activities from models (b) and (c) are identical. The remaining constant after differentiation

$$\left(\frac{\partial S^{con}}{\partial n_i} \right) = -R \ln a_i^{con} \tag{11}$$

of model (c) is added to the entropy for tschermakite endmember.

Neither of these models considers Al-avoidance, however. On the other hand, the introduced error is probably low. As shown above, tremolite-tschermakite solid solutions are in the range between $tr_{100}ts_0$ and $tr_{40}ts_{60}$ and do not extend to Al-richer compositions. Assuming random distribution, even for the highest experimentally observed X_{ts} of about

Table 7. Configurational entropies and ideal mixing models of amphibole and ideal mixing models of Al-bearing phases.

ideal mixing model	compositional variable	S^{con}	a_{tr}	a_{ts}
amphibole				
(a) Al-Mg mixing at one M3-site charge coupled with Al-Si substitution at a "specific" T1-site (one-site coupled model)	$X_{ts} = \dfrac{X_{Al}^{M3}}{2}$ $(X_{ts} \leq 0.5)$	$-R(X_{tr} \ln X_{tr} + X_{ts} \ln X_{ts})$	$(1-X_{ts})$	X_{ts}
(b) Al-Mg mixing at two M2-sites charge coupled with Al-Si substitution at two "specific" T1-sites (two-site coupled model)	$X_{ts} = X_{Al}^{M2}$	$-2R(X_{tr} \ln X_{tr} + X_{ts} \ln X_{ts})$	$(1-X_{ts})^2$	X_{ts}^2
(c) Mixing of two charge coupled clusters of type $Si_{T1}Mg_{M2}Si_{T1}$ (A), $Al_{T1}Al_{M2}Si_{T1}$ (B), and $Si_{T1}Al_{M2}Al_{T1}$ (C)	$X_{ts} = (1-X_{(A)})$ $= 2X_{(B)} = 2X_{(C)}$	$-2R\left(X_{tr}\ln X_{tr} + X_{ts} \ln \dfrac{X_{ts}}{2}\right)$	$(1-X_{ts})^2$	X_{ts}^2
(d) Al-Mg mixing at two M2 and one M3-sites charge coupled with tetrahedral Al-Si substitution (three-site coupled model)	$X_{ts} = \dfrac{3}{2}X_{Al}^{M2} = \dfrac{3}{2}X_{Al}^{M3}$	$-3R\left(\left(\dfrac{1+2X_{tr}}{3}\right)\ln\left(\dfrac{1+2X_{tr}}{3}\right) + \dfrac{2}{3}X_{ts}\ln\dfrac{2}{3}X_{ts}\right)$	$\left(1-\dfrac{2}{3}X_{ts}\right)^3$	$X_{ts}^2(3-2X_{ts})$
(e) Al-Si mixing at four T1-sites charge coupled with a "specific" octahedral Al-Mg substitution (four-site coupled model)	$X_{ts} = X_{Al}^{M2}$	$-4R\left(\left(\dfrac{1+X_{tr}}{2}\right)\ln\left(\dfrac{1+X_{tr}}{2}\right) + \dfrac{X_{ts}}{2}\ln\dfrac{X_{ts}}{2}\right)$	$\left(1-\dfrac{X_{ts}}{2}\right)^4$	$4X_{ts}^2\left(1-\dfrac{X_{ts}}{2}\right)^2$
(f) random mixing of Al-Mg at two M2-sites and four Al-Si-sites at four T1-sites (random mixing model)	$X_{ts} = X_{Al}^{M2}$	$-R\left(2(X_{tr} \ln X_{tr} + X_{ts} \ln X_{ts}) + 4\left(\left(\dfrac{1+X_{tr}}{2}\right)\ln\left(\dfrac{1+X_{tr}}{2}\right) + \dfrac{X_{ts}}{2}\ln\left(\dfrac{X_{ts}}{2}\right)\right)\right)$	$(1-X_{ts})^2\left(1-\dfrac{X_{ts}}{2}\right)^4$	$4X_{ts}^4\left(1-\dfrac{X_{ts}}{2}\right)^2$
(g) random mixing of Al-Mg at two M2-sites and four Al-Si-sites at two T1-sites (reduced random mixing model)	$X_{ts} = X_{Al}^{M2}$	$-R\left(2(X_{tr} \ln X_{tr} + X_{ts} \ln X_{ts}) + 2\left(\left(\dfrac{1+X_{tr}}{2}\right)\ln\left(\dfrac{1+X_{tr}}{2}\right) + \dfrac{X_{ts}}{2}\ln\left(\dfrac{X_{ts}}{2}\right)\right)\right)$	$(1-X_{ts})^2\left(1-\dfrac{X_{ts}}{2}\right)^2$	$2X_{ts}^3\left(1-\dfrac{X_{ts}}{2}\right)^2$
clinopyroxene random Al-Mg mixing at one M1-site and Al-Si at two T-sites	$X_{Cats} = X_{Al}^{M1}$		$a_{di} = (1-X_{Cats})\left(1-\dfrac{X_{Cats}}{2}\right)^2$	
orthopyroxene random Al-Mg mixing at one M1-site and Al-Si at two T-sites	$X_{Mgts} = X_{Al}^{M1}$		$a_{en} = (1-X_{Mgts})\left(1-\dfrac{X_{Mgts}}{2}\right)^2$	
talc random Al-Mg mixing at one M3-site and Al-Si at two T-sites	$X_{tats} = X_{Al}^{M3}$		$a_{tc} = \dfrac{(1-X_{tats})(2-X_{tats})^2}{4}$	
clinochlore random Al-Mg mixing at one M1-site and Al-Si at two T2-sites	$X_{cln} \leq X_{Mg}^{M1}$		$a_{cln} = X_{cln}^2(2-X_{cln})$	

note: X_{Al}^{M2}, X_{Al}^{M3} mole fractions of Al at M2 and M3 in amphibole; X_{Al}^{M1} mole fraction of Al at M1 in pyroxene; X_{Al}^{M3} mole fraction of Al at M3 in talc; X_{Mg}^{M1} mole fraction of Mg at M1 in clinochlore.

140

0.60 (Cho and Ernst 1991), the probability of Al-occupancy on adjacent tetrahedral or octahedral sites is still less than 9%. Consideration of Al-avoidance or more complex mixing models, e.g. adding mixing at M3 to model (c), would require the application of Monte-Carlo simulations or cluster variation methods (Vinograd and Putnis 1999).

Using the different activity models (a) to (g) from Table 7 and their contributions to the configurational entropy (Fig. 6), a series of $\Delta_f H_{ts}^o$ and S_{ts}^o values are derived (Table 8). The best fit to the experimental data (see r^2-values in Table 8) was achieved using the two-site coupled model (b) and the three-site coupled model (d). Using the two-site coupled model (b) for tschermakite, $\Delta_f H_{ts}^o$ = -12528.3 ± 11.7 kJ/mol and S_{ts}^o = 556.5 ± 12.0 J/mol/K were derived (Fig. 7a). Model (b) is believed to represent the most vigorous mixing model for which a closed formulation exists.

Similar calculations were carried out using magnesiohornblende instead of tschermakite as endmember. Again, the best fits were attained with two-site and three-site coupled models. For magnesiohornblende, values of $\Delta_f H_{Mghb}^o$ = -12418.7 ± 5.9 kJ/mol and S_{Mghb}^o = 562.8 ± 6.1 J/mol/K were extracted when the two-site coupled model was applied (Fig. 7b).
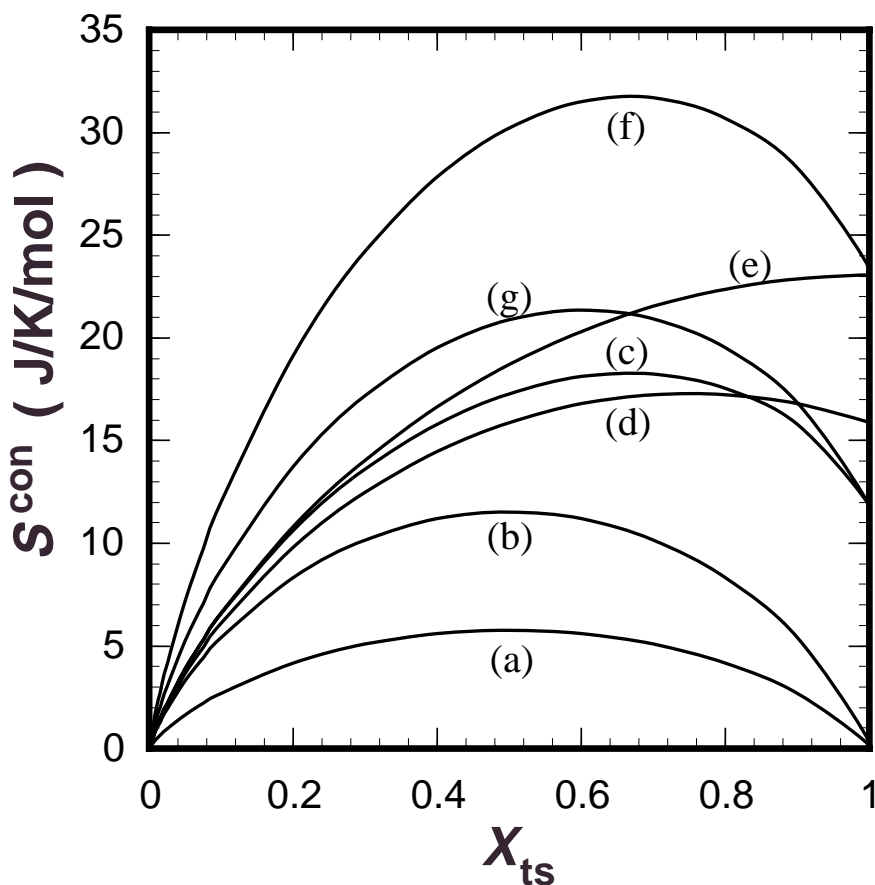
In addition to the configurational entropy, a term considering excess enthalpy and activity coefficients can be added in eq. (10) to the equilibrium constant $K_{(P,T)}$. Applying a two-site regular solution model for the mixing model (b), the excess enthalpy for the tremolite-tschermakite solid solution series is expressed by:

$$H^{excess} = 2X_{tr}X_{ts}W_{Mg-Al}^{M2} + (1+X_{tr})X_{ts}W_{Si-Al}^{T1} = X_{tr}X_{ts}\left(2W_{Mg-Al}^{M2} + W_{Si-Al}^{T1}\right) + X_{ts}W_{Si-Al}^{T1} \tag{12}$$

$$RT\ln\gamma_{tr} = X_{ts}^2\left(2W_{Mg-Al}^{M2} + W_{Si-Al}^{T1}\right) \tag{13}$$

$$RT\ln\gamma_{ts} = X_{tr}^2\left(2W_{Mg-Al}^{M2} + W_{Si-Al}^{T1}\right) + W_{Si-Al}^{T1} \tag{14}$$

The term for γ_{ts} involves a constant (W_{Si-Al}^{T1}) which can not be distinguished from the parameter $\Delta_f H_{ts}^o$. Therefore, only a value for $2W_{Mg-Al}^{M2} + W_{Si-Al}^{T1}$ of −1.2 ± 7.3 kJ/mol was derived. In conjunction with this excess enthalpy, the corresponding values for $\Delta_f H_{ts}^o$ and S_{ts}^o are −12528.7 ±12 kJ/mol and 555.3 ± 14 J/mol/K. The low value for $2W_{Mg-Al}^{M2} + W_{Si-Al}^{T1}$ indicates that an additional excess enthalpy term is not necessary to fit the data (see Table 8, columns 3 and 4).

Fig. 6. Calculated configurational entropies *versus* X_{ts} for the different mixing models (a) to (g) given in Table 7.

The comparison with previously reported entropy and enthalpy values is shown in Table 9. The entropy of tschermakite is about 3% higher than indicated in previous studies. Within error limits, the entropy is comparable with the value from Holland and Powell (1998). Our derived enthalpy of tschermakite agrees with other studies, particularly with the calorimetrically measured value of Smelik et al. (1994).

Our value of the entropy of magnesiohornblende is between the reported values from other studies (Table 9). A significantly higher entropy and a lower enthalpy were suggested by Smelik et al. (1994). Quirion and Jenkins (1998) used Smelik's enthalpy data of magnesiohornblende and also derived a significant higher entropy. The enthalpy of magnesiohornblende is in reasonable agreement with the value from Holland and Powell (1990).

Table 8. Fits of $\Delta_f H^o_{ts}$ and S^o_{ts} for tschermakite and $2W^{M2}_{Mg-Al} + W^{T1}_{Si-Al}$ using different mixing models

	model (a) one-site coupled	model (b) two-site coupled	including excess enthalpy term	model (d) three-site coupled	model (e) four-site coupled	model (f) random mixing	model (g) reduced random mixing
$\Delta_f H^o_{ts}$ (kJ/mol)	-12521.2 ± 13.5	-12528.3 ± 11.7	-12528.7 ± 12.3	-12525.2 ± 12.4	-12523.8 ± 12.2	-12556.3 ± 16.7	-12542.3 ± 13.2
S^o_{ts} (J/K/mol)	585.1 ± 13.9	556.5 ± 12.0	555.3 ± 14.3	567.4 ± 12.0	570.5 ± 12.6	513.3 ± 17.2	534.9 ± 13.6
$2W^{M2}_{Mg-Al} + W^{T1}_{Si-Al}$ (kJ/mol)	-	-	-1.2 ± 7.3	-	-	-	-
r^2	0.9861	0.9884	0.9879	0.9882	0.9880	0.9727	0.9841

Table 9. Comparison of thermodynamic data of tschermakite and magnesiohornblende

$\Delta_f H^o$ (kJ/mol)	S^o (J/K/mol)	references
tschermakite		
-12528.3 ± 11.7	556.5 ± 12.0	this study (two-site model)
-12540.57 ± 2.91	545.00	Holland and Powell (1998)
-12527.7 ± 16.4	-	Smelik et al. (1994)**
-12534.4 ± 13.0	542.5 ± 12.7	Jenkins (1994)
-12534.67	538.6	Leger and Ferry (1991)*
magnesiohornblende		
-12418.7 ± 5.9	562.8 ± 6.1	this study (two-site model)
-	575.4 ± 1.6	Quirion and Jenkins (1998)
-12401.2	575.3 ± 3.5	Smelik et al. (1994)**
-12420.29 ± 12.7	551.0	Holland and Powell (1990)

note: *Values were derived from natural samples. **Calorimetric study.
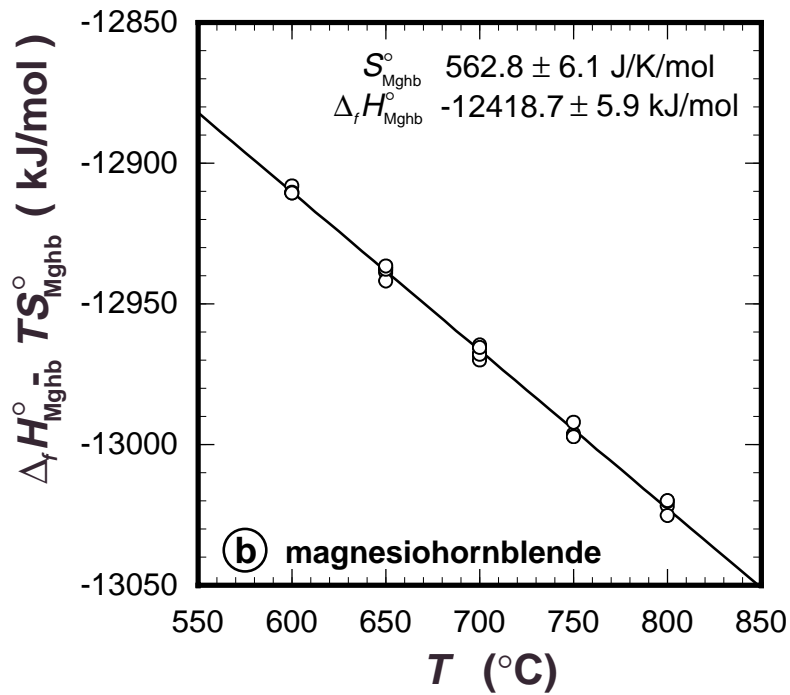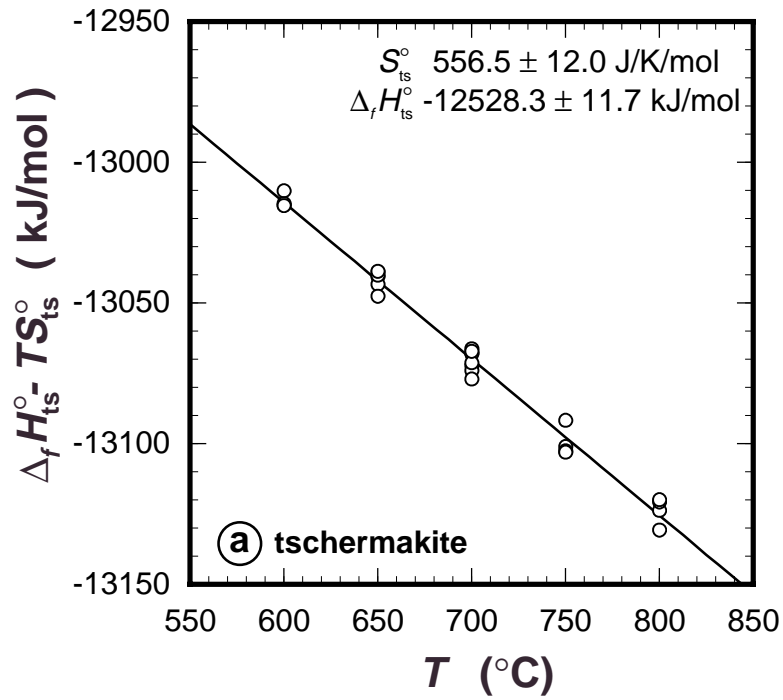
Fig. 7. Plot of $\Delta_f H^\circ_{ts} - TS^\circ_{ts}$ *versus* temperature for exchange reactions (1) to (6) using compositional data from Table 2 and mixing models explained in the text. **a)** tschermakite, **b)** magnesiohornblende.

Calculation of Al-isoplethes

The derived thermodynamic data for tschermakite and the two-site coupled mixing model (b) for tremolite-tschermakite solid solutions were used for calculations the of P-T phase relations in the CMASH-system shown in Fig.s 4a-d. For the assemblages amphibole-anorthite-quartz-diopside and amphibole-anorthite-quartz-talc the resulting X_{ts}-isopleths for Al-incorporation in amphibole are nearly horizontal in P-T-space (Fig.s 4a, b) and provide excellent geobarometers. The X_{ts}-isopleths in amphibole for the assemblage amphibole-anorthite-clinochlore-talc are both pressure and temperature dependent and show a negative slope in P-T-space whereas for amphibole-anorthite-enstatite-forsterite, the slope is positive (Fig. 4c). The X_{ts}-isopleths for the assemblage amphibole-zoisite-quartz-talc show only a slight pressure and a strong temperature dependence (Fig. 4d).

In general, the measured X_{ts} in amphiboles are nicely reproduced by the calculated isopleths, at least within the stability fields of the assemblages amphibole-anorthite-quartz-diopside, amphibole-anorthite-quartz-talc, amphibole-anorthite-enstatite-forsterite, and amphibole-zoisite-quartz-talc. Less agreement exists for the assemblage amphibole-anorthite-clinochlore-talc where isopleths indicate somewhat enhanced Al-incorporation compared to the measured data. This is possibly due to the poor thermodynamic properties of clinochlore in chlorite solid solutions for which a good model is not available up to now. In general, the phase relations in the CMASH-system were calculated accurately with the proposed thermodynamic data of tschermakite and the two-site coupled mixing model. Observed small deviations between experimental and calculated Al-concentrations are mostly due to the fact that ideal mixing was assumed along the tremolite-tschermakite join. Up to now, however, information about ordering of Al^{3+} between different sites, e.g. M2 and M3, in Al-bearing tremolite is not sufficient enough to calibrate a more rigorous model.

Concluding remark

In natural rocks, the Al concentration in amphibole coexisting with plagioclase is widely used as a geobarometer because Al concentrations increase mainly with pressure. Our results suggest that, at a given pressure, more Al is incorporated than indicated by previous experimental studies. Thus, pressure estimations indicated by the "Al in hornblende" geobarometer that used experimental data yielded pressure values that were probably too high.

ACKNOWLEDGMENTS

REFERENCES CITED

Baker, J., and Holland, T.J.B. (1996) Experimental reversals of chlorite composition in divariant $MgO + Al_2O_3 + SiO_2 + H_2O$ assemblages. American Mineralogist, 81, 676-684.

Baker, J., and Matthews (1994) Textural and isotopic development of marble assemblages during the Barrovian-style M2 metamorphic event, Naxos, Greece. Contributions to Mineralogy and Petrology, 116, 130-144.

Cao, R.-L., Ross, C., and Ernst, W.G. (1986) Experimental studies to 10 kb of the bulk composition $tremolite_{50}$-$tschermakite_{50}$ + excess H_2O. Contributions to Mineralogy and Petrology, 93, 160-167.

Cho, M., and Ernst, W.G. (1991) An experimental determination of calcic amphibole solid solution along the join tremolite-tschermakite. American Mineralogist, 76, 985-1001.

Connolly, J. A. D. (1990): Multivariate phase diagrams: an algorithm based on generalized thermodynamics. American Journal of Science, 290, 266-718.

Danckwerth, P.A., and Newton, R.C. (1978) Experimental determination of the spinel peridotite to garnet peridotite reaction in the system MgO-Al_2O_3-SiO_2 in the range 900-1100 °C and Al_2O_3 isopleths of enstatite in the spinel field. Contributions to Mineralogy and Petrology, 66, 189-201.

Gasparik, T. (1986) Experimental study of subsolidus phase relations and mixing properties of clinopyroxene in the silica saturated system CaO-MgO- Al_2O_3-SiO_2. American Mineralogist, 71, 686-693.

Gottschalk, M. (1997) Internally consistent thermodynamic data for rock forming minerals. European Journal of Mineralogy, 9, 175-223.

Gottschalk, M., Andrut, M., and Melzer, S. (1999) The determination of cummingtonite content of synthetic tremolite. European Journal of Mineralogy, 11, 967-982.

Gottschalk, M., Najorka, J., and Andrut, M. (1998) Structural and compositional characterisation of synthetic (Ca,Sr)-tremolite and (Ca,Sr)-diopside solid solutions. Physics and Chemistry of Minerals, 25, 415-428.

Hammarstrom, J.M., and Zen, E.-A. (1986) Aluminium in hornblende: an empirical igneous geobarometer. American Mineralogist, 71, 1297-1313.

Hawthorne, F.C. (1983) The crystal chemistry of the amphiboles. Canadian Mineralogist, 21, 173-480.

Hawthorne, F.C. (1997) Short-range order in amphiboles: a bond-valence approach. The Canadian Mineralogist, 35, 201-216.

Hawthorne, F.C., Welch, M., Della Ventura, G., Liu, S., Robert, J.-L., and Jenkins, D. (2000) Short -range order in synthetic aluminous tremolites: An infrared and triple-quantum MAS NMR study. American Mineralogist, 85, 1716-1724.

Holland, T.J.B., and Powell, R. (1990) An enlarged and updated internally consistent thermodynamic dataset with uncertainties and correlations: the system K_2O-Na_2O-CaO-MgO-MnO-FeO-Fe_2O_3-Al_2O_3-TiO_2-SiO_2-C-H-O_2. Journal of Metamorphic Geology, 8, 89-124.

Holland, T.J.B., and Powell, R. (1998) An internally consistent thermodynamic dataset for phases of petrological interest. Journal of Metamorphic Geology, 16, 309-343.

Hollister, L.S., Grissom, G.C., Peters, E.K., Stowell, H.H., and Sisson, V.B. (1987) Confirmation of the empirical correlation of Al in hornblende with pressure of solidification of calc-alkaline plutons. American Mineralogist, 72, 231-239.

Hoschek, G. (1995) Stability relations and Al content of tremolite and talc in CMASH assemblages with kyanite + zoisite + quartz + H_2O. European Journal of Mineralogy, 7, 353-362.

Jasmund, K., and Schäfer, R. (1972) Experimentelle Bestimmung der P-T-Stabilitätsbereiche in der Mischkristallreihe Tremolit-Tschermakite. Contributions to Mineralogy and Petrology, 34, 101-115.

Jenkins, D.M. (1981) Experimental phase relations of hydrous peridotites modelled in the system H_2O-CaO-MgO-Al_2O_3-SiO_2. Contributions to Mineralogy and Petrology, 77, 166-176.

Jenkins, D.M. (1983) Stability and composition relations of calcic amphiboles in ultramafic rocks. Contributions to Mineralogy and Petrology, 83, 375-384.

Jenkins, D.M. (1988) Experimental study of the join tremolite-tschermakite: A reinvestigation. Contributions to Mineralogy and Petrology, 99, 392-400.

Jenkins, D.M. (1994) Experimental reversal of the aluminium content in tremolitic amphiboles in the system H_2O-CaO-MgO-Al_2O_3-SiO_2. American Journal of Science, 294, 593-620.

Jenkins, D.M., Sherriff, B.L., Cramer, J., and Xu, Z. (1997) Al, Si, and Mg occupancies in tetrahedrally and octahedrally coordinated sites in synthetic aluminous tremolite. American Mineralogist, 82, 280-290.

Johnson, M.C., and Rutherford, M.J. (1989) Experimental calibration of the aluminum-in-hornblende geobarometer with application to Long Valley caldera (California) volcanic rocks. Geology, 17, 837-841.

Kerrick, D.M., and Jacobs, G.K. (1981) A modified Redlich-Kwong equation for H_2O, CO_2, and H_2O-CO_2 mixtures at elevated pressures and temperatures. American Journal of Science, 281, 735-767.

Léger, A., and Ferry, J.M. (1991) Highly aluminous hornblende from low-pressure metacarbonates and a preliminary thermodynamic model for the Al content of calcic amphibole. American Mineralogist, 76, 1002-1017.

Makino, K., and Tomita, K. (1989) Cation distribution in the octahedral sites of hornblendes. American Mineralogist, 74, 1097-1105.

Melzer, S., Gottschalk, M., and Heinrich, W. (1998) Experimentally determined partitioning of Rb between richterites and aqueuos (Na,K)-chloride solutions. Contributions to Mineralogy and Petrology, 133, 315-328.

Najorka J., Gottschalk M., Franz G., and Heinrich W. (1999) Experimental determination of the Sr-Ca distribution between amphibole, clinopyroxene and chloridic aqueous solution. American Mineralogist 84, 596-606.

Najorka, J., and Gottschalk, M., submitted Crystal chemistry of tremolite-tschermakite solid solutions. Submitted to American Mineralogist.

Oba, T. (1978) Phase relationship of $Ca_2Mg_3Al_2Si_6Al_2O_{22}(OH)_2$-$Ca_2Mg_3Fe_2^{3+}Si_6Al_2O_{22}(OH)_2$ join at high temperature and high pressure - the stability of tschermakite. Journal of Faculty of Science, Hokkaido University, 18, Ser. IV, 339-350.

Oberti, R., Hawthorne, F.C., Ungaretti, L., and Cannillo, E. (1995a) [6]Al disorder in amphiboles from mantle peridotites. Canadian Mineralogist, 33, 867-878.

Oberti, R., Ungaretti, L., Cannillo, E., Hawthorne, F.C., and Memmi, I. (1995b) Temperature-dependent Al order-disorder in the tetrahedral double chain of C2/m amphiboles. European Journal of Mineralogy, 7, 1049-1063.

Quirion, D.M., and Jenkins, D.M. (1998) Dehydration and partial melting of tremolitic amphibole coexisting with zoisite, quartz, anorthite, diopside, and water in the system H_2O-CaO-MgO-Al_2O_3-SiO_2. Contributions to Mineralogy and Petrology, 130, 379-389.

Robinson, P., Spear, F.S., Schumacher, J.C., Laird, J., Klein, C., Evans, B.W., and Doolan, B.L. (1982) Phase relations of metamorphic amphiboles: natural occurance and theory. In D.R. Veblen, and P.H. Ribbe, Eds. Amphiboles: Petrology and experimental phase relations, 9B, p. 1-228. Mineralogical Society of America.

Schmidt, M.W. (1992) Amphibole composition in tonalite as a function of pressure: an experimental calibration of the Al-in-hornblende barometer. Contributions to Mineralogy and Petrology, 110, 304-310.

Shannon, R.D. (1976) Revised effective ionic radii and systematic studies of interatomic distances in halides and chalcogenides. Acta Crystallographica Section A, 32, 751-767.

Smelik, E.A., Jenkins, D.M., and Navrotsky, A. (1994) A calorimetric study of synthetic amphiboles along the tremolite-tschermakite join and the heats of formation of magnesiohornblende and tschermakite. American Mineralogist, 79, 1110-1122.

Thomas, W.M., and Ernst, W.G. (1990) The aluminium content of hornblende in calc-alkaline granitic rocks: A mineralogic barometer calibrated experimentally to 12 kbars. Geochemical Society Special Publication, 2, 59-63.

Vinograd, V., and Putnis, A. (1999) The description of Al, Si ordering in alumosilicates using the cluster variation method. American Mineralogist, 84, 311-324.

Welch, M.D., and Knight, K.S. (1999) A neutron powder diffraction study of cation ordering in high-temperature synthetic amphiboles. European Journal of Mineralogy, 11, 321-331.

Welch, M.D., Shuangxi, L., and Klinowski, J. (1998) ^{29}Si MAS NMR systematics of calcic and sodic-calcic amphiboles. American Mineralogist, 83, 85-96.

Zimmermann, R., Heinrich, W., and Franz, G. (1996) Tremolite synthesis from $CaCl_2$-bearing aqueous solutions. European Journal of Mineralogy, 8, 767-776.

Zimmermann R., Gottschalk M., Heinrich W., and Franz G. (1997) Experimental Na-K distribution between amphiboles and aqueous chloride solutions, and a mixing model along the richterite – K-richterite join. Contributions to Mineralogy and Petrology 126, 252-264.

ZUSAMMENFASSUNG

Die Zusammensetzung synthetischer Amphibole wurde experimentell entlang der Tremolit-Tschermakit–Mischkristallreihe im System CaO-MgO-Al_2O_3-SiO_2-H_2O-Br_2 untersucht.

Die Amphibole wurden in folgenden Paragenesen betrachtet: Amphibol-Anorthit-Diopsid-Quartz (I) Amphibol-Anorthit-Quartz-Talk (II), Amphibol-Anorthit-Quartz-Enstatit (III), Amphibol-Anorthit-Talk-Klinochlor (IV), Amphibol-Zoisit-Talk-Quartz (V), and Amphibol-Zoisit-Talk-Klinochlor (VI). Die Paragenesen wurden aus Oxid-Hydroxidmischungen in Anwesenheit einer $CaBr_2$-Lösung im Bereich zwischen 600-800°C und 200–2000 MPa untersucht. Die festen Phasen wurden mit SEM, HRTEM, EMP und XRD-Methoden untersucht. Die Mikrosondendaten zeigten, daß die Amphibole Mischkristalle des ternären Systems Tremolit-Tschermakit-Cummingtonit darstellen. Geringe Abweichungen von der Endgliedzusammensetzung wurden in den Phasen Enstatit, Diopsit, Talk und Klinochlor beobachtet.

Die thermodynamischen Eigenschaften des Tschermakitendgliedes und die Mischungseigenschaften entlang der Tremolit-Tschermakit–Mischkristallreihe wurden mittels der korrespondierenden Austauschreaktionen der experimentell beobachteten Paragenesen (I-VI) extrahiert.

Verschiedene ideale Mischungsmodelle wurden für die Al-Mg- und Al-Si-Substitution auf den Oktaederpositionen M2 und M3 sowie den Tetraederpositionen T1 getestet. Der beste Fit für die thermodynamischen Daten für Tschermakit wurde mit der Verwendung des "two-side coupled"-Modell erzielt. Für Tschermakit konnte eine Enthalpie von $\Delta_f H^o_{ts}$ = -12528.3 ± 11.7 kJ/mol und eine Entropie von S^o_{ts} = 556.5 ± 12.0 J/mol/K abgeleitet werden. Ähnliche Berechnungen wurden für Magnesiohornblende als Endglied anstelle des Tschermakits durchgeführt. Für Magnesiohornblende konnte eine Enthalpie von $\Delta_f H^o_{Mghb}$ = -12418.7 ± 5.9 kJ/mol und eine Entropie von S^o_{Mghb} = 562.8 ± 6.1 J/mol/K extrahiert werden. Mit der Verwendung der abgeleiteten thermodynamischen Daten für Tschermakit und des "two-side coupled"- Mischungsmodells zeigten die berechneten Phasenbeziehungen im CMASH-System und der berechnete Tschermakitgehalt im Amphibol eine gute Übereinstimmung mit den experimentellen Daten.

Lebenslauf

Jens Najorka
geboren am 22.04.1967 in Berlin

Ausbildungsweg

1992-1996	Hauptstudium Mineralogie an der TU-Berlin
1990-1992	Grundstudium Mineralogie an der Bergakademie Freiberg
1989-1990	Erlangung der Hochschulreife an der Bergakademie Freiberg
1983-1985	Ausbildung zum Geologiefacharbeiter am Zentralen Geologischen Institut Berlin
1973-1983	Polytechnische Oberschule in Berlin

Beschäftigungsverhältnisse

2001	Wissenschaftlicher Mitarbeiter an der Universität in Bristol (England), Department of Earth Sciences
1996-2000	Wissenschaftlicher Mitarbeiter am GeoForschungsZentrum Potsdam, Abteilung Stoffparameter und Transportprozesse
1998-2000	Leiter des Schmuckstein-Schleifkurses in den Künstlerischen Werkstätten, Berlin-Prenzlauer Berg
1994, 1995-1996	Studentischer Mitarbeiter an der TU-Berlin, Institute für Petrologie und Kristallographie
1986-1989	Wehrdienst
1985-1986	Geologiefacharbeiter am Zentralen Geologischen Institut Berlin